

# ИЗВЕСТИЯ ВЫСШИХ УЧЕБНЫХ ЗАВЕДЕНИЙ ЧЕРНАЯ МЕТАЛЛУРГИЯ

IZVESTIYA. FERROUS METALLURGY

[fermet.misis.ru](http://fermet.misis.ru)

2025 Том 68 № 2  
Vol. No.

## МЕТАЛЛУРГИЧЕСКИЕ ТЕХНОЛОГИИ

Опыт производства рельсов из бейнитной стали  
марок 30ХГ2С2АФМ и 30ХГ2САФН

## МАТЕРИАЛОВЕДЕНИЕ

К вопросу о влиянии добавок оксидов редкоземельных элементов  
на кинетику образованию борированных слоев и диффузию бора  
по границам зерен при борировании сталей

## ФИЗИКО-ХИМИЧЕСКИЕ ОСНОВЫ МЕТАЛЛУРГИЧЕСКИХ ПРОЦЕССОВ

Термодинамическое моделирование процесса восстановления  
железорудных материалов водородсодержащими газами



ISSN 0368-0797  
eISSN 2410-2091

# ИЗВЕСТИЯ ВЫСШИХ УЧЕБНЫХ ЗАВЕДЕНИЙ ЧЕРНАЯ МЕТАЛЛУРГИЯ

Научно-технический журнал

Издается с января 1958 г. Выпускается 6 раз в год

2025 Том 68 № 2  
Vol. No.

# IZVESTIYA FERROUS METALLURGY

Scientific and Technical Journal

Published since January 1958. Issued 6 times a year

# IZVESTIYA FERROUS METALLURGY

www.fermet.misis.ru

ISSN 0368-0797 (Print) ISSN 2410-2091 (Online)

## Alternative title:

Izvestiya vuzov. Chernaya metallurgiya

## Founders:



## Editorial Board:

**Sailaubai O. Baisanov**, Dr. Sci. (Eng.), Prof., Abishev Chemical-Metallurgical Institute, Karaganda, Republic of Kazakhstan  
**Vladimir D. Belov**, Dr. Sci. (Eng.), Prof., NUST MISIS, Moscow  
**Anatolii A. Brodov**, Cand. Sci. (Econ.), Bardin Central Research Institute for Ferrous Metallurgy, Moscow  
**Il'ya V. Chumanov**, Dr. Sci. (Eng.), Prof., South Ural State Research University, Chelyabinsk  
**Andrei N. Dmitriev**, Dr. Sci. (Eng.), Prof., Academician, RANS, A.M. Prokhorov Academy of Engineering Sciences, Institute of Metallurgy, Ural Branch of RAS, Ural Federal University, Yekaterinburg  
**Aleksei V. Dub**, Dr. Sci. (Eng.), Prof., JSC "Science and Innovations", Moscow  
**Mikhail R. Filonov**, Dr. Sci. (Eng.), Prof., NUST MISIS, Moscow  
**Sergei M. Gorbatyuk**, Dr. Sci. (Eng.), Prof., NUST MISIS, Moscow  
**Konstantin V. Grigorovich**, Academician of RAS, Dr. Sci. (Eng.), Baikov Institute of Metallurgy and Materials Science of RAS, Moscow  
**Victor E. Gromov**, Dr. Sci. (Eng.), Prof., Siberian State Industrial University, Novokuznetsk  
**Aleksei G. Kolmakov**, Dr. Sci. (Eng.), Corresponding Member of RAS, Baikov Institute of Metallurgy and Materials Science of RAS, Moscow  
**Valerii M. Kolokol'tsev**, Dr. Sci. (Eng.), Prof., Magnitogorsk State Technical University, Magnitogorsk  
**Mariya V. Kostina**, Dr. Sci. (Eng.), Baikov Institute of Metallurgy and Materials Science of RAS, Moscow  
**Konstantin L. Kosyrev**, Dr. Sci. (Eng.), Academician of RANS, Electrosteel Heavy Engineering Works JSC, Moscow  
**Yuliya A. Kurganova**, Dr. Sci. (Eng.), Prof., Bauman Moscow State Technical University, Moscow  
**Linn Horst**, Linn High Therm GmbH, Hirschbach, Germany  
**Vladimir I. Lysak**, Academician of RAS, Dr. Sci. (Eng.), Prof., Rector, Volgograd State Technical University, Volgograd  
**Valerii P. Meshalkin**, Dr. Sci. (Eng.), Academician of RAS, Prof., D.I. Mendeleev Russian Chemical-Technological University, Moscow  
**Radik R. Mulyukov**, Dr. Sci. (Phys.-Chem.), Prof., Corresponding Member of RAS, Institute of Metals Superplasticity Problems of RAS, Ufa

*In accordance with paragraph 5 of the Rules for the formation of the Higher Attestation Commission list journal "Izvestiya. Ferrous metallurgy" is included in the list of leading peer-reviewed scientific journals, publication in which is taken into account in the defense of candidate and doctoral dissertations, as indexed in international data bases.*

## Editor-in-Chief:

**Leopol'd I. Leont'ev**, Academician, Adviser of the Russian Academy of Sciences; Dr. Sci. (Eng.), Prof., NUST "MISIS"; Chief Researcher, Institute of Metallurgy UB RAS, Moscow  
4 Leninskii Ave., Moscow 119049, Russian Federation  
National University of Science and Technology "MISIS"

## Deputy Editor-in-Chief:

**Evgenii V. Protopopov**, Dr. Sci. (Eng.), Prof., Siberian State Industrial University, Novokuznetsk

## Publisher:

National University of Science and Technology "MISIS"

## Editorial Office Address:

**in Moscow**  
4 Leninskii Ave., Moscow 119049, Russian Federation  
National University of Science and Technology "MISIS"  
Tel.: +7 (495) 638-44-11  
E-mail: fermet.misis@mail.ru, ferrous@misis.ru

**in Novokuznetsk**  
42 Kirova Str., Novokuznetsk, Kemerovo Region – Kuzbass  
654007, Russian Federation  
Siberian State Industrial University  
Tel.: +7 (3843) 74-86-28 E-mail: redjizvz@sibsiu.ru

**Sergei A. Nikulin**, Dr. Sci. (Eng.), Prof., Corresponding Member of RANS, NUST MISIS, Moscow  
**Asylbek Kh. Nurumgaliev**, Dr. Sci. (Eng.), Prof., Karaganda State Industrial University, Karaganda, Republic of Kazakhstan  
**Oleg I. Ostrovski**, Dr. Sci. (Eng.), Prof., University of New South Wales, Sydney, Australia  
**Loris Pietrelli**, Dr., Scientist, Italian National Agency for New Technologies, Energy and Sustainable Economic Development, Rome, Italy  
**Igor' Yu. Pyshmintsev**, Dr. Sci. (Eng.), Russian Research Institute of the Pipe Industry, Chelyabinsk  
**Andrei I. Rudskoi**, Academician of RAS, Dr. Sci. (Eng.), Prof., Rector, Peter the Great Saint-Petersburg Polytechnic University, Saint-Petersburg  
**Oleg Yu. Sheshukov**, Dr. Sci. (Eng.), Prof., Ural Federal University, Yekaterinburg  
**Laura M. Simonyan**, Dr. Sci. (Eng.), Prof., NUST MISIS, Moscow  
**Robert F. Singer**, Dr. Sci. (Eng.), Prof., Friedrich-Alexander University, Germany  
**Boris A. Sivak**, Cand. Sci. (Eng.), Prof., VNIIMETMASH Holding Company, Moscow  
**Leonid A. Smirnov**, Dr. Sci. (Eng.), Prof., Academician of RAS, OJSC "Ural Institute of Metals", Yekaterinburg  
**Sergei V. Solodov**, Cand. Sci. (Eng.), NUST MISIS, Moscow  
**Marcus Speidel**, Dr. Natur. Sci., Prof., Swiss Academy of Materials, Switzerland  
**Nikolai A. Spirin**, Dr. Sci. (Eng.), Prof., Ural Federal University, Yekaterinburg  
**Guoi Tang**, Institute of Advanced Materials of Tsinghua University, Shenzhen, China  
**Mikhail V. Temlyantsev**, Dr. Sci. (Eng.), Prof., Siberian State Industrial University, Novokuznetsk  
**Ekaterina P. Volynkina**, Dr. Sci. (Eng.), Advisor, ALE "Kuzbass Association of Waste Processors", Novokuznetsk  
**Aleksei B. Yur'ev**, Dr. Sci. (Eng.), Prof., Rector, Siberian State Industrial University, Novokuznetsk  
**Vladimir S. Yusupov**, Dr. Sci. (Eng.), Prof., Baikov Institute of Metallurgy and Materials Science of RAS, Moscow  
**Vladimir I. Zhuchkov**, Dr. Sci. (Eng.), Prof., Institute of Metallurgy, Ural Branch of RAS, Ural Federal University, Yekaterinburg  
**Michael Zinigrad**, Dr. Sci. (Physical Chemistry), Prof., Rector, Ariel University, Israel  
**Vladimir I. Zolotukhin**, Dr. Sci. (Eng.), Prof., Tula State University, Tula

**Indexed:** Scopus, Russian Science Citation Index (RSCI), Research Bible, Chemical Abstracts, OCLC and Google Scholar

Registered in Federal Service for Supervision in the Sphere of Mass Communications **PI number FS77-35456.**



Articles are available under Creative Commons Attribution 4.0 License.

# ИЗВЕСТИЯ ВЫСШИХ УЧЕБНЫХ ЗАВЕДЕНИЙ ЧЕРНАЯ МЕТАЛЛУРГИЯ

www.fermet.misis.ru

ISSN 0368-0797 (Print) ISSN 2410-2091 (Online)

## Варианты названия:

Известия вузов. Черная металлургия

Izvestiya. Ferrous Metallurgy

## Учредители:



## Редакционная коллегия:

**С. О. Байсанов**, д.т.н., профессор, ХМИ им. Ж.Абишева, г. Караганда, Республика Казахстан

**В. Д. Белов**, д.т.н., профессор, НИТУ МИСИС, г. Москва

**А. А. Бродов**, к.экон.н., ФГУП «ЦНИИчермет им. И.П. Бардина», г. Москва

**Е. П. Волынкина**, д.т.н., советник, ОЮЛ «Кузбасская Ассоциация переработчиков отходов», г. Новокузнецк

**С. М. Горбатько**, д.т.н., профессор, НИТУ МИСИС, г. Москва

**К. В. Григорович**, академик РАН, д.т.н., ИМЕТ им. А.А. Байкова РАН, г. Москва

**В. Е. Громов**, д.ф.-м.н., профессор, СибГИУ, г. Новокузнецк

**А. Н. Дмитриев**, д.т.н., профессор, академик РАЕН, академик АИН РФ, г. Екатеринбург

**А. В. Дуб**, д.т.н., профессор, ЗАО «Наука и инновации», г. Москва

**В. И. Жучков**, д.т.н., профессор, ИМЕТ УрО РАН, г. Екатеринбург

**Р. Ф. Зингер**, д.т.н., профессор, Институт Фридриха-Александра, Германия

**М. Зиниград**, д.т.н., профессор, Институт Ариэля, Израиль

**В. И. Золотухин**, д.т.н., профессор, ТулГУ, г. Тула

**А. Г. Колмаков**, д.т.н., чл.-корр. РАН, ИМЕТ им. А.А. Байкова РАН, г. Москва

**В. М. Колокольцев**, д.т.н., профессор, МГТУ им. Г.И. Носова, г. Магнитогорск

**М. В. Костина**, д.т.н., ИМЕТ им. А.А. Байкова РАН, г. Москва

**К. Л. Косырев**, д.т.н., академик РАЕН, ОАО «Электростальский завод тяжелого машиностроения», г. Москва

**Ю. А. Курганова**, д.т.н., профессор, МГТУ им. Н.Э. Баумана, г. Москва

**Х. Линн**, ООО «Линн Хай Терм», Германия

**В. И. Лысак**, академик РАН, д.т.н., профессор, ВолГТУ, г. Волгоград

**В. П. Мешалкин**, академик РАН, д.т.н., профессор, РХТУ им. Д.И. Менделеева, г. Москва

*В соответствии п. 5 Правил формирования перечня ВАК журнал «Известия вузов. Черная металлургия» входит в перечень ведущих рецензируемых научных журналов и изданий, публикация в которых учитывается при защитах кандидатских и докторских диссертаций как индексируемый в МБД.*

## Главный редактор:

**Леопольд Игоревич Леонтьев**, академик РАН, советник, Президиум РАН; д.т.н., профессор, НИТУ «МИСИС»; главный научный сотрудник, Институт металлургии УрО РАН  
Россия, 119049, Москва, Ленинский просп., д. 4, стр. 1, Национальный исследовательский технологический университет «МИСИС»

## Заместитель главного редактора:

**Евгений Валентинович Протопопов**, д.т.н., профессор, Сибирский государственный индустриальный университет г. Новокузнецк

## Издатель:

Национальный исследовательский технологический университет «МИСИС»

## Адреса подразделений редакции:

### в Москве

Россия, 119049, Москва, Ленинский просп., д. 4, стр. 1  
Национальный исследовательский технологический университет «МИСИС»

Тел.: +7 (495) 638-44-11 E-mail: ferrous@misis.ru

### в Новокузнецке

Россия, 654007, Новокузнецк,  
Кемеровская обл. – Кузбасс, ул. Кирова, зд. 42  
Сибирский государственный индустриальный университет  
Тел.: +7 (3843) 74-86-28 E-mail: redjizvz@sibsiu.ru

**Р. Р. Мулюков**, д.ф.м.-н., профессор, чл.-корр. ФГБУН ИПСМ РАН, г. Уфа  
**С. А. Никулин**, д.т.н., профессор, чл.-корр. РАЕН, НИТУ МИСИС, г. Москва  
**А. Х. Нурумгалиев**, д.т.н., профессор, КГИУ, г. Караганда, Республика Казахстан  
**О. И. Островский**, д.т.н., профессор, Университет Нового Южного Уэльса, Сидней, Австралия  
**Л. Пиетрелли**, д.т.н., итальянское национальное агентство по новым технологиям, энергетике и устойчивому экономическому развитию, Рим, Италия  
**И. Ю. Пышминцев**, д.т.н., РосНИТИ, г. Челябинск  
**А. И. Рудской**, академик РАН, д.т.н., профессор, СПбПУ Петра Великого, г. Санкт-Петербург  
**Б. А. Сивак**, к.т.н., профессор, АО АХК «ВНИИМТМАШ», г. Москва  
**Л. М. Симонян**, д.т.н., профессор, НИТУ МИСИС, г. Москва  
**Л. А. Смирнов**, академик РАН, д.т.н., профессор, ОАО «Уральский институт металлов», г. Екатеринбург  
**С. В. Солодов**, к.т.н., НИТУ МИСИС, г. Москва  
**Н. А. Спирин**, д.т.н., профессор, УрФУ, г. Екатеринбург  
**Г. Танг**, Институт перспективных материалов университета Циньхуа, г. Шеньжень, Китай  
**М. В. Темлянецев**, д.т.н., профессор, СибГИУ, г. Новокузнецк  
**М. Р. Филонов**, д.т.н., профессор, НИТУ МИСИС, г. Москва  
**И. В. Чуманов**, д.т.н., профессор, ЮУрГУ, г. Челябинск  
**О. Ю. Шешуков**, д.т.н., профессор УрФУ, г. Екатеринбург  
**М. О. Шпайдель**, д.ест.н., профессор, Швейцарская академия материаловедения, Швейцария  
**А. Б. Юрьев**, д.т.н., профессор, ректор, СибГИУ, г. Новокузнецк  
**В. С. Юсупов**, д.т.н., профессор, ИМЕТ им. А.А. Байкова РАН, г. Москва

**Индексирование:** Scopus, Russian Science Citation Index (RSCI), Research Bible, Chemical Abstracts, OCLC и Google Scholar

Зарегистрирован Федеральной службой по надзору в сфере связи и массовых коммуникаций ПИ № ФС77-35456.



Статьи доступны под лицензией Creative Commons Attribution 4.0 License.

## HISTORY OF METALLURGY

- Tresvyatskii L.A., Protopopov E.V., Umanskii A.A., Khudoleev A.N. Kuznetsk armor: The first frontiers of victory ..... 112

## METALLURGICAL TECHNOLOGIES

- Yunusov A.M., Polevoi E.V., Yunin G.N., Oskolkova T.N. Experience in producing rails from bainitic steels 30KhG2S2AFM and 30KhG2SAFN ..... 122

## ECOLOGY AND RATIONAL USE OF NATURAL RESOURCES

- Ulyeva G.A., Tuyskhan K., Matsugina E.M., Volokitina I.E., Akhmetova G.E. Actual progress of production waste disposal problems ..... 129

## MATERIALS SCIENCE

- Zorya I.V., Poletaev G.M., Bebikhov Yu.V., Semenov A.S. Initiation of melting at tilt grain boundaries in austenite depending on the misorientation angle ..... 137
- Ishmametov D.A., Pomel'nikova A.S., Petelin A.L. On the influence of rare-earth oxide additives on kinetics of borated layer formation and boron diffusion along grain boundaries during steel boriding ..... 146

## PHYSICO-CHEMICAL BASICS OF METALLURGICAL PROCESSES

- Bol'shov L.A., Korneichuk S.K., Bol'shova E.L. Thermodynamic second-order interaction coefficients of nitrogen with nickel and chromium in liquid steel ..... 156
- Dmitriev A.N., Burova Yu.E., Vit'kina G.Yu., Barbin N.M., Terent'ev D.I. Thermodynamic modelling of reduction of iron ore materials by hydrogen-containing gases ..... 161
- Smirnov K.I., Gamov P.A., Roshchin V.E., Samolin V.S. Thermodynamic analysis of conditions for iron and titanium separation in ilmenite concentrate by selective reduction of elements ..... 169
- Sheshukov O.Yu., Mikheenkova M.A., Egiazar'yan D.K., Mikheenkova A.M., Kleonovskii M.V., Matyukhin O.V. Peculiarities of the phase composition formation of steelmaking slags and evaluation of the possibility of obtaining mineral binders with low CO<sub>2</sub> generation on their basis ..... 177

## ИСТОРИЯ ОТРАСЛИ

- Тресвятский Л.А., Протопопов Е.В., Уманский А.А., Худолеев А.Н. Кузнецкая броня: первые рубежи победы ..... 112

## МЕТАЛЛУРГИЧЕСКИЕ ТЕХНОЛОГИИ

- Юнусов А.М., Полевой Е.В., Юнин Г.Н., Осколкова Т.Н. Опыт производства рельсов из бейнитной стали марок 30ХГ2С2АФМ и 30ХГ2САФН ..... 122

## ЭКОЛОГИЯ И РАЦИОНАЛЬНОЕ ПРИРОДОПОЛЬЗОВАНИЕ

- Ульева Г.А., Туысхан К., Мацугина Е.М., Волокитина И.Е., Ахметова Г.Е. Современное состояние проблемы утилизации отходов производства ..... 129

## МАТЕРИАЛОВЕДЕНИЕ

- Зоря И.В., Полетаев Г.М., Бибихов Ю.В., Семенов А.С. Инициация плавления на границах зерен наклона в аустените в зависимости от угла разориентации ..... 137
- Ишмаматов Д.А., Помельникова А.С., Петелин А.Л. К вопросу о влиянии добавок оксидов редкоземельных элементов на кинетику образования борированных слоев и диффузию бора по границам зерен при борировании сталей ..... 146

## ФИЗИКО-ХИМИЧЕСКИЕ ОСНОВЫ МЕТАЛЛУРГИЧЕСКИХ ПРОЦЕССОВ

- Большов Л.А., Корнейчук С.К., Большова Э.Л. Термодинамические параметры взаимодействия второго порядка азота с никелем и хромом в жидкой стали... 156
- Дмитриев А.Н., Бурова Ю.Е., Г.Ю. Витькина Г.Ю., Барбин Н.М., Терентьев Д.И. Термодинамическое моделирование процесса восстановления железорудных материалов водородсодержащими газами .... 161
- Смирнов К.И., Гамов П.А., Рощин В.Е., Самолин В.С. Термодинамический анализ условий разделения железа и титана в ильменитовом концентрате селективным восстановлением элементов ..... 169
- Шешуков О.Ю., Михеенков М.А., Егизарьян Д.К., Михеенков А.М., Клеоновский М.В., Матюхин О.В. Особенности формирования фазового состава сталеплавильных шлаков и оценка возможности получения на их основе минеральных вяжущих веществ с низкой генерацией CO<sub>2</sub> ..... 177

**CONTENTS** *(Continuation)*

**СОДЕРЖАНИЕ** *(продолжение)*

**INFORMATION TECHNOLOGIES  
AND AUTOMATIC CONTROL  
IN FERROUS METALLURGY**

**ИНФОРМАЦИОННЫЕ ТЕХНОЛОГИИ  
И АВТОМАТИЗАЦИЯ  
В ЧЕРНОЙ МЕТАЛЛУРГИИ**

**Zimin A.V., Kornet M.E., Burkova I.V., Zimin V.V.**  
Using digital simulation models to optimize the operation of complex production facilities ..... 198

**Зимин А.В., Корнет М.Е., Буркова И.В., Зимин В.В.**  
Использование цифровых имитационных моделей для оптимизация сложных производственных объектов ..... 198

---



UDC 669:93

DOI 10.17073/0368-0797-2025-2-114-123



Original article

Оригинальная статья

To the 80<sup>th</sup> anniversary of the Great Victory

To the 95<sup>th</sup> anniversary of SibSIU – the first university in Kuzbass

## KUZNETSK ARMOR: THE FIRST FRONTIERS OF VICTORY

L. A. Tresvyatskii<sup>1</sup>, E. V. Protopopov<sup>1</sup>✉, A. A. Umanskii<sup>1</sup>,  
A. N. Khudoleev<sup>2</sup>

<sup>1</sup> Siberian State Industrial University (42 Kirova Str., Novokuznetsk, Kemerovo Region – Kuzbass 654007, Russian Federation)

<sup>2</sup> Kuzbass Humanitarian and Pedagogical Institute Kemerovo State University (23 Tsiolkovskogo Str., Novokuznetsk, Kemerovo Region – Kuzbass 654007, Russian Federation)

✉ protopopov@sibsiu.ru

**Abstract.** The article discusses issues related to the accelerated transition of the Kuznetsk Metallurgical Plant (KMK) to production of armored steel in the conditions of the Great Patriotic War. The prerequisites and conditions for the transition from the production of exclusively peaceful products to the mass production of armored metal were determined. The authors clarified the stages of mastering new production technologies, the contribution of individual departments and production scientists, scientists from the Siberian Metallurgical Institute (SMI) to production of steel for victory. The emergence of Kuznetsk armor is viewed through the prism of contribution of the whole country and people to the common cause of the fight against fascism.

**Keywords:** ferrous metallurgy, armored steel, defense products, Kuznetsk Metallurgical Plant, the Great Patriotic War

**For citation:** Tresvyatskii L.A., Protopopov E.V., Umanskii A.A., Khudoleev A.N. Kuznetsk armor: The first frontiers of victory. *Izvestiya. Ferrous Metallurgy*. 2025;68(2):114–123. <https://doi.org/10.17073/0368-0797-2025-2-114-123>

## КУЗНЕЦКАЯ БРОНЯ: ПЕРВЫЕ РУБЕЖИ ПОБЕДЫ

Л. А. Тресвятский<sup>1</sup>, Е. В. Протопопов<sup>1</sup>✉, А. А. Уманский<sup>1</sup>,  
А. Н. Худолеев<sup>2</sup>

<sup>1</sup> Сибирский государственный индустриальный университет (Россия, 654007, Кемеровская обл. – Кузбасс, Новокузнецк, ул. Кирова, 42)

<sup>2</sup> Кузбасский гуманитарно-педагогический институт Кемеровского государственного университета (Россия, 654007, Кемеровская область – Кузбасс, Новокузнецк, ул. Циолковского, 23)

✉ protopopov@sibsiu.ru

**Аннотация.** В статье рассмотрены вопросы, связанные с ускоренным переходом «Кузнецкого металлургического комбината» (КМК) к производству броневой стали в условиях Великой Отечественной войны. Определены предпосылки и условия перехода от выпуска исключительно мирной продукции к массовому производству броневых металлов. Описаны этапы освоения новых технологий производства, вклада отдельных подразделений и ученых-производственников, ученых Сибирского металлургического института (СМИ) в производство металла Победы. Появление кузнецкой брони рассматривается через призму вклада всей страны, народа в общее дело борьбы с фашизмом.

**Ключевые слова:** черная металлургия, броневая сталь, оборонная продукция, Кузнецкий металлургический комбинат, Великая Отечественная война

**Для цитирования:** Тресвятский Л.А., Протопопов Е.В., Уманский А.А., Худолеев А.Н. Кузнецкая броня: первые рубежи победы. *Известия вузов. Черная металлургия*. 2025;68(2):114–123. <https://doi.org/10.17073/0368-0797-2025-2-114-123>

## INTRODUCTION

From the very beginning of the Great Patriotic War, the country's metallurgical industry was tasked with a strategic objective: to ensure the rapid launch of armored steel production. The development and transition to mass production of armored steel in 1941 at the Kuznetsk Metallurgical Plant (KMK) in the city of Stalinsk (now Novokuznetsk) was of great significance for strengthening the country's defense capability during the difficult initial defensive stage of the war. played a crucial role in strengthening the nation's defense capabilities during the initial and most challenging phase of the war. Due to the urgency and complexity of mastering new technologies and restructuring the plant's infrastructure, many specific features and nuances of this transformation were not thoroughly documented and were subsequently lost to historical memory. Soviet-era scholarly literature addressed certain aspects of this transition but often reflected ideological, institutional, or other biases. In the post-Soviet period, this topic received limited attention; available accounts either reproduced established narratives or remained superficial.

As the 80<sup>th</sup> anniversary of Victory in the Great Patriotic War approaches, the need to reassess and recognize KMK's contribution to the labor feat of the Soviet people becomes increasingly evident. The time has come to address several historical blind spots.

## STUDYING THE ISSUE

The 1930s in the USSR were marked by a major shift in national policy. The Soviet leadership identified fascist Germany and militarist Japan as the primary threats to peace and security. In response, a course was set

to strengthen the country's defense-industrial base. As part of the accelerated industrialization program, dozens of large industrial enterprises were established to provide the economic foundation for the anticipated confrontation with potential aggressors. Leadership of the newly emerging Soviet industry was centralized in the People's Commissariat of Heavy Industry, headed by G.K. Ordzhonikidze. At the Kuznetsk Metallurgical Plant, among the metallurgists of Stalinsk, the People's Commissar of Heavy Industry enjoyed exceptional respect. This was evidenced by the fact that, in 1933, the Siberian Metallurgical Institute (SMI) was named after Sergo Ordzhonikidze (then known as SICHM – Siberian Institute of Ferrous Metals), at the initiative of local workers.

Despite the significant achievements in the development of ferrous metallurgy during the prewar decade, they remained insufficient: the rapidly expanding domestic industry demanded ever-growing volumes of metal. While ferrous metals were mainly used for the production of civilian goods, defense manufacturing was concentrated at designated enterprises. The pace of industrial growth necessitated the creation of specialized commissariats. From 1939 onward, KMK fell under the jurisdiction of the People's Commissariat of Ferrous Metallurgy of the USSR. This commissariat was responsible for producing civilian products but was also tasked with switching to defense production in the event of war.

Between April 1932 and January 1941, KMK experienced rapid development – from the launch of its first blast furnace to the commissioning of the fifteenth 300-ton open-hearth furnace. The rate of equipment commissioning was remarkable:

- 1932: Blast furnaces No. 1 and 2, open-hearth furnaces No. 1, 2, and 3, and the blooming mill were commissioned;



Legendary T-34 tank (active, taking part in the Victory Day celebrations) at the plant administration square

Легендарный танк Т-34 (действующий, принимает участие на праздновании Дня победы) на площади заводоуправления

- 1933: Open-hearth furnaces No. 4, 5, 6, and 7;
- 1934: Blast furnaces No. 3 and 4, and open-hearth furnaces No. 6, 8, and 9;
- 1935: Open-hearth furnaces No. 11 and 12, and a sheet-rolling mill;
- 1936: Open-hearth furnace No. 13 and rolling mill “500”;
- 1937: Rolling mill “900”;
- 1940: Open-hearth furnace No. 14;
- 1941: Open-hearth furnace No. 15.

The final two open-hearth furnaces were designed for 300-ton charges. The plant had to overcome the challenges of a “growth crisis” in steel production – problems that were, to a large extent, successfully resolved. By mid-1941, the KMK had achieved stable operation and was consistently exceeding production targets across the full metallurgical cycle.

In 1941, KMK began considering the possibility of transitioning to defense production. This is confirmed by the fact that on the very day of the fascist Germany’s attack, the plant’s engineering and technical personnel convened to discuss the organization of defense production [1].

Under the conditions of the Great Patriotic War, the entire industry – particularly ferrous metallurgy – had

to respond swiftly to wartime demands. This required not only increasing output volumes but also a radical restructuring of production. There was an urgent need to boost the output of high-alloy steels required for armored vehicles and other military applications. It is important to note that, at the time, most alloyed steel production was concentrated in the southern and central regions of the country – territories that were soon either occupied or under serious threat due to the enemy’s rapid advance. This created enormous challenges for the metallurgical industry, as many of its leading enterprises were either destroyed or severely damaged by air raids.

In the year preceding the war, alloy steel accounted for only 2.2 % of KMK’s total rolled metal output. However, beginning on June 22, the range of steel grades produced at the plant began to shift [2]. KMK reached its maximum pig iron output, and both open-hearth and rolling mill crews met their performance targets. Already in July 1941, open-hearth furnace No. 11 delivered its first batch of armored steel. rapid and effective transition of the national economy to a wartime footing was made possible by the mobilization-based economic model established during the first Five-Year Plans. This system demanded results from all levels of the production chain – from government officials and plant managers to engineers and workers. The socioeconomic and political structures shaped during the 1930s laid the foundation



From an open-hearth furnace

Из мартеновской печи

for Soviet society and gave rise to a new type of Soviet engineer-specialist: a skilled technician who was also a member of the working class.

On June 22, 1941, KMK director R.V. Belan was in Moscow. He had been on vacation and was planning a trip to Sochi. Upon learning of Germany's invasion of the USSR, he immediately traveled that same Sunday to meet with the People's Commissar of Ferrous Metallurgy, I.F. Tevosyan. At that point, it appears that the issue of organizing defense steel production at KMK had not yet been discussed with the plant's leadership.

The following day, reports of the rapid advance of German forces into Soviet territory prompted the Commissar to make a strategic decision: to involve the industrial capacities of the eastern regions – the Urals and Siberia – in defense production. Upon reviewing KMK's operational capabilities, it became clear that the existing equipment was not suited for producing armored steel. The plant would either need new open-hearth furnaces or significant upgrades to the current ones. Equally pressing was the question of whether the plant could handle the rolling of armor plate. Late in the evening of June 23, Tevosyan called chief engineer L. Vaisberg in Stalinsk and posed a key question: *did KMK have the technical capacity to roll armor plate?* Vaisberg requested a few hours to provide a definitive answer and, that same night, urgently organized a rolling test [3].

Chief engineer L. Vaisberg, blooming mill head V.D. Smirnov, along with the senior operator and roller, carried out a trial run: the ingots were first passed through the blooming mill and then through the sheet-rolling mill. Within a few hours, the team successfully rolled a steel ingot into a maximum-width plate. The test revealed that rolling armored steel – due to its greater mass and increased strength – would require technical modifications to the equipment. Specifically, it was necessary to reinforce the lifting tables for heavier blooms, implement autogenous cutting, and introduce other improvements. With this knowledge, a definitive answer was ready. Five hours after the last call from Moscow, Vaisberg contacted the People's Commissariat of Ferrous Metallurgy with the positive result. At that moment, Tevosyan attending a meeting with the head of state and the Defense Committee, I.V. Stalin. In his absence, Deputy commissar P.I. Korobov received the update and *was satisfied with the result.*

As a consequence, the People's Commissariat of Ferrous Metallurgy issued an order for KMK to begin producing armored steel for tanks. At that time, however, KMK had neither the necessary technology nor the proper equipment. Previously, armored steel had only been produced at specialized defense facilities using small-capacity open-hearth furnaces with acid linings. The large open-hearth furnaces at KMK were not technically suitable for smelting alloyed steel grades, and the roll-

ing mills lacked the capacity for processing armor plate. Commissariat decided to transfer heat treatment furnaces from the Izhora Plant to Stalinsk, and a dedicated workshop section had to be built to house them.

The People's Commissar of Ferrous Metallurgy instructed the implementation of large-scale changes to the steel production process, particularly involving the open-hearth furnaces. The top priority was to reconstruct and convert the furnaces to basic linings, which would improve both the quality and mechanical properties of the steel. This required major technological revisions, including reducing the volume of the metal charge. A fundamentally new smelting technology for armored steel had been developed at the Izhora Plant in June 1941, but there was no time for extensive testing. Complicating matters further, both the relevant classified documents and experienced personnel had already been redirected to the Magnitogorsk Metallurgical Plant. On June 26, 1941, an official order was issued instructing KMK to begin producing tank armor by August 1 of that year [4]. This urgent decision was a direct response to the intensifying war and the critical need to increase production of high-quality armored metal for tank manufacturing.

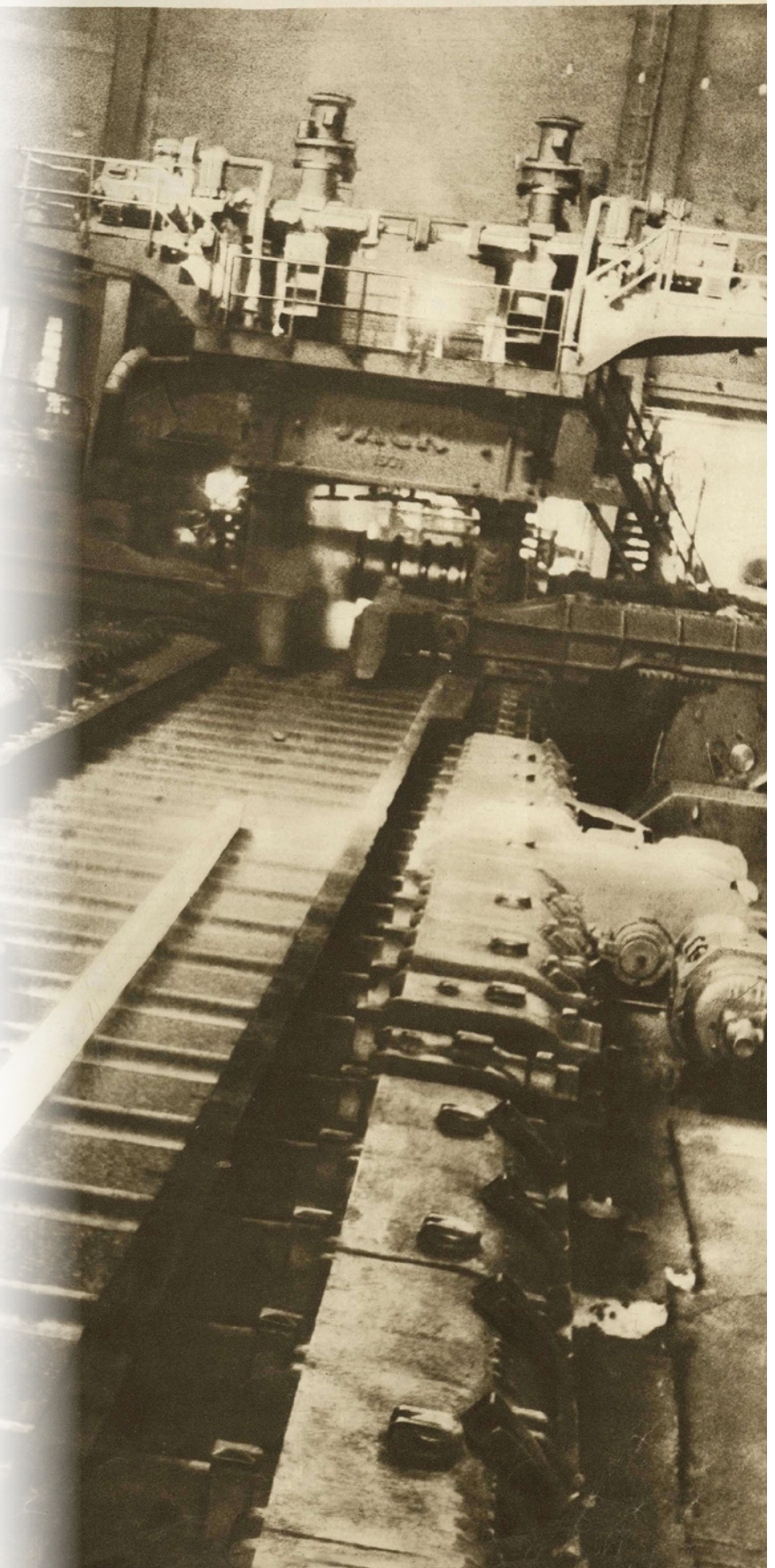
In June 1941, a group of engineers from the Izhora Plant – including M.N. Popov, A.F. Yakimovich, D.Ya. Badyagin, I.A. Frumkin, P.A. Romanov, and Ya.I. Mashchuk – collaborated with specialists from the Central Research Institute of Structural Materials (TsNII-48, the “Armor Institute”), such as A.S. Zav'yalov, S.I. Sakhin, E.E. Levin, and A.Ya. Vergazov, to develop a new technology for smelting armored steel in basic-lined open-hearth furnaces. As previously mentioned, armored steel had traditionally been produced in acid-lined furnaces at specialized defense facilities. The new process was first tested at the Izhora Plant on Furnace No. 8 – the largest of its kind there – which allowed engineers to replicate, to some extent, the operating conditions of the high-capacity furnaces used at KMK. This innovative technology was formalized into a set of technical guidelines just as enemy forces approached the outskirts of Leningrad [5]. Due to its novelty and complexity, the technology could not be adopted immediately on a wide scale. However, as the blockade of Leningrad tightened, a crucial decision was made. On September 8, 1941, with the city under full siege, engineer I.A. Frumkin transported the technical documentation out of Leningrad via a special air mission. The availability of these instructions, developed at the Izhora Plant, enabled Soviet ferrous metallurgy facilities to promptly initiate large-scale production of tank armor in the early stages of the Great Patriotic War.

A special “armor bureau” was established, composed not only of metallurgical scientists from TsNII-48 but also of KMK plant personnel. This bureau developed a fundamentally new technology for smelting armored

steel in large-capacity open-hearth furnaces with basic lining. On July 23, 1941, the first heat of armored steel using this new method was successfully carried out at the Magnitogorsk Metallurgical Plant. As a result, between September 1941 and January 1942, the output of armored steel increased almost one hundredfold. Following Magnitogorsk, the production of alloyed and armored steels using similar technologies – adapted with the support of TsNII-48 experts – was launched at both the Nizhny Tagil Metallurgical Plant and KMK [6].

On June 27, 1941, open-hearth furnace No. 11 in KMK's second open-hearth shop was shut down for scheduled repairs. The design department promptly finalized and submitted the full technical documentation for the furnace's reconstruction and modernization. Repair crews – comprising refractory specialists, boilermakers, and assemblers – worked around the clock to meet the urgent deadlines. First, the outdated equipment was dismantled; then the installation of new components began. These upgrades were intended to boost the furnace's efficiency and enhance its production performance. The entire plant was gripped by a sense of shared responsibility, as every worker understood the strategic importance of their efforts. On July 4, the furnace was fired up again. Its successful adaptation to the new smelting technology was essential for maintaining the operational capacity of the entire shop. This achievement became not only a technical milestone but also a symbol of hope – marking a decisive step toward large-scale production of armored steel and, ultimately, toward victory.

Simultaneously with the furnace reconstruction, work was underway to establish a heat treatment section within the sheet-rolling mill. On the eve of the Great Patriotic War had no furnaces for the heat treatment of rolled metal – creating a major obstacle to fulfilling its new production tasks, particularly in light of the decision to launch armor plate production. Recognizing the strategic significance of the project, the People's Commissariat of Ferrous Metallurgy ordered the dismantling of six heat treatment furnaces at the Izhora Plant in Kolpino,



Rolling mill. KMK. 1930s

Прокатный стан. КМК. 1930-е годы

near Leningrad. These furnaces were to be shipped over 3,000 kilometers to KMK. On the same day the order was received, dismantling began at the Izhora Plant, while construction work commenced simultaneously at KMK. The deadlines set by the Commissariat were extremely strict: the heat treatment furnaces were to be fully operational by September 1, 1941. It was decided to install them in the fourth span of the blanking shop, which was still under construction – requiring additional effort from builders and designers. Foundations for the first two furnace blocks were laid in the completed portion of the span, while the rest of the space had to be expanded – necessitating design changes and a significantly faster pace of construction.

On July 3, 1941, KMK director R.M. Belan and N.G. Kratenko, head of the Stalinskpromstroï trust, signed an order establishing a strict project schedule. It defined the deadlines for issuing design documentation, which were subject to tight oversight. The final set of construction drawings had to be delivered to the site no later than 8:00 p.m. on July 7. The urgency of the task created a highly charged atmosphere at the construction site. Chief Mechanic I.S. Lyulenkov committed to delivering all required equipment by 10:00 a.m. on July 16. To support uninterrupted work, temporary lighting had to be installed at the site by 10:00 p.m. on the day the order was issued, and the power supply was to be connected by 8:00 p.m. on July 4.

Work continued around the clock. Both workers and engineers invested enormous effort and displayed remarkable enthusiasm throughout the construction process. Among those involved were renowned assemblers from Kuznetskstroï: V.E. Kashkarov, I.A. Dubovik, M.M. Kalyuzhnyi, S.V. Yudakov, N.I. Osipov, and G.I. Podoroga. Their professionalism and experience played a crucial role in the project's successful execution. Engineers G.F. Rybochkin and S.Ya. Selyukov also deserve recognition for their technical supervision and quality control during the entire construction phase.

Furnace masonry foreman I.A. Klenov, actively coordinated work crews and closely monitored adherence to the construction timeline. Daily on-site meetings were held to review progress, address emerging issues, and propose practical solutions. The workers clearly understood the importance of their task: the successful completion of the heat treatment section would not only enable the plant to meet its production targets but also make a vital contribution to the country's defense capabilities. With each passing day, the construction pace accelerated. Despite growing fatigue, the construction teams maintained high morale and unwavering commitment.

In the third ten-day period of July, smelting operations resumed in open-hearth furnace No. 11. Initially, standard heats of the plant's existing steel grades were produced.

Soon thereafter, armored steel was added to the production schedule [7]. Smelting armored steel in an acid-lined open-hearth furnace requires a specific approach. One of the key conditions was the use of exceptionally clean charge materials with reduced phosphorus and sulfur content. Unfortunately, the pig iron produced at KMK contained elevated levels of these impurities, rendering it unsuitable for smelting in acid-lined furnaces. To address this, the duplex process – a two-stage smelting method – was employed. In the first stage, a semi-finished melt was produced in a basic-lined furnace and refined to remove sulfur and phosphorus. This was followed by a transfer of the molten metal into an acid-lined furnace for final refining. However, the process necessitated a reduction in charge volume in the main 185-ton furnace, which led to decreased production capacity and significantly increased the workload on plant personnel.

Highly qualified foremen A.N. Tomilin, A.A. Akridin, and V.A. Matyushkin were assigned to open-hearth furnace No. 11, while steelmakers D.V. Merzlyakov, F.A. Ryabov, and D.P. Sinenko were appointed to conduct the melting operations. As noted in the records, “the primary role in the technical oversight and organization of armored steel production belonged to chief engineer L.E. Vaisberg” [8]. At the time, KMK steelmakers had no previous experience working with acid-lined open-hearth furnaces. During the initial heats, they received expert guidance from specialists dispatched from the Izhora Plant. This knowledge transfer played a critical role in preparing and adapting the local workforce to the new process requirements. The learning curve proved to be relatively short. The first heats were carried out by A.N. Tomilin, in collaboration with G.V. Gurskii, head of Open-Hearth Shop No. 2, a widely respected expert in the field. Gurskii, known for his technical competence and strong theoretical foundation, took a creative and systematic approach to solving emerging process challenges. His experience, combined with the determination of shift foreman A.N. Tomilin, led to rapid progress. By the third ten-day period of July, the first successful heats of armored steel had been completed – a major achievement for the plant.

The process of mastering armor plate production presented a serious challenge for KMK's rolling mill operators. On June 26, 1941, the plant issued an internal order outlining the urgent measures required to prepare the blooming mill and the sheet-rolling mill – both of which would be adapted for armor plate production – for their new roles. This involved modifying the equipment to meet the technical demands of rolling heavy, high-strength steel, and called for intense effort across the plant's workforce. By the time the first heats of armored steel were ready, a team of specialists had already begun developing new roll pass designs for the breakdown stand – an essential step toward launching full-scale production. Under the leadership of chief

electrician V.G. Prokoshin, chief mechanic I.S. Lyulenkov, and plate mill head S.I. Pavlovskii, a modernization plan was prepared within just one month. The plan called for reinforcing several key mechanical and electrical components of the rolling equipment. Its implementation demanded not only deep technical expertise but also close coordination between departments.

In parallel, the plant's technical department, working with alongside specialists from the Central Research Institute of Structural Materials (TsNII-48), who had arrived to assist with the transition, began developing technical guidelines for armor plate rolling. A key advantage at this stage was the prior experience accumulated at the Izhora Plant, which served as a practical foundation for creating process standards [9].

Close collaboration with faculty members from the Siberian Metallurgical Institute (SMI) also made it possible to incorporate advanced approaches and modern methods in organizing the production of this new type of defense product – armor plate – significantly improving the prospects for success [10]. Major contributions to the development of armor steel production technology were made by professor Yu.V. Grdina and Associate Professors I.S. Nazarov and E.Ya. Zarvin. SMI researchers and instructors – N.N. Shubina, D.L. Polyakova, and A.A. Govorov – worked almost continuously under real production conditions to optimize the parameters of the heat treatment process for armor plate. Associate professors E.Kh. Shamovskii and N.I. Kunitsyn designed a highly efficient gas torch specifically for cutting thick slabs of armor steel.

Finally, the long-anticipated moment arrived: the first ingot of armored steel was placed onto the blooming mill's roller table. This ingot differed significantly from standard ones – both in mass and dimensions – creating additional challenges during rolling. It required 25 to 28 passes to achieve the desired reduction, and by the end of the process, the slab had cooled significantly, complicating further handling. It was no longer possible to cut the slab with standard shears, so a crane was used to transfer it to the plate rolling mill's storage area, where it was cut with an oxy-fuel torch. Unfortunately, the heating and rolling temperature modes developed at the Izhora Plant proved incompatible with KMK's equipment. As a result, the steel from this first heat exhibited surface defects that required immediate correction. The mill scale had to be removed manually using pneumatic chisels – a time-consuming and labor-intensive process. Surface defects were smoothed using handheld electric grinders, which also demanded significant time and physical effort. In this way, the introduction of armor plate production became a true test for the entire KMK workforce. Ultimately, the transition to this new production line not only expanded the workers' knowledge and skills, but also marked a turning point in the broader evolution of Soviet

steelmaking. The successful implementation of new processing methods for armored steel paved the way for continued innovation and industrial advancement.

Thanks to the extraordinary efforts of the workforce and the full mobilization of available resources, KMK surpassed the government's August production target for armored steel – achieving an impressive 190 % of the planned volume. This accomplishment marked the plant's first major wartime success and became a source of pride and inspiration not only for KMK employees but for the entire city of Stalinsk. The achievements of the Kuznetsk steelmakers were of national significance – especially considering that, by autumn 1941, over 48 % of rolling mills across the Soviet Union had been rendered inoperable due to bombing and destruction. Despite material shortages and mounting fatigue, KMK's metallurgists continued to optimize production processes and increase output to meet the urgent needs of the war effort.

On August 16, 1941, the Central Committee of the All-Union Communist Party (Bolsheviks) and the Council of People's Commissars of the USSR approved a military-economic plan for industry covering the fourth quarter of 1941 and the entirety of 1942 [11]. The plan aimed to mobilize key industrial regions – such as the Volga region, the Urals, Western Siberia, Kazakhstan, and Central Asia – for defense production. One of its top priorities was to expand the output of specialty metals critical to the war effort, particularly in response to the growing intensity of military operations. At that point, the nationwide demand for high-quality armored steel had reached an unprecedented level. However, the available technologies could not ensure the required production volumes. The widespread use of the duplex process – based on melting in separate furnaces – remained common at many facilities, but it entailed significant production losses and became increasingly inefficient under the pressure of wartime requirements. As a result of the reconstruction of open-hearth furnace No. 11, the average heat mass had to be reduced by about 65 tons – a critical limitation during wartime. Furthermore, the charge for this furnace was prepared separately in a unit with a basic hearth, which further compromised both the quality and quantity of the steel produced. Daily losses from operating a single acid-lined furnace reached approximately 450 – 460 tons of metal – an unacceptable figure, particularly under government pressure to meet armored steel production targets. Meeting those targets would have required converting several more furnaces to acid lining, which would have drastically lowered the plant's overall steelmaking capacity – an undesirable outcome in wartime. This situation created an urgent need to optimize production processes and reduce losses wherever possible.

One of the key solutions was to use the plant's high-capacity 185-ton open-hearth furnaces with basic lining for the production of armored steel. This strategy offered

the potential to significantly increase output while minimizing material losses. In addition to increasing the mass of each heat, there was also a strong focus on improving product quality. Another critical goal was the introduction of a fundamentally new rolling technology that could enhance both productivity and the quality of finished armor plate. As a result, the steelmaking and rolling shops became the central fronts in the broader industrial campaign to supply urgently needed armored steel for tanks and military vehicles.

At KMK, alongside the conventional production of armored steel in acid-lined furnaces, experimental trials were launched to develop new melting techniques using basic-lined open-hearth furnaces. Unlike acid linings, basic linings provided more stable smelting conditions and enabled more effective removal of harmful impurities, resulting in higher-quality steel. A key element of this transition was the study of prior developments at the Izhora Plant, where metallurgists had already achieved success in this area. Their experience had been adopted at the Magnitogorsk Metallurgical Plant and served to significantly accelerate KMK's shift toward large-scale production of alloyed steels.

The first experimental heats of armored steel in the newly retrofitted furnace were entrusted to master steelmaker P.D. Nikitin, an experienced specialist in new steel grades. However, the task before him was excep-

tionally demanding. Producing armored steel required not only technical knowledge and skill but also effective desulfurization and dephosphorization pig iron. It was necessary to completely drain the slag and form a new slag layer during the melting process, which complicated operations and extended the overall smelting time. By September 1941, both of KMK's open-hearth shops had begun mass production of armored steel using 185-ton basic-lined furnaces. This milestone was made possible by successful trials and the operational experience accumulated in previous months. By that time, newly developed technologies had significantly improved both the quality and output of the steel.

The Office of the Chief Steelmaker became the center for developing and implementing these new technologies and making critical production decisions. The team shared a deep sense of urgency and responsibility. Engineers and workers not only handled everyday challenges but also actively sought ways to optimize technological processes. Thanks to their combined efforts, KMK achieved major advances in armored steel production. Under wartime conditions, these results were nothing short of heroic – attained through unity and the growing expertise of the workforce.

Beginning in October 1941, KMK achieved a major breakthrough in both armored steel and plate production, marking a significant milestone in the plant's war-



Conquering metal

Покорение металла

time history. In the third quarter, the plant fulfilled 112 % of its armor plate production plan – a testament to organizational effectiveness and operational discipline. In the fourth quarter, despite a nearly fivefold increase in targets, the plant exceeded the plan by reaching 125 % [7].

As production volumes increased, rolling mill specialists actively explored new ways to enhance process efficiency. Leading engineers played a central role in developing and implementing improved rolling technologies. Chief engineer L.E. Vaisberg, whose technical knowledge and experience were widely recognized, became a driving force behind these efforts. Significant contributions were also made by plate mill head S.I. Pavlovskii and blooming mill head V.D. Smirnov, both of whom played key roles in streamlining operations and achieving high-performance outcomes. Senior foreman of the plate rolling shop M.I. Korchemnyi, deputy head of the Technical Department G.V. Sharov, blooming mill operators P.A. Zavarykin and M.I. Merkulov, and plate mill rollers P.A. Novokreshchin and I.P. Maksimov II demonstrated exceptional dedication – an essential factor in the plant's overall success. Within a remarkably short time, a fundamentally new armor plate rolling technology was developed. It featured advanced processing techniques and improved quality control measures. Specialists identified optimal heat treatment temperature regimes, significantly improving the strength and durability of the final product. As a result of these innovations, productivity at both the blooming and plate rolling mills increased severalfold, while surface defects were reduced to a minimum.

## CONCLUSIONS

The Kuznetsk Metallurgical Plant (КМК) played a critical role in supplying armored steel to the Soviet Union during the Great Patriotic War. The scale of the challenges faced by КМК was unprecedented. It was not simply a matter of increasing output – it required a complete restructuring of production to manufacture high-quality armored steel that met the extreme demands of wartime. This effort entailed solving a wide range of technical and organizational problems, many of which had previously seemed insurmountable. The launch of armored steel production at КМК in the second half of 1941 represented a major industrial breakthrough and demanded extraordinary dedication from the residents of Stalinsk. Workers often remained at the plant around the clock, fully committed to the production effort. The rapid technical re-equipment of the plant posed a particular challenge. New production technologies for armored steel had to be developed and implemented within an extremely short timeframe, including improvements under severe time constraints. This included improvements in the mechanical properties of the steel – such as hardness and strength – as well as new processes for smelting, rolling, and heat

treating armor plate. The successful transition to mass production of armored steel at КМК in Stalinsk (now Novokuznetsk) in 1941 became a strategically important contribution to the defense capabilities of the country during the critical initial phase of the war.

## REFERENCES / СПИСОК ЛИТЕРАТУРЫ

1. Berlin A.B. Novokuznetsk in a Soldier's Overcoat: In the Year of the 50<sup>th</sup> Anniversary of the Great Victory, Dedicated to the Younger Generation of Novokuznetsk Residents. Novokuznetsk: Kuznetsk Fortress: Writers' Union; 1995:297. (In Russ.).  
Берлин А.Б. Новокузнецк в солдатской шинели: В год 50-летия Великой Победы – молодому поколению новокузнецчан посвящается. Новокузнецк: Кузнецкая крепость: Союз писателей; 1995:297.
2. Dokuchaev G.A. The Siberian rear in the Great Patriotic War. Novosibirsk: Nauka, Siberian Branch; 1968:322. (In Russ.).  
Докучаев Г.А. Сибирский тыл в Великой Отечественной войне. Новосибирск: Наука, Сибирское отделение; 1968:322.
3. Weisberg L. Not a minute to rock. In: *The Steel Heart of Siberia*. Titova A.M. ed. Kemerovo: Kemerovskoe knizhnoe izdatel'stvo; 1982:121–125. (In Russ.).  
Вайсберг Л. Ни минуты на раскачку. В кн.: *Стальное сердце Сибири* / Сост. М.Ф. Беркович, Н.М. Шидловский; ред. А.М. Титова; предисл. А. Кузнецова. Кемерово: Кемеровское книжное издательство; 1982:121–125.
4. Belan R. Contribution of Kuznetsk residents to the victory. In: *The Steel Heart of Siberia*. Titova A.M. ed. Kemerovo: Kemerovskoe knizhnoe izdatel'stvo; 1982:125–129. (In Russ.).  
Белан Р. Вклад кузнецчан в победу. В кн.: *Стальное сердце Сибири* / Сост. М.Ф. Беркович, Н.М. Шидловский; ред. А.М. Титова; предисл. А. Кузнецова. Кемерово: Кемеровское книжное издательство; 1982:125–129.
5. Frumkin-Rybakov Yu. The history of the creation of new armored steel grades at the Izhora plant in 1936 – 1941. Report to the plenary session “Development of Science and Technology in the USSR in the pre-war years”, section 14, at the XXXVI Int. Conf. of the St. Petersburg Branch of the Russian National Committee for the History and Philosophy of Science and Technology of the Russian Academy of Sciences. [Electronic resource]. Available at URL: <https://kolpino.ru/news/1/yulian-frumkin-rybakov-istoriya-sozdaniya-novykh-bronevykh-marok-stali-na-izhorskom-zavode-v-1936-1941-gg/>. (Accessed: 09.03.2025). (In Russ.).  
Фрумкин-Рыбаков Ю. История создания новых броневых марок стали на Ижорском заводе в 1936 – 1941 гг. Доклад к пленарному заседанию «Развитие науки и техники в СССР в предвоенные годы», секция 14, на XXXVI международной конференции СПб отделения Российского национального комитета по истории и философии науки и техники РАН. [Электронный ресурс]. URL: <https://kolpino.ru/news/1/yulian-frumkin-rybakov-istoriya-sozdaniya-novykh-bronevykh-marok-stali-na-izhorskom-zavode-v-1936-1941-gg/> (Дата обращения: 09.03.2025).

6. Serikbol A. The military and economic task of ferrous metallurgy during the Great Patriotic War. In: *Salute, Victory! Proceedings of the International Scientific and Practical Military Historical Conference, May 13, 2015, Yurga*. Tomsk: TPU; 2015:134–137. (In Russ.).  
Серикбол А. Военно-хозяйственная задача черной металлургии в годы Великой Отечественной войны. В кн.: *Салют, Победа! Сб. трудов Международной научно-практической военно-исторической конференции, 13 мая 2015 г., г. Юрга*. Томск: Изд-во ТПУ; 2015: 134–137.
7. Polyanskaya E.M., Susakin G.N., Shparog Yu.A., etc. History of the Kuznetsk Metallurgical Plant named after V.I. Lenin. Zherebin B.N. ed. Moscow: Metallurgiya; 1973:463. (In Russ.).  
История Кузнецкого металлургического комбината имени В.И. Ленина / Е.М. Полянская, Г.Н. Сусакин, Ю.А. Шпарог и др.; под общ. ред. Б.Н. Жеребина. Москва: Металлургия; 1973:463.
8. Zaparii V.I., Zaparii V.V., Sheshukov O.Yu. Going through old paper, or correcting an error after half a century. *Problemy cherno metallurgii i materialovedeniya*. 2024;(4):122–126. (In Russ.). [https://doi.org/10.52351/00260827\\_2024\\_4\\_122](https://doi.org/10.52351/00260827_2024_4_122)
- Запарий В.И., Запарий В.В., Шешуков О.Ю. Перебирая старые бумаги, или исправление ошибки через полвека. *Проблемы черной металлургии и материаловедения*. 2024;(4):122–126.  
[https://doi.org/10.52351/00260827\\_2024\\_4\\_122](https://doi.org/10.52351/00260827_2024_4_122)
9. Novokuznetsk is a City of Labor Valor. Lizogub P.P. ed. Novokuznetsk: Lotus Press; 2021:168. (In Russ.).  
Новокузнецк – город трудовой доблести / Составитель П.П. Лизогуб. Новокузнецк: Лотус-Пресс; 2021:168.
10. Gromov V. Metal and People [Electronic resource]. Available at URL: [https://www.sibsiu.ru/news/?ELEMENT\\_ID=13351](https://www.sibsiu.ru/news/?ELEMENT_ID=13351). (Accessed: 09.03.2025). (In Russ.).  
Громов В. Металл и люди [Электронный ресурс]. URL: [https://www.sibsiu.ru/news/?ELEMENT\\_ID=13351](https://www.sibsiu.ru/news/?ELEMENT_ID=13351). (Дата обращения: 09.03.2025).
11. Butakov P.V. The industrial policy of the USSR during the Great Patriotic War. *Problemnyi analiz i gosudarstvennoe upravlencheskoe proektirovanie: politologiya, ekonomika, pravo*. 2013;6(4):61–72. (In Russ.).  
Бутаков П.В. Промышленная политика СССР в годы Великой Отечественной войны. *Проблемный анализ и государственное управленческое проектирование: политология, экономика, право*. 2013;6(4):61–72.

## Information about the Authors

## Сведения об авторах

**Lev A. Tresvyatskii**, Dr. Sci. (Cultural), Assist. Prof., Prof. of the Chair of Pedagogical Education, Siberian State Industrial University  
**E-mail:** lev-35@mail.ru

**Evgenii V. Protopopov**, Dr. Sci. (Eng.), Prof. of the Chair of Ferrous Metallurgy and Chemical Technology, Siberian State Industrial University  
**ORCID:** 0000-0002-7554-2168  
**E-mail:** protopopov@sibsiu.ru

**Aleksandr A. Umanskiy**, Dr. Sci. (Eng.), Prof. of the Chair of Ferrous Metallurgy and Chemical Technology, Siberian State Industrial University  
**ORCID:** 0000-0003-4403-9006  
**E-mail:** umanskiy@bk.ru

**Aleksei N. Khudoleev**, Dr. Sci. (Historical), Assist. Prof., Prof. of the Chair of History and Social Sciences, Kuzbass Humanitarian and Pedagogical Institute of Kemerovo State University  
**E-mail:** khudoleev73@mail.ru

**Лев Алексеевич Тресвятский**, доктор культурологии, доцент, профессор кафедры педагогического образования, Сибирский государственный индустриальный университет  
**E-mail:** lev-35@mail.ru

**Евгений Валентинович Протопопов**, д.т.н., профессор кафедры металлургии черных металлов и химической технологии, Сибирский государственный индустриальный университет  
**ORCID:** 0000-0002-7554-2168  
**E-mail:** protopopov@sibsiu.ru

**Александр Александрович Уманский**, д.т.н., профессор кафедры металлургии черных металлов и химической технологии, Сибирский государственный индустриальный университет  
**ORCID:** 0000-0003-4403-9006  
**E-mail:** umanskiy@bk.ru

**Алексей Николаевич Худолеев**, д.ист.н., доцент, профессор кафедры истории и общественных наук, Кузбасский гуманитарно-педагогический институт Кемеровского государственного университета  
**E-mail:** khudoleev73@mail.ru

## Contribution of the Authors

## Вклад авторов

**L. A. Tresvyatskii** – analysis of historical materials, literary search, compilation of bibliographic list.  
**E. V. Protopopov** – literary analysis of the technology of armor metal smelting, editing the text.  
**A. A. Umanskiy** – literary analysis of the technology of rolling armor plate, editing the text.  
**A. N. Khudoleev** – literary search, compilation of a bibliographic list, drawing up a conclusion.

**Л. А. Тресвятский** – анализ исторических материалов, литературный поиск, составление библиографического списка.  
**Е. В. Протопопов** – анализ материалов по технологии выплавки броневго металла, редактирование текста.  
**А. А. Уманский** – анализ материала по технологии прокатки броневго листа, редактирование текста.  
**А. Н. Худолеев** – литературный поиск, составление библиографического списка, составление заключения.

Received 14.02.2025  
Revised 20.02.2025  
Accepted 20.02.2025

Поступила в редакцию 14.02.2025  
После доработки 20.02.2025  
Принята к публикации 20.02.2025



UDC 621.373.826:621.78+620.18

DOI 10.17073/0368-0797-2025-2-124-130



Original article

Оригинальная статья

## EXPERIENCE IN PRODUCING RAILS FROM BAINITIC STEELS 30KhG2S2AFM AND 30KhG2SAFN

A. M. Yunusov<sup>1</sup>, E.V. Polevoi<sup>1</sup>, G. N. Yunin<sup>1</sup>, T. N. Oskolkova<sup>2</sup> <sup>1</sup> JSC EVRAZ United West Siberian Metallurgical Plant (16 Kosmicheskoe Route, Novokuznetsk, Kemerovo Region – Kuzbass 654007, Russian Federation)<sup>2</sup> Siberian State Industrial University (42 Kirova Str., Novokuznetsk, Kemerovo Region – Kuzbass 654007, Russian Federation)

oskolkovatiana@yandex.ru

**Abstract.** The operational resistance of railway rails is mainly determined by the resistance to contact fatigue defects and wear resistance, and, in addition to the impact characteristics of rolling stock wheels, depends on the chemical composition, structure and mechanical properties of rail steel. Currently, the ways to improve the operational properties of traditional pearlitic rails by increasing the microstructure dispersion are almost exhausted. One of the solutions to increase the service life of rails may be the transition to their production from bainitic steels, characterized by higher mechanical properties, resistance to the formation of surface contact and fatigue defects and increased cold resistance. Operational tests conducted abroad in the early 2000s showed that rails made of bainitic steel do indeed have increased resistance to formation of contact fatigue defects compared to rails made of pearlitic steel, but they are subject to more intensive wear. It was concluded that the resistance of bainitic rails to head damage by surface contact and fatigue defects is a consequence of the removal of the damaged rolling surface layer as a result of wear. In 2004–2006, JSC EVRAZ United West Siberian Metallurgical Plant conducted research and produced an experimental batch of bainitic rails, which showed the promise of using such steel and the possibility of simultaneously providing increased wear resistance and low-temperature reliability. However, at that time, the plant did not have the full capabilities to ensure the high metallurgical quality of steel: the identified shortcomings are related to the insufficient purity of the metal for non-metallic inclusions. As part of the resumption of work on the development of bainitic rails, two experimental medium-carbon steels B1 and B2, differing in alloying schemes, were smelted, rolled onto rails of type P65 and cooled in calm air. The presented results of mechanical tests showed the positive effect of increased chromium and nickel alloying on mechanical properties and structure.

**Keywords:** rail rolling, bainitic steel, tempering, microstructure, impact strength, resistance to formation of contact fatigue defects, scanning electron microscopy

**For citation:** Yunusov A.M., Polevoi E.V., Yunin G.N., Oskolkova T.N. Experience in producing rails from bainitic steels 30KhG2S2AFM and 30KhG2SAFN. *Izvestiya. Ferrous Metallurgy*. 2025;68(2):124–130. <https://doi.org/10.17073/0368-0797-2025-2-124-130>

## ОПЫТ ПРОИЗВОДСТВА РЕЛЬСОВ ИЗ БЕЙНИТНОЙ СТАЛИ МАРОК 30ХГ2С2АФМ И 30ХГ2САФН

А. М. Юнусов<sup>1</sup>, Е. В. Полевой<sup>1</sup>, Г. Н. Юнин<sup>1</sup>, Т. Н. Осколкова<sup>2</sup> <sup>1</sup> АО «ЕВРАЗ Объединенный Западно-Сибирский металлургический комбинат» (Россия, 654043, Кемеровская обл. – Кузбасс, Новокузнецк, шоссе Космическое, 16)<sup>2</sup> Сибирский государственный индустриальный университет (Россия, 654007, Кемеровская обл. – Кузбасс, Новокузнецк, ул. Кирова, 42)

oskolkovatiana@yandex.ru

**Аннотация.** Эксплуатационная стойкость железнодорожных рельсов определяется в основном сопротивлением возникновению дефектов контактной усталости и износостойкостью, и зависит, помимо характеристик воздействия колес подвижного состава, от химического состава, структуры и механических свойств рельсовой стали. В настоящее время пути повышения эксплуатационных свойств традиционных перлитных рельсов за счет увеличения дисперсности микроструктуры практически исчерпаны. Одним из решений для повышения срока службы рельсов может стать переход на производство их из сталей бейнитного класса, отличающихся более высокими механическими свойствами, стойкостью к образованию поверхностных контактно-усталостных дефектов и повышенной хладостойкостью. Проведенные в начале 2000-х годов за рубежом эксплуатационные испытания показали, что рельсы из бейнитной стали действительно обладают повышенной по сравнению с рельсами из стали перлитного класса сопротивляемостью к зарождению контактно-усталостных дефектов, однако подвержены более интенсивному износу. Был сделан вывод, что стойкость бейнитных рельсов к повреждениям головки поверхностными контактно-усталостными дефектами является следствием удаления поврежденного слоя поверхности катания в резуль-

тате износа. В 2004 – 2006 гг. на АО «ЕВРАЗ Объединенный Западно-Сибирский металлургический комбинат» проведены исследования и выпуск опытной партии бейнитных рельсов, которые показали перспективность применения такой стали и возможность обеспечения одновременно повышенной износостойкости и низкотемпературной надежности. Однако в тот период комбинат не располагал в полной мере возможностями обеспечения высокого металлургического качества стали: выявленные недостатки связаны с недостаточной чистотой металла по неметаллическим включениям. В рамках возобновления работ по освоению рельсов бейнитного класса проведена выплавка, прокатка рельсов типа Р65 и охлаждение на спокойном воздухе двух опытных среднеуглеродистых сталей Б1 и Б2, отличающихся схемами легирования. Представленные результаты механических испытаний показали положительное влияние повышенного легирования хромом и никелем на механические свойства и структуру.

**Ключевые слова:** прокатка рельсов, бейнитная сталь, отпуск, микроструктура, ударная вязкость, стойкость к образованию контактно-усталостных дефектов, сканирующая электронная микроскопия

**Для цитирования:** Юнусов А.М., Полевой Е.В., Юнин Г.Н., Осколкова Т.Н. Опыт производства рельсов из бейнитной стали марок 30ХГ2С2АФМ и 30ХГ2САФН. *Известия вузов. Черная металлургия.* 2025;68(2):124–130.

<https://doi.org/10.17073/0368-0797-2025-2-124-130>

## INTRODUCTION

As is well known [1 – 3], the service life of railway rails is influenced by numerous technological and operational factors. Among the latter, the most critical – judging by the number of rails removed due to defects or severe damage – are the resistance of rail steel to contact fatigue defects and its wear resistance. These properties, in turn, depend largely on technological parameters such as chemical composition, microstructure, mechanical properties, the level of non-metallic inclusions, and the magnitude and distribution of residual stresses.

Traditionally [4], rail steels have a high carbon content (0.6 – 0.8 wt. %) and a pearlitic microstructure. Improvements in the wear resistance of pearlitic steels have been achieved by optimizing both chemical composition and heat treatment parameters, which allow for a reduction in the interlamellar spacing of cementite plates within pearlite colonies. This refinement enhances the strength, ductility, and hardness of the steel.

In modern pearlitic rail steels, the interlamellar spacing has reached its theoretical lower limit [5], estimated at 0.06 – 0.07  $\mu\text{m}$ . Therefore, further improvements in the performance of pearlitic rails appear to be nearly exhausted. A promising alternative is the production of rails from bainitic steels, which feature a finer microstructure and, as a result, offer superior mechanical properties and increased resistance to contact fatigue defect (CFD) formation.

In the late 1990s and early 2000s, with support from railways in Western Europe and the United States, several experimental bainitic steel grades suitable for manufacturing heat-treated rails were developed by metallurgical institutes and industrial enterprises [6 – 10].

Initial field trials of hot-rolled rails made from B360 bainitic steel, conducted near Frick Station in Switzerland in 1999, confirmed that this material offers significantly improved resistance to the initiation and growth of contact fatigue defects [8].

However, some bainitic rail grades have shown more intensive wear compared to the widely used heat-

treated pearlitic rails. According to studies conducted by the Materials and Processing Research Center (NKK Corporation, Japan), the wear resistance of pearlitic steels is primarily determined by their hardness and microstructural characteristics. It has been concluded in [10; 11] that the high resistance of bainitic rails to contact fatigue damage is due to the gradual removal of the surface layer affected by rolling contact – a phenomenon referred to as the so-called “magic grinding effect”.

These findings suggest that bainitic rails require further investigation before they can be considered a reliable alternative to heat-treated pearlitic rails [7].

## MATERIALS AND RESEARCH RESULTS

Studies conducted at EVRAZ United West Siberian Metallurgical Plant (EVRAZ ZSMK) between 2004 and 2006 demonstrated that a lower bainite microstructure – typically used in critical structural applications requiring high strength – can be obtained in rails made from medium-carbon steel alloyed with chromium, molybdenum, nickel, and vanadium [12; 13]. Test results for experimental rails after rolling, normalizing, and tempering confirmed the potential of using such steel to simultaneously achieve enhanced wear resistance and improved low-temperature reliability. Field testing of an experimental batch of bainitic rails produced in 2005 by the EVRAZ Novokuznetsk Metallurgical Plant using E30KhG2SAFM steel showed promising results, provided that further improvements in steel purity – specifically with respect to non-metallic inclusions – could be achieved. At the time, however, the plant did not yet have the full technical capabilities to ensure consistently high metallurgical quality and precision rolling using modern equipment. In light of increasingly stringent performance requirements for rails operating under the extremely harsh conditions of the Eastern Railway Network – characterized by prolonged exposure to very low temperatures – it has become necessary to develop a new bainitic steel composition and define a suitable production route, taking into account the current capabilities of the modernized rail manufacturing facilities.

In 2022, EVRAZ ZSMK resumed the development of bainitic rail steel production technology aimed at meeting modern operational demands. Two pilot heats with improved chemical compositions were produced. Rolling was carried out in the rail and beam shop using the plant’s standard process flow, with the use of a tandem universal mill and a separate finishing stand. Complete cooling of the experimental rolled products was carried out in bundles on a cooling bed, in still air, without forced convection.

Two medium-carbon steels, provisionally designated B1 and B2, were tested. Steel B1 featured a higher content of molybdenum and silicon, while steel B2 was characterized by increased levels of chromium and nickel (Table 1). For comparison, the chemical composition of the E30KhG2SAFM bainitic steel grade produced in 2004 is also provided [13].

The chemical compositions of the experimental grades differ considerably in their silicon, chromium, nickel, and molybdenum content. Compared to E30KhG2SAFM, steel B1 has a higher silicon content and slightly elevated levels of chromium and molybdenum.

To determine the mechanical properties of the rails, tensile tests were carried out using cylindrical specimens with a diameter of 6 mm and a gauge length of 30 mm (Type III, GOST 1497–84). Impact bending tests were performed at +20 °C and –60 °C using U-notch specimens (Type I, GOST 9454–78), in accordance with GOST standards for impact strength. Hardness was measured both on the running surface and across the cross-section of the rail head.

The results of the mechanical tests (Table 2) show that, compared to rails made from B1 steel, rails made from B2 steel exhibit higher strength properties: yield strength is 20 % higher, and ultimate tensile strength is 9.2 % higher. However, B2 steel has a 27 % lower elongation at fracture, while the values of area reduction are similar for both steels.

At +20 °C, the impact strength values of the two steels are fairly close. However, at –60 °C, the B2 steel demonstrates a significantly higher impact strength – 48 % higher than that of B1 steel. These results indicate a positive effect of nickel on impact strength at sub-zero temperatures.

Compared to rails made from E30KhG2SAFM steel, the B1 steel rails show higher strength properties (yield strength is 9.6 % higher, and tensile strength is 10.1 % higher), although their elongation is somewhat lower (by 9.4 %) at comparable values of area reduction. It is worth noting that the impact strength of B1 steel rails is significantly higher than that of E30KhG2SAFM rails. This improvement is attributed to the higher purity of the steel in terms of trace elements and non-metallic inclusions, as well as better structural refinement achieved through processing in the universal rail rolling mill.

The hardness distribution across the cross-sections of the experimental rails is presented in Table 3.

Rails made from B2 steel generally exhibit higher hardness compared to those made from B1 steel, which is attributed to differences in the overall level of alloying. Notably high hardness was also recorded in the foot fillet regions of both steel grades. This is primarily due

Table 1. Chemical composition of the studied steels

Таблица 1. Химический состав исследуемых сталей

Steel	Chemical composition, wt. %					
	C	Mn	Si	Cr	Mo	Ni
B1	0.30 – 0.35	1.40 – 1.60	1.30 – 1.50	1.00 – 1.10	0.20 – 0.30	–
B2	0.30 – 0.35	1.40 – 1.60	0.80 – 1.10	1.30 – 1.50	–	1.00 – 1.10
E30KhG2SAFM	0.32	1.48	1.21	1.00	0.20	0.07

Table 2. Mechanical properties of bainitic steel rails

Таблица 2. Механические свойства рельсов из бейнитной стали

Steel	Tensile properties				Impact strength, KCU, J/cm <sup>2</sup>	
	$\sigma_y$ , N/mm <sup>2</sup>	$\sigma_t$ , N/mm <sup>2</sup>	$\delta$ , %	$\psi$ , %	at +20 °C	at –60 °C
B1	960 – 980	1390 – 1430	14.0 – 15.0	27 – 32	50 – 65	24 – 34
B2	1150 – 1180	1510 – 1570	10.0 – 11.5	27 – 30	58 – 64	36 – 47
E30KhG2SAFM	880 – 890	1270 – 1290	15.0 – 17.0	25 – 33	32 – 37	11 – 17

Note.  $\sigma_y$  – yield strength;  $\sigma_t$  – tensile strength;  $\delta$  – elongation at fracture;  $\psi$  – reduction of area; KCU – impact strength.

Table 3. Hardness on the head rolling surface and on the cross section of the experimental rails

Таблица 3. Твердость на поверхности катания головки и по сечению опытных рельсов

Steel	Hardness, HB							
	rail head					web	rail foot	
	running surface	10 mm from running surface	left fillet	right fillet	22 mm from running surface		fillet 1	fillet 2
B1	394 – 399	392 – 398	380 – 395	392 – 396	380 – 384	376 – 387	414 – 426	418 – 422
B2	444 – 462	440 – 448	454 – 458	446 – 450	418 – 421	410 – 420	508 – 520	510 – 516
E30KhG2SAFM	375	375	–	–	363	363	388	388

to the increased cooling rate in these areas, resulting from the thinner cross-sections of the rail profile. A similar hardness pattern was observed previously in rails made from E30KhG2SAFM steel.

Microstructural analysis conducted using an Olympus GX71 optical microscope revealed zones of structural heterogeneity in the rail head of B2 steel. These inhomogeneities were caused by uneven plastic deformation during rolling and appeared as alternating carbon-enriched and carbon-depleted regions. Upon cooling from rolling heat, martensitic transformation occurred in the carbon-rich zones, while bainitic structures formed in the carbon-depleted ones (Fig. 1). The combination of high strength, ductility, and toughness observed in the material is a result of this mixed microstructure. As the distance from the fillet surface increases, the proportion of bainite in the structure also grows, which is consistent with variations in the cooling rate across the rail head section.

The microstructure at the base of the B2 rail foot and in its fillets consists predominantly of martensite (Fig. 2). The formation of martensite in this region is associated

with the relatively high cooling rate under still air conditions, which is intensified by the smaller cross-sectional area compared to the head.

The microstructure of the B1 rail head is shown in Fig. 3. Near the fillet surface, a partially decarburized layer is visible, along with fine polygonal ferrite grains. The microstructure is predominantly composed of lower bainite exhibiting a needle-like morphology. As the depth increases, upper bainite begins to appear. This phase has a feathery morphology, comprising alternating fragmented ferrite and cementite plates. Beyond a depth of 20 mm, the structure transitions almost entirely to upper bainite.

The microstructures of the rail foot and fillet regions are shown in Fig. 4. In the foot, both lower and upper bainite are present (Fig. 4, a), while the fillet areas consist mainly of lower bainite with isolated regions of martensite (Fig. 4, b).

According to published studies [14–17], the most favorable microstructure for bainitic rail steels is a combination of lower bainite and lath martensite. This is because, during the transformation of austenite into

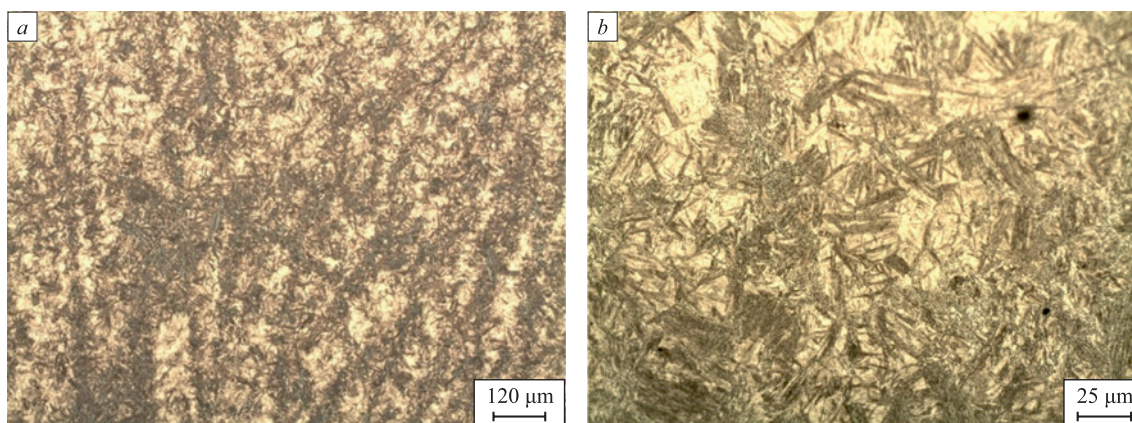
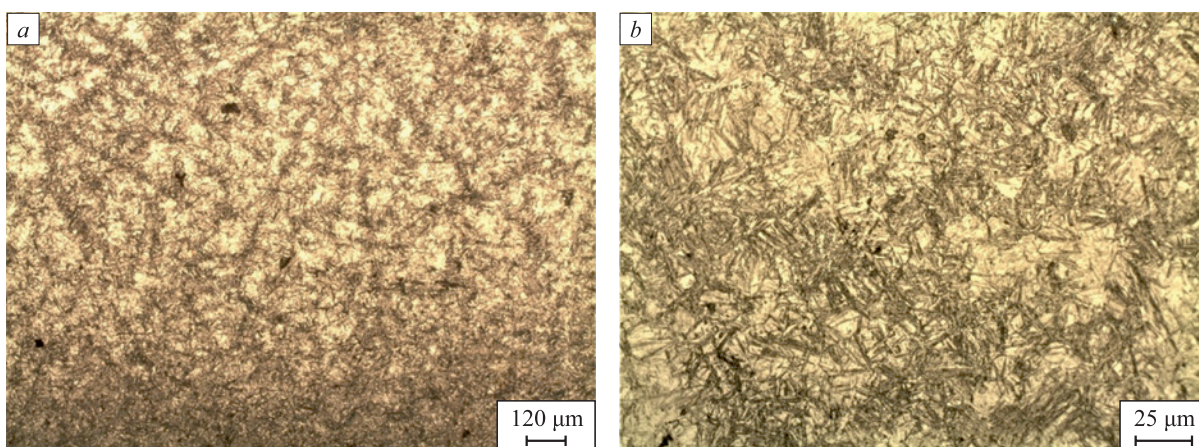


Fig. 1. Microstructure of B2 steel rail head:

a – structural heterogeneity at a depth of about 2 mm (sections of lower bainite (dark), sections of martensite (light));  
b – microstructure at a depth of up to 10 mm from the head rolling surface

Рис. 1. Микроструктура головки рельса из стали Б2:

a – структурная неоднородность на глубине около 2 мм (участки бейнита нижнего (темные), участки мартенсита (светлые));  
b – микроструктура на глубине до 10 мм от поверхности катания головки



**Fig. 2.** Microstructure of B2 steel rail foot:  
*a* – martensite at foot base; *b* – martensite in foot fillets

**Рис. 2.** Микроструктура подошвы рельса из стали Б2:  
*a* – мартенсит в основании подошвы; *b* – мартенсит в перьях

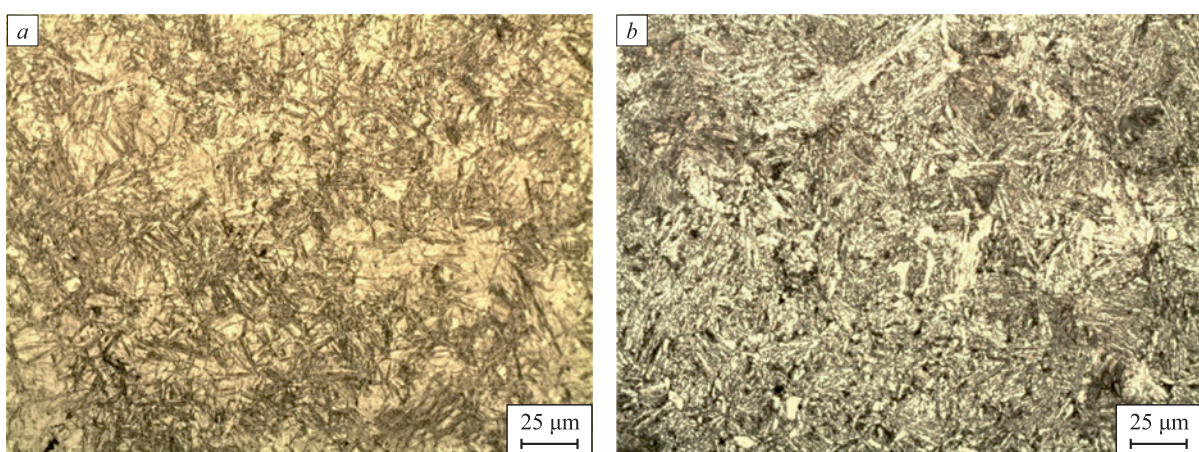


**Fig. 3.** Microstructure of B1 steel rail head:  
*a* – lower bainite and small grains of polygonal ferrite near the fillet surface;  
*b* – microstructure at a depth of about 20 mm (mainly upper bainite)

**Рис. 3.** Микроструктура головки рельса из стали марки Б1:  
*a* – нижний бейнит и мелкие зерна полигонального феррита вблизи поверхности выкружки;  
*b* – микроструктура на глубине около 20 мм (преимущественно верхний бейнит)

lower bainite, retained austenite becomes segmented into thin regions by the bainitic laths. Subsequent martensitic transformation within these confined regions leads to the formation of an extremely fine lath martensite structure. The finer the microstructure, the greater the strength and toughness of the steel. Steels with this type of mixed structure exhibit both high ductility and fracture toughness. Moreover, as contact stress increases, the wear rate of such steels rises more slowly than that of pearlitic rail steels [10; 17 – 19].

The results of the study suggest that B2 steel is suitable for the production of rails cooled in still air after rolling. To improve processability – specifically, to facilitate straightening and reduce internal microstresses – it is recommended to test a reduced carbon content

of 0.28 – 0.30 %, while maintaining the levels of the other alloying elements.

## CONCLUSIONS

A comparative evaluation of the hot-rolled rail steel produced from experimental compositions B1 and B2 demonstrated that increased alloying with chromium (1.2 – 1.5 %) and nickel (1.0 – 1.1 %) leads to a 20 % increase in yield strength, a 9.2 % increase in ultimate tensile strength, and a 48 % increase in impact strength at –60 °C compared to the alloying scheme based on molybdenum at 0.20 – 0.30 %.

Microstructural analysis of the rails made from both experimental steel grades revealed the formation of nee-

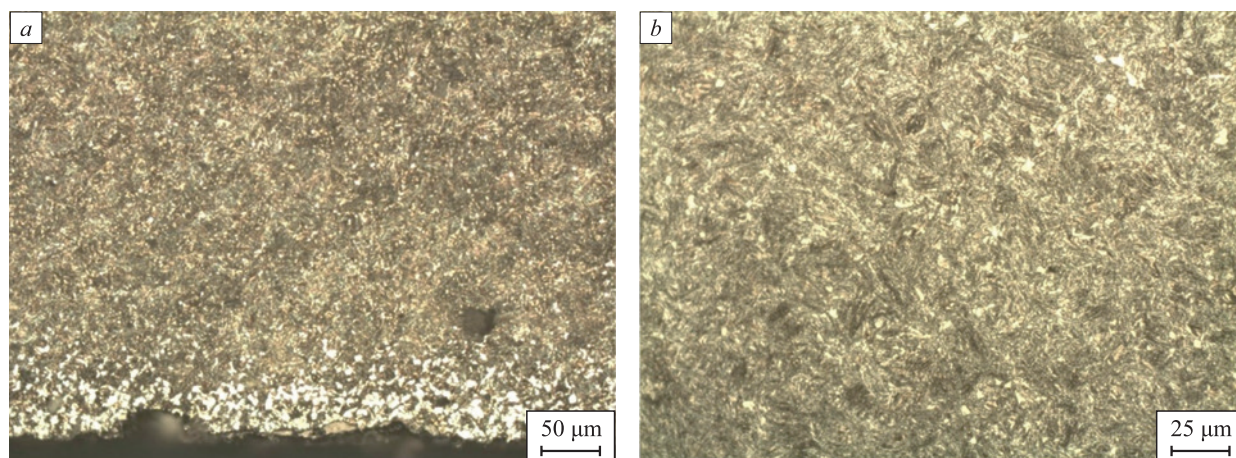


**Fig. 4.** Microstructure of the foot and foot fillets of rail:

- a* – decarbonized layer, bainite near the foot base;  
*b* – lower bainite, areas of martensite (dark areas of needle-like structure) in the foot fillets

**Рис. 4.** Микроструктура подошвы и перьев рельса:

- a* – обезуглероженный слой, бейнит вблизи основания подошвы;  
*b* – нижний бейнит, участки мартенсита (темные участки игольчатой структуры) в перьях

dle-like upper and lower bainite during continuous cooling in still air. In the B2 steel rails, a higher fraction of martensite was observed in the head, which contributed to increased strength and hardness.

To further develop the technology and achieve a more stable structure consisting predominantly of lower bainite, it is recommended to use B2 steel as a base composition, while reducing the carbon content to 0.25 – 0.30 %.

#### REFERENCES / СПИСОК ЛИТЕРАТУРЫ

- Shur E.A. Rail Damage. Moscow: Intekst; 2012:192. (In Russ.).  
Шур Е.А. Повреждения рельсов. Москва: Интекст; 2012:192.
- Pavlov V.V., Godik L.A., Korneva L.V., Kozyrev N.A., Gizatuln R.A. Production of rails with increased wear resistance. *Izvestiya. Ferrous Metallurgy*. 2007;50(10):35–37. (In Russ.).  
Павлов В.В., Годик Л.А., Корнева Л.В., Козырев Н.А., Гизатулин Р.А. Производство рельсов повышенной износостойкости. *Известия вузов. Черная металлургия*. 2007; 50(10):35–37.
- Ermakov V.M. About some issues of rail management. In: *Improving the Quality and Operating Conditions of Rails and Rail Fasteners (based on the Materials of the Meeting of the Non-Profit Partnership “Rail Commission”, October 7–9, 2014): Proceedings*. St. Petersburg: UIM; 2015:137–148. (In Russ.).  
Ермаков В.М. О некоторых вопросах ведения рельсового хозяйства. В кн.: *Улучшение качества и условий эксплуатации рельсов и рельсовых скреплений (по материалам заседания некоммерческого партнерства «Рельсовая комиссия» 7–9 октября 2014 г.): Сборник научных докладов*. Санкт-Петербург: ОАО «УИМ»; 2015:137–148.
- Pavlov V.V., Temlyantsev M.V., Korneva L.V., Syusyukin A.Yu. Promising Technologies of Thermal and Heat Treatment in Production of Rails. Moscow: Teplotekhnik; 2007:280. (In Russ.).  
Перспективные технологии тепловой и термической обработки в производстве рельсов / В.В. Павлов, М.В. Темлянцева, Л.В. Корнева, А.Ю. Сюсюкин. Москва: Теплотехник; 2007:280.
- Korneva L.V., Yunin G.N., Kozyrev N.A., Atkonova O.P., Polevoi E.V. Comparative analysis of quality indicators of rails of JSC Novokuznetsk Metallurgical Plant and foreign manufacturers. *Izvestiya. Ferrous Metallurgy*. 2010;53(12):38–42. (In Russ.).  
Корнева Л.В., Юнин Г.Н., Козырев Н.А., Атконова О.П., Полевой Е.В. Сравнительный анализ показателей качества рельсов ОАО «Новокузнецкий металлургический комбинат» и зарубежных производителей. *Известия вузов. Черная металлургия*. 2010;53(12):38–42.
- Hlavatý I., Sigmund M., Krejčí L., Mohyla P. The bainitic steels for rails applications. *Materials Science Engineering*. 2009;16(4):44–50.
- Rail steel – evolution and prospects. *Zheleznye dorogi mira*. 2008;(5):59–64. (In Russ.).  
Рельсовая сталь – эволюция и перспективы. *Железные дороги мира*. 2008;(5):59–64.
- Bainitic steel rails on Swiss railways. *Zheleznye dorogi mira*. 2011;(5):71–75. (In Russ.).  
Рельсы из бейнитной стали на железных дорогах Швейцарии. *Железные дороги мира*. 2011;(5):71–75.
- Racyna J. The microstructure and properties of the new bainitic rail steels. *Journal of Achievements in Materials and Manufacturing Engineering*. 2008;28(1):19–22.
- Yokoyama H., Mitao S., Yamamoto S., Kataoka Y., Sugiyama T. High strength bainitic steel rails for heavy haul railways with superior damage resistance. *NKK Technical Review*. 2001;(84):44–51.
- Yokoyama H., Mitao S., Yamamoto S., Fujikake M. Effect of the angle of attack on flaking behavior in pearlitic and

- bainitic steel rails. *Wear*. 2002;253(1-2):60–66.  
[https://doi.org/10.1016/S0043-1648\(02\)00083-2](https://doi.org/10.1016/S0043-1648(02)00083-2)
12. Pavlov V.V., Godik L.A., Korneva L.V., Kozyrev N.A., Kuznetsov E.P. The railway rails from bainite steel. *Metal-lurg*. 2007;(4):51–53. (In Russ.).  
 Павлов В.В., Годик Л.А., Корнева Л.В., Козырев Н.А., Кузнецов Е.П. Железнодорожные рельсы из бейнитной стали. *Металлург*. 2007;(4):51–53.
  13. Korneva L.V., Oskolkova T.N. Structure of bainitic steel rails. *Izvestiya. Ferrous Metallurgy*. 2006;49(12):26–27. (In Russ.).  
 Корнева Л.В., Осколкова Т.Н. Структура рельсов из стали бейнитного класса. *Известия вузов. Черная металлур-гия*. 2006;49(12):26–27.
  14. Dobuzhskaya A.B., Galitsyn G.A., Smirnov L.A., Yunin G.N., Koshkarov D.A., Kirichkov A.A., Pavlov V.V., Polevoi E.V., Belokurova E.V. Outlook for manufacture of rails of bainitic steel. *Stal'*. 2023;(2):41–46.  
 Добужская А.Б., Галицын Г.А., Смирнов Л.А., Юнин Г.Н., Кошкарлов Д.А., Киричков А.А., Павлов В.В., Поле-вой Е.В., Белокурова Е.В. Перспективы производства рельсов из бейнитной стали. *Сталь*. 2023;(2):41–46.
  15. Zajac S., Schwinn V., Tacke K.-H. Characterisation and quantification of complex bainitic microstructures in high and ultra-high strength linepipe steels. *Materials Science Forum*. 2005;500-501:387–394.  
<https://doi.org/10.4028/www.scientific.net/MSF.500-501.387>
  16. Qiu J., Zhang M., Tan Z., Gao G., Bai B. Research on the microstructures and mechanical properties of bainite/martensite rail treated by the controlled-cooling process. *Materials*. 2019;12(19):3061.  
<https://doi.org/10.3390/ma12193061>
  17. Adamczyk-Cieślak B., Korallnik M., Kuziak R., Majchro-wicz K., Mizera J. Studies of bainitic steel for rail applica-tions based on carbide-free, low-alloy steel. *Metallurgical and Materials Transactions*. 2021;52:5429–5442.  
<https://doi.org/10.1007/s11661-021-06480-6>
  18. Wiedorn J., Kammerhofer C., Scheriau S. 340 Dobain HSH – Schienenwerkstoff gegen Head Checks. *FAHRWEG*. 2021;31–35. (In Germ.).
  19. Girsch G., Heyder R. Advanced pearlitic and bainitic high rails promise to improve rolling contact fatigue resistance. In: *Proceedings of 7<sup>th</sup> World Congress on Railway Research*. 2006;43–51.

## Information about the Authors

## Сведения об авторах

**Anatolii M. Yunusov**, Head of the Research and Development Department of the Research Center, JSC EVRAZ United West Siberian Metallurgical Plant

**E-mail:** Anatoly.Yunusov@evraz.com

**Egor V. Polevoi**, Cand. Sci. (Eng.), Head of the Research Center, JSC EVRAZ United West Siberian Metallurgical Plant

**E-mail:** egor.polevoj@evraz.com

**Gennadii N. Yunin**, Advisor on the Technology of Production of Rolled Rails, JSC EVRAZ United West Siberian Metallurgical Plant

**E-mail:** Gennady.Yunin@evraz.com

**Tat'yana N. Oskolkova**, Dr. Sci. (Eng.), Prof. of the Chair of Ferrous Metallurgy and Chemical Technology, Siberian State Industrial University

**ORCID:** 0000-0003-1310-1284

**E-mail:** oskolkovatiana@yandex.ru

**Анатолий Майдарисович Юнусов**, начальник отдела научно-исследовательских разработок научно-исследовательского центра, АО «ЕВРАЗ Объединенный Западно-Сибирский металлургический комбинат»

**E-mail:** Anatoly.Yunusov@evraz.com

**Егор Владимирович Полевой**, к.т.н., начальник научно-исследовательского центра, АО «ЕВРАЗ Объединенный Западно-Сибирский металлургический комбинат»

**E-mail:** egor.polevoj@evraz.com

**Геннадий Николаевич Юнин**, советник по технологии производства рельсового проката, АО «ЕВРАЗ Объединенный Западно-Сибирский металлургический комбинат»

**E-mail:** Gennady.Yunin@evraz.com

**Татьяна Николаевна Осколкова**, д.т.н., профессор кафедры металлургии черных металлов и химической технологии, Сибирский государственный индустриальный университет

**ORCID:** 0000-0003-1310-1284

**E-mail:** oskolkovatiana@yandex.ru

## Contribution of the Authors

## Вклад авторов

**A. M. Yunusov** – organization and control of experimental rolling, collection and analysis of data on production stages, laboratory research, report preparation.

**E. V. Polevoi** – analysis and proposals for the development of experimental chemical compositions of bainitic steels, management of research work.

**G. N. Yunin** – preparation of recommendations for production, organization of work on smelting and rolling of experimental rails.

**T. N. Oskolkova** – consulting work on preparation for production of experimental rails, assistance in the article formation.

**А. М. Юнусов** – организация и контроль проведения опытной прокатки, сбор и анализ данных по этапам производства, проведение лабораторного исследования опытного металла, подготовка отчета.

**Е. В. Полевой** – анализ и внесение предложений по разработке опытных химических составов бейнитным марок сталей, руководство при проведении научно-исследовательской работы.

**Г. Н. Юнин** – подготовка рекомендаций по производству, организация работ по выплавке и прокатке опытных рельсов.

**Т. Н. Осколкова** – проведение консультационных работ по подготовке к производству опытных рельсов, помощь в формировании статьи.

Received 03.06.2024

Revised 20.10.2024

Accepted 27.01.2025

Поступила в редакцию 03.06.2024

После доработки 20.10.2024

Принята к публикации 27.01.2025



UDC 658.567.1

DOI 10.17073/0368-0797-2025-2-131-138



Original article

Оригинальная статья

## ACTUAL PROGRESS OF PRODUCTION WASTE DISPOSAL PROBLEMS

G. A. Ulyeva<sup>1,2</sup>, K. Tuyskhan<sup>2</sup>, E. M. Matsugina<sup>2</sup>,  
I. E. Volokitina<sup>2</sup>, G. E. Akhmetova<sup>2</sup>

<sup>1</sup>JSC «Qarmet» (1 Respubliki Ave., Timertau, Karaganda Region 101400, Republic of Kazakhstan)

<sup>2</sup>Karaganda State Industrial University (30 Respubliki Ave., Timertau, Karaganda Region 101400, Republic of Kazakhstan)

✉ irinka.vav@mail.ru

**Abstract.** For many countries the problem of industrial and household waste disposal is particularly acute, since the annual accumulation of all types of waste is quite large (about 7 billion tons), and their reuse does not exceed 30 %. At the same time, industrial waste has a negative impact on living organisms and the environment. Therefore, ways of recycling household and production wastes are necessary. This article considers the problems of utilization, processing (recycling) of industrial and household waste and the prospects of their application in various industries. The influence of different formulations of initial components (microsilica, blast furnace slag, slaked lime), their fractions on physical and mechanical properties of the obtained new composite materials is considered. The obtained materials were investigated in order to determine the values of compressive strength and percentage of water absorption. Thus, all samples have low water absorption percentage (0 – 13.12 %), except for Sample 7 (41.34 %), consisting of 2 parts of microsilica, 1 part of slag and 1 part of lime. It was found that high values of compressive strength are observed in the samples which include microsilica. Samples 3 and 4, composed of microsilica and slag jointly, have the lowest compressive strength of 14.74 and 17.18 kgf/cm<sup>2</sup>, respectively. However, Sample 8, which is composed of 2 parts of microsilica, slag and lime simultaneously, is characterized by the highest compressive strength value of 51.16 kgf/cm<sup>2</sup>. Microsilica has a greater influence on the increase of strength properties. At the same time, the use of industrial waste in the creation of new secondary materials leads to a reduction in the cost of production, expansion of the raw material base of the country, as well as reducing the environmental load of the region.

**Keywords:** industrial waste, production waste, domestic waste, silicon production waste, microsilica, brick scrap, ash, blast furnace slag, environmental protection

**For citation:** Ulyeva G.A., Tuyskhan K., Matsugina E.M., Volokitina I.E., Akhmetova G.E. Actual progress of production waste disposal problems. *Izvestiya. Ferrous Metallurgy*. 2025;68(2):131–138. <https://doi.org/10.17073/0368-0797-2025-2-131-138>

## СОВРЕМЕННОЕ СОСТОЯНИЕ ПРОБЛЕМЫ УТИЛИЗАЦИИ ОТХОДОВ ПРОИЗВОДСТВА

Г. А. Ульева<sup>1,2</sup>, К. Туысхан<sup>2</sup>, Е. М. Мацугина<sup>2</sup>,  
И. Е. Волокитина<sup>2</sup>, Г. Е. Ахметова<sup>2</sup>

<sup>1</sup>АО «Qarmet» (Республика Казахстан, 101400, Карагандинская обл., Темиртау, пр. Республики, 1)

<sup>2</sup>Карагандинский государственный индустриальный университет (Республика Казахстан, 101400, Карагандинская обл., Темиртау, пр. Республики, 30)

✉ irinka.vav@mail.ru

**Аннотация.** Для многих стран проблема утилизации отходов производства и быта стоит особенно остро, поскольку ежегодное накопление всех видов отходов достаточно велико (около 7 млрд т), а их повторное использование не превышает 30 %. При этом отходы производства отрицательно влияют на живые организмы и окружающую среду, поэтому необходимо расширение их переработки. В данной работе рассмотрены проблемы утилизации, переработки (рециклинга) промышленных и бытовых отходов и перспективы их применения в различных отраслях. Рассмотрено влияние различных рецептур исходных компонентов (микросилики, доменного шлака, гашеной извести) и их фракций на физико-механические свойства полученных новых композиционных материалов. Проведены исследования полученных материалов с целью определения значений предела прочности на сжатие и процент водопоглощения. Так, все образцы имеют низкий процент водопоглощения (0 – 13,12 %), кроме образца 7 (41,34 %), состоящего из двух частей микросилики, одной части шлака и одной части извести. Выявлено, что в образцах, в состав которых входит микросилика, наблюдаются

высокие значения предела прочности на сжатие. Образцы 3 и 4, состоящие из микросилики и шлака, обладают самым низким пределом прочности – 14,74 и 17,18 кгс/см<sup>2</sup> соответственно. Однако образец 8, в состав которого одновременно входят две части микросилики, шлак и известь, характеризуется самым высоким значением предела прочности на сжатие – 51,16 кгс/см<sup>2</sup>. Таким образом, микросилика оказывает большее влияние на увеличение прочностных свойств. При этом применение отходов производства при создании новых вторичных материалов приводит к снижению себестоимости продукции, расширению сырьевой базы страны, а также снижению экологической нагрузки региона.

**Ключевые слова:** отходы производства, промышленные отходы, бытовые отходы, отходы кремниевого производства, микросилика, кирпичный лом, зола, доменный шлак, защита окружающей среды

**Для цитирования:** Ульева Г.А., Туысхан К., Мацугина Е.М., Волокитина И.Е., Ахметова Г.Е. Современное состояние проблемы утилизации отходов производства. *Известия вузов. Черная металлургия*. 2025;68(2):131–138. <https://doi.org/10.17073/0368-0797-2025-2-131-138>

## INTRODUCTION

In recent years, the fields of metallurgy, engineering and materials science have been rapidly evolving [1 – 4]. However, the problem of solid and household waste remains unresolved in every country worldwide<sup>1, 2</sup>. For example, in the CIS countries, this issue is particularly severe, as the annual accumulation of all types of waste reaches approximately 7 billion tons, with the reuse rate of less than 30 %. A major concern is the direct impact of waste on human life as it is concentrated in residential and recreational areas. To address this issue, waste must be integrated into natural cycles, removed and utilized. The most viable solution is to develop efficient recycling methods and establish a new industry sector [5 – 8]. However, many challenges along must be overcome, some of which are complex but solvable [9].

Currently, industrial waste in Kazakhstan amounts to 31.6 billion tons, with an annual increase of approximately 1 million tons in recent years<sup>3</sup>.

However, according to the 2022 report *On the state of the environment and use of natural resources of the Republic of Kazakhstan*, the volume of industrial waste exceeds 895 million tons. Kostanai, Pavlodar, and Karaganda regions are the leaders in generating this waste. Approximately half of the waste from these regions is recycled. However, regions such as Turkestan (0.76 %), Almaty (9.32 %), and Zhambyl (7.38 %) have low recycling rates. In 2022, the percentage of recycled and disposed industrial waste reached 40.03 %, which is higher than the 38.2 % recorded in 2021<sup>4</sup>.

<sup>1</sup> Improving legislation to increase the efficiency of processing and use of production and consumption waste. URL: <https://council.gov.ru/activity/activities/roundtables/29479> (Accessed: 06.03.2025).

<sup>2</sup> Problem of industrial waste. URL: <https://msd.com.ua/tehnologiya-teploizolyacii/problema-promyshlennyx-otxodov> (Accessed: 06.03.2025).

<sup>3</sup> National report on the state of environment and the use of natural resources of the Republic of Kazakhstan for 2021. URL: <https://www.gov.kz/memleket/entities/ecogeo/documents/details/383692?lang=ru> (Accessed: 06.03.2025).

<sup>4</sup> For discussion, the draft National Report on the state of environment and the use of natural resources of the Republic of Kazakhstan for 2022. URL: <https://www.gov.kz/memleket/entities/ecogeo/documents/details/144658?lang=ru> (Accessed: 26.09.2024).

Forced storage of huge amounts of waste and their disposal in dumps cause significant losses to the national economy due to unused opportunities for utilizing secondary raw materials, while industrial waste production results in damage amounting to tens of millions [10 – 12]. Another equally important aspect of the issue is the negative impact of industrial waste on the environment. The atmosphere is being severely polluted at an alarming rate by a variety of industrial emissions<sup>2</sup> [12].

Scientists from both domestic and foreign institutions are engaged in addressing the problem of industrial and household waste disposal [13 – 15]. One known method involves processing dusty silicon waste by remelting it in a solid-liquid aluminum medium [13; 16]. This method allows the use of pulverized silicon waste in the smelting of aluminum alloys. However, it is not suitable for recycling other silicon-containing powdered materials.

It is known that crystalline silicon in the 20 – 50 mm fraction is used for the production of aluminum-silicon alloys, while dust-like and fine fractions resulting from crushing and screening are sent to dumps, leading to a decrease in silicon utilization in the production of the these alloys. Papers [17 – 19] proposed a method for processing waste silicon, which includes introducing silicon into the aluminum melt with stirring. This method is distinguished by the fact that silicon fractions of 0.1 – 20.0 mm are introduced onto the surface of the melt at 670 – 680 °C, followed by heating to 720 – 750 °C at a rate of 2.5 – 4.0 °C/mm to improve silicon assimilation and reduce metal losses from oxidation by shortening the melting duration.

Technologists and scientists in Kazakhstan are developing methods to recover captured dust in order to obtain high-quality technical silicon. This will not only reduce production cost but also lessen the environmental impact by decreasing emissions. Microsilica processing technologies are also being developed to produce briquette mono-blends.

The paper [20] presents a technology for obtaining silica filler intended for use in the production of rubber materials at the Karaganda Rubber Technical Plant, as well as other industries.

Existing technologies for the disposal of silicon-containing powdery waste, despite their diversity, have one common feature: the silicon remains present in silicon-containing waste even after recycling. In other words, its chemical state does not change [21; 22].

Thus, based on the given literature review, the authors of this article present a technology for the disposal of industrial and domestic waste, specifically microsilica, to obtain secondary composite materials [23].

**MATERIAL AND METHODS**

The ratio of initial components was 1:1 (Samples 1, 3, 5), 2:1 (Samples 2, 4, 6), 1:1:1 (Sample 7), and 2:1:1 (Sample 8). Table 1 shows the composition of the obtained samples.

All materials were sieved through a sieve with a fraction of 1 – 2 mm, followed by weighing. The initial components were then combined in a dry state and mixed until evenly distributed. After thorough mixing, 5 – 7 g of water was gradually added and mixed to form a homogeneous mixture. The resulting composition was transferred into molds, shaken, and tamped down. The complete drying time of the molds was 14 days (see Fig. 1). After drying, the samples were removed, inspected for integrity, and weighed. At the same time, all dried samples produced a metallic sound when tapped.

The study of the physical and mechanical properties of the obtained secondary materials was carried out in three stages:

- Stage 1 – study of samples for water absorption without coating;
- Stage 2 – study of coated samples for water absorption;
- Stage 3 – compression testing of samples.

The samples were then tested for water absorption according to GOST 12730.3–2020. In this process, the samples were completely immersed in water. Bubbles were released during soaking, which may indicate the presence of internal pores. The samples remained in water until bubble release was complete. After soaking, the samples were weighed. Then, they were placed in a SNOL-type furnace heated to 150 – 200 °C and dried until their mass became constant, with re-weighing.

*Table 1. Ratio of initial components*

*Таблица 1. Соотношение исходных компонентов*

Material	Quantity of material in sample, g							
	1	2	3	4	5	6	7	8
Microsilica	25	50	25	50	–	–	25	50
Lime	25	25	–	–	25	25	25	25
Slag	–	–	25	25	25	50	25	25

The calculation of water absorption  $W_m$  of the samples was performed according to the formula (GOST 12730.3–2020)

$$W_m = \frac{m_w - m_d}{m_d} \cdot 100 \%,$$

where  $m_d$  is dried sample weight, g, and  $m_w$  is water-saturated sample weight, g.

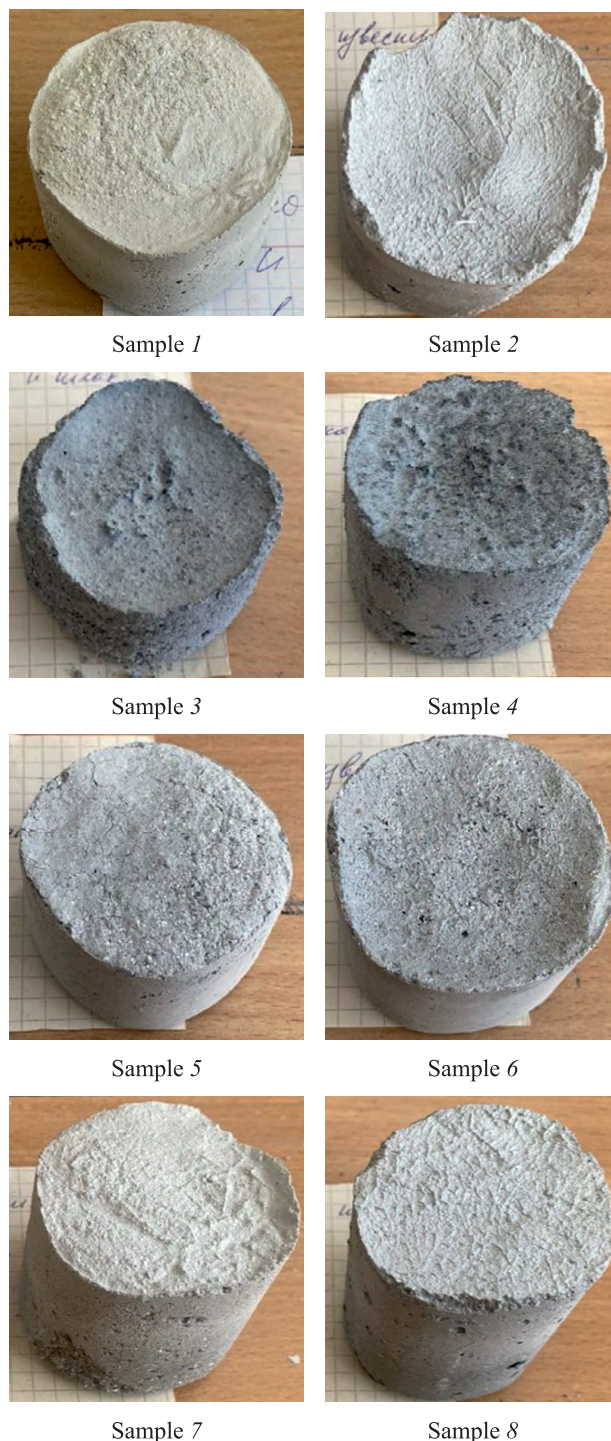


*Fig. 1. Samples obtained after drying*

*Рис. 1. Полученные образцы после высыхания*

For optimal water absorption performance, the authors suggest applying a protective varnish to the samples and re-testing them for water absorption. After coating,

the samples were dried at room conditions for 24 h. After drying, they were checked and weighed.

When the samples were kept in water, no bubbles were released, unlike in the first water absorption test, because all pores were completely blocked by the varnish. However, some samples floated to the surface, suggesting the presence of internal pores.

After soaking in water, the samples were weighed and left to dry for 24 h under room conditions. Re-weighing was performed every 24 h until the samples reached a constant mass, and the percentage of water absorption was re-determined (Table 2).

Then, the samples were subjected to compression testing on a 40KU testing machine according to GOST 10180–2012. The behavior of the samples during compression testing corresponded to GOST 10180–2012.

Prior to testing, each sample underwent side grinding to ensure parallelism of the sample sides (Fig. 2).

## RESULTS

The water absorption results are presented in Table 2, and the compression test results are summarized in Table 3.

Table 3 shows that Samples 3 and 4 have the lowest compressive strength, at 14.74 and 17.18 kgf/cm<sup>2</sup>, respectively. The composition of these samples includes microsilica and slag, with slag having a greater weakening effect. It should be noted that in Sample 4 the microsilica content was doubled, which resulted in an increase in the strength index. However, when comparing Samples 5 and 6, which contain slag and lime, the combination and interaction of these components enhance compressive strength, especially as the slag content increases.

Samples 1 and 2, containing microsilica and lime, have moderate compressive strength values of 28.20 and 24.64 kgf/cm<sup>2</sup>, respectively.

Table 2. Water absorption percentage after two stages

Таблица 2. Процент водопоглощения после двух этапов

Sample No.	Water absorption $W_m$ , %	
	stage 1	stage 2
1	44.70	<b>1.93</b>
2	53.30	<b>2.64</b>
3	<b>16.60</b>	<b>2.33</b>
4	<b>15.70</b>	13.12
5	<b>27.60</b>	<b>0</b>
6	<b>24.30</b>	12.50
7	58.30	41.34
8	62.20	<b>4.66</b>

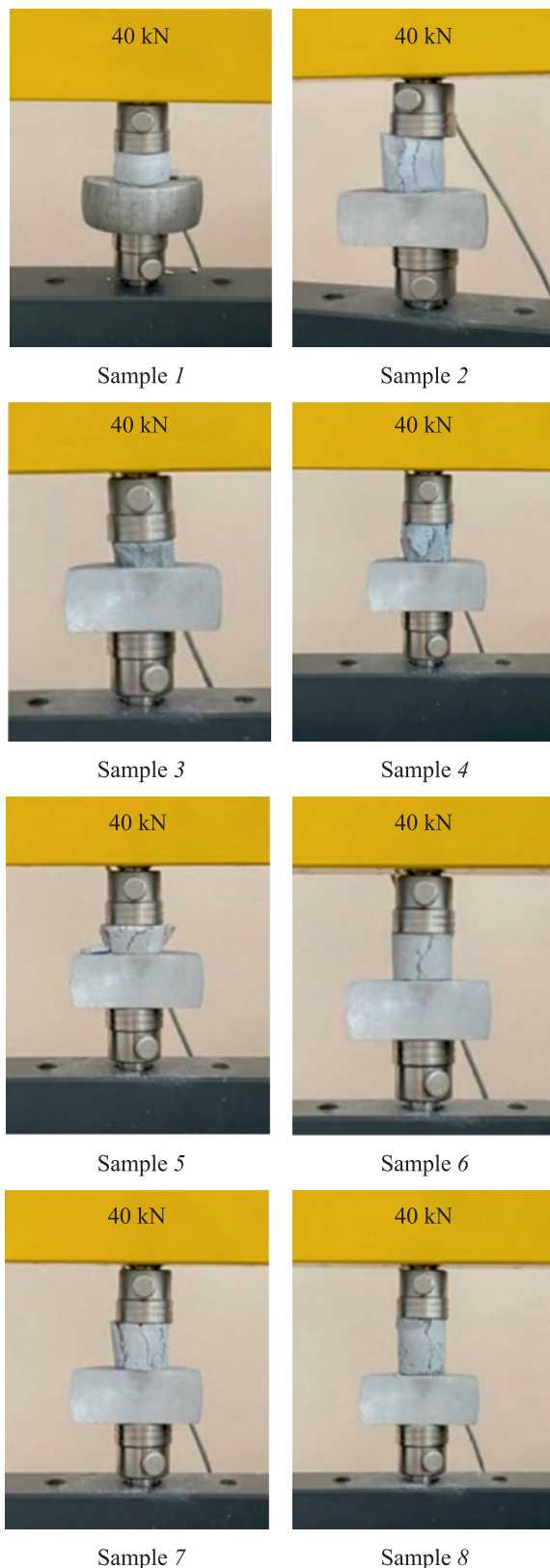


Fig. 2. Sample on the testing machine before and after fracture

Рис. 2. Образец на испытательной машине до и после разрушения

Table 3. Compression test results

Таблица 3. Результаты испытания на сжатие

Sample No.	Loading P, kgf	Cross-sectional area, F, cm <sup>2</sup>	Compressive strength, $\sigma_{st}$ , kgf/cm <sup>2</sup>	Behavior of samples in compression testing
1	509.90	18.08	28.20	A crack appeared on the lateral surface of the sample, accompanied by a small fracture
2	445.60	18.08	24.64	Several cracks appeared on the sample, but no fracture occurred
3	234.50	15.90	14.74	Cracks appeared at the edges of the sample without fracture as the load was applied
4	273.30	15.90	17.18	Cracks appeared at the edges with slight fracture
5	416.04	21.22	19.60	Gradual cracking and slight fracture at the edges of the sample
6	662.80	18.84	35.18	Cracking across the entire cross-section without fracture
7	705.60	18.08	39.02	Cracking and slight fracture at the edges of the sample
8	887.20	17.34	51.16	Cracking along the edges of the sample without fracture

It is also worth noting that samples with a three-component composition of microsilica, slag, and lime exhibit the highest compressive strength, particularly Sample 8 (51.16 kgf/cm<sup>2</sup>). In this sample, the microsilica content is doubled compared to Sample 7, which contributes to the material’s hardening.

Thus, the properties of the material vary depending on the composition. For example, microsilica has been shown to enhance strength, as seen in Sample 4. Similarly, slag contributes to increase strength, as observed in Sample 6, where lime is the second component.

The compression diagrams of the tested samples are shown in Fig. 3.

Fractures of Samples 3 and 8 (samples with the lowest and the highest compressive strength value) were studied using a scanning electron microscope EVO18 (Qarmet JSC) (Fig. 4).

DISCUSSION

**Stage 1.** Samples 1 and 2 show unsatisfactory result according to Table 2. Their composition consists of microsilica and lime in a 1:1 and 2:1 ratio, with water absorption values of 44.7 and 53.3 %. The negative effect is probably due to the second component, hygroscopic lime.

Samples 3 and 4, composed of microsilica and slag in a 1:1 and 2:1 ratio, demonstrate good water absorption values of 16.6 and 15.7 %, respectively. This suggests that these initial components reduce hydrophilicity.

Similarly, Samples 5 and 6, with slag-to-lime ratios of 1:1 and 2:1, also showed favorable results: water absorption decreased from 27.6 to 24.32 % as the slag content increased from 25 to 50 g.

Samples 7 and 8, composed of microsilica, slag, and lime in a 1:1:1 and 2:1:1 ratio, exhibited unsatisfactory results, with water absorption values of 58.3 and 62.2 %, respectively. Notably, higher microsilica content correlates with higher water absorption.

**Stage 2.** It is evident that water absorption results improved significantly in samples coated with protective varnish. Specifically, Samples 1, 2, 3, and 8 demonstrated

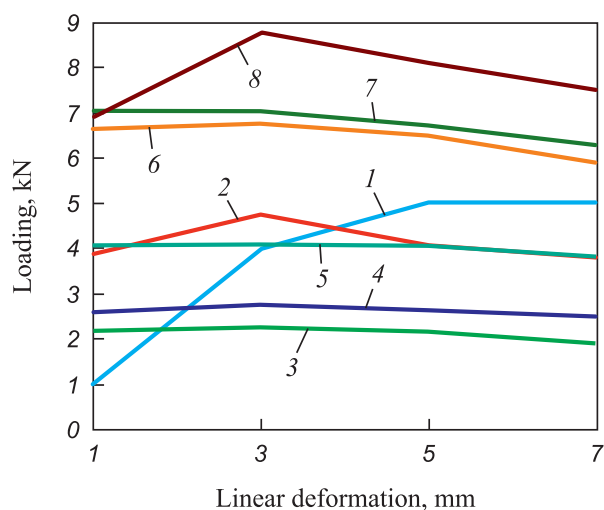


Fig. 3. Compression test diagrams (numbers on curves indicate sample number)

Рис. 3. Диаграммы сжатия при испытании (цифры у кривых – номер образца)

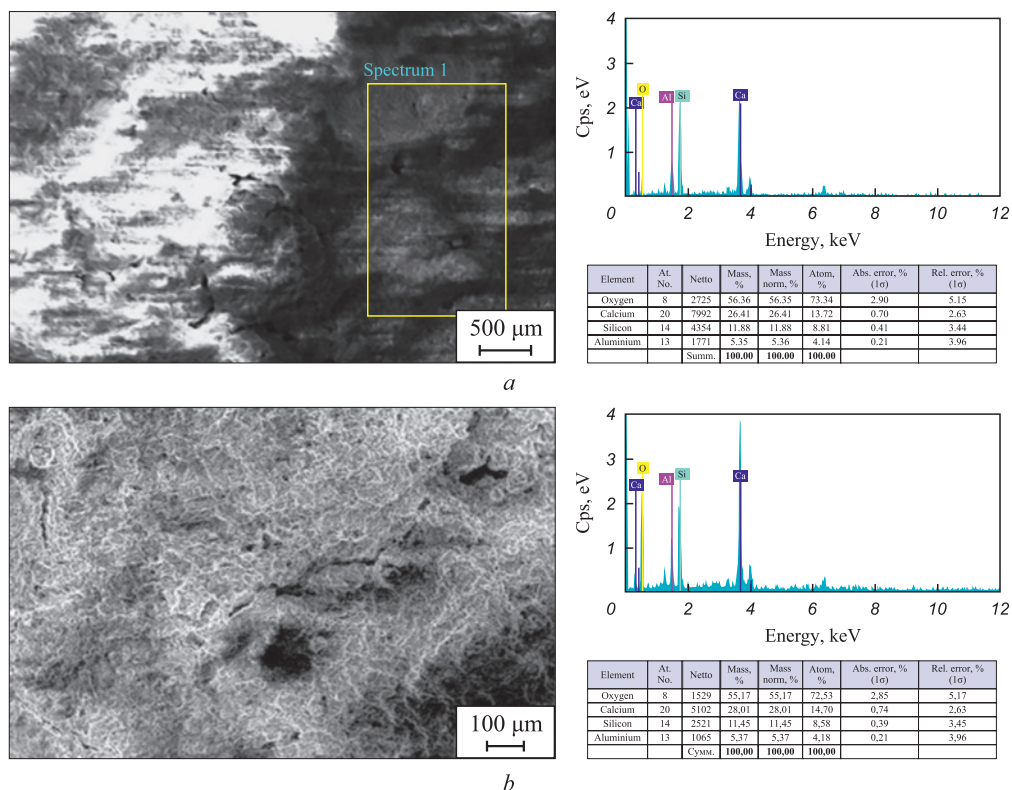


Fig. 4. Material structure:  
a – Sample 3, b – Sample 8

Рис. 4. Строение материала:  
a – образец 3, b – образец 8

the lowest water absorption values of 1.93, 2.64, 2.33, and 4.66 % respectively. Sample 5 achieved an excellent water absorption rate of 0 %.

Samples 4 and 7 exhibited moderate water absorption values of 13.12 and 12.5 %, respectively.

However, Sample 7 has the worst water absorption performance (41.34 %). This may be due to the presence of macropores and the unpredictable behavior of the original components in a 1:1:1 ratio with the protective varnish.

Thus, different compositions and ratios lead to varying final properties. Each component interacts differently, allowing for the selection of optimal properties through proper material composition. It is also worth noting that Sample 5, with a slag-lime composition in a 1:1 ratio, has the best water absorption performance, while Sample 7, with a microsilica-slag-lime composition in a 1:1:1 ratio, showed the worst results.

The structure of Sample 3, which exhibited the lowest value of compressive strength, is characterized by a loose structure and uneven distribution of microsilica and slag throughout its volume. The sample is friable.

The experimental data comply with GOST 12730.3–2020 “Water absorption”, GOST 10180–2012 “Compressive strength”.

## CONCLUSION

This study demonstrates the feasibility of using industrial and household waste to produce secondary materials with a functional set of physical and mechanical properties. The developed samples with high water absorption values can be used as interior cladding material. However, when coated with a protective layer, these materials can also serve as exterior cladding. At the same time, materials based on microsilica and blast furnace slag exhibit satisfactory strength properties (17.18 – 51.16 kgf/cm<sup>2</sup>), expanding their potential applications.

The development of waste disposal and recycling methods remains a major economic challenge. Addressing this issue will change the perception of industrial waste as an end product, promoting more active use of recycling methods while shifting the focus toward generating economic benefits from this process.

## REFERENCES / СПИСОК ЛИТЕРАТУРЫ

1. Volokitin A.V., Volokitina I.E., Latypova M.A., Chigirinsky V.V., Kolesnikov A.S. Effect of controlled rolling on the structural and phase transformation. *Progress in Physics of Metals*. 2023;24(1):132–156. <https://doi.org/10.15407/ufm.24.01.132>

2. Volokitina I., Volokitin A., Denissova A., Fedorova T., Lawrinuk D., Kolesnikov A., Yerzhanov A., Kuatbay Y., Liseitsev Yu. Effect of thermomechanical processing of building stainless wire to increase its durability. *Case Studies in Construction Materials*. 2023; 19:e02346. <https://doi.org/10.1016/j.cscm.2023.e02346>
3. Volokitina I., Bychkov A., Volokitin A., Kolesnikov A. Natural aging of aluminum alloy 2024 after severe plastic deformation. *Metallography, Microstructure, and Analysis*. 2023;12(3):564–566. <https://doi.org/10.1007/s13632-023-00966-y>
4. Volokitina I., Sapargaliyeva B., Agabekova A., Ulyeva G., Yerzhanov A., Kozlov P. Study of changes in microstructure and metal interface Cu/Al during bimetallic construction wire straining. *Case Studies in Construction Materials*. 2023;18:e02162. <https://doi.org/10.1016/j.cscm.2023.e02162>
5. Gelmanova Z.S., Bazarov B.A., Mezentsseva A.V., Konakbaeva A.N., Tolshov A.K. Industrial safety management at mining enterprises in Kazakhstan. *Mining Informational and Analytical Bulletin*. 2021;(2-1):184–198. (In Russ.). <https://doi.org/10.25018/0236-1493-2021-21-0-184-198>  
Гельманова З.С., Базаров Б.А., Мезенцева А.В., Конакбаева А.Н., Толшов А.К. Управление производственной безопасностью на горнодобывающих предприятиях Казахстана. *Горный информационно-аналитический бюллетень*. 2021;(2-1):184–198. <https://doi.org/10.25018/0236-1493-2021-21-0-184-198>
6. Zhangabay N., Baidilla I., Tagybayev A., Suleimenov U., Kurganbekov Zh., Kambarov M., Kolesnikov A., Ibraimbayeva G., Abshenov Kh., Volokitina I., Nsanbayev B., Anarbayev Y., Kozlov P. Thermophysical indicators of elaborated sandwich cladding constructions with heat-reflective coverings and air gaps. *Case Studies in Construction Materials*. 2023; 18:e02161. <https://doi.org/10.1016/j.cscm.2023.e02161>
7. Volokitina I.E., Volokitin A.V. Changes in microstructure and mechanical properties of steel-copper wire during deformation. *Metallurgist*. 2023;67:232–239. <https://doi.org/10.1007/s11015-023-01510-7>  
Волокитина И.Е., Волокитин А.В. Изменение микроstructures и механических свойств сталемедной проволоки в процессе деформирования. *Металлург*. 2023;(2): 93–99. [https://doi.org/10.52351/00260827\\_2023\\_02\\_93](https://doi.org/10.52351/00260827_2023_02_93)
8. Nurumgaliyev A., Zhuniskaliyev T., Shevko V., Mukhambetgaliyev Y., Yerekeyeva G., Kelamanov B., Kuatbay Y., Badikova A. Modeling and development of technology for smelting a complex alloy (ligature) Fe-Si-Mn-Al from manganese-containing briquettes and high-ash coals. *Scientific Reports*. 2024;14(1):7456. <https://doi.org/10.1038/s41598-024-57529-6>
9. Ruberti M. The chip manufacturing industry: Environmental impacts and eco-efficiency analysis. *Science of the Total Environment*. 2023;858(2):159873. <https://doi.org/10.1016/j.scitotenv.2022.159873>
10. Ma M., Wang T., Ke X., Liu Y., Song Y., Shang X., Li J., Han Q. A novel slag composite for the adsorption of heavy metals: Preparation, characterization and mechanisms. *Environmental Research*. 2023;216(2):114442. <https://doi.org/10.1016/j.envres.2022.114442>
11. Ulyeva G.A., Akhmetova G.E., Tuyskhan K., Tulegenov A.V. State-of-the-Art and analysis of characteristics, properties, significance and application prospects of metallurgical slags. *Progress in Physics of Metals*. 2022;23:108–130. <https://doi.org/10.15407/ufm.23.01.108>
12. Chang Z., Long G., Zhou J., Cong M. Valorization of sewage sludge in the fabrication of construction and building materials: A review. *Resources Conservation and Recycling*. 2020;154:104606. <https://doi.org/10.1016/j.resconrec.2019.104606>
13. Raheem A., Sikarwar V., He J., Dastyar W., Dionysiou D.D., Wang W., Zhao M. Opportunities and challenges in sustainable treatment and resource reuse of sewage sludge: A review. *Chemical Engineering Journal*. 2018;337:616–641. <http://dx.doi.org/10.1016/j.cej.2017.12.149>
14. Ulyeva G.A., Akhmetova G.E., Tuyskhan K., Reshotrina E.N. Development of new composite materials based on “Metal-Non-metal” with improved functional properties. *Metallophysics and Advanced Technologies*. 2022;44:1137–1146. <http://dx.doi.org/10.15407/mfint.44.09.1137>
15. Nowaka O., Enderle P., Varbanov P. Ways to optimize the energy balance of municipal wastewater systems: Lessons learned from Austrian applications. *Journal of Cleaner Production*. 2015;88:125–131. <https://doi.org/10.1016/j.jclepro.2014.08.068>
16. Gavrilin I.V., Kechin V.A., Koltyshev V.I. Method of remelting of dusty silicon waste in the medium of solid liquid aluminum. Patent RU 2180013 C1. Publ. 27.02.2002. Пат. 2180013 C1 RU. Способ переплава пылевидных отходов кремния в среде твердотекучего алюминия / Гаврилин И.В., Кечин В.А., Колтышев В.И.; заявл. 17.07.2000; опубл. 27.02.2002.
17. Lisai V.E., Malen'kikh A.N., Zverev Yu.A., Teplyakov F.K., Gorbunov V.A., Danilov S.N. Method of silicon waste processing. Patent RU 2016110 C1. Publ. 15.07.1994. Пат. 2016110 C1 RU. Способ переработки отходов кремния / Лисай В.Э., Маленьких А.Н., Зверев Ю.А., Тепляков Ф.К., Горбунов В.А., Данилов С.Н.; заявл. 29.12.1991; опубл. 15.07.1994.
18. Wang S., Zhou P., Liu X., Zhang S., Jia Q. Effect of modified coal tar pitch addition on the microstructure and properties of Al<sub>2</sub>O<sub>3</sub>-SiC-C castables for solid waste incinerators. *Ceramics International*. 2022;48(14):20778–20790. <https://doi.org/10.1016/j.ceramint.2022.04.060>
19. Chen G., Li Y., Huang L., Zhang C., Luo X. Preparation of Al-Si alloy from silicon cutting waste: Enabling oxide surface removing and silicon utilization improving via vacuum sintering. *Science of the Total Environment*. 2023;863:161038. <https://doi.org/10.1016/j.scitotenv.2022.161038>
20. Sal'keeva L.K., Sevost'yanova K.A., Kakolina G.M., Tazhbaev E.M., Sugralina L.M., Omasheva A.V. Method of obtaining precipitated silica filler. Patent C01B 33/18. *Bulleten' izobretenii*. 2016;15. Пат. C01B 33/18 RU. Способ получения осажденного кремнеземного наполнителя / Салькеева Л.К., Севостьянова К.А., Каколина Г.М., Тажбаев Е.М., Сугралина Л.М., Омашева А.В.; заявл. 04.02.2013; опубл. 15.11.2016. Бюл. № 15.
21. Liang S., Zhou X., Ruan S., Kastiukas G., Sun Y. Milled waste glass powder in magnesium-silicate-hydrate cement: Technical and environmental assessment. *Journal of Materials in Civil Engineering*. 2023;35(1):04022379. [https://doi.org/10.1061/\(ASCE\)MT.1943-5533.000455](https://doi.org/10.1061/(ASCE)MT.1943-5533.000455)

22. Beskopylny A.N., Stel'makh S.A., Shcherban' E.M., Beskopylny N., El'shaeva D. A study on the cement gel formation process during the creation of nanomodified high-performance concrete based on nanosilica. *Gels*. 2022;8(6):346. <https://doi.org/10.3390/gels8060346>
23. Abdurakhmanov B.M., Kurbanov M.S., Nuraliev U.M., Andriyko L.S. Application of methane and micro silica for silicon carbide synthesis. *Powder Metallurgy and Metal Ceramics*. 2022;61(5–6):298–307. <https://doi.org/10.1007/s11106-022-00317-6>

### Information about the Authors

### Сведения об авторах

**Gulnara A. Ulyeva**, Leading Specialist of the Laboratory of Metallography and Defectoscopy of the Analytical Control Center, JSC "Qarmet"; Cand. Sci. (Eng.), Assist. Prof. of the Chair of Metallurgy and Materials Science, Karaganda State Industrial University

ORCID: 0000-0002-3600-1318

E-mail: [g.ulyeva@tttu.edu.kz](mailto:g.ulyeva@tttu.edu.kz)

**Kurmetbek Tuyskhan**, Master Student, Doctoral, Karaganda State Industrial University

ORCID: 0000-0003-4272-2637

E-mail: [k.tuyskhan@tttu.edu.kz](mailto:k.tuyskhan@tttu.edu.kz)

**Ekaterina M. Matsugina**, MA Student, Karaganda State Industrial University

ORCID: 0009-0002-2550-4822

E-mail: [y.matsugina@tttu.edu.kz](mailto:y.matsugina@tttu.edu.kz)

**Irina E. Volokitina**, PhD, Prof. of the Chair of Metallurgy and Materials Science, Karaganda State Industrial University

ORCID: 0000-0002-2190-5672

E-mail: [irinka.vav@mail.ru](mailto:irinka.vav@mail.ru)

**Gulzhainat E. Akhmetova**, PhD, Assist. Prof. of the Chair of Metallurgy and Materials Science, Karaganda State Industrial University

ORCID: 0000-0001-8244-5027

E-mail: [g.akhmetova@tttu.edu.kz](mailto:g.akhmetova@tttu.edu.kz)

**Гулнара Анатольевна Ульева**, ведущий специалист лаборатории металловедения и дефектоскопии Центра аналитического контроля, АО «Qarmet»; к.т.н, доцент кафедры «Металлургия и материаловедение», Карагандинский государственный индустриальный университет

ORCID: 0000-0002-3600-1318

E-mail: [g.ulyeva@tttu.edu.kz](mailto:g.ulyeva@tttu.edu.kz)

**Курметбек Туысхан**, магистр, докторант, Карагандинский государственный индустриальный университет

ORCID: 0000-0003-4272-2637

E-mail: [k.tuyskhan@tttu.edu.kz](mailto:k.tuyskhan@tttu.edu.kz)

**Екатерина Михайловна Мацугина**, магистрант, Карагандинский государственный индустриальный университет

ORCID: 0009-0002-2550-4822

E-mail: [y.matsugina@tttu.edu.kz](mailto:y.matsugina@tttu.edu.kz)

**Ирина Евгеньевна Волокитина**, к.т.н., профессор кафедры «Металлургия и материаловедение», Карагандинский государственный индустриальный университет

ORCID: 0000-0002-2190-5672

E-mail: [irinka.vav@mail.ru](mailto:irinka.vav@mail.ru)

**Гулъжайнат Есенжоловна Ахметова**, к.т.н., доцент кафедры «Металлургия и материаловедение», Карагандинский государственный индустриальный университет

ORCID: 0000-0001-8244-5027

E-mail: [g.akhmetova@tttu.edu.kz](mailto:g.akhmetova@tttu.edu.kz)

### Contribution of the Authors

### Вклад авторов

**G. A. Ulyeva** – complex metallographic study.

**K. Tuyskhan** – compression testing of samples, tabular and graphical presentation of results.

**E. M. Matsugina** – water absorption testing of samples, statistical processing of obtained data.

**I. E. Volokitina** – problem statement, analysis of research results, formulation of conclusions.

**G. E. Akhmetova** – description of results, formulation of conclusions, critical literary analysis.

**Г. А. Ульева** – комплексное металлографическое исследование.

**К. Туысхан** – испытание образцов на сжатие, табличное и графическое представление результатов.

**Е. М. Мацугина** – испытание образцов на водопоглощение, статистическая обработка полученных данных.

**И. Е. Волокитина** – постановка задачи, анализ результатов исследований, формулировка выводов.

**Г. Е. Ахметова** – описание результатов, формулировка выводов, критический анализ литературы.

Received 13.09.2024

Revised 10.12.2024

Accepted 28.02.2025

Поступила в редакцию 20.10.2024

После доработки 10.12.2024

Принята к публикации 28.02.2025



UDC 538.953

DOI 10.17073/0368-0797-2025-2-139-147



Original article

Оригинальная статья

## INITIATION OF MELTING AT TILT GRAIN BOUNDARIES IN AUSTENITE DEPENDING ON THE MISORIENTATION ANGLE

I. V. Zorya<sup>1</sup>, G. M. Poletaev<sup>2</sup>, Yu. V. Bebikhov<sup>3</sup>, A. S. Semenov<sup>3</sup><sup>1</sup> Siberian State Industrial University (42 Kirova Str., Novokuznetsk, Kemerovo Region – Kuzbass 654007, Russian Federation)<sup>2</sup> Polzunov Altai State Technical University (46 Lenina Ave., Barnaul, Altai Territory 656038, Russian Federation)<sup>3</sup> Mirny Polytechnic Institute (branch) of North-Eastern Federal University (5 Tikhonova Str., Mirnyi, Republic of Sakha (Yakutia) 678170, Russian Federation)

✉ zorya.i@mail.ru

**Abstract.** Using molecular dynamics simulation, the authors studied the influence of misorientation angle and energy of tilt grain boundaries with the misorientation axes  $\langle 100 \rangle$ ,  $\langle 110 \rangle$  and  $\langle 111 \rangle$  on the melting temperature and nature of early initiation of melting at grain boundaries in austenite. It is shown that with gradual heating, melting begins from the grain boundaries, where there is a violation of the crystal structure and, accordingly, the atoms are located in less deep potential wells. In the case of large-angle boundaries, melting begins simultaneously along the entire boundary, in the case of small-angle boundaries – in the cores of grain-boundary dislocations. Dependences of the melting temperature of the simulated calculation cells on the angle of grain misorientation and excess energy were obtained. For the misorientation axes  $\langle 100 \rangle$ ,  $\langle 110 \rangle$  and  $\langle 111 \rangle$ , the results were similar. In the region of small misorientation angles (less than  $15^\circ$ ), the melting point decreases almost linearly with increasing angle, then, for large-angle boundaries, the decrease becomes less intense. These dependences correlate with the energy of grain boundary formation or with the associated excess energy of the calculation cell. The main quantitative criterion determining the effect of defects on a decrease in melting temperature is excess energy, that is, the energy difference between the considered structure and the ideal crystal, which can also be interpreted as the energy of the considered structure formation. The melting point decreases linearly with increasing excess energy. Obviously, the effect of grain boundaries on the melting point becomes significant only for materials with a very high content of grain boundaries, for example, for materials with a nanocrystalline structure.

**Keywords:** molecular dynamics, melting, grain boundary, misorientation angle, austenite

**Acknowledgements:** The research was supported by the Ministry of Science and Higher Education of the Russian Federation (project FZMM-2023-0003) and the Russian Science Foundation (project No. 24-22-00092).

**For citation:** Zorya I.V., Poletaev G.M., Bebikhov Yu.V., Semenov A.S. Initiation of melting at tilt grain boundaries in austenite depending on the misorientation angle. *Izvestiya. Ferrous Metallurgy*. 2025;68(2):139–147. <https://doi.org/10.17073/0368-0797-2025-2-139-147>

## ИНИЦИАЦИЯ ПЛАВЛЕНИЯ НА ГРАНИЦАХ ЗЕРЕН НАКЛОНА В АУСТЕНИТЕ В ЗАВИСИМОСТИ ОТ УГЛА РАЗОРИЕНТАЦИИ

И. В. Зоря<sup>1</sup>, Г. М. Полетаев<sup>2</sup>, Ю. В. Бебихов<sup>3</sup>, А. С. Семенов<sup>3</sup><sup>1</sup> Сибирский государственный индустриальный университет (Россия, 654007, Кемеровская обл. – Кузбасс, Новокузнецк, ул. Кирова, 42)<sup>2</sup> Алтайский государственный технический университет им. И.И. Ползунова (Россия, 656038, Алтайский край, Барнаул, пр. Ленина, 46)<sup>3</sup> Политехнический институт Северо-Восточного федерального университета им. М.К. Аммосова (Россия, 678170, Республика Саха (Якутия), Мирный, ул. Тихонова, 5)

✉ zorya.i@mail.ru

**Аннотация.** С помощью молекулярно-динамического моделирования проведено исследование влияния угла разориентации и энергии границ зерен наклона с осями разориентации  $\langle 100 \rangle$ ,  $\langle 110 \rangle$  и  $\langle 111 \rangle$  на температуру плавления и характер начальной инициации плавления на границе зерен в аустените. Показано, что при постепенном нагревании плавление начинается от границ зерен, там, где имеются нарушения кристаллической структуры и, соответственно, атомы находятся в менее глубоких потенциальных ямах. В случае большеугловых границ плавление начинается одновременно вдоль всей границы, в случае малоугловых – в ядрах зернограницных дислокаций. Получены зависимости температуры плавления моделируемых расчетных ячеек от угла разориентации зерен и избыточной энергии. Для осей разориентации  $\langle 100 \rangle$ ,  $\langle 110 \rangle$  и  $\langle 111 \rangle$  результаты оказались аналогичными. В области малых углов разориентации (менее  $15^\circ$ ) темпе-

ратура плавления с ростом угла падает почти линейно, затем, для большеугловых границ, снижение становится менее интенсивным. Эти зависимости коррелируют с энергией образования границ зерен или со связанной с ней величиной избыточной энергии расчетной ячейки. Главным количественным критерием, определяющим влияние дефектов на снижение температуры плавления, является избыточная энергия, то есть разность энергий рассматриваемой структуры и идеального кристалла, которую еще можно интерпретировать как энергию образования рассматриваемой структуры. Температура плавления линейно уменьшается с ростом избыточной энергии. Очевидно, что данный эффект, то есть влияние границ зерен на температуру плавления, становится существенным только для материалов с очень высоким содержанием границ зерен, например, для материалов с нанокристаллической структурой.

**Ключевые слова:** молекулярная динамика, плавление, граница зерен, угол разориентации, аустенит

**Благодарности:** Исследование выполнено при финансовой поддержке Министерства науки и высшего образования Российской Федерации (проект FZMM-2023-0003) и Российского научного фонда (проект № 24-22-00092).

**Для цитирования:** Зоря И.В., Полетаев Г.М., Бебихов Ю.В., Семенов А.С. Инициация плавления на границах зерен наклона в аустените в зависимости от угла разориентации. *Известия вузов. Черная металлургия.* 2025;68(2):139–147.

<https://doi.org/10.17073/0368-0797-2025-2-139-147>

## INTRODUCTION

In recent decades, considerable attention has been paid to nanocrystalline materials, which include polycrystals with an average grain size of less than 100 nm. These materials exhibit size-dependent physical and mechanical properties, primarily due to a significantly higher volume fraction of grain boundaries, triple junctions, and other defects compared to conventional coarse-grained counterparts [1–3]. Ultrafine grain sizes are achieved using various methods, which typically include severe plastic deformation. Such materials can also be produced by sintering nanopowders, vapor-phase condensation, or other nanostructuring methods. A characteristic feature of nanocrystalline materials is their highly non-equilibrium structure, associated with a significant level of excess (or stored) energy [1–3]. Excess energy, i.e., the difference between the free energy of the material and that of an ideal crystal at the same temperature (or, in other words, the energy that can potentially be released during structural transformations such as recrystallization), in nanocrystalline materials arises from the high density of defects: grain boundaries, triple junctions, dislocations, disclinations, and others. The specific set and types of defects largely depend on the method used to produce the nanocrystalline structure and the subsequent treatment [1–4].

The unique properties of nanomaterials are largely determined by the high volume fraction of surface area and other interfaces (interphase or intergranular boundaries). One of these properties, which is important from both an application and manufacturing standpoint, is the dependence of melting temperature on effective size: grain size, film thickness, or nanoparticle diameter. The dependence of the melting point of nanoparticles on their size is the most thoroughly studied. It is currently well established that the melting temperature of spherical nanoparticles is inversely proportional to their diameter, a finding demonstrated both experimentally [5–9] and through molecular dynamics (MD) simulations [10–14], as well as supported by theoretical models [15–20].

As for materials with a nanocrystalline structure, studies [21–25] employing MD simulations have shown that melting in such materials is not a homogeneous process: it usually starts from free surfaces and grain boundaries. A reduction in the average grain size leads to a decrease in the melting temperature of nanocrystalline silver [22; 23] and aluminum [24; 25]. Similar findings were reported in [14; 26], where nanocrystalline nickel particles exhibited a lower melting point compared to monocrystalline counterparts.

The phenomenon of melting point reduction as a function of average grain size in nanocrystalline materials, in comparison with monocrystalline nanoparticles, is more complex and less thoroughly understood. This complexity arises from the presence of not a single type of defect (such as particle surfaces), but rather a broad spectrum of grain boundaries with varying energies, along with other structural defects. This study investigates the influence of the misorientation angle and the corresponding energy of tilt grain boundaries on the melting temperature and the mechanism of melting initiation at the boundary. Tilt boundaries with misorientation axes  $\langle 100 \rangle$ ,  $\langle 110 \rangle$  and  $\langle 111 \rangle$  are examined. Austenite is chosen as the model material due to its widespread practical applications.

## MODEL DESCRIPTION

To describe interatomic interactions in the molecular dynamics model, an embedded atom method (EAM) potential was employed [27]. This potential was developed based on comparisons with experimental data and *ab initio* calculations of various properties of austenite. It reliably reproduces a wide range of mechanical and structural-energetic properties and has been successfully validated in simulations of various processes, including melting [27–29].

The calculation cells had a parallelepiped shape with approximate dimensions of  $9.9 \times 10.8 \times 13.5$  nm and contained about 118,000 atoms (Fig. 1). A tilt grain boundary was introduced at the center of the calculation cell by rotating two crystals, i.e., the two halves of the cell, by

a misorientation angle  $\theta$  around the  $\langle 100 \rangle$ ,  $\langle 110 \rangle$  or  $\langle 111 \rangle$  axis, which coincided with the  $x$ -axis in Fig. 1. To keep the grain boundary positioned at the center of the calculation cell throughout the simulation, fixed boundary conditions were applied along the  $z$ -axis (at the top and bottom of the calculation cell in Fig. 1): atoms shown in dark gray remained stationary during the simulation. Periodic boundary conditions were applied along the other directions. As a result, two parallel, identical grain boundaries were present in the calculation cell. Fig. 1 shows an example of the calculation cell visualized using the *Common Neighbor Analysis* (CNA) method [30], highlighting the presence of two boundaries – one in the center and one at the edge of the cell – with a misorientation axis of  $\langle 111 \rangle$  and a misorientation angle of  $30^\circ$  (hereafter referred to as  $\langle 111 \rangle 30^\circ$ ). After the rotation of the crystals and the removal of overlapping atoms, the structure was relaxed for 20 ps at a constant temperature of 1000 K. During relaxation, atoms shifted into positions cor-

responding to the local energy minimum. Fig. 1 shows the calculation cell after structural relaxation.

The misorientation angle  $\theta$  for the  $\langle 100 \rangle$ ,  $\langle 110 \rangle$  and  $\langle 111 \rangle$  grain boundaries was varied from  $0^\circ$  to  $30^\circ$ . Thus, half of the boundaries considered (up to  $15^\circ$ ) corresponded to small-angle grain boundaries, i.e., boundaries with clearly distinguishable geometrically necessary grain-boundary dislocations, while the other half (above  $15^\circ$ ) represented large-angle grain boundaries. As will be shown below, the main characteristic influencing the melting process is the grain boundary energy, which is typically nearly constant for large-angle boundaries. This is why, for example, most angles between boundaries at triple junctions tend to be close to  $120^\circ$  [31; 32]. For this reason, the misorientation angle was limited to  $30^\circ$  for all types of tilt boundaries considered in the present study.

The model employed an NPT ensemble in combination with a Nosé–Hoover thermostat. During melting, the specific volume increases due to the destruction of the crystal lattice; therefore, it was important to maintain constant pressure at zero. Thermal expansion with increasing temperature was taken into account, including for the fixed regions at the boundaries of the calculation cell (the dark gray regions in Fig. 1). A time integration step of 2 fs was used in the molecular dynamics simulations.

To determine the melting temperature, the gradual heating method was applied, involving the construction of dependence of the average atomic potential energy on temperature – a commonly used approach in similar studies [10–14; 26; 33–35]. The temperature was increased linearly at a rate of  $10^{12}$  K/s by correspondingly scaling the magnitudes of atomic velocities at regular time intervals (5 ps in this case).

## RESULTS AND DISCUSSION

Fig. 2 shows examples of the dependencies of the average atomic potential energy on temperature for calculation cells with  $\langle 111 \rangle 6^\circ$  (curve 3) and  $\langle 111 \rangle 30^\circ$  (curve 4) grain boundaries, as well as for monocrystalline austenite (curves 1 and 2), during gradual heating at a rate of  $10^{12}$  K/s in the range from 1500 to 2300 K. As the temperature increases, the average atomic energy within the same phase increases almost linearly due to enhanced thermal vibrations of the atoms and thermal expansion. A sharp rise in the average atomic energy on the plots corresponds to a phase transition, i.e., melting.

As previously noted, the structure in the fixed boundary regions (Fig. 1) remained crystalline even after melting, which clearly affects the melting behavior and temperature of the entire calculation cell. Nevertheless, the use of fixed boundaries was necessary to preserve the grain boundaries with the initially assigned

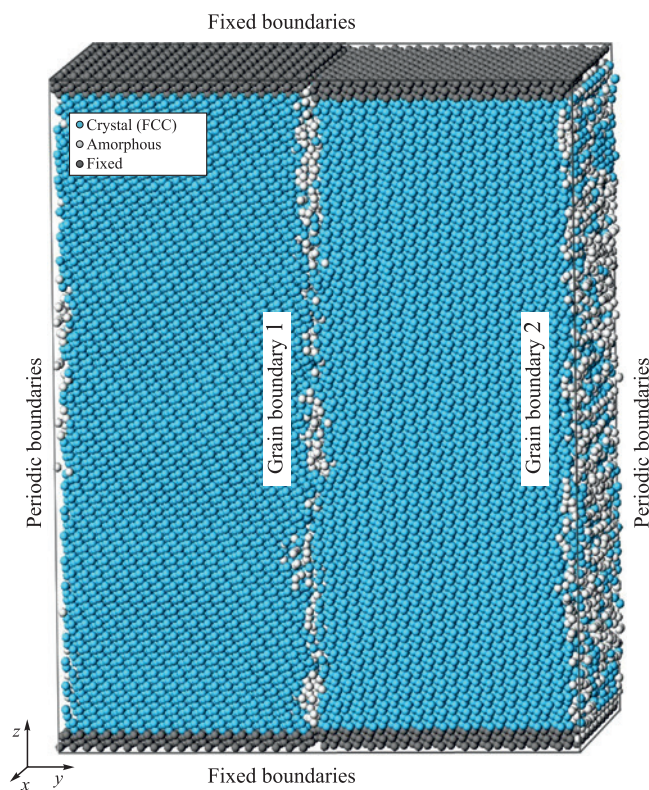


**Fig. 1.** Example of a calculation cell containing two tilt boundaries  $\langle 111 \rangle 30^\circ$

(blue – atoms whose immediate environment corresponds to the FCC crystal lattice of austenite; white – crystal lattice was not identified; dark gray – atoms remained stationary during the simulation)

**Рис. 1.** Пример расчетной ячейки, содержащей две границы наклона  $\langle 111 \rangle 30^\circ$

(голубым цветом показаны атомы, ближайшее окружение которых соответствует ГЦК кристаллической решетки аустенита; белым – кристаллическая решетка не идентифицирована; темно-серым – атомы, которые оставались неподвижными в течение моделирования)

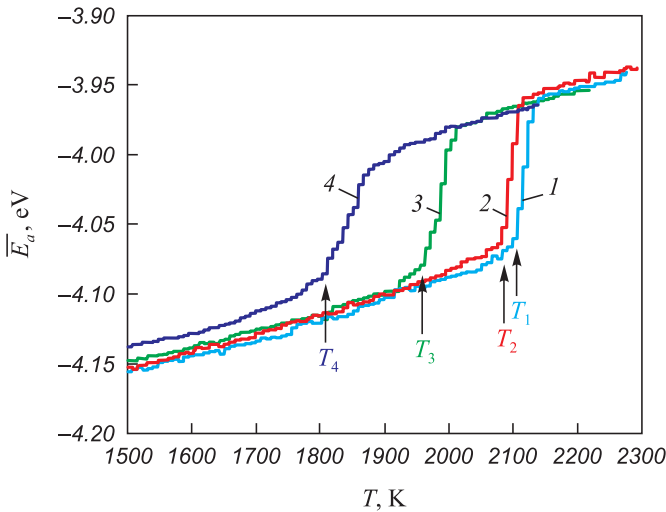


**Fig. 2.** Dependences of the average potential energy of an atom on temperature when heated at a rate of  $10^{12}$  K/s: 1 – for monocrystalline austenite with boundaries fixed along  $z$  axis; 2 – with periodic boundary conditions on all sides; 3 – for a computational cell with two tilt boundaries  $\langle 111 \rangle 6^\circ$ ; 4 – with two tilt boundaries  $\langle 111 \rangle 30^\circ$  at corresponding melting temperatures  $T_1, T_2, T_3$  and  $T_4$

**Рис. 2.** Зависимости средней потенциальной энергии атома от температуры при нагревании со скоростью  $10^{12}$  К/с: 1 – для монокристаллического аустенита с зафиксированными вдоль оси  $z$  границами; 2 – с периодическими граничными условиями со всех сторон; 3 – для расчетной ячейки с двумя границами наклона  $\langle 111 \rangle 6^\circ$ ; 4 – с двумя границами наклона  $\langle 111 \rangle 30^\circ$  при соответствующих температурах плавления  $T_1, T_2, T_3$  и  $T_4$

characteristics within the cell throughout the simulation. For monocrystalline austenite, i.e., a calculation cell without any defects, an additional analysis was carried out to evaluate the influence of fixed boundaries on the melting temperature. Fig. 2 presents the temperature dependence of the average atomic energy for the monocrystal: with fixed boundaries (curve 1) and with periodic boundaries on all sides (curve 2). As can be seen, melting in the presence of fixed boundaries indeed occurred at a higher temperature compared to the case with fully periodic boundary conditions. However, this difference was minor and had little effect on the qualitative results of the study.

In the presence of grain boundaries within the calculation cell, melting proceeded heterogeneously, meaning that it was initiated at the grain boundary, after which the solid–liquid front advanced from the boundary toward the center of the grains at a finite velocity, which is known to depend on temperature. The velocity was on the order of several tens of meters per second [36; 37]. Static two-phase coexistence, i.e., the simultaneous presence of part of the calculation cell in the liquid state and another part in the crystalline state for a relatively long period, was not observed: the solid–liquid front consistently advanced in one direction or another. Therefore, the melting temperature was determined based on the onset of the phase tran-

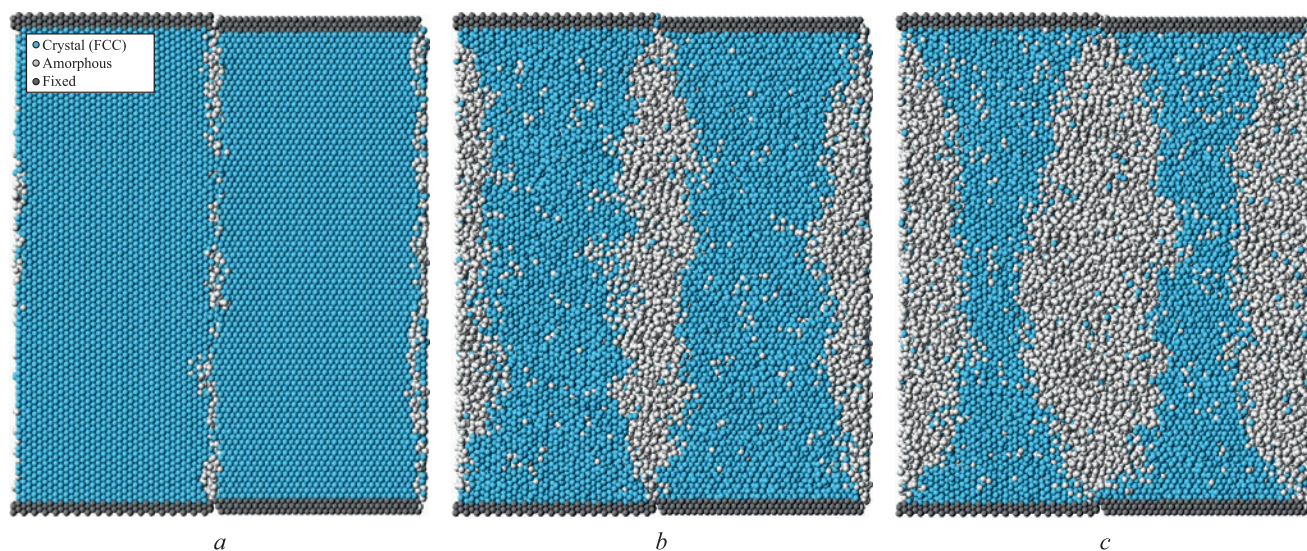
sition (indicated by arrows in Fig. 2), which in turn was identified as the intersection point of the linear approximations before and after the start of melting.

Fig. 2 clearly shows that the calculation cell containing a large-angle  $\langle 111 \rangle 30^\circ$  grain boundary melts at a significantly lower temperature (1835 K) than the one with the small-angle  $\langle 111 \rangle 6^\circ$  boundary (2013 K), confirming the influence of grain boundary type on melting behavior. The grain boundary energy, and consequently the degree of disruption of the crystalline structure, is higher in the case of the large-angle boundary.

Fig. 3 shows a calculation cell in the  $yz$ -plane containing two large-angle  $\langle 111 \rangle 30^\circ$  boundaries at different stages of melting, visualized using a structure identification tool based on the *Common Neighbor Analysis* (CNA) method [30]. This method allows each atom to be classified according to its local crystalline environment by analyzing the arrangement of its neighboring atoms. In the present case, an atom was considered to belong to an FCC lattice if more than 75 % of its nearest neighbors were located near the lattice sites of an ideal FCC crystal (taking into account thermal expansion), within a tolerance of 25 % of the first coordination sphere radius. Atoms that did not satisfy these conditions, or the conditions for classification as HCP, were considered to be part of an amorphous structure (shown in white in Fig. 3).

Fig. 3, *a* shows the relaxed initial structure of the calculation cell with two parallel  $\langle 111 \rangle 30^\circ$  boundaries. In the case of a large-angle boundary, the defect appears almost continuous: disruption of the crystalline structure is observed along the entire boundary. As the temperature increased, melting began almost uniformly along the boundary (Fig. 3, *b*), except near the fixed boundaries (at the top and bottom of the calculation cell), which is expected, as the influence of the constrained crystalline structure at those boundaries becomes significant in those regions.

With further temperature increase, the solid–liquid front propagated from the grain boundaries into the bulk of the material (Fig. 3, *c*). The number of atoms in the amorphous phase (shown in white) increased accordingly. It can be observed that melting initiation at the boundary occurred even at a lower temperature than the melting point determined from the energy – temperature plot for the entire calculation cell (Fig. 2). This is due to the fact that the melting temperature of the entire calculation cell is influenced by the grain boundary density. A similar dependence was observed in [22 – 25] as the average grain size in nanocrystalline silver or aluminum decreased, the melting temperature also decreased. In the present case, this implies that, for example, an increase in the size of the cell along the  $y$ -axis would reduce the influence of the grain boundary on the overall melting temperature.



**Fig. 3.** Melting from large-angle grain boundaries  $\langle 111 \rangle 30^\circ$  during heating at a rate of  $10^{12}$  K/s:

*a* – initial structure of the calculation cell at *yz* plane; *b* and *c* – structure of the calculation cell when temperature reaches 1810 and 1830 K

**Рис. 3.** Плавление от большеугловых границ зерен  $\langle 111 \rangle 30^\circ$  в процессе нагревания со скоростью  $10^{12}$  К/с:

*a* – начальная структура расчетной ячейки в плоскости *yz*; *b* и *c* – структура расчетной ячейки при достижении температуры 1810 и 1830 К

Melting initiates at grain boundaries because the crystalline structure is more easily disrupted in their vicinity. This occurs because atoms located in defect regions are situated in shallower potential wells compared to those in a perfect crystal, and can escape more easily due to thermal vibrations. Atoms located near the solid–liquid interface on the crystalline side are also found in relatively shallow potential wells, as the atomic arrangement on the molten side is more disordered. In addition, the melt exhibits more intense self-diffusion and a greater amount of free volume compared to the crystal. These factors also

contribute to easier disruption of the crystal structure near the interface than within the bulk of the crystal, and thus drive the motion of the solid–liquid front.

Fig. 4 shows a calculation cell containing two small-angle  $\langle 111 \rangle 6^\circ$  grain boundaries at different time points during the heating process. The structure of small-angle tilt boundaries is known to consist of an array of geometrically necessary grain-boundary dislocations, provided that no additional defects are introduced. Fig. 4, *a* displays the initial structure of the calculation cell, where the cores of the grain-boundary dislocations are clearly

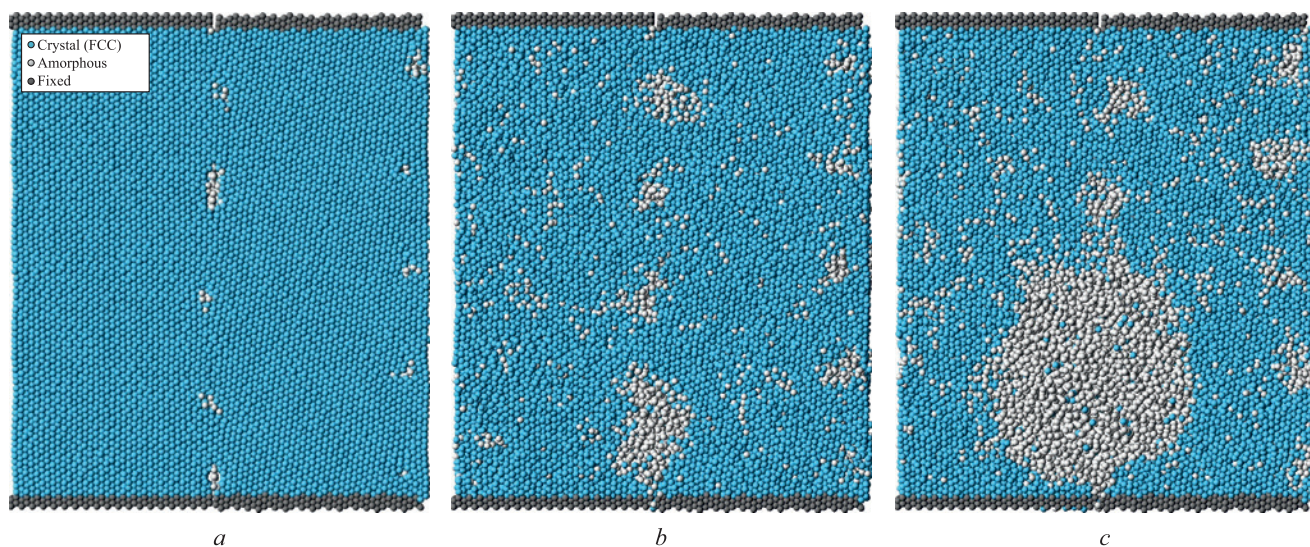


**Fig. 4.** Melting from small-angle grain boundaries  $\langle 111 \rangle 6^\circ$  during heating at a rate of  $10^{12}$  K/s:

*a* – initial structure of the calculation cell at *yz* plane; *b* and *c* – structure of the calculation cell when temperature reaches 1980 and 2000 K

**Рис. 4.** Плавление от малоугловых границ зерен  $\langle 111 \rangle 6^\circ$  в процессе нагревания со скоростью  $10^{12}$  К/с:

*a* – начальная структура расчетной ячейки в плоскости *yz*; *b* и *c* – структура расчетной ячейки при достижении температуры 1980 и 2000 К

visible. These appear as small regions of disrupted crystalline order (white atoms) periodically arranged along the boundaries. For a misorientation angle of 6°, the distance between dislocations is sufficiently large, and it is clearly seen that the structure between them remains fully crystalline, with no visible disorder. Melting initiated from the dislocation cores (Fig. 4, b) as the crystalline structure began to break down. In this case, melting began at a higher temperature compared to that observed for the large-angle grain boundary. As the temperature continued to increase, some amorphous regions grew more rapidly, merged, and eventually spread throughout the entire volume.

Fig. 5, a shows the dependences of the melting point  $T_m$  of the calculation cell on the misorientation angle  $\theta$  for all grain boundaries considered in the study. The resulting dependences were identical for all three grain boundary misorientation axes  $\langle 100 \rangle$ ,  $\langle 110 \rangle$  and  $\langle 111 \rangle$ . It should be noted that special misorientation angles, i.e., those characterized by a high degree of atomic coincidence between adjacent grains, were not considered in this study.

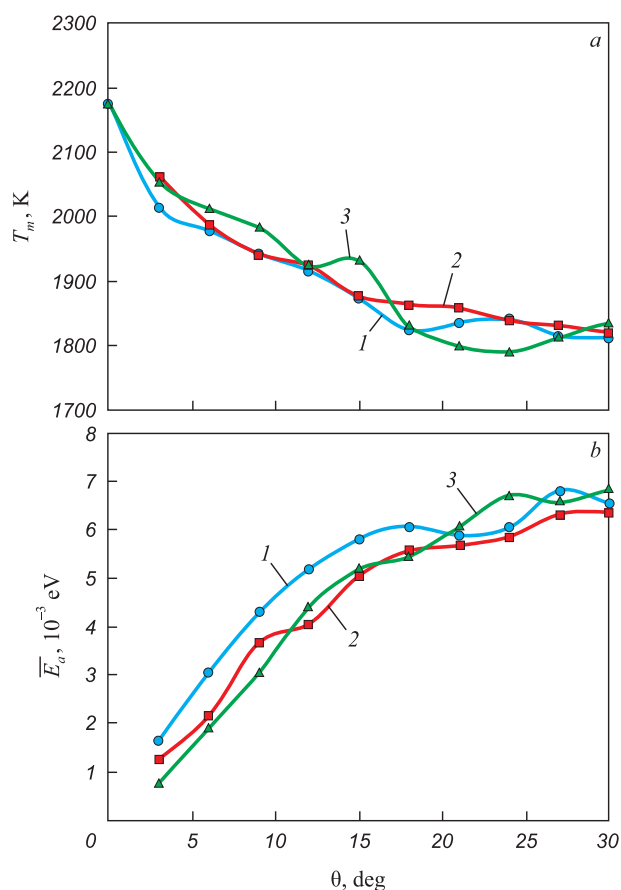


**Fig. 5.** Dependences of the melting point of the calculation cell  $T_m$  (a) and the excess energy per atom,  $\Delta E_a$  (b) on misorientation angle: 1 –  $\langle 100 \rangle$ ; 2 –  $\langle 110 \rangle$ ; 3 –  $\langle 111 \rangle$

**Рис. 5.** Зависимости температуры плавления расчетной ячейки  $T_m$  (a) и избыточной энергии  $\Delta E_a$ , приходящейся на один атом (b), от угла разориентации  $\theta$ : 1 –  $\langle 100 \rangle$ ; 2 –  $\langle 110 \rangle$ ; 3 –  $\langle 111 \rangle$

As the misorientation angle  $\theta$  increases in the low-angle range (less than 15°), the melting point decreases almost linearly. For large-angle grain boundaries, the decrease becomes less pronounced. The obtained  $T_m(\theta)$  dependences correlate with the grain boundary energy or with the associated value of excess energy of the calculation cell. Fig. 5, b shows the dependences of the excess energy per atom  $\Delta E_a$ , on the misorientation angle  $\theta$ . This excess energy was calculated as the difference between the average potential energy per atom in a calculation cell containing a pair of the studied grain boundaries, and that in an ideal crystal containing the same number of atoms.

The obtained  $\Delta E_a(\theta)$  dependences are typical of the angular dependences of grain boundary energy [38 – 40]. Initially, up to approximately  $\theta = 15^\circ$  (i.e., for small-angle grain boundaries), the excess energy increases almost linearly, which is due to the linear increase in the density of grain-boundary dislocations. At larger misorientation angles (above  $\sim 15^\circ$ ), the dislocation cores merge into a single extended defect, and the energy increases more slowly with increasing  $\theta$ .

The obtained dependencies indicate a correlation between  $T_m$  and  $\Delta E_a$ . To verify this, the  $T_m(\Delta E_a)$  dependence was plotted (Fig. 6). Within the studied range of  $\Delta E_a$  values, the relationship is approximately linear and follows the equation  $T_m = -49,828\Delta E_a + 2,135$  (shown as a dashed line).

Thus, it can be concluded that the main quantitative criterion determining the influence of defects on the reduction of the melting point is the excess energy – that is, the difference between the energy of the structure under consideration and that of an ideal crystal. This

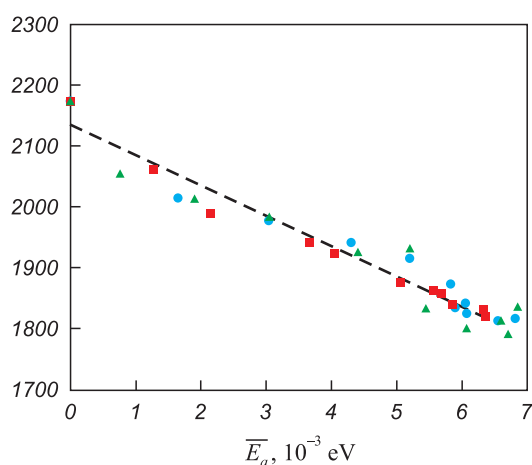


**Fig. 6.** Dependence of the melting point on the excess energy per atom: ●, ■, ▲ – results of the model for misorientation axes  $\langle 100 \rangle$ ,  $\langle 110 \rangle$  and  $\langle 111 \rangle$ , dashed line – linear approximation

**Рис. 6.** Зависимость температуры плавления от избыточной энергии, приходящейся на один атом: ●, ■, ▲ – результаты модели для осей разориентации  $\langle 100 \rangle$ ,  $\langle 110 \rangle$  и  $\langle 111 \rangle$ , штриховая линия – линейная аппроксимация

quantity can also be interpreted as the formation energy of the given structure or as the energy potentially released during structural transformation, such as recrystallization. The observed linear dependence is likely due to the fact that the excess energy reflects the reduction in work required to break the crystal lattice during melting – or, put differently, the corresponding decrease in the material's heat of fusion.

## CONCLUSIONS

Molecular dynamics simulations were used to investigate the effect of the misorientation angle and grain boundary energy of tilt boundaries with misorientation axes  $\langle 100 \rangle$ ,  $\langle 110 \rangle$  and  $\langle 111 \rangle$  on the melting temperature and the nature of melting initiation at grain boundaries in austenite. The results show that during gradual heating, melting begins at the grain boundaries, where the crystal structure is disrupted and atoms are located in shallower potential wells. For large-angle boundaries, melting is initiated simultaneously along the entire boundary, whereas for small-angle boundaries, it starts at the cores of grain-boundary dislocations. Dependences of the melting temperature of the simulated calculation cells on the grain misorientation angle and excess energy were obtained. Similar results were observed for the  $\langle 100 \rangle$ ,  $\langle 110 \rangle$  and  $\langle 111 \rangle$  misorientation axes. In the range of low misorientation angles (less than  $15^\circ$ ), the melting point decreases almost linearly as the angle increases. For large-angle boundaries, the decrease becomes less pronounced. These dependences correlate with the grain boundary energy or the corresponding excess energy of the calculation cell. The key quantitative parameter determining the influence of defects on the reduction of the melting point is the excess energy – that is, the difference between the energy of the structure under consideration and that of an ideal crystal. This value can also be interpreted as the formation energy of the given structure. A linear decrease in melting point with increasing excess energy was observed. It is clear that this effect – the influence of grain boundaries on the melting point – becomes significant only in materials with a very high content of grain boundaries, such as those with a nanocrystalline structure.

## REFERENCES / СПИСОК ЛИТЕРАТУРЫ

- Gleiter H. Nanostructured materials: Basic concepts and microstructure. *Acta Materialia*. 2000;48(1):1–29. [https://doi.org/10.1016/S1359-6454\(99\)00285-2](https://doi.org/10.1016/S1359-6454(99)00285-2)
- Meyers M.A., Mishra A., Benson D.J. Mechanical properties of nanocrystalline materials. *Progress in Materials Science*. 2006;51(4):427–556. <https://doi.org/10.1016/j.pmatsci.2005.08.003>
- Kumar K.S., Van Swygenhoven H., Suresh S. Mechanical behavior of nanocrystalline metals and alloys. *Acta Materialia*. 2003;51(19):5743–5774. <https://doi.org/10.1016/j.actamat.2003.08.032>
- Nazarov A.A., Murzaev R.T. A method for the construction of initial structures for molecular dynamics simulations of nanocrystals with nonequilibrium grain boundaries containing extrinsic dislocations. *Letters on Materials*. 2018;8(1):5–10. <https://doi.org/10.22226/2410-3535-2018-1-5-10>
- Castro T., Reifemberger R., Choi E., Andres R.P. Size-dependent melting temperature of individual nanometer-sized metallic clusters. *Physical Review B*. 1990;42:8548–8556. <https://doi.org/10.1103/PhysRevB.42.8548>
- Dick K., Dhanasekaran T., Zhang Z., Meisel D. Size-dependent melting of silica-encapsulated gold nanoparticles. *Journal of the American Chemical Society*. 2002;124(10):2312–2317. <https://doi.org/10.1021/ja017281a>
- Hirasawa M., Orii T., Seto T. Size-dependent crystallization of Si nanoparticles. *Applied Physics Letters*. 2006;88(9):093119. <https://doi.org/10.1063/1.2182018>
- Tang S., Zhu S., Lu H., Meng X. Shape evolution and thermal stability of Ag nanoparticles on spherical SiO<sub>2</sub> substrates. *Journal of Solid State Chemistry*. 2008;181(3):587–592. <https://doi.org/10.1016/j.jssc.2008.01.014>
- Kim H.K., Huh S.H., Park J.W., Jeong J.W., Lee G.H. The cluster size dependence of thermal stabilities of both molybdenum and tungsten nanoclusters. *Chemical Physics Letters*. 2002;354(1-2):165–172. [https://doi.org/10.1016/S0009-2614\(02\)00146-X](https://doi.org/10.1016/S0009-2614(02)00146-X)
- Qi Y., Cagin T., Johnson W.L., Goddard III W.A. Melting and crystallization in Ni nanoclusters: The mesoscale regime. *The Journal of Chemical Physics*. 2001;115:385–394. <https://doi.org/10.1063/1.1373664>
- Shim J.-H., Lee B.-J., Cho Y.-W. Thermal stability of unsupported gold nanoparticle: A molecular dynamics study. *Surface Science*. 2002;512(3):262–268. [https://doi.org/10.1016/S0039-6028\(02\)01692-8](https://doi.org/10.1016/S0039-6028(02)01692-8)
- Li X. Modeling the size- and shape- dependent cohesive energy of nanomaterials and its applications in heterogeneous systems. *Nanotechnology*. 2014;25(18):185702. <https://doi.org/10.1088/0957-4484/25/18/185702>
- Chepkasov I.V., Gafner Yu.Ya., Vysotin M.A., Redel' L.V. A study of melting of various types of Pt-Pd nanoparticles. *Physics of the Solid State*. 2017;59:2076–2081. <https://doi.org/10.1134/S1063783417100109>
- Poletaev G.M., Gafner Y.Y., Gafner S.L. Molecular dynamics study of melting, crystallization and devitrification of nickel nanoparticles. *Letters on Materials*. 2023;13(4):298–303.
- Nanda K.K., Sahu S.N., Behera S.N. Liquid-drop model for the size-dependent melting of low-dimensional systems. *Physical Review A*. 2002;66:013208. <https://doi.org/10.1103/PhysRevA.66.013208>
- Qi W.H., Wang M.P., Zhou M., Shen X.Q., Zhang X.F. Modeling cohesive energy and melting temperature of nanocrystals. *Journal of Physics and Chemistry of Solids*. 2006;67(4):851–855. <https://doi.org/10.1016/j.jpccs.2005.12.003>
- Luo W., Hu W., Xiao S. Size effect on the thermodynamic properties of silver nanoparticles. *The Journal of Physical Chemistry C*. 2008;112(7):2359–2369. <https://doi.org/10.1021/jp0770155>

18. Luo W., Deng L., Su K., Li K., Liao G., Xiao S. Gibbs free energy approach to calculate the thermodynamic properties of copper nanocrystals. *Physica B: Condensed Matter*. 2011;406(4):859–863. <https://doi.org/10.1016/j.physb.2010.12.014>
19. Li H., Han P.D., Zhang X.B., Li M. Size-dependent melting point of nanoparticles based on bond number calculation. *Materials Chemistry and Physics*. 2013;137(3):1007–1011. <https://doi.org/10.1016/j.matchemphys.2012.11.016>
20. Zhu J., Fu Q., Xue Y., Cui Z. Accurate thermodynamic relations of the melting temperature of nanocrystals with different shapes and pure theoretical calculation. *Materials Chemistry and Physics*. 2017;192:22–28. <http://dx.doi.org/10.1016/j.matchemphys.2017.01.049>
21. Phillpot S.R., Lutsko J.F., Wolf D., Yip S. Molecular-dynamics study of lattice-defect-nucleated melting in silicon. *Physical Review B*. 1989;40:2831. <https://doi.org/10.1103/PhysRevB.40.2831>
22. Xiao S., Hu W., Yang J. Melting behaviors of nanocrystalline Ag. *The Journal of Physical Chemistry B*. 2005;109(43):20339–20342. <https://doi.org/10.1021/jp054551t>
23. Xiao S., Hu W., Yang J. Melting temperature: From nanocrystalline to amorphous phase. *Journal of Chemical Physics*. 2006;125(18):184504. <https://doi.org/10.1063/1.2371112>
24. Wejrzanowski T., Lewandowska M., Sikorski K., Kurzydowski K.J. Effect of grain size on the melting point of confined thin aluminum films. *Journal of Applied Physics*. 2014;116(16):164302. <https://doi.org/10.1063/1.4899240>
25. Noori Z., Panjepour M., Ahmadian M. Study of the effect of grain size on melting temperature of Al nanocrystals by molecular dynamics simulation. *Journal of Materials Research*. 2015;30:1648–1660. <https://doi.org/10.1557/jmr.2015.109>
26. Poletaev G.M., Bebikhov Y.V., Semenov A.S. Molecular dynamics study of the formation of the nanocrystalline structure in nickel nanoparticles during rapid cooling from the melt. *Materials Chemistry and Physics*. 2023;309:128358. <https://doi.org/10.1016/j.matchemphys.2023.128358>
27. Lau T.T., Först C.J., Lin X., Gale J.D., Yip S., Van Vliet K.J. Many-body potential for point defect clusters in Fe–C alloys. *Physical Review Letters*. 2007;98:215501. <https://doi.org/10.1103/PhysRevLett.98.215501>
28. Oila A., Bull S.J. Atomistic simulation of Fe–C austenite. *Computational Materials Science*. 2009;45(2):235–239. <https://doi.org/10.1016/j.commatsci.2008.09.013>
29. Зоря И.В., Поletaев Г.М., Бибихов Ю.В., Семенов А.С. Молекулярно-динамическое исследование влияния примеси углерода на процесс кристаллизации наночастиц аустенита при быстром охлаждении. *Известия вузов. Черная металлургия*. 2024;67(4):440–448. <https://doi.org/10.17073/0368-0797-2024-4-440-448>  
Zorya I.V., Poletaev G.M., Bebikhov Yu.V., Semenov A.S. Molecular dynamics study of the influence of carbon impurity on austenite nanoparticles crystallization during rapid cooling. *Izvestiya. Ferrous Metallurgy*. 2024;67(4):440–448. <https://doi.org/10.17073/0368-0797-2024-4-440-448>
30. Tsuzuki H., Branicio P.S., Rino J.P. Structural characterization of deformed crystals by analysis of common atomic neighborhood. *Computer Physics Communications*. 2007;177(6):518–523. <https://doi.org/10.1016/j.cpc.2007.05.018>
31. Fortes M.A., Deus A.M. Effects of triple grain junctions on equilibrium boundary angles and grain growth kinetics. *Materials Science Forum*. 2004;455–456:648–652. <https://doi.org/10.4028/www.scientific.net/MSF.455-456.648>
32. Perevalova O.B., Konovalova E.V., Koneva N.A., Kozlov E.V. Energy of grain boundaries of different types in fcc solid solutions, ordered alloys and intermetallics with L1(2) superstructure. *Journal of Materials Science & Technology*. 2003;19(6):593–596.
33. Poletaev G., Gafner Y., Gafner S., Bebikhov Y., Semenov A. Molecular dynamics study of the devitrification of amorphous copper nanoparticles in vacuum and in a silver shell. *Metals*. 2023;13(10):1664. <https://doi.org/10.3390/met13101664>
34. Poletaev G.M., Sannikov A.V., Gafner Y.Y., Gafner S.L. Molecular dynamics study of the effect of structural defects, impurities, and the presence of a shell on the melting temperature of metallic nanoparticles. *Letters on Materials*. 2024;14(4):332–339. <https://doi.org/10.48612/letters/2024-4-332-339>
35. Poletaev G.M., Bebikhov Yu.V., Semenov A.S., Sitnikov A.A. Molecular dynamics investigation of the effect of the interface orientation on the intensity of titanium dissolution in crystalline and amorphous aluminum. *Journal of Experimental and Theoretical Physics*. 2023;136(4):477–483. <https://doi.org/10.1134/S1063776123040118>
36. Chan W.-L., Averback R.S., Cahill D.G., Ashkenazy Y. Solidification velocities in deeply undercooled silver. *Physical Review Letters*. 2009;102:095701. <https://doi.org/10.1103/PhysRevLett.102.095701>
37. Zhang H.Y., Liu F., Yang Y., Sun D.Y. The molecular dynamics study of vacancy formation during solidification of pure metals. *Scientific Reports*. 2017;7:10241. <https://doi.org/10.1038/s41598-017-10662-x>
38. Li S., Yang L., Lai C. Atomistic simulations of energies for arbitrary grain boundaries. Part I: Model and validation. *Computational Materials Science*. 2019;161:330–338. <https://doi.org/10.1016/j.commatsci.2019.02.003>
39. Olmsted D.L., Foiles S.M., Holm E.A. Survey of computed grain boundary properties in face-centered cubic metals: I. Grain boundary energy. *Acta Materialia*. 2009;57(13):3694–3703. <https://doi.org/10.1016/j.actamat.2009.04.007>
40. Van Beers P.R.M., Kouznetsova V.G., Geers M.G.D., Tschopp M.A., McDowell D.L. A multiscale model of grain boundary structure and energy: From atomistics to a continuum description. *Acta Materialia*. 2015;82:513–529. <https://doi.org/10.1016/j.actamat.2014.08.045>

## Information about the Authors

## Сведения об авторах

**Irina V. Zorya**, Dr. Sci. (Phys.-Math.), Prof., Head of the Chair of Heat-Gas-Water Supply, Water Disposal and Ventilation, Siberian State Industrial University

ORCID: 0000-0001-5748-813X

E-mail: zorya.i@mail.ru

**Ирина Васильевна Зоря**, д.ф.-м.н., доцент, заведующий кафедрой теплогазоводоснабжения, водоотведения и вентиляции, Сибирский государственный индустриальный университет

ORCID: 0000-0001-5748-813X

E-mail: zorya.i@mail.ru

**Gennadii M. Poletaev**, Dr. Sci. (Phys.-Math.), Prof., Leading Researcher, Polzunov Altai State Technical University  
**ORCID:** 0000-0002-5252-2455  
**E-mail:** gmpoletaev@mail.ru

**Yurii V. Bebikhov**, Dr. Sci. (Phys.-Math.), Assist. Prof., Mirny Polytechnic Institute (branch) of North-Eastern Federal University  
**ORCID:** 0000-0002-8366-4819  
**E-mail:** bebikhov.yura@mail.ru

**Aleksandr S. Semenov**, Dr. Sci. (Phys.-Math.), Director of the Institute, Mirny Polytechnic Institute (branch) of North-Eastern Federal University  
**ORCID:** 0000-0001-9940-3915  
**E-mail:** as.semenov@s-vfu.ru

**Геннадий Михайлович Поletaев**, д.ф.-м.н., профессор, ведущий научный сотрудник, Алтайский государственный технический университет им. И.И. Ползунова  
**ORCID:** 0000-0002-5252-2455  
**E-mail:** gmpoletaev@mail.ru

**Юрий Владимирович Бебихов**, д.ф.-м.н., доцент, Политехнический институт Северо-Восточного федерального университета им. М.К. Аммосова  
**ORCID:** 0000-0002-8366-4819  
**E-mail:** bebikhov.yura@mail.ru

**Александр Сергеевич Семенов**, д.ф.-м.н., директор института, Политехнический институт Северо-Восточного федерального университета им. М.К. Аммосова  
**ORCID:** 0000-0001-9940-3915  
**E-mail:** as.semenov@s-vfu.ru

## Contribution of the Authors

## Вклад авторов

**I. V. Zorya** – problem statement, analysis of literary sources, processing of results, writing the main text of the article.

**G. M. Poletaev** – problem statement, development of a computer model, analysis of literary sources, processing of results, editing the final version of the article.

**Yu. V. Bebikhov** – performing calculations, obtaining results, obtaining drawings and graphs.

**A. S. Semenov** – performing calculations, obtaining results, obtaining drawings and graphs.

**И. В. Зоря** – постановка задачи, анализ литературных источников, обработка результатов, написание основного текста статьи.

**Г. М. Поletaев** – постановка задачи, разработка компьютерной модели, анализ литературных источников, обработка результатов, редактирование финальной версии статьи.

**Ю. В. Бебихов** – проведение расчетов, получение результатов, получение рисунков и графиков.

**А. С. Семенов** – проведение расчетов, получение результатов, получение рисунков и графиков для статьи.

Received 14.11.2024

Revised 25.12.2024

Accepted 10.01.2025

Поступила в редакцию 14.11.2024

После доработки 25.12.2024

Принята к публикации 10.01.2025



UDC 621.785.5

DOI 10.17073/0368-0797-2025-2-148-157



Original article

Оригинальная статья

## ON THE INFLUENCE OF RARE-EARTH OXIDE ADDITIVES ON KINETICS OF BORATED LAYER FORMATION AND BORON DIFFUSION ALONG GRAIN BOUNDARIES DURING STEEL BORIDING

D. A. Ishmametov<sup>1,2</sup>, A. S. Pomel'nikova<sup>1</sup>, A. L. Petelin<sup>1,3</sup><sup>1</sup> Bauman Moscow State Technical University (5/1 Baumanskaya 2-ya Str., Moscow 105005, Russian Federation)<sup>2</sup> Federal State Research and Design Institute of Rare Metal Industry (2, bld. 1 Ehlektrodnaya Str., Moscow 111141, Russian Federation)<sup>3</sup> National University of Science and Technology "MISIS" (4 Leninskii Ave., Moscow 119049, Russian Federation)✉ [ishmametv@yandex.ru](mailto:ishmametv@yandex.ru)

**Abstract.** Metallographic studies showed that the use of rare-earth oxide (REO) additives during liquid electrolysis-free boriding increases the borated layers depth, with these additives not interacting with the treated product material. Addition of lanthanum and yttrium oxides increases the borated layer depth by 30 – 40 %, while addition of scandium oxide either has no effect or decreases the layer depth. X-ray phase analysis of boriding alloys with REO additives was conducted in this study. It was shown that REO additions to the melt result in formation of low-melting rare-earth borates ( $\text{LaBO}_3$ ,  $\text{YBO}_3$ ,  $\text{ScBO}_3$ ), which enhance grain boundary diffusion and significantly intensify the boriding process. Estimated values of bulk and grain boundary diffusion coefficients were obtained. The addition of yttrium oxide increased the bulk diffusion coefficient in VKS-5 steel by 280 %. In Kh12MF steel, addition of lanthanum oxide resulted in an 83 % increase in the bulk diffusion coefficient. For 40Kh steel, no increase in the bulk diffusion coefficient was recorded in any of the investigated cases. The grain boundary diffusion coefficient increased in VKS-5 and Kh12MF steels by 1000 % with addition of lanthanum oxide. Addition of yttrium oxide increased the grain boundary diffusion coefficient by 1000 % in VKS-5 steel, by 135 % in Kh12MF steel, and by 87 % in 40Kh steel. Addition of scandium oxide increased the grain boundary diffusion coefficient by 160 % in VKS-5 steel. The diffusion coefficient values at grain boundaries obtained through modeling calculations agree well with the experimental data.

**Keywords:** boriding, borated layers, rare-earth element, lanthanum oxide, yttrium oxide, scandium oxide, liquid borating, modification, morphology of borated layers, diffusion

**For citation:** Ishmametov D.A., Pomel'nikova A.S., Petelin A.L. On the influence of rare-earth oxide additives on kinetics of borated layer formation and boron diffusion along grain boundaries during steel boriding. *Izvestiya. Ferrous Metallurgy*. 2025;68(2):148–157.

<https://doi.org/10.17073/0368-0797-2025-2-148-157>

# К ВОПРОСУ О ВЛИЯНИИ ДОБАВОК ОКСИДОВ РЕДКОЗЕМЕЛЬНЫХ ЭЛЕМЕНТОВ НА КИНЕТИКУ ОБРАЗОВАНИЯ БОРИРОВАННЫХ СЛОЕВ И ДИФфуЗИЮ БОРА ПО ГРАНИЦАМ ЗЕРЕН ПРИ БОРИРОВАНИИ СТАЛЕЙ

Д. А. Ишмаматов<sup>1,2</sup> , А. С. Помельникова<sup>1</sup>, А. Л. Петелин<sup>1,3</sup>

<sup>1</sup> Московский государственный технический университет им. Н.Э. Баумана (Россия, 105005, Москва, ул. 2-я Бауманская, 5/1)

<sup>2</sup> Государственный научно-исследовательский и проектный институт редкометаллической промышленности (АО «Гиредмет») (Россия, 111141, Москва, Электродная ул., 2, стр. 1)

<sup>3</sup> Национальный исследовательский технологический университет «МИСИС» (Россия, 119049, Москва, Ленинский пр., 4)

 ishmametu@yandex.ru

**Аннотация.** Проведены металлографические исследования, показывающие, что применение добавок оксидов редкоземельных элементов (РЗЭ) при жидкостном безэлектролизном борировании приводит к увеличению глубины борированных слоев, причем данные добавки не взаимодействуют с материалом обрабатываемого изделия. Добавка оксидов лантана и иттрия увеличивает глубину борированного слоя на 30 – 40 %, добавка оксида скандия не влияет или приводит к снижению глубины борированного слоя. В данной работе проведен рентгенофазовый анализ сплавов для борирования с добавками оксидов РЗЭ. Показано, что при добавке оксида РЗЭ в расплаве образуется легкоплавкий борат РЗЭ ( $\text{LaBO}_3$ ,  $\text{YBO}_3$ ,  $\text{ScBO}_3$ ), который способствует зернограничной диффузии, что приводит к значительной интенсификации процессов борирования. Получены оценочные значения коэффициентов объемной и зернограничной диффузии. Добавка оксида иттрия увеличивает коэффициент объемной диффузии в стали ВКС-5 на 280 %. В стали Х12МФ добавка оксида лантана привела к увеличению коэффициента объемной диффузии на 83 %. На стали 40Х во всех исследуемых случаях увеличение коэффициента объемной диффузии не зафиксировано. Коэффициент зернограничной диффузии увеличился в сталях ВКС-5 и Х12МФ на 1000 % при добавке оксида лантана. Добавка оксида иттрия привела к увеличению коэффициента зернограничной диффузии на 1000 % в стали ВКС-5, на 135 % в стали Х12МФ и на 87 % в стали 40Х. Добавка оксида скандия позволила увеличить коэффициент зернограничной диффузии на 160 % в стали ВКС-5. Значения коэффициентов диффузии по границам зерен, полученные путем модельных расчетов, хорошо согласуются с экспериментальными данными.

**Ключевые слова:** борирование, борированные слои, редкоземельный элемент, оксид лантана, оксид иттрия, оксид скандия, жидкостное борирование, модифицирование, морфология борированных слоев, диффузия

**Для цитирования:** Ишмаматов Д.А., Помельникова А.С., Петелин А.Л. К вопросу о влиянии добавок оксидов редкоземельных элементов на кинетику образования борированных слоев и диффузию бора по границам зерен при борировании сталей. *Известия вузов. Черная металлургия*. 2025;68(2):148–157. <https://doi.org/10.17073/0368-0797-2025-2-148-157>

## INTRODUCTION

Although the use of rare-earth metal (REM) additives in liquid boriding increases the depth of borated layers, promotes the formation of complex borides, and improves mechanical properties [1; 2], their application has not become widespread in boriding technologies due to the high cost of such additives. Recent studies on the use of rare-earth oxide (REO) additives in powder boriding [3 – 5] have shown that they produce similar effects. Research into REO additives in liquid electrolysis-free boriding has demonstrated an increase in the depth of borated layers and, in some cases, changes in their morphology [6; 7]. It has been noted that REO additives do not interact with the material being treated and instead act as catalysts in the boriding process [8; 9].

A key factor in controlling the boriding process when using REO additives is understanding the mechanism by which they influence the kinetics of borated layer formation and boron diffusion into the metal [10 – 12].

Although no traces of rare-earth elements are detected in the structure of the treated steels, their presence in the melt can affect the boriding process in several ways [13 – 14].

- Rare-earth oxides may act as catalysts that accelerate chemical reactions in the melt. This can lead to an increased rate of formation of active boron atoms, which diffuse into the steel and ultimately result in deeper borated layers.

- The presence of REO additives alters the physico-chemical properties of the melt, such as viscosity, surface tension, and ion distribution. These changes may promote more uniform and active interaction between boron and the steel surface, enhancing boron penetration depth.

- REO additives may influence the structure and defectiveness of the oxide layer on the steel surface, facilitating more active diffusion of boron atoms into the metal.

- Rare-earth oxides can affect the formation of intermediate phases in the melt or at the steel–melt interface, thereby intensifying the boriding process.

A study reported in the international literature [15] describes the positive effect of cerium oxide addition on the depth of borated layers produced on a Ti6Al4V titanium alloy. The beneficial effect is attributed to the formation of low-melting rare-earth borates, which enhance the transport capacity of the boriding agent. However, that study focuses solely on powder boriding and does not consider the contribution of low-melting RE borate phases to grain boundary diffusion of boron into the material.

The aim of this study is to analyze the effect of rare-earth oxide additives on boron diffusion during the formation of borated layers in steels with different compositions.

## MATERIALS AND METHODS

The steel samples were subjected to liquid electrolysis-free boriding in a melt composed of sodium tetraborate and boron carbide, with lanthanum, yttrium, or scandium oxides added in amounts of 1, 5, 10, and 20 wt. %. The boriding process was conducted at 1000 °C for 8 h, followed by air cooling of the samples.

This study investigated VKS-5, Kh12MF, and 40Kh steels, selected for their varying carbon content and alloying element composition. Their chemical compositions are listed in Table 1.

The microstructure of the samples was examined using a Jeol JXA-iSP100 electron probe microanalyzer. Microstructure images were obtained with a backscattered electron detector.

X-ray phase analysis of the boriding alloy was performed using a BRUKER D2 PHASER X-ray diffractometer.

## RESULTS AND DISCUSSION

As previously shown, the addition of rare-earth oxides has a significant impact on the depth, properties, and, in some cases, the morphology of the resulting borated layers. All steel samples treated in the various melts described in this study were examined using an electron microscope. Fig. 1 presents the microstructures

of borated layers formed on VKS-5 steel in a standard melt and in melts containing 1, 5, 10, and 20 wt. % lanthanum oxide. These images were selected as they clearly illustrate the characteristic features of borated layer formation during liquid boriding with REO additives.

As seen in Fig. 1, the addition of 1 wt. % lanthanum oxide promotes the formation of higher-quality borated layers. With 5 wt. % lanthanum oxide, the penetration depth of the dark, boron-rich FeB phase increases, although this phase forms unevenly. Increasing the additive content to 10 wt. % leads to even deeper FeB penetration, with the dark phase displaying greater continuity. Notably, the deepening zone of the borated layer consists of light, acicular regions that appear as a continuation of the dark layer. This zone reflects the initial accelerated diffusion of boron along the grain boundaries of the matrix, followed by boron penetration into the grain volume from the boundaries, which act as diffusion sources. However, as the diffusant concentration at the boundaries decreases beyond a certain depth, the grains are no longer fully saturated with boron, resulting in a jagged interface at the bottom of the borated layer. Boron partially decorates the grain boundaries, which become visible in the transition to the underlying structure. A network of boride phases along the grain boundaries in the transition zone is observed in all the presented microstructures.

Table 2 presents the data on the depth of borated layers formed in melts with various additives for the steels studied.

Analysis of the data in Table 2 indicates that rare-earth oxide additives influence the depth of the borated layers. However, there appears to be a critical concentration of these additives, beyond which the boriding process slows down and the layer depth decreases. Notably, the addition of scandium oxide does not result in any increase in layer depth. The chemical composition of the steel also plays a significant role in determining the depth of borated layers formed in melts without additives. While previous studies [6; 18] have identified carbon content as the primary factor influencing layer depth, the data in Table 1 show no clear correlation. For example, the low-carbon VKS-5 steel exhibited a layer

Table 1. Chemical composition of the studied steels

Таблица 1. Химический состав исследуемых сталей

Alloy	Element content, wt. %										
	Fe	C	Si	Mn	Cr	Ni	W	V	Mo	Nb	Ce
VKS-5	base	0.15	0.68	0.41	2.80	1.30	1.20	0.41	0.58	0.10	0.03
Kh12MF	base	1.62	0.33	0.30	12.20	0.36	–	0.26	0.41	–	–
40Kh	base	0.41	0.24	0.62	1.10	0.21	–	–	–	–	–

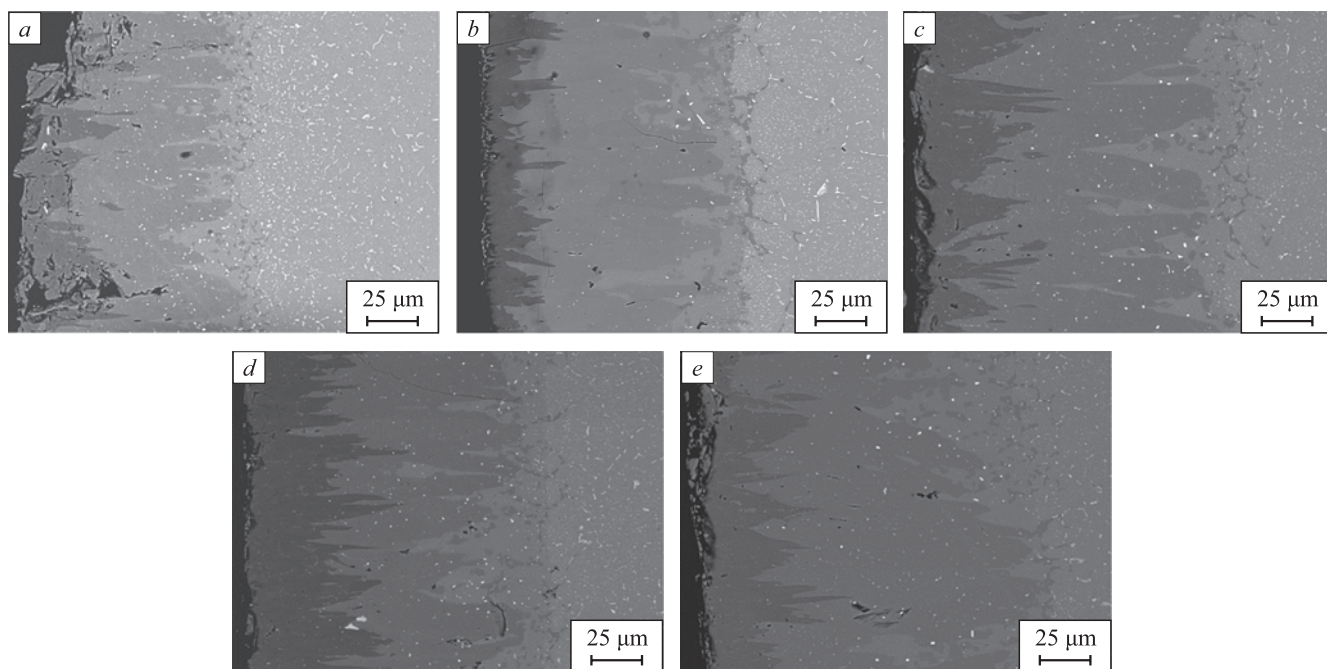


**Fig. 1.** Microstructure of borated layers on VKS-5 steel:

*a* – without lanthanum oxide addition, *b* – with 1 wt. % lanthanum oxide addition, *c* – with 5 wt. % lanthanum oxide addition, *d* – with 10 wt. % lanthanum oxide addition, *e* – with 20 wt. % lanthanum oxide addition

**Рис. 1.** Микроструктура борированных слоев, полученных на стали ВКС-5:

*a* – без добавления оксида лантана; *b* – с добавлением 1 мас. % оксида лантана; *c* – с добавлением 5 мас. % оксида лантана; *d* – с добавлением 10 мас. % оксида лантана; *e* – с добавлением 20 мас. % оксида лантана

depth of 120 – 130 μm; the medium-carbon 40Kh steel reached 240 – 250 μm; whereas the high-carbon Kh12MF steel showed a depth of only 95 – 105 μm.

**Table 2. Depth data of borated layers in melts with various additives on steels**

**Таблица 2. Данные по глубинам борированных слоев, полученных в расплавах с разными добавками на сталях**

Composition	Depth of borated layers, μm		
	VKS-5	Kh12MF	40Kh
No additive	120 – 130	95 – 105	240 – 250
1 % La <sub>2</sub> O <sub>3</sub>	120 – 130	100 – 105	240 – 250
5 % La <sub>2</sub> O <sub>3</sub>	150 – 160	140 – 145	260 – 270
10 % La <sub>2</sub> O <sub>3</sub>	160 – 170	118 – 124	270 – 275
20 % La <sub>2</sub> O <sub>3</sub>	150 – 160	100 – 105	268 – 274
1 % Y <sub>2</sub> O <sub>3</sub>	100 – 105	95 – 105	200 – 220
5 % Y <sub>2</sub> O <sub>3</sub>	235 – 245	120 – 130	140 – 150
10 % Y <sub>2</sub> O <sub>3</sub>	165 – 170	95 – 100	210 – 230
20 % Y <sub>2</sub> O <sub>3</sub>	105 – 115	100 – 105	160 – 170
1 % Sc <sub>2</sub> O <sub>3</sub>	122 – 126	95 – 110	235 – 245
5 % Sc <sub>2</sub> O <sub>3</sub>	128 – 134	76 – 82	155 – 162
10 % Sc <sub>2</sub> O <sub>3</sub>	127 – 133	87 – 96	158 – 164
20 % Sc <sub>2</sub> O <sub>3</sub>	64 – 79	0	103 – 113

Given that the addition of 5 wt. % rare-earth oxide (REO) consistently resulted in increased borated layer depth, the compositions of melts containing 5 wt. % REO were analyzed in detail.

Figs. 2 – 4 show the X-ray diffraction patterns of boriding melts with various REO additives.

These diffraction patterns reveal the formation of a new phase in all melts – rare-earth borates (LaBO<sub>3</sub>, YBO<sub>3</sub>, ScBO<sub>3</sub>). According to previous studies [14 – 16], these compounds are low-melting. It was also observed during melt preparation that adding up to 10 wt. % REO improved melt fluidity.

X-ray phase analysis suggests that the presence of a low-melting phase in the melt increases its fluidity and likely promotes faster diffusion of boron atoms into the steel. Given that the boriding temperature is 1000 °C – within the range where grain boundary diffusion dominates over bulk diffusion ( $T < 0.7T_m$  [17]) – it can be assumed that boron initially diffuses rapidly along grain boundaries (GB), followed by penetration into the grain interiors from these boundaries, which serve as diffusion sources. This is due to the fact that the activation energy for grain boundary diffusion is considerably lower than for bulk diffusion, making it the preferred pathway under these conditions. This assumption is supported by the observed morphology of the borated layers – specifically, the presence of light acicular regions within

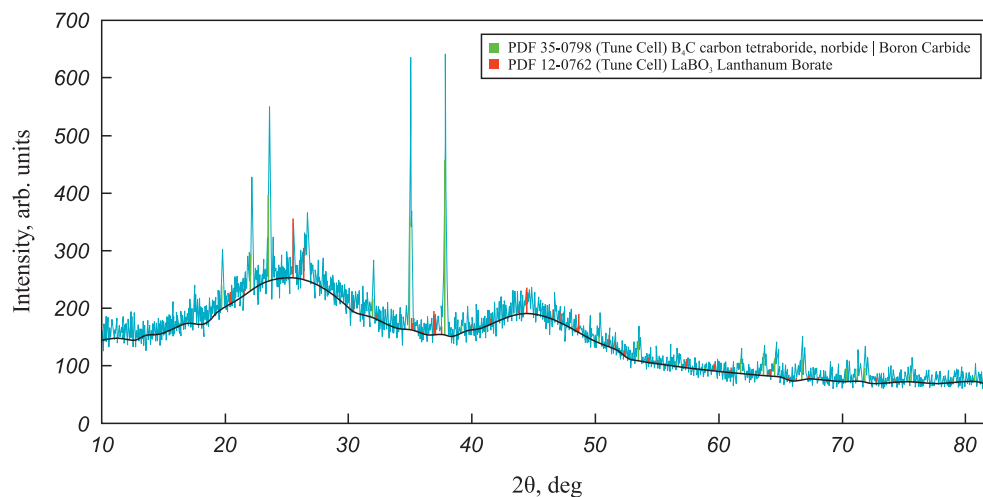


**Fig. 2.** Diffraction pattern of the melt with 5 wt. % lanthanum oxide addition

**Рис. 2.** Дифрактограмма расплава с добавкой 5 мас. % оксида лантана

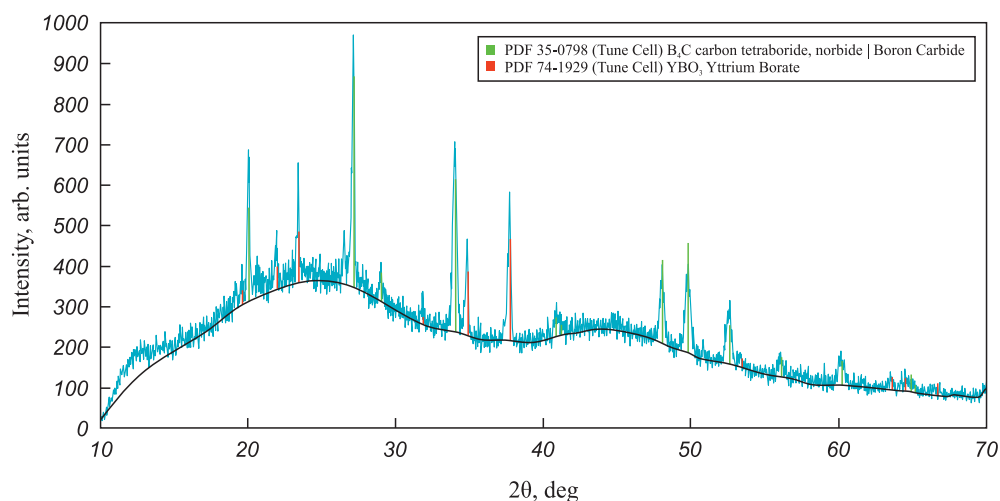


**Fig. 3.** Diffraction pattern of the melt with 5 wt. % yttrium oxide addition

**Рис. 3.** Дифрактограмма расплава с добавкой 5 мас. % оксида иттрия

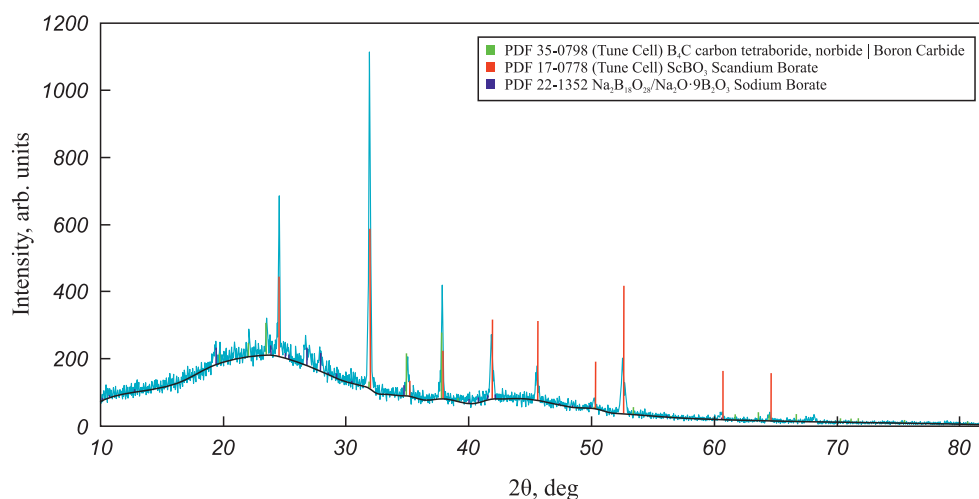


**Fig. 4.** Diffraction pattern of the melt with 5 wt. % scandium oxide addition

**Рис. 4.** Дифрактограмма расплава с добавкой 5 мас. % оксида скандия

the layer and a boride network along grain boundaries in the transition zone.

It is also reasonable to hypothesize that the low-melting RE borate phase acts as a transport medium, enhancing the delivery of boron atoms to grain boundary outlets at the matrix surface. Grain boundary diffusion, being faster than bulk diffusion, creates leading boron fluxes into the steel. This results in a higher concentration of boron in the reaction zone, thereby accelerating the boriding process.

In light of the presumed substantial role of REO additives in promoting grain boundary diffusion, it is appropriate to assess the depth of boron penetration for different melt compositions and to estimate the bulk and grain boundary diffusion coefficients of boron in the studied steels.

Based on the metallographic analysis, the following characteristic depths were determined.

- $h$  – the depth of the borated layer where bulk diffusion is the dominant mechanism. In this zone, boron enrichment occurs primarily through lattice diffusion, as the supply of boron atoms to the grain boundaries (GBs) is limited and no low-melting transport medium is present. The contribution of grain boundary diffusion in this region is minimal or absent, and the boron distribution is governed solely by bulk diffusion.

- $L_b$  – the grain boundary diffusion path, defined as the distance from the sample surface to the depth where boron enrichment along grain boundaries significantly decreases (approximately by a factor of  $e$ ).

- $L_v$  – the bulk diffusion path of boron during the saturation of grain interiors from the grain boundaries, which act as sources of boron atoms – that is, in the presence of grain boundary diffusion fluxes.

Fig. 5 illustrates the zones within the borated layer corresponding to these parameters.

The bulk diffusion coefficient of boron in the steels was estimated using the equation provided in [18]:

$$h = \sqrt{D\tau}, \quad (1)$$

where  $h$  is the layer depth,  $\mu\text{m}$ ;  $D$  is the bulk diffusion coefficient of boron,  $\text{m}^2/\text{s}$ ;  $\tau$  is the boriding time,  $\text{s}$ .

Table 3 summarizes the average values of  $h$ ,  $L_b$ ,  $L_v$  obtained from metallographic observations.

Analysis of the data in Table 3 shows that rare-earth oxide (REO) additives significantly affect the depth of the borated layers. In VKS-5 steel, which has a fine-grained structure (approximately  $5 - 8 \mu\text{m}$ ), grain boundary diffusion contributes most prominently – particularly with the addition of yttrium and lanthanum oxides – reflected in the increased  $L_b$  values. Kh12MF steel, with a slightly larger grain size ( $8 - 12 \mu\text{m}$ ),

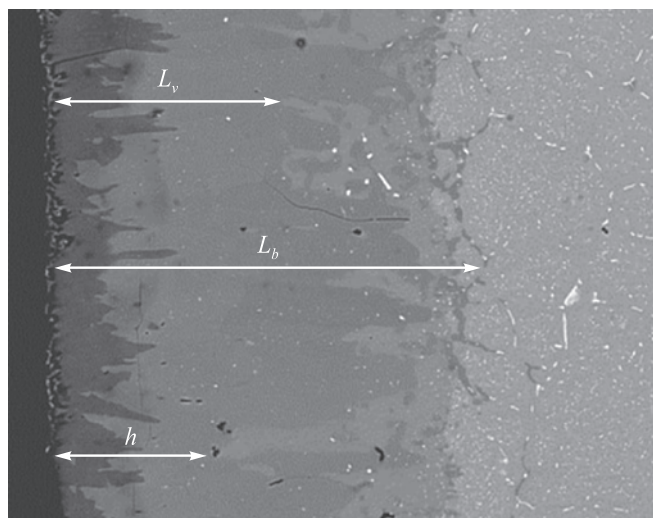


Fig. 5. Structure of the borated layer with marked depths  $h$ ,  $L_b$ ,  $L_v$ .

Рис. 5. Структура борированного слоя с отмеченными глубинами  $h$ ,  $L_b$ ,  $L_v$ .

demonstrates similar trends, though the effect is less pronounced. In contrast, 40Kh steel, with coarser grains ( $12 - 18 \mu\text{m}$ ), shows the weakest response to REO additions. These findings confirm that fine-grained structures enhance grain boundary diffusion, while in steels with larger grains, bulk diffusion plays a more dominant role in borated layer formation.

To predict the kinetics of borated layer formation during liquid boriding with REO additions, estimated calculations of the grain boundary diffusion coefficient ( $D_b$ ) can be performed. The  $L_b$  values can also be estimated using the formulas proposed in [19; 20] and compared with experimental values obtained through microstructural analysis. This comparison helps validate the reliability of the grain boundary diffusion coefficients derived from the experimental data.

An estimated calculation of  $L_b$  was performed using Equation (2), as proposed in [19; 20], with  $L_v$  and  $D$  values taken from Table 2. The average grain sizes were  $5 - 8 \mu\text{m}$  for VKS-5 steel,  $8 - 12 \mu\text{m}$  for Kh12MF steel, and  $12 - 18 \mu\text{m}$  for 40Kh steel:

$$L_v = L_b \left[ 1 + \ln \left( 1 - \frac{4}{\pi} e^{-\frac{\pi^2 D \tau}{l^2}} \right) \right], \quad (2)$$

where  $l$  is the grain size,  $\mu\text{m}$ .

Table 4 presents the  $L_b$  values obtained through estimated calculations using Equation (2) ( $L_{b, \text{calc}}$ ), alongside those determined through microstructural analysis ( $L_{b, \text{exp}}$ ).

The comparison shows that the calculated diffusion lengths closely match the experimental data, with deviations not exceeding 12 %. This consistency supports

Table 3. Average values of  $h$ ,  $L_b$ ,  $L_v$ ,  $D$  for all studied borated layers

Таблица 3. Средние значения  $h$ ,  $L_b$ ,  $L_v$ ,  $D$  для всех исследуемых борированных слоев

Composition	VKS-5				Kh12MF				40Kh			
	$h$ , $\mu\text{m}$	$L_b$ , $\mu\text{m}$	$L_v$ , $\mu\text{m}$	$D$ , $\text{m}^2/\text{s}$	$h$ , $\mu\text{m}$	$L_b$ , $\mu\text{m}$	$L_v$ , $\mu\text{m}$	$D$ , $\text{m}^2/\text{s}$	$h$ , $\mu\text{m}$	$L_b$ , $\mu\text{m}$	$L_v$ , $\mu\text{m}$	$D$ , $\text{m}^2/\text{s}$
No additive	39	140	91	$0.05 \cdot 10^{-12}$	42	105	73	$0.06 \cdot 10^{-12}$	100	250	150	$0.34 \cdot 10^{-12}$
1 % $\text{La}_2\text{O}_3$	52	144	91	$0.09 \cdot 10^{-12}$	42	105	61	$0.06 \cdot 10^{-12}$	75	273	125	$0.19 \cdot 10^{-12}$
5 % $\text{La}_2\text{O}_3$	64	176	96	$0.14 \cdot 10^{-12}$	58	145	102	$0.12 \cdot 10^{-12}$	54	270	162	$0.10 \cdot 10^{-12}$
10 % $\text{La}_2\text{O}_3$	68	187	119	$0.16 \cdot 10^{-12}$	50	124	87	$0.09 \cdot 10^{-12}$	83	303	165	$0.24 \cdot 10^{-12}$
20 % $\text{La}_2\text{O}_3$	62	180	112	$0.13 \cdot 10^{-12}$	42	104	73	$0.06 \cdot 10^{-12}$	81	274	164	$0.23 \cdot 10^{-12}$
1 % $\text{Y}_2\text{O}_3$	31	116	78	$0.03 \cdot 10^{-12}$	31	105	42	$0.03 \cdot 10^{-12}$	66	220	132	$0.15 \cdot 10^{-12}$
5 % $\text{Y}_2\text{O}_3$	74	269	171	$0.19 \cdot 10^{-12}$	52	130	78	$0.09 \cdot 10^{-12}$	45	150	75	$0.07 \cdot 10^{-12}$
10 % $\text{Y}_2\text{O}_3$	68	189	136	$0.16 \cdot 10^{-12}$	30	100	70	$0.03 \cdot 10^{-12}$	69	230	138	$0.17 \cdot 10^{-12}$
20 % $\text{Y}_2\text{O}_3$	46	127	80	$0.07 \cdot 10^{-12}$	51	100	63	$0.09 \cdot 10^{-12}$	51	170	102	$0.09 \cdot 10^{-12}$
1 % $\text{Sc}_2\text{O}_3$	38	139	76	$0.05 \cdot 10^{-12}$	44	110	66	$0.07 \cdot 10^{-12}$	73	245	171	$0.18 \cdot 10^{-12}$
5 % $\text{Sc}_2\text{O}_3$	40	147	94	$0.05 \cdot 10^{-12}$	24	82	57	$0.02 \cdot 10^{-12}$	48	162	113	$0.08 \cdot 10^{-12}$
10 % $\text{Sc}_2\text{O}_3$	53	146	93	$0.09 \cdot 10^{-12}$	29	96	54	$0.03 \cdot 10^{-12}$	49	164	98	$0.08 \cdot 10^{-12}$
20 % $\text{Sc}_2\text{O}_3$	23	87	55	$0.02 \cdot 10^{-12}$	0	0	0	0	34	113	68	$0.04 \cdot 10^{-12}$

the reliability of the calculation method and validates the experimental findings.

Using Equation (3), proposed in [19; 20], and the  $L_b$  values from Table 3, the grain boundary diffusion coefficient ( $D_b$ ) can be estimated:

$$L_b = \sqrt{\frac{D_b \delta l}{8D}} e^{\frac{\pi^2 D \tau}{l^2}}, \quad (3)$$

where  $\delta$  is the interatomic spacing, nm, used to estimate the average grain boundary thickness.

The estimated grain boundary diffusion coefficients are summarized in Table 5.

Analysis of the data in Table 5 shows that the calculated grain boundary diffusion coefficients are generally in good agreement with the experimental values, confirming the adequacy of the chosen calculation approach. In all

Table 4.  $L_{b,calc}$  and  $L_{b,exp}$  values

Таблица 4. Значения  $L_{b,расч}$  и  $L_{b,эксп}$

Composition	VKS-5		Kh12MF		40Kh	
	$L_{b,calc}$	$L_{b,exp}$	$L_{b,calc}$	$L_{b,exp}$	$L_{b,calc}$	$L_{b,exp}$
No additive	137.9	140	95.7	105	213.3	250
1 % $\text{La}_2\text{O}_3$	138.8	144	103.9	105	268.1	273
5 % $\text{La}_2\text{O}_3$	164.8	176	138.5	145	274.4	270
10 % $\text{La}_2\text{O}_3$	164.1	187	136.9	124	306.2	303
20 % $\text{La}_2\text{O}_3$	196.7	180	100.4	104	260.2	274
1 % $\text{Y}_2\text{O}_3$	112.9	116	102.1	105	214.1	220
5 % $\text{Y}_2\text{O}_3$	271.6	269	118.9	130	157.1	150
10 % $\text{Y}_2\text{O}_3$	195.7	189	94.9	100	223.6	230
20 % $\text{Y}_2\text{O}_3$	123.8	127	105.9	100	171.6	170
1 % $\text{Sc}_2\text{O}_3$	127.9	139	104.9	110	249.5	245
5 % $\text{Sc}_2\text{O}_3$	135.4	147	85.2	82	169.1	162
10 % $\text{Sc}_2\text{O}_3$	130.4	146	106.2	96	168.9	164
20 % $\text{Sc}_2\text{O}_3$	81.8	87	0	0	117.3	113

Table 5. Estimated values of grain boundary diffusion coefficients

Таблица 5. Оценочные значения коэффициентов диффузии по ГЗ

Composition	Diffusion coefficients, m <sup>2</sup> /s					
	VKS-5		Kh12MF		40Kh	
	<i>D</i> <sub>b.calc</sub>	<i>D</i> <sub>b.exp</sub>	<i>D</i> <sub>b.calc</sub>	<i>D</i> <sub>b.exp</sub>	<i>D</i> <sub>b.calc</sub>	<i>D</i> <sub>b.exp</sub>
No additive	0.6·10 <sup>-9</sup>	0.6·10 <sup>-9</sup>	0.3·10 <sup>-9</sup>	0.4·10 <sup>-9</sup>	0.9·10 <sup>-8</sup>	0.1·10 <sup>-7</sup>
La <sub>2</sub> O <sub>3</sub> 1 %	0.1·10 <sup>-8</sup>	0.1·10 <sup>-8</sup>	0.4·10 <sup>-9</sup>	0.4·10 <sup>-9</sup>	0.8·10 <sup>-8</sup>	0.9·10 <sup>-8</sup>
La <sub>2</sub> O <sub>3</sub> 5 %	0.2·10 <sup>-8</sup>	0.3·10 <sup>-8</sup>	0.1·10 <sup>-8</sup>	0.2·10 <sup>-8</sup>	0.5·10 <sup>-8</sup>	0.4·10 <sup>-8</sup>
La <sub>2</sub> O <sub>3</sub> 10 %	0.3·10 <sup>-8</sup>	0.3·10 <sup>-8</sup>	0.9·10 <sup>-9</sup>	0.8·10 <sup>-9</sup>	0.1·10 <sup>-7</sup>	0.1·10 <sup>-7</sup>
La <sub>2</sub> O <sub>3</sub> 20 %	0.3·10 <sup>-8</sup>	0.3·10 <sup>-8</sup>	0.4·10 <sup>-9</sup>	0.4·10 <sup>-9</sup>	0.9·10 <sup>-8</sup>	0.1·10 <sup>-7</sup>
Y <sub>2</sub> O <sub>3</sub> 1 %	0.3·10 <sup>-9</sup>	0.3·10 <sup>-9</sup>	0.2·10 <sup>-9</sup>	0.2·10 <sup>-9</sup>	0.4·10 <sup>-8</sup>	0.4·10 <sup>-8</sup>
Y <sub>2</sub> O <sub>3</sub> 5 %	0.8·10 <sup>-8</sup>	0.8·10 <sup>-8</sup>	0.8·10 <sup>-9</sup>	0.9·10 <sup>-9</sup>	0.1·10 <sup>-8</sup>	0.9·10 <sup>-9</sup>
Y <sub>2</sub> O <sub>3</sub> 10 %	0.4·10 <sup>-8</sup>	0.3·10 <sup>-8</sup>	0.2·10 <sup>-9</sup>	0.2·10 <sup>-9</sup>	0.5·10 <sup>-8</sup>	0.5·10 <sup>-8</sup>
Y <sub>2</sub> O <sub>3</sub> 20 %	0.7·10 <sup>-9</sup>	0.7·10 <sup>-9</sup>	0.6·10 <sup>-9</sup>	0.5·10 <sup>-9</sup>	0.2·10 <sup>-8</sup>	0.1·10 <sup>-8</sup>
Sc <sub>2</sub> O <sub>3</sub> 1 %	0.5·10 <sup>-9</sup>	0.6·10 <sup>-9</sup>	0.4·10 <sup>-9</sup>	0.5·10 <sup>-9</sup>	0.7·10 <sup>-8</sup>	0.6·10 <sup>-8</sup>
Sc <sub>2</sub> O <sub>3</sub> 5 %	0.6·10 <sup>-9</sup>	0.7·10 <sup>-9</sup>	0.1·10 <sup>-9</sup>	0.1·10 <sup>-9</sup>	0.1·10 <sup>-8</sup>	0.1·10 <sup>-8</sup>
Sc <sub>2</sub> O <sub>3</sub> 10 %	0.9·10 <sup>-9</sup>	0.1·10 <sup>-9</sup>	0.2·10 <sup>-9</sup>	0.2·10 <sup>-9</sup>	0.1·10 <sup>-8</sup>	0.1·10 <sup>-8</sup>
Sc <sub>2</sub> O <sub>3</sub> 20 %	0.1·10 <sup>-9</sup>	0.1·10 <sup>-9</sup>	0	0	0.3·10 <sup>-9</sup>	0.3·10 <sup>-9</sup>

the steels studied – particularly in VKS-5 – an increase in boron penetration into the matrix was observed with the addition of lanthanum and yttrium oxides.

## CONCLUSIONS

The structure of borated layers formed in melts containing 5, 10, and 20 wt. % of lanthanum, yttrium, and scandium oxides was investigated. The depth of the resulting layers was measured. It was found that additions of lanthanum and yttrium oxides significantly increase the depth of the borated layers, whereas scandium oxide either has no effect or reduces the layer depth.

X-ray phase analysis revealed the formation of low-melting rare-earth borates (LaBO<sub>3</sub>, YBO<sub>3</sub>, ScBO<sub>3</sub>) in the boriding melts. These phases improve the fluidity of the melt, facilitating more efficient transport of boron atoms to the grain boundaries and enhancing their delivery into the steel. This leads to higher boron concentrations within the grains and plays a key role in forming deeper and more uniform borated layers.

Estimated values of both bulk and grain boundary diffusion coefficients were obtained. The addition of yttrium oxide increased the bulk diffusion coefficient in VKS-5 steel by 280 %. In Kh12MF steel, lanthanum oxide led to an 83 % increase. In 40Kh steel, no increase in the bulk diffusion coefficient was recorded in any of the studied cases. The addition of lanthanum oxide resulted in a 1000 % increase in the grain boundary diffusion coefficient in VKS-5 and Kh12MF steels. The addition

of yttrium oxide resulted in a 1000 % increase in grain boundary diffusion in VKS-5 steel, 135 % in Kh12MF, and 87 % in 40Kh. The addition of scandium oxide led to a 160 % increase in grain boundary diffusion in VKS-5.

VKS-5 steel exhibited the strongest response to REO additions, attributed to its fine-grained structure and the dominant role of grain boundary diffusion. In Kh12MF steel, which has a medium grain size, the effect was noticeable but less pronounced. In 40Kh steel, which has a coarser grain structure, REO additions in some cases contribute to an increase in boriding depth, although bulk diffusion remains significant.

The grain boundary diffusion coefficients obtained through modeling were in good agreement with experimental values, confirming the reliability of the calculation methods and their suitability for modeling diffusion processes in steels.

## REFERENCES / СПИСОК ЛИТЕРАТУРЫ

1. Dozmorov S.V., Bakhmat V.V., Antipov I.A., Lozmorova E.V., Brynskii A.A., Kopachev V.Ya. Composition for boriding steel products from melt. Patent SU no. 1617046. MPK C23C 8/44. *Bulleten' izobretenii*. 1990;(48). (In Russ.). Пат. 1617046 SU. Состав для борирования стальных изделий из расплава / Дозморов С.В., Бахмат В.В., Антипов И.А., Лозморова Е.В., Брынский А.А., Копачев В.Я.; заявлено 20.06.1988; опубликовано 30.12.1990. Бюллетень № 48.
2. Kovalevskii A.V., Prismotrov E.P., Savel'ev Yu.D., Soroka V.V. Melt for boriding steel products. Patent SU no.

1093727. МПК C23C 8/44. *Bulleten' izobretenii*. 1984;(19). (In Russ.).
- Пат. 1093727 SU. Расплав для борирования стальных изделий / Ковалевский А.В., Присмотров Е.П., Савельев Ю.Д., Сорока В.В.; заявлено 20.10.1982; опубликовано 23.05.1984. Бюллетень № 19.
3. Mei S., Zhang Y., Zheng Q., Fan Y., Lygdenov B., Guryev A. Compound boronizing and its kinetics analysis for H13 steel with rare earth CeO<sub>2</sub> and Cr<sub>2</sub>O<sub>3</sub>. *Applied Sciences*. 2022;12(7):3636. <https://doi.org/10.3390/app12073636>
  4. Zhang Y.W., Zheng Q., Fan Y., Mei S.Q., Lygenov B., Guryev A. Effects of CeO<sub>2</sub> content, boronizing temperature and time on the microstructure and properties of boronizing layer of H13 steel. *Materials for Mechanical Engineering*. 2021;45(7):22–26. <https://doi.org/10.4028/www.scientific.net/KEM.45.22>
  5. Santaella C.R.K., Cotinho S.P., Correa O.V., Pillis M.F. Enhancement of the RE-boronizing process through the use of La, Nd, Sm, and Gd compounds. *Journal of Engineering Research*. 2022;2(14):2–7. <https://doi.org/10.22533/at.ed.3172142206074>
  6. Ishmametov D.A., Pomel'nikova A.S. Study of structure and properties of borated layers obtained on steels with different alloying elements by method of liquid electrolysis-free borating in melt with addition of yttrium oxide. *Zagotovitel'nye proizvodstva v mashinostroenii*. 2023;21(11):511–520. (In Russ.). <https://doi.org/10.36652/1684-1107-2023-21-11-511-520>
- Ишмаматов Д.А., Помельникова А.С. Изучение структуры и свойств борированных слоев, полученных на разнOLEгированных сталях методом жидкостного безэлектродного борирования в расплаве с добавкой оксида иттрия. *Zagotovitel'nye proizvodstva v mashinostroenii*. 2023;21(11):511–520. <https://doi.org/10.36652/1684-1107-2023-21-11-511-520>
7. Ishmametov D.A., Pomel'nikova A.S., Romyantseva S.B. Effect of lanthanum oxide on structure and properties of borated layers obtained on low-carbon complex-alloyed steel. *Tekhnologiya metallov*. 2024;(5):2–9. (In Russ.). <https://doi.org/10.31044/1684-2499-2024-0-5-2-9>
- Ишмаматов Д.А., Помельникова А.С., Румянцева С.Б. Влияние оксида лантана на структуру и свойства борированных слоев, полученных на низкоуглеродистой сложнOLEгированной стали. *Технология металлов*. 2024;(5):2–9. <https://doi.org/10.31044/1684-2499-2024-0-5-2-9>
8. Ishmametov D.A., Pomel'nikova A.S., Romyantseva S.B. Study of effect of lanthanum oxide on kinetics, morphology and properties of borated layers obtained by liquid method on different carbon content steels. *Uprochnyayushchie tekhnologii i pokrytiya*. 2024;20(4):174–180. (In Russ.). <https://doi.org/10.36652/1813-1336-2024-20-4-174-180>
- Ишмаматов Д.А., Помельникова А.С., Румянцева С.Б. Исследование влияния оксида лантана на кинетику, морфологию и свойства борированных слоев, полученных жидкостным методом на сталях с разным содержанием углерода. *Упрочняющие технологии и покрытия*. 2024;20(4):174–180. <https://doi.org/10.36652/1813-1336-2024-20-4-174-180>
9. Greco A., Mistry K., Sista V., Eryilmaz O., Erdemir A. Friction and wear behaviour of boron-based surface treatment and nano-particle. *Wear*. 2011;271(9–10):1754–1760. <https://doi.org/10.1016/j.wear.2010.11.060>
  10. Lin N., Zhou P., Zhou H., Guo J., Zhang H., Zou J., Ma Y., Han P., Tang B. Pack boronizing of P110 oil casing tube steel to combat wear and corrosion. *International Journal of Electrochemical Science*. 2015;10(3):2694–2706. [https://doi.org/10.1016/S1452-3981\(23\)04878-2](https://doi.org/10.1016/S1452-3981(23)04878-2)
  11. Wang D., Li Y.D., Zhang X.L. A novel steel RE-borosulphurizing and mechanical properties of the produced RE-borosulfide layer. *Applied Surface Science*. 2013;276:236–241. <https://doi.org/10.1016/j.apsusc.2013.03.094>
  12. Chapter 12 – Steel Transformations. In: *Modern Physical Metallurgy*. 8<sup>th</sup> ed. Smallman R.E., Ngan A.H.W. eds. Oxford: Butterworth-Heinemann; 2014:473–498.
  13. Kulka M. Trends in thermochemical techniques of boriding. In: *Current Trends in Boriding*. Cham: Springer; 2019:17–98.
  14. Agarwal S., Kim H.I., Park K., Lee J.Y. Thermodynamic aspects for rare earth metal production. In: *Rare Metal Technology 2020*. Springer; 2020:39–56. [https://doi.org/10.1007/978-3-030-38106-6\\_3](https://doi.org/10.1007/978-3-030-38106-6_3)
  15. Yuan K. A study on RE boronizing process in a titanium alloy. *Journal of Thermal Spray Technology*. 2021;30(4):977–986. <https://doi.org/10.1007/s11666-021-01157-3>
  16. Liu Y.H. *Study on the solid boronizing agents, boronizing process, microstructure and properties of titanium alloy (Ti6Al4V): PhD thesis*. Jiangsu University; 2013.
  17. Bokshstein B.S., Bokshstein S.Z., Zhukhovitskii A.A. Thermodynamics and Kinetics of Diffusion in Solids. Moscow: Metallurgiya; 1974:280. (In Russ.).  
Бокштейн Б.С., Бокштейн С.З., Жуховицкий А.А. Термодинамика и кинетика диффузии в твердых телах. Москва: Metallurgiya; 1974:280.
  18. Krukovich M.G., Prusakov B.A., Sizov I.G. Plasticity of Borated Layers. Moscow: Fizmatlit; 2010:384. (In Russ.).  
Крукович М.Г., Прусаков Б.А., Сизов И.Г. Пластичность борированных слоев. Москва: Физматлит; 2010:384.
  19. Petelin A.L., Plohih A.I. The model of the layer boundary diffusion in multilayer materials. *Izvestiya. Ferrous Metallurgy*. 2015;56(11):45–48. (In Russ.). <https://doi.org/10.17073/0368-0797-2013-11-45-48>
- Петелин А.Л., Плохих А.И. Модель диффузии по границам слоев в многослойных материалах. *Известия вузов. Черная металлургия*. 2015;56(11):45–48. <https://doi.org/10.17073/0368-0797-2013-11-45-48>
20. Polikevich K.B., Petelin A.L., Plokhikh A.I., Fomina L.P. Nitrogen diffusion along the layer boundaries after nitriding of multilayer materials. *Izvestiya. Ferrous Metallurgy*. 2024;67(3):318–324. <https://doi.org/10.17073/0368-0797-2024-3-318-324>
- Поликевич К.Б., Петелин А.Л., Плохих А.И., Фомина Л.П. Диффузия азота по границам слоев при азотировании многослойных материалов. *Известия вузов. Черная металлургия*. 2024;67(3):318–324. <https://doi.org/10.17073/0368-0797-2024-3-318-324>

## Information about the Authors

## Сведения об авторах

**Dmitrii A. Ishmametov**, Postgraduate of the Chair “Materials Science”, Bauman Moscow State Technical University; Head of the Laboratory, Federal State Research and Design Institute of Rare Metal Industry

**ORCID:** 0009-0008-8541-5147

**E-mail:** ishmametu@yandex.ru

**Alla S. Pomel'nikova**, Dr. Sci. (Eng.), Prof. of the Chair “Materials Science”, Bauman Moscow State Technical University

**E-mail:** pomelnikovalla@rambler.ru

**Aleksandr L. Petelin**, Dr. Sci. (Phys.–Math.), Prof., Bauman Moscow State Technical University; Prof. of the Chair of Physical Chemistry, National University of Science and Technology “MISIS”

**E-mail:** alexander-petelin@yandex.ru

**Дмитрий Амирович Ишмаматов**, аспирант кафедры «Материаловедение», Московский государственный технический университет им. Н.Э. Баумана; начальник лаборатории, Государственный научно-исследовательский и проектный институт редкометаллической промышленности (АО «Гиредмет»)

**ORCID:** 0009-0008-8541-5147

**E-mail:** ishmametu@yandex.ru

**Алла Сергеевна Помельникова**, д.т.н., профессор кафедры «Материаловедение», Московский государственный технический университет им. Н.Э. Баумана

**E-mail:** pomelnikovalla@rambler.ru

**Александр Львович Петелин**, д.ф.-м.н., профессор, Московский государственный технический университет им. Н.Э. Баумана; профессор кафедры физической химии, Национальный исследовательский технологический университет «МИСИС»

**E-mail:** alexander-petelin@yandex.ru

## Contribution of the Authors

## Вклад авторов

**D. A. Ishmametov** – literature review, selecting and preparing the research objects.

**A. S. Pomel'nikova** – formation of the research task, conceptualization.

**A. L. Petelin** – development of the mathematical model, calculation of diffusion coefficients for the studied samples.

**Д. А. Ишмаматов** – литературный обзор, выбор и подготовка объектов исследования.

**А. С. Помельникова** – определение проблематики исследования, разработка концепции.

**А. Л. Петелин** – разработка математической модели, расчет коэффициентов диффузии для рассматриваемых объектов исследования.

Received 13.11.2024

Revised 07.02.2025

Accepted 28.02.2025

Поступила в редакцию 13.11.2024

После доработки 07.02.2025

Принята к публикации 28.02.2025



UDC 669.15:544.353:517.26:(546.74+546.76)

DOI 10.17073/0368-0797-2025-2-158-162



Original article

Оригинальная статья

## THERMODYNAMIC SECOND-ORDER INTERACTION COEFFICIENTS OF NITROGEN WITH NICKEL AND CHROMIUM IN LIQUID STEEL

L. A. Bol'shov, S. K. Korneichuk<sup>✉</sup>, E. L. Bol'shova

Vologda State University (15 Lenina Str., Vologda 16000, Russian Federation)

✉ korn62@mail.ru

**Abstract.** The authors propose a simple theory of thermodynamic properties of liquid nitrogen solutions in alloys of the Fe–Ni and Fe–Cr systems. The theory is analogous to the theory of these systems proposed previously by the authors in 2019 and 2021. It is based on lattice model of the Fe–Ni and Fe–Cr solutions. The model assumes a FCC lattice. At the sites of this lattice are the atoms of iron, nickel and chromium. Nitrogen atoms are located in octahedral interstices. Nitrogen atom interacts only with the metal atoms located in the lattice sites neighboring to it. This interaction is pairwise. It is assumed that the energy of this interaction depends neither on composition nor on temperature and the liquid solutions of Fe–Ni and Fe–Cr systems are perfect. For an infinitely nitrogen-diluted solution of this element in the Fe–*j* alloy (*j* = Ni, Cr), a rational nitrogen activity coefficient  $\gamma_N^0$  is determined. Next, we considered the expansion of the function  $\ln \gamma_N^0$  at a constant temperature in a series in powers of the argument  $c_j$ , where  $c_j$  is the concentration of the *j* component, expressed in mole fractions. The coefficient  $J_n$  in the term of the  $n^{\text{th}}$  degree of this expansion is called the thermodynamic  $n^{\text{th}}$  order interaction coefficient of nitrogen with *j* element in liquid steel. In this case,  $J_1 = \varepsilon_N^j$  is called Wagner interaction coefficient,  $J_2 = \rho_N^j$  – the second order interaction coefficient. Within the framework of the presented theory the simplest relationship between the interaction coefficients  $\rho_N^j$  and  $\varepsilon_N^j$  was found. The formula looks like:  $\rho_N^j = \frac{1}{12} (\varepsilon_N^j)^2$ . To verify this formula, experimental data on the solubility of nitrogen in liquid alloys of the Fe–Ni and Fe–Cr systems at a temperature of 1873 K, obtained by Satir-Kolorz and Feichtinger (1991) were used. From these data follows:  $\varepsilon_N^{\text{Ni}} = 2.6$ ;  $\varepsilon_N^{\text{Cr}} = -10.2$ ;  $\rho_N^{\text{Ni}} = 0.8$ ;  $\rho_N^{\text{Cr}} = 6.3$ . The theoretical values calculated using the above formula are as follows:  $\rho_N^{\text{Ni}} = 0.56$ ;  $\rho_N^{\text{Cr}} = 8.67$ . Bearing in mind the significant uncertainty in the experimental determination of the second order interaction coefficient of nitrogen with alloying elements in iron-based binary alloys, the correspondence between the theoretical and experimental results should be considered satisfactory.

**Keywords:** thermodynamics, solution, nitrogen, iron, nickel, chromium, activity coefficient,  $n^{\text{th}}$  order interaction coefficient, Wagner interaction coefficient, Langenberg interaction coefficient

**For citation:** Bol'shov L.A., Korneichuk S.K., Bol'shova E.L. Thermodynamic second-order interaction coefficients of nitrogen with nickel and chromium in liquid steel. *Izvestiya. Ferrous Metallurgy*. 2025;68(2):158–162. <https://doi.org/10.17073/0368-0797-2025-2-158-162>

## ТЕРМОДИНАМИЧЕСКИЕ ПАРАМЕТРЫ ВЗАИМОДЕЙСТВИЯ ВТОРОГО ПОРЯДКА АЗОТА С НИКЕЛЕМ И ХРОМОМ В ЖИДКОЙ СТАЛИ

Л. А. Большов, С. К. Корнейчук<sup>✉</sup>, Э. Л. Большова

Вологодский государственный университет (Россия, 160000, Вологда, ул. Ленина, 15)

✉ korn62@mail.ru

**Аннотация.** Предложена простая теория термодинамических свойств жидких растворов азота в бинарных сплавах систем Fe–Ni и Fe–Cr, которая аналогична теории, предложенной авторами ранее (2019 – 2021). Данная теория основана на решеточной модели растворов Fe–Ni и Fe–Cr. Предполагается модельная решетка типа ГЦК, в узлах которой располагаются атомы железа, никеля и хрома. Атомы азота располагаются в октаэдрических междоузлиях. Атом азота взаимодействует лишь с атомами металлов, находящимися в соседних с этим атомом узлах решетки, и это взаимодействие парное. Предполагается, что энергия этого взаимодействия не зависит ни от состава сплава, ни от температуры, и жидкие растворы систем Fe–Ni и Fe–Cr являются совершенными. Для бесконечно разбавленного по азоту раствора этого элемента в сплаве Fe–*j* (*j* = Ni, Cr) рассматривается рациональный коэффициент активности азота  $\gamma_N^0$ . Далее анализируется разложение функции  $\ln \gamma_N^0$  при постоянной температуре в ряд по степеням аргумента  $c_j$ , где  $c_j$  – концентрация компонента *j*, выраженная в мольных долях. Коэффициент  $J_n$  в члене  $n$ -й степени этого разложения называется термодинамическим параметром взаимодействия  $n$ -го порядка азота с элементом *j* в жидкой стали. При этом  $J_1 = \varepsilon_N^j$  называется вагнеровским параметром взаимодействия, а  $J_2 = \rho_N^j$  – параметром взаимодействия второго порядка. В рамках представленной теории найдена простая связь между параметрами

взаимодействия  $\rho_N^j$  и  $\varepsilon_N^j$ . Формула имеет вид  $\rho_N^j = \frac{1}{12}(\varepsilon_N^j)^2$ , для ее проверки были использованы экспериментальные данные по растворимости азота в жидких сплавах систем Fe–Ni и Fe–Cr при температуре 1873 К, полученные в работе Затир-Колорц и Файхтингера (1991 г.). Из этих данных следует:  $\varepsilon_N^{\text{Ni}} = 2,6$ ;  $\varepsilon_N^{\text{Cr}} = -10,2$ ;  $\rho_N^{\text{Ni}} = 0,8$ ;  $\rho_N^{\text{Cr}} = 6,3$ . Теоретические значения, рассчитанные по приведенной формуле, получились следующими:  $\rho_N^{\text{Ni}} = 0,56$ ;  $\rho_N^{\text{Cr}} = 8,67$ . Имея ввиду значительную экспериментальную неопределенность для параметров взаимодействия  $\rho_N^{\text{Ni}}$  и  $\rho_N^{\text{Cr}}$ , согласие теоретических результатов с экспериментальными следует признать удовлетворительным.

**Ключевые слова:** термодинамика, раствор, азот, железо, никель, хром, коэффициент активности, параметр взаимодействия  $n$ -го порядка, вагнеровский параметр взаимодействия, лангенберговский параметр взаимодействия

**Для цитирования:** Большов Л.А., Корнейчук С.К., Большова Э.Л. Термодинамические параметры взаимодействия второго порядка азота с никелем и хромом в жидкой стали. *Известия вузов. Черная металлургия*. 2025;68(2):158–162.

<https://doi.org/10.17073/0368-0797-2025-2-158-162>

Nitrogen is an element that plays a significant role in steel production [1]. In recent decades, special attention has been given to the production and application of high-nitrogen steels [2; 3], as well as to the behavior of nitrogen in various manufacturing processes [4 – 6]. The solubility of nitrogen in liquid steel is of primary importance [7 – 10]. Research in this area aims to improve the accuracy of solubility predictions and the potential for nitride formation.

Let us consider the thermodynamics of nitrogen solutions in liquid binary Fe– $j$  alloys, where  $j$  represents nickel and chromium. The concentrations of elements in the Fe– $j$ –N solution, expressed in mole fractions, will be denoted as  $c_{\text{Fe}}$ ,  $c_j$  and  $c_N$ , respectively. In practical metallurgy, these concentrations are typically expressed as mass percentages and designated as [% Fe], [%  $j$ ] and [% N].

We will proceed from the concept of the absolute [11] activity of nitrogen in the solution, denoted as  $a_N$ . The rational activity coefficient will be represented as  $\gamma_N$  ( $\gamma_N = a_N/c_N$ ). The mass-percent activity coefficient of nitrogen will be denoted as  $f_N$  ( $f_N = a_N/[\% \text{ N}]$ ). The activity coefficients in an infinitely nitrogen-diluted solution ( $c_N \rightarrow 0$ ; [% N]  $\rightarrow 0$ ) will be denoted as  $\gamma_N^0$  and  $f_N^0$ , respectively. These coefficients will be normalized based on the condition:  $\gamma_N^0 \rightarrow 1$  as  $c_{\text{Fe}} \rightarrow 1$ ;  $f_N^0 \rightarrow 1$  as [% Fe]  $\rightarrow 100$ .

The fundamental concept of the phenomenological thermodynamics of multicomponent dilute alloys was introduced by Wagner [12]. Wagner's idea was applied to the calculation of nitrogen solubility in steel by Langenberg [13]. A significant development of Wagner's approach was presented in [14]. According to this study, within a certain convergence interval, the following expansion holds

$$\ln \gamma_N^0 = \sum_{n=1}^{\infty} J_n c_j^n, \quad (1)$$

where  $J_n$  is the rational  $n$ -th order interaction coefficient. A similar expansion can be written.

$$\lg f_N^0 = \sum_{n=1}^{\infty} \widetilde{J}_n [\% j]^n, \quad (2)$$

where  $\widetilde{J}_n$  is the mass-percent  $n$ -th order interaction coefficient.

For first- and second-order interaction coefficients, there exist more specific notations [12 – 14]:  $J_1 = \varepsilon_N^j$ ;  $J_2 = \rho_N^j$ ;  $\widetilde{J}_1 = e_N^j$ ;  $\widetilde{J}_2 = r_N^j$ , where  $\varepsilon_N^j$  and  $e_N^j$  are the Wagner and Langenberg interaction coefficients, respectively.

Next, we will limit our consideration to the condition of constant temperature  $T = \text{const}$ .

Under this condition, from the invariance of the differential of the logarithm of the activity coefficient, the following relationship was obtained [15]

$$\varepsilon_N^j = 230,3 \frac{A_j}{A_{\text{Fe}}} e_N^j + \frac{A_{\text{Fe}} - A_j}{A_{\text{Fe}}}, \quad (3)$$

where  $A_{\text{Fe}}$  is the atomic mass of iron, and  $A_j$  is the atomic mass of the alloying element  $j$ . Similarly, the following relationship was derived [14]

$$\rho_N^j = \frac{230,3}{A_{\text{Fe}}^2} [100 A_j^2 r_N^j + A_j (A_{\text{Fe}} - A_j) e_N^j] + \frac{1}{2} \left( \frac{A_{\text{Fe}} - A_j}{A_{\text{Fe}}} \right)^2. \quad (4)$$

To measure the thermodynamic parameters of nitrogen interaction with element  $j$  in liquid steel, it is, in principle, sufficient to experimentally study the dependence of nitrogen solubility in a binary Fe– $j$  alloy on the concentration of element  $j$ . The solubility of nitrogen in liquid iron was first measured in 1938 [16]. Shortly thereafter, research on nitrogen solubility in liquid binary iron alloys began [17]. The first-order thermodynamic interaction parameters of nitrogen with alloying elements were thoroughly investigated in studies [18 – 21]. The results of the main stage of experimental research on these parameters were summarized in a review article [22]. Such studies continue to this day [23].

Truncating the power series expansions (1) and (2) while retaining only the linear terms does not allow for an adequate description of the concentration dependence of nitrogen solubility in liquid binary iron alloys for a number of systems. Therefore, it is necessary to account for at least the quadratic terms as well. The technical

capabilities of experimental methods allow for the reliable determination of second-order thermodynamic interaction parameters of nitrogen with an alloying metal only in specific cases. Therefore, a theoretical approach capable of predicting these values would be useful for assessing the reliability of the obtained experimental results.

In this study, we propose a simple model of nitrogen solutions in liquid Fe–*j* (*j* = Ni, Cr) alloys that allows expressing the second-order thermodynamic interaction coefficient  $\rho_N^j$  in terms of the Wagner interaction coefficient  $\varepsilon_N^j$ . The theory is based on a lattice model of Fe–*j* solution. The model assumes a face-centered cubic (FCC) lattice, where the lattice sites are occupied by iron atoms and atoms of element *j*. Nitrogen atoms are located in octahedral interstices. A nitrogen atom interacts only with metal atoms occupying the neighboring lattice sites, and this interaction is pairwise. It is assumed that the energy of this interaction is independent of the alloy composition and temperature. The liquid solutions in the Fe–*j* system are considered ideal. Within the framework of the proposed theory, we express the logarithm of the nitrogen activity coefficient,  $\ln\gamma_N^0$ , in an infinitely nitrogen-diluted solution as a function of the concentration  $c_j$ . In doing so, we use the result obtained in studies [24; 25]:

$$\ln\gamma_N^0 = -\delta \ln\left(1 - \frac{1}{\delta} \varepsilon_N^j c_j\right), \quad (5)$$

where  $\delta$  is the number of FCC lattice sites surrounding an octahedral interstice ( $\delta = 6$ ).

Next, we use the logarithmic expansion

$$\ln(1+x) = \sum_{n=1}^{\infty} (-1)^{n+1} \frac{x^n}{n}.$$

It follows that

$$\ln(1-x) = -\sum_{n=1}^{\infty} \frac{x^n}{n}. \quad (6)$$

The radius of convergence for these expansions is equal to 1.

From expressions (5) and (6), we obtain

$$\ln\gamma_N = \delta \sum_{n=1}^{\infty} \frac{1}{n} \left(\frac{\varepsilon_N^j c_j}{\delta}\right)^n. \quad (7)$$

### Thermodynamic interaction coefficients of nitrogen with nickel and chromium in liquid steel

#### Термодинамические параметры взаимодействия азота с никелем и хромом в жидкой стали

<i>j</i>	Experiment [26]				Theory
	$e_N^j$	$\varepsilon_N^j$ , equation (3)	$r_N^j \cdot 10^5$	$\rho_N^j$ , equation (4)	$\rho_N^j$ , equation (8)
Ni	0.110	2.6	3.5	0.8	0.56
Cr	-0.048	-10.2	35.0	6.3	8.67

Thus, for the *n*-th order interaction coefficient of nitrogen with element *j*, we have

$$J_n = \frac{1}{n} \left(\frac{\varepsilon_N^j}{\delta}\right)^n$$

or

$$J_n = \frac{6^{1-n}}{n} \left(\varepsilon_N^j\right)^n.$$

The radius of convergence of expansion (7) is  $\frac{6}{|\varepsilon_N^j|}$ .

For the second-order interaction coefficient  $\rho_N^j = J_2$  we obtain

$$\rho_N^j = \frac{1}{12} \left(\varepsilon_N^j\right)^2. \quad (8)$$

As an experimental validation of equation (8), this study utilizes the results of nitrogen solubility measurements in liquid binary Fe–Ni and Fe–Cr alloys at a temperature of 1873 K and partial nitrogen pressures  $P_{N_2}$  up to 100 bar [26]. A comparison between the theoretical predictions and experimental data is presented in the Table. The results obtained in [26] appear to be more reliable than the data reported in [7–10].

From the Table, it follows that the theoretical calculations based on equation (8) show satisfactory agreement with the experimental data from [26].

### CONCLUSIONS

A model-based theory of structure and interatomic interaction has been applied to nitrogen solutions in liquid alloys of the Fe–Ni and Fe–Cr systems.

Equation (8) has been derived, expressing the second-order thermodynamic interaction coefficients  $\rho_N^{Ni}$  and  $\rho_N^{Cr}$  in liquid steel in terms of the Wagner interaction coefficients  $\varepsilon_N^{Ni}$  and  $\varepsilon_N^{Cr}$  in liquid iron-based alloys. The equation is given by  $\rho_N^j = \frac{1}{12} \left(\varepsilon_N^j\right)^2$ , where *j* = Ni, Cr.

Theoretical values of the second-order interaction coefficients in liquid steel at  $T = 1873$  K were obtained:  $\rho_N^{Ni} = 0.56$  and  $\rho_N^{Cr} = 8.67$ , which show satisfactory agreement with the experimental estimates:  $\rho_N^{Ni} = 0.8$  and  $\rho_N^{Cr} = 6.3$ , as reported in [26].

## REFERENCES / СПИСОК ЛИТЕРАТУРЫ

1. Kostina M.B., Rigina L.G. Nitrogen-containing steels and methods of their production. *Izvestiya. Ferrous Metallurgy*. 2020;63(8):606–622. (In Russ.).  
<https://doi.org/10.17073/0368-0797-2020-8-606-622>  
Костина М.В., Ригина Л.Г. Азотосодержащие стали и способы их производства. *Известия вузов. Черная металлургия*. 2020;63(8):606–622.  
<https://doi.org/10.17073/0368-0797-2020-8-606-622>
2. Rashev Ts. High-Nitrogen Steels. Metallurgy under Pressure. Sofia: Publishing house of the Bulgarian Academy of Science "Professor Marin Drinov"; 1998:268. (In Russ.).  
Рашев Ц. Высокоазотистые стали. Металлургия под давлением. София: Издательство Болгарской АН «Профессор Марин Дринов»; 1998:268.
3. Gavriljuk V.G., Berns H. High Nitrogen Steels: Structure, Properties, Manufacture, Applications. Berlin, Heidelberg, New York: Springer Verlag; 1999:379.
4. Riipi J., Fabritius T., Heikinen E.-P., Kupari P., Kärnä A. Behavior of nitrogen during AOD process. *ISIJ International*. 2009;49(10):1468–1473.  
<https://doi.org/10.2355/isijinternational.49.1468>
5. Sun L.-Y., Li J.-S., Zhang L.-F., Yang S.-F., Chen Y.-F. Production of nitrogen bearing stainless steel by injecting nitrogen gas. *Journal of Iron and Steel Research, International*. 2011;18(11):7–11.  
[https://doi.org/10.1016/S1006-706X\(11\)60109-X](https://doi.org/10.1016/S1006-706X(11)60109-X)
6. Gobinat T.R., Vertivel Murugan R. Denitrogenation model for vacuum tank degasser. *IOP Conference Proceedings: Materials Science and Engineering*. 208;314:012006.  
<https://doi.org/10.1088/1757-899X/314/1/012006>
7. Anson D., Pomfret R., Hendry A. Predicting of the solubility of nitrogen in molten duplex stainless steel. *ISIJ International*. 1966;36(7):750–758.
8. Siwka J. Equilibrium constants and nitrogen activity in liquid metals and iron alloys. *ISIJ International*. 2008;48(4):385–394.  
<https://doi.org/10.2355/isijinternational.48.385>
9. Lysenkova E.V. Improving the accuracy of calculating the solubility of nitrogen and titanium nitride in iron-based melts. Application to nitrogen and titanium alloyed steel: Cand. Tech. Sci. Diss. Moscow: NUST MISIS; 2015:75. (In Russ.).  
Лысенкова Е.В. Повышение точности расчетов растворимости азота и нитрида титана в сплавах на основе железа. Применение к сталям, легированным азотом и титаном: Диссертация ... кандидата технических наук. Москва: МИСиС; 2015:75.
10. Pitkälä J., Hollala L., Jokilockast A. A study of the effect of alloying elements and temperature on nitrogen solubility in industrial stainless steelmaking. *Metallurgical and Materials Transactions B*. 2022;53(4):2364–2376.  
<https://doi.org/10.1007/s11663-022-02534-1>
11. Fowler R.H., Guggenheim E.A. Statistical Thermodynamics. Cambridge: Addison-Wesley Press; 1939:693.  
Фаулер Р., Гуггенгейм Э. Статистическая термодинамика. Москва: Издательство иностранной литературы; 1949:612.
12. Wagner C. Thermodynamics of Alloys. Cambridge; Addison-Wesley Press; 1952:162.
13. Langenberg F.C. Predicting solubility of nitrogen in molten steel. *JOM*. 1956;8(8):1099–1101.  
<https://doi.org/10.1007/BF03377828>
14. Lupis C.H.P., Elliott J.F. Generalized interaction coefficients. Part I. Definitions. *Acta Metallurgica*. 1966;14(4):529–538.  
[https://doi.org/10.1016/0001-6160\(66\)90320-8](https://doi.org/10.1016/0001-6160(66)90320-8)
15. Lupis C.H.P., Elliott J.F. The relation between interaction coefficients  $\epsilon$  and  $e$ . *Transactions of the Metallurgical Society of AIME*. 1965;233(1):257–258.
16. Sieverts A., Zapf G., Moritz H. Die Löslichkeit von Wasserstoff, Deuterium und Stickstoff in Eisen. *Zeitschrift für physikalische Chemie*. 1938;183(1):19–37. (In Germ.).  
<https://doi.org/10.1515/zpch-1939-18304>
17. Brick R.M., Creevy J.A. Solubility of nitrogen in liquid Fe-Cr and Fe-V alloys. *Metals Technology*. 1940;1165:1–10.
18. Schenck H., Froberg M.G., Graf H. Untersuchungen über die Beeinflussung der Gleichgewichte von Stickstoff mit flüssigen Eisenlösungen durch den Zusatz weiterer Elemente (I). *Archiv für das Eisenhüttenwesen*. 1958;29(11):673–676 (In Germ.). <https://doi.org/10.1002/srin.195803011>
19. Schenck H., Froberg M.G., Graf H. Untersuchungen über die Beeinflussung der Gleichgewichte von Stickstoff mit flüssigen Eisenlösungen durch den Zusatz weiterer Elemente (II). *Archiv für das Eisenhüttenwesen*. 1959;30(9):533–537. (In Germ.). <https://doi.org/10.1002/srin.195903074>
20. Maekawa S., Nakagawa Y. Effect of nickel, cobalt, molybdenum, chromium and vanadium on the solubility of nitrogen in liquid iron. (Solubility of nitrogen in liquid iron and liquid alloys. – II.). *Tetsu-to-Hagane*. 1960;46(9):972–976. (In Japan.).  
[https://doi.org/10.2355/tetsutohagane1955.46.9\\_972](https://doi.org/10.2355/tetsutohagane1955.46.9_972)
21. Pehlke R.D., Elliott J.F. Solubility of nitrogen in liquid iron alloys. I. Thermodynamics. *Transactions of the Metallurgical Society of AIME*. 1960;218(6):1088–1101.
22. Sigworth G.K., Elliott J.F. The thermodynamics of liquid dilute iron alloys. *Metal Science*. 1974;8(1):298–310.  
<https://doi.org/10.1179/msc.1974.8.1.298>
23. Shin J., Lee J., Min D.J., Park J. Solubility of nitrogen in high manganese steel (HMnS) melts: Interaction parameter between Mn and N. *Metallurgical and Materials Transactions B*. 2011;42(6):1081–1085.  
<https://doi.org/10.1007/s11663-011-9582-6>
24. Bol'shov L.A. On solubility of nitrogen in liquid multicomponent iron alloys with transition metals. *Izvestiya. Ferrous Metallurgy*. 1982;25(1):8–10. (In Russ.).  
Большов Л.А. О растворимости азота в жидких многокомпонентных сплавах железа с переходными металлами. *Известия вузов. Черная металлургия*. 1982;25(1):8–10.
25. Bol'shov L.A. Statistical theory of multicomponent and low-concentration alloys: Dr. Phys.-Math. Sci. Diss. Moscow: 1991:496. (In Russ.).  
Большов Л.А. Статистическая теория многокомпонентных и малокоцентрированных сплавов. Диссертация ... доктора физико-математических наук. Москва, МГУ; 1991:496.
26. Satir-Kolorz A.H., Feichtinger H.K. On the solubility of nitrogen in liquid iron and steel alloys using elevated pressure. *Zeitschrift für Metallkunde*. 1991;82(9):689–697.

## Information about the Authors

## Сведения об авторах

**Leonid A. Bol'shov**, Dr. Sci. (Phys.–Math.), Prof. of the Chair of Mathematics and Informatics, Vologda State University  
**E-mail:** labolshov@mail.ru

**Svetlana K. Korneichuk**, Cand. Sci. (Phys.–Math.), Assist. Prof. of the Chair of Physics, Vologda State University  
**E-mail:** korn62@mail.ru

**Elina L. Bol'shova**, Assist. Prof. of the Chair of English, Vologda State University  
**E-mail:** labolshov@mail.ru

**Леонид Абрамович Большов**, д.ф.-м.н., профессор кафедры математики и информатики, Вологодский государственный университет  
**E-mail:** labolshov@mail.ru

**Светлана Константиновна Корнейчук**, к.ф.-м.н., доцент кафедры физики, Вологодский государственный университет  
**E-mail:** korn62@mail.ru

**Элина Леонидовна Большова**, доцент кафедры английского языка, Вологодский государственный университет  
**E-mail:** labolshov@mail.ru

## Contribution of the Authors

## Вклад авторов

**L. A. Bol'shov** – formation of the article idea, writing the text.

**S. K. Korneichuk** – verification of the proposed method and results, formatting the paper and accompanying documents.

**E. L. Bol'shova** – translation of English articles, translation into English of the abstract and references.

**Л. А. Большов** – формулировка идеи работы, написание статьи.

**С. К. Корнейчук** – анализ метода и результатов, оформление текста и сопровождающих документов, переписка с редакцией.

**Э. Л. Большова** – перевод англоязычных статей на русский язык, перевод аннотации и библиографического списка на английский язык.

Received 05.06.2024

Revised 26.07.2024

Accepted 12.11.2024

Поступила в редакцию 05.06.2024

После доработки 26.07.2024

Принята к публикации 12.11.2024



UDC 669.12.094.1

DOI 10.17073/0368-0797-2025-2-163-170



Original article

Оригинальная статья

## THERMODYNAMIC MODELLING OF REDUCTION OF IRON ORE MATERIALS BY HYDROGEN-CONTAINING GASES

A. N. Dmitriev<sup>1</sup>, Yu. E. Burova<sup>1</sup>, G. Yu. Vit'kina<sup>1</sup>,  
N. M. Barbin<sup>1,2</sup>, D. I. Terent'yev<sup>2</sup>

<sup>1</sup> Institute of Metallurgy, Ural Branch of the Russian Academy of Sciences (101 Amundsen Str., Yekaterinburg 620016, Russian Federation)

<sup>2</sup> Ural Institute of State Fire Service of EMERCOM of Russia (22 Mira Str., Yekaterinburg 620062, Russian Federation)

✉ [menestrelfox@gmail.com](mailto:menestrelfox@gmail.com)

**Abstract.** The article presents the results of studying the processes of reduction of iron ore titanomagnetite pellets with synthesis gas by means of thermodynamic modeling using the Terra software package. Its use made it possible to model and predict chemical and phase transformations in iron ore titanomagnetite pellets during reduction using hydrogen-containing synthesis gas, taking into account the effect of temperature, hydrogen concentration and other parameters on reduction. Calculations were performed with different gas mixture contents to evaluate the model efficiency. Content of the CO–N<sub>2</sub>–H<sub>2</sub>–CH<sub>4</sub> gas mixture for calculations varied with an increase in CO and H<sub>2</sub>, decrease in N<sub>2</sub> and constant CH<sub>4</sub>. Thermodynamic modeling showed that when balance of the main phases in high-temperature systems is achieved during reduction with various gas mixtures, the concentration of distribution of silicon, aluminum, titanium, magnesium, and calcium elements remains constant. Significant changes are observed in the concentration of iron, vanadium, and manganese, which is associated with the features of reduction process and composition of the gases used. Dependences of the system equilibrium composition on temperature at various element contents were obtained. The constructed thermodynamic model describes the reduction process and can be used to optimize it under various production conditions.

**Keywords:** thermodynamic modeling, reduction, hydrogen, synthesis gas, pellets, titanomagnetite, iron

**Acknowledgements:** The work was performed within the framework of the State assignment of the Institute of Metallurgy, Ural Branch of the Russian Academy of Sciences.

**For citation:** Dmitriev A.N., Burova Yu.E., Vit'kina G.Yu., Barbin N.M., Terent'ev D.I. Thermodynamic modelling of reduction of iron ore materials by hydrogen-containing gases. *Izvestiya. Ferrous Metallurgy*. 2025;68(2):163–170. <https://doi.org/10.17073/0368-0797-2025-2-163-170>

## ТЕРМОДИНАМИЧЕСКОЕ МОДЕЛИРОВАНИЕ ПРОЦЕССА ВОССТАНОВЛЕНИЯ ЖЕЛЕЗОРУДНЫХ МАТЕРИАЛОВ ВОДОРОДСОДЕРЖАЩИМИ ГАЗАМИ

А. Н. Дмитриев<sup>1</sup>, Ю. Е. Бурова<sup>1</sup>, Г. Ю. Витькина<sup>1</sup>,  
Н. М. Барбин<sup>1,2</sup>, Д. И. Терентьев<sup>2</sup>

<sup>1</sup> Институт металлургии Уральского отделения РАН (Россия, 620016, Екатеринбург, ул. Амундсена, 101)

<sup>2</sup> Уральский институт государственной противопожарной службы МЧС России (Россия, 620062, Екатеринбург, ул. Мира, 22)

✉ [menestrelfox@gmail.com](mailto:menestrelfox@gmail.com)

**Аннотация.** В статье представлены результаты исследования процессов восстановления железорудных титаномагнетитовых окатышей синтез-газом с помощью термодинамического моделирования с использованием программного комплекса «Терра». Его применение позволило смоделировать и спрогнозировать химические и фазовые превращения в железорудных титаномагнетитовых окатышах при восстановлении с использованием водородсодержащего синтез-газа, учитывая влияние температуры, концентрации водорода и других параметров. Расчеты проводились с различным содержанием газовой смеси для оценки эффективности модели. Содержание газовой смеси CO–N<sub>2</sub>–H<sub>2</sub>–CH<sub>4</sub> для расчетов изменялось с увеличением CO и H<sub>2</sub>, уменьшением N<sub>2</sub> и постоянным CH<sub>4</sub>. Термодинамическое моделирование показало, что при достижении баланса основных фаз в высокотемпературных системах при восстановлении различными газовыми смесями концентрация распределения кремния, алюминия, титана, магния и кальция остается постоянной. Значительные изме-

нения наблюдаются в концентрации содержания железа, ванадия и марганца, что связано с особенностями процесса восстановления и составом используемых газов. Получены зависимости равновесного состава системы от температуры при различных содержаниях элементов. Построенная термодинамическая модель описывает процесс восстановления и может быть использована для оптимизации данного процесса в различных условиях производства.

**Ключевые слова:** термодинамическое моделирование, восстановление, водород, синтез-газ, окатыши, титаномагнетит, железо

**Благодарности:** Работа выполнена в рамках реализации государственного задания Института металлургии Уральского отделения РАН.

**Для цитирования:** Дмитриев А.Н., Бурова Ю.Е., Витькина Г.Ю., Барбин Н.М., Терентьев Д.И. Термодинамическое моделирование процесса восстановления железорудных материалов водородсодержащими газами. *Известия вузов. Черная металлургия*. 2025;68(2):163–170. <https://doi.org/10.17073/0368-0797-2025-2-163-170>

## INTRODUCTION

Currently, considerable attention is being paid to the development of various approaches to decarbonizing metallurgical production. The conventional blast furnace process for metal production involves the emission of large volumes of carbon dioxide into the atmosphere. One of the possible solutions is to move toward decarbonization without radical changes to the production process by capturing CO<sub>2</sub> emissions followed by their utilization or storage. A more fundamental approach involves replacing carbon monoxide with pure hydrogen or, more feasibly, using synthesis gas – a combination of hydrogen and carbon monoxide – which can substitute a significant portion of solid carbon-based fuel in the blast furnace process and offers the potential for progress toward decarbonization while meeting high environmental standards [1 – 3].

One approach to reducing CO<sub>2</sub> emissions during pig iron production is the injection of coke oven gas and blast furnace gas into the blast furnace in order to decrease the specific coke consumption. For the effective injection of blast furnace gas, the CO<sub>2</sub> and H<sub>2</sub>O content must be minimized as much as possible [4 – 5]. In this regard, coke oven gas is far more suitable from a process standpoint – its CO<sub>2</sub> content is approximately 3 vol. %. For instance, ArcelorMittal has announced the implementation of a coke oven gas injection technology at its plant in Spain<sup>1</sup>. The companies Dillinger and Saarstahl have invested €14 million in a new coke oven gas conversion plant for blast furnace injection at the Rogesa plant<sup>2</sup>. According to various estimates, injecting 100 m<sup>3</sup> of coke oven gas per ton of pig iron can reduce the carbon consumption from coke by 30 kg per ton of pig iron.

Due to technical limitations, the use of hydrogen alone in a blast furnace is not feasible; therefore, its application within the blast furnace–converter route may only

be regarded as an interim step toward the transition to direct reduced iron production<sup>3</sup> [6 – 8].

Many studies have focused on the production of hydrogen-enriched gas through the gasification of various types of biomass [9 – 13], including charcoal, tar, hydrocarbons, wood, and synthetic natural gas. At small-scale enterprises, this approach is becoming one of the measures aimed at reducing CO<sub>2</sub> emissions.

The reduction of iron ore materials by hydrogen-containing gases during pig iron production is associated with certain challenges [14 – 17]. Computational experiments make it possible to analyze the state of the system and the physicochemical processes involved, and, based on the resulting models, draw conclusions about the behavior of the substances under study.

The depletion of traditional iron ore reserves in the Urals, which have been exploited for over 300 years, poses a challenge for the ferrous metallurgy industry, prompting a transition to alternative types of iron ore. One such alternative is titanium-bearing ore, which contains, in addition to iron, vanadium and titanium. Its integrated processing – including the production of steel, vanadium pentoxide, pigment-grade titanium dioxide, and titanium sponge – represents a technologically and economically complex task that requires the optimization of the recovery processes for all valuable components. As demonstrated by the experience of the Institute of Metallurgy of the Ural Branch of the Russian Academy of Sciences, a promising solution lies in the use of information systems that describe the physicochemical and thermophysical processes occurring in metallurgical units. These systems enable the optimization of process parameters and enhance the recovery efficiency of target components – both of which are critical for the economic viability of titanium-bearing ore processing.

The aim of this study is to examine the thermodynamics of the reduction of iron ore titanomagnetite pellets in atmospheres of various gas mixtures, including those similar in composition to synthesis gas, blast furnace gas, coke oven gas, and other hydrogen-containing process gases viewed as promising for recycling applications.

## RESEARCH METHODOLOGY

This study employed the method of thermodynamic modeling based on the analysis of the equilibrium state

<sup>1</sup> Gas in Metal Production [Electronic resource]. URL: <https://stal-kom.ru/gaz-pri-proizvodstve-metalla/> (accessed 07 March 2025).

<sup>2</sup> Germany launches first hydrogen-based steel production [Electronic resource]. URL: <https://gmk.center/news/v-germanii-zapustili-pervoe-proizvodstvo-stali-na-vodorode/> (accessed 07 March 2025)

<sup>3</sup> Thyssenkrupp Converts One of Its Blast Furnaces to Hydrogen [Electronic resource]. URL: <https://metallurgprom.org/articles/analytics/877-thyssenkrupp-perevodit-odnu-iz-domennyh-pechej-na-vodorod.html> (accessed 07 March 2025)

of systems. The research was conducted using the Terra software package developed at Bauman Moscow State Technical University [18–20]. The advantages of this software include:

- the ability to define equilibrium conditions of a thermodynamic system with the environment using any pair of thermodynamic parameters ( $P$  – pressure,  $V$  – specific volume,  $T$  – temperature,  $S$  – entropy,  $H$  – enthalpy, and  $U$  – internal energy);

- the ability to perform equilibrium calculations for thermodynamic systems of arbitrary elemental composition;

- the inclusion of any individual substances in the expected composition of the system by adjusting the input data, and the determination of the equilibrium phase composition without the need to predefine thermodynamically permissible states;

- the option to exclude any substances from the equilibrium composition;

- the assignment of specific concentrations for substances, with the remaining composition calculated accordingly;

- the ability to account for the volume occupied by condensed phases, and more.

The material used in the study consisted of titanium-bearing iron ore pellets. The initial chemical composition of the pellets is presented in Table 1. The reduction modeling was carried out for atmospheres composed of CO–N<sub>2</sub>–H<sub>2</sub>–CH<sub>4</sub> gas mixtures. The compositions of the reducing gases are shown in Table 2.

The thermodynamic database used for the calculations was compiled based on data from IVTANTHERMO and HSC, and includes thermodynamic property sets for both the initial components of the gas phase (CO, CH<sub>4</sub>, H<sub>2</sub>, N<sub>2</sub>) and the expected products of their interactions (CO<sub>2</sub>, H<sub>2</sub>O and many others), as well as condensed carbon (graphite).

Two independent parameters were used: temperature (in the range of 493–1793 K, in 100 K increments) and pressure (0.1 MPa).

## RESULTS AND DISCUSSION

The initial system for the reduction of pellets in an atmosphere of hydrogen-containing gases consists of a gas phase and condensed phases. The gas phase

includes CO, N<sub>2</sub>, H<sub>2</sub>, and CH<sub>4</sub>. The condensed phase consists of a metallic solution ( $s1$ ) and an oxide solution ( $s2$ ).

The composition of the condensed oxide phase is shown in Fig. 1.

According to the graphical data, the most significant components are Fe( $s1$ ), FeO( $s2$ ), and Fe<sub>3</sub>O<sub>4</sub>( $s2$ ), each with a concentration exceeding 10<sup>-1</sup> mol. fraction. In the temperature range of 1100–1793 K (Fig. 1, *a*), Fe( $s1$ ) becomes the dominant component, with a concentration of 0.88 mol. fraction. Under reduction in gas mixtures 2 and 3, Fe( $s1$ ) also becomes the predominant component in the temperature range of 1193–1793 K (Fig. 1, *b, c*).

Changes in the composition of the gas phase are shown in Fig. 2. At temperatures above 900 K, the main components of the gas phase are H<sub>2</sub>, N<sub>2</sub> ( $p \sim 0.58$  atm), and CO.

The phase distribution of iron, vanadium, and manganese as a function of temperature is presented in Fig. 3. In the temperature range of 500–893 K, the dominant iron phase is Fe<sub>3</sub>O<sub>4</sub>( $s2$ ) with a concentration of up to 86 mol. %. In the 593–993 K range, FeO( $s2$ ) in appears in concentrations ranging from 11 to 40 mol. %. At 993 K, the formation of iron carbide Fe<sub>3</sub>C( $s2$ ) occurs, reaching concentrations of 88, 94, and 95 mol. %, respectively. The formation of Fe<sub>3</sub>C( $s2$ ) is attributed to an increase in carbon content in the gas phase, which is confirmed by the rise in CO and CO<sub>2</sub> concentrations. A further temperature increase to 1000–1793 K leads to the appearance of metallic iron Fe( $s1$ ), with concentrations ranging from 89 to 98 mol. %.

At 500 K, condensed manganese silicate Mn<sub>2</sub>SiO<sub>4</sub>( $s2$ ) dominates, accounting for approximately 85 mol. %. Between 593 and 1093 K, the concentration of Mn<sub>2</sub>SiO<sub>4</sub>( $s2$ ) decreases to 15, 13, and 12 mol. %, respectively, accompanied by an increase in condensed manganese oxide MnO( $s2$ ) from 34 to 86 mol. %. Further heating to 1700 K results in an increase in the concentration of gaseous manganese hydride MnH, reaching 9, 34, and 55 mol. %, respectively.

In the temperature range of 500–793 K, the dominant vanadium phase is condensed V<sub>2</sub>O<sub>3</sub>( $s2$ ), accounting for about 96 mol. %. As the temperature rises to 1700 K, the share of V<sub>2</sub>O<sub>3</sub>( $s2$ ) gradually decreases to 26, 22, and 19 mol. %. At the same time, an increase in the concentration of condensed vanadium oxide VO( $s2$ ) is observed above 893 K. Additionally, the concentration of con-

Table 1. Initial composition of the gas reducing system

Таблица 1. Исходный состав системы для восстановления газами

Composition, wt. %								
Fe <sub>2</sub> O <sub>3</sub>	FeO	CaO	SiO <sub>2</sub>	V <sub>2</sub> O <sub>5</sub>	TiO <sub>2</sub>	MgO	MnO	Al <sub>2</sub> O <sub>3</sub>
82.83	3.00	1.19	4.20	0.54	2.75	2.85	0.24	2.40

Table 2. Compositions of reducing gases

Таблица 2. Составы восстановительных газов

Mixture No.	Composition, wt. %			
	CO	N <sub>2</sub>	H <sub>2</sub>	CH <sub>4</sub>
1	20	65	10	5
2	35	35	25	5
3	50	5	40	5

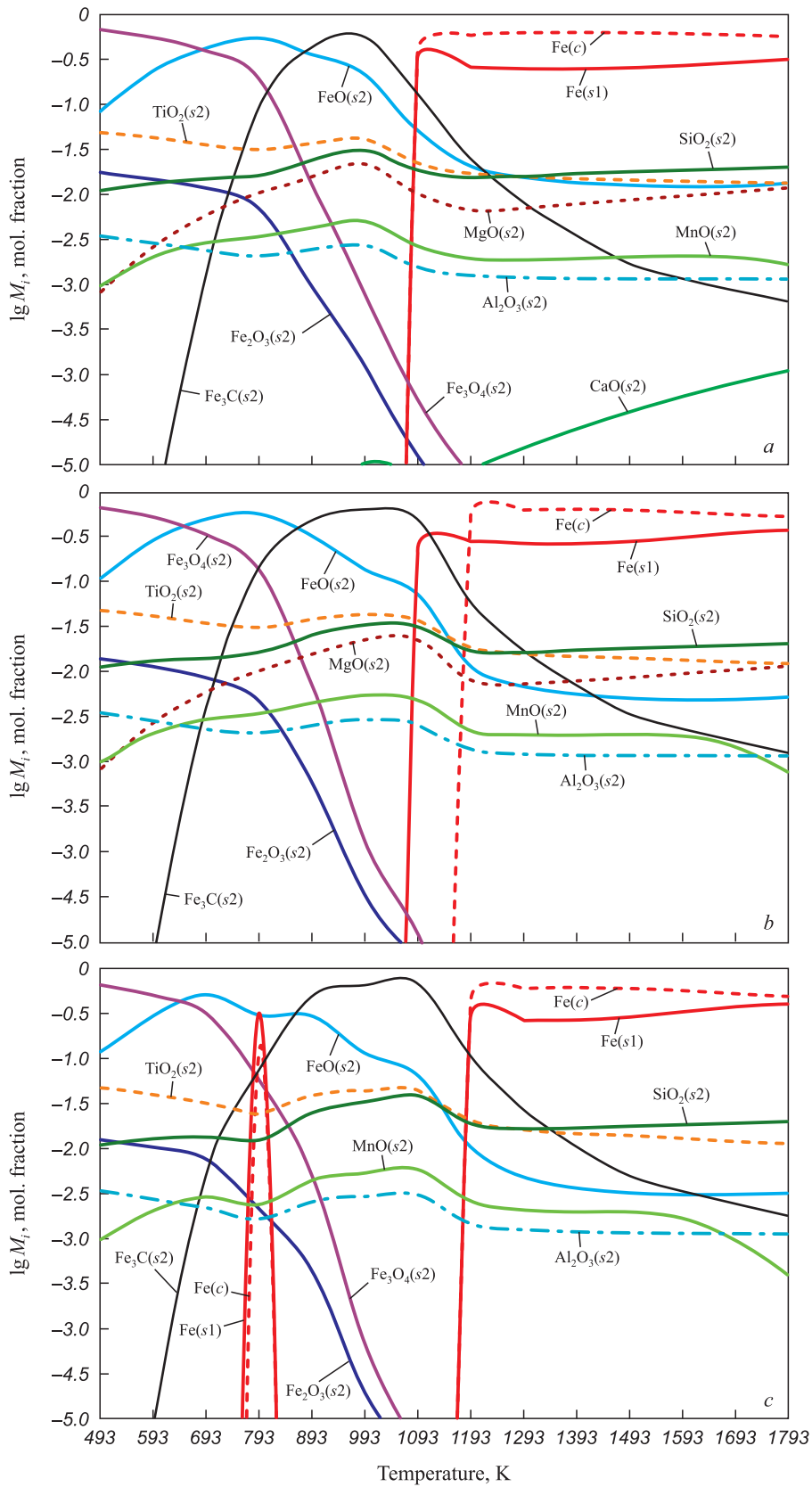


**Fig 1.** Composition of the condensed oxide phase during gas reduction:

$M_i$  – concentration of the  $i$ -th component in the system of mole fractions (1.00 mol. fr. = 100 mol. %):  
 a – gas mixture 1; b – gas mixture 2; c – gas mixture 3

**Рис. 1.** Состав конденсированной оксидной фазы при восстановлении газом:

$M_i$  – концентрация  $i$ -го компонента в системе мольных долей (1,00 мол. дол. = 100 мол. %):  
 а – смесь газов 1; б – смесь газов 2; в – смесь газов 3

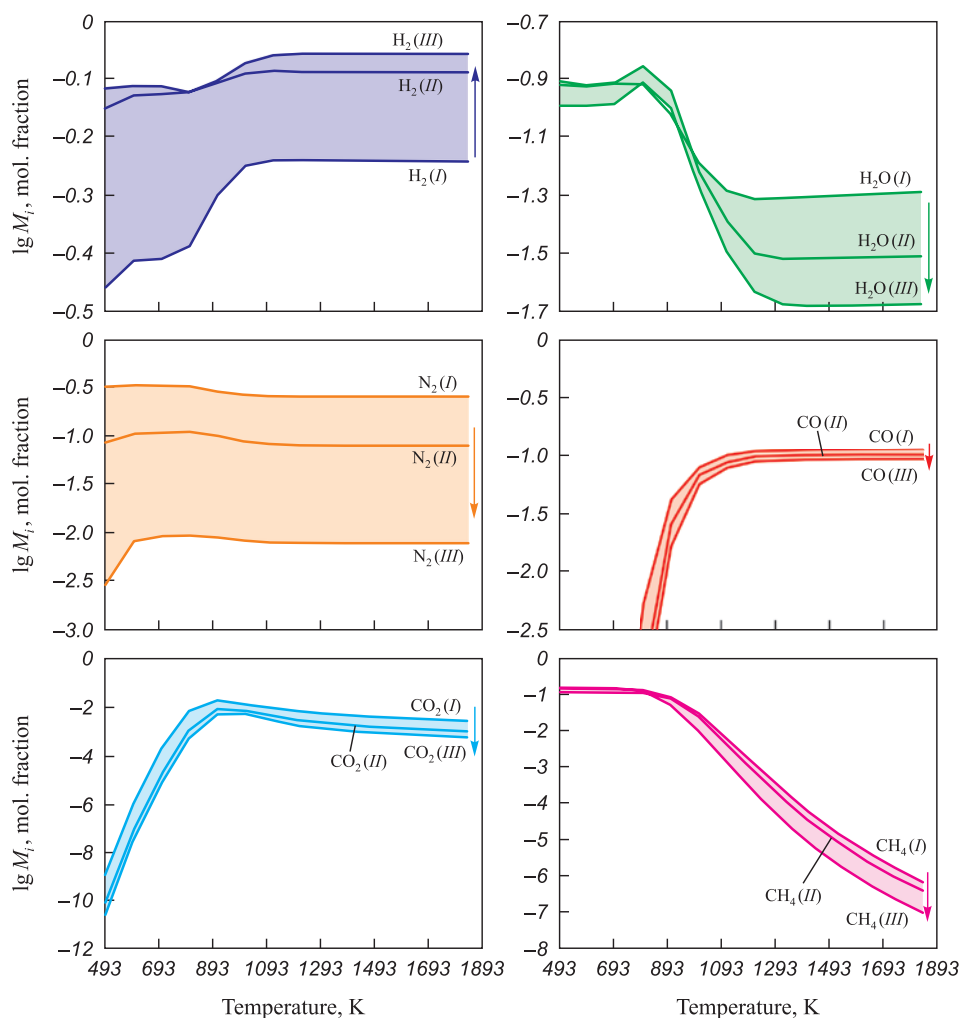


**Fig. 2.** Gas phase composition during reduction with different mixtures of gases (I, II, III)

**Рис. 2.** Состав газовой фазы при восстановлении различными смесями газов (I, II, III)

densified  $V_3O_5(s_2)$  increases with temperature, reaching 29, 16, and 10 mol. % at 1700 K.

In the temperature range of 500 – 1493 K, the majority of silicon is present in the form of condensed magnesium silicate  $MgSiO_3(s_2)$ , with a concentration ranging from 27 to 43 mol. %. The concentrations of calcium silicate  $CaSiO_3(s_2)$  (approximately 16 mol. %) and magnesium silicate  $Mg_2SiO_4(s_2)$  (22 to 26 mol. %) remain nearly constant throughout the 500 – 1700 K range. A temperature increase to 1500 – 1700 K leads to a rise in the content of condensed silicon dioxide  $SiO_2(s_2)$  to 34 mol. %.

The investigation of the sample's phase composition over the 500 – 1793 K temperature range revealed the following patterns. In the initial state (500 K),  $Al_2O_3(s_2)$  is the dominant mineral phase of aluminum, accounting for 70 mol. %. Upon heating to 1700 K, the  $Al_2O_3(s_2)$  content decreases to 58 mol. %, indicating the occurrence of phase transformations. Simultaneously, the concentration of  $MgAl_2O_4(s_2)$  increases from 30 to 42 mol. %, pointing to the formation of a new phase. In the 500 – 1700 K range, the primary mineral phase of tita-

nium is  $TiO_2(s_2)$ . Between 993 and 1700 K, the concentration of  $TiO_2(s_2)$  decreases from 70 to 43 mol. %. The  $CaTiO_3(s_2)$  content remains stable at approximately 28 mol. % throughout the entire temperature interval. At temperatures above 1093 K, the concentrations of  $MgTi_2O_5(s_2)$  and  $Mg_2TiO_4(s_2)$  increase to 12 and 6 mol. %, respectively, indicating the formation of new mineral phases. The predominant magnesium phase throughout the 500 – 1793 K range is  $Mg_2SiO_4(s_2)$ , with a molar fraction of 43 – 54 mol. %. Heating to 1793 K leads to a decrease in  $MgSiO_3(s_2)$  content from 43 to 27 mol. %. A slight increase in the  $Mg_2TiO_4(s_2)$  concentration to 6 mol. % is also observed. Between 500 and 1793 K, most of the calcium remains in the form of condensed  $CaSiO_3(s_2)$  (~49 – 55 mol. %), while the  $CaTiO_3(s_2)$  content (~45 mol. %) remains unchanged in all three cases.

Thus, increasing the temperature to 1793 K results in significant restructuring of the mineral composition due to reactions between various phases. Changes in the CO,  $N_2$ , and  $H_2$  content of the gas mixture do not affect the elemental distribution of silicon, aluminum, titanium, mag-

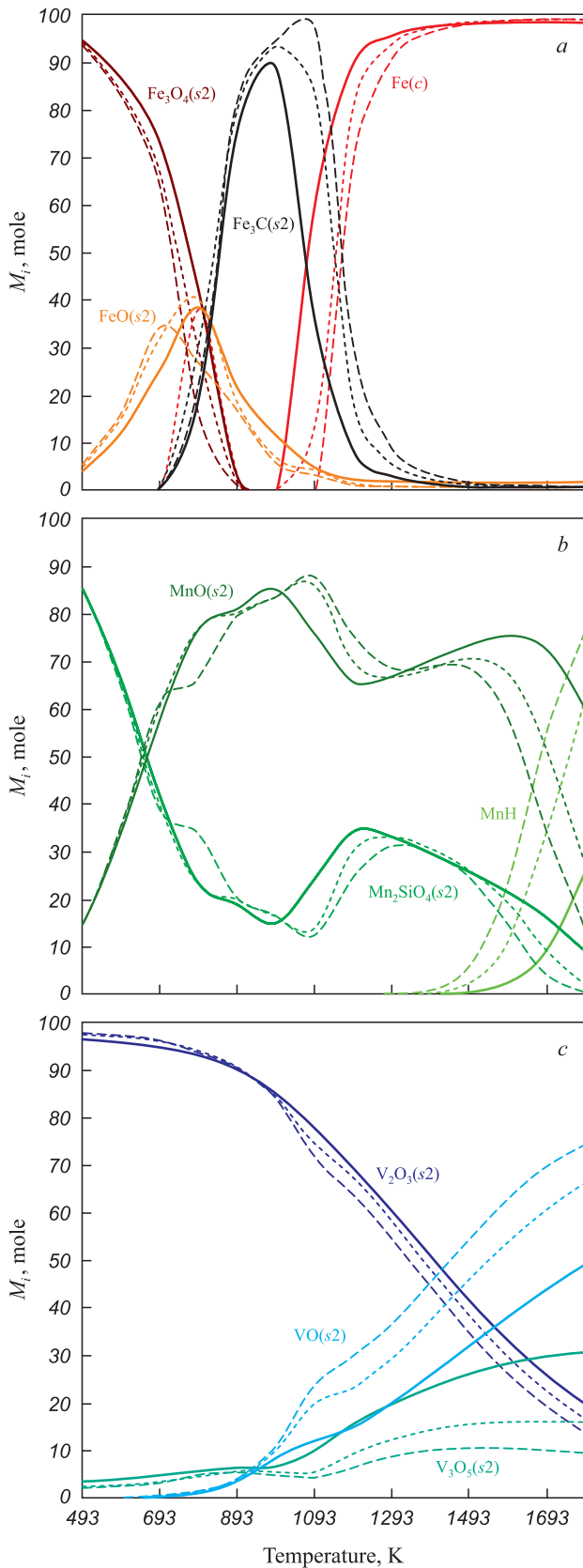


**Fig 3.** Iron (a), manganese (b), vanadium (c) balance by phase during gas reduction:

— gas mixture 1; - - - gas mixture 2; - · - gas mixture 3

**Рис. 3.** Баланс железа (а), марганца (б), ванадия (с) по фазам при восстановлении газом:

— смесь газов 1; - - - смесь газов 2; - · - смесь газов 3

nesium, and calcium. However, substantial changes are observed for iron, vanadium, and manganese.

In the temperature range of 500 – 893 K, the amount of condensed  $\text{Fe}_3\text{O}_4(s2)$  phase decreases, with gas mixture 3 showing a lower  $\text{Fe}_3\text{O}_4(s2)$  content than mixture 1. The maximum concentration of  $\text{FeO}(s2)$  in the system is approximately 40 mol. % at 793 K for gas mixtures 1 and 2, and 34 mol. % at 693 K for mixture 1. The maximum content of iron carbide  $\text{Fe}_3\text{C}(s2)$  is about 96 mol. % at 1093 K in gas mixture 3, approximately 94 mol. % at 993 K in mixture 2, and ~88 mol. % in mixture 1. The formation of  $\text{Fe}(s1)$  begins at 993 K in mixtures 1 and 2, and at 1193 K in mixture 3. The amount of  $\text{Fe}(s1)$  formed in reducing gas mixture 1 is higher than in mixtures 2 and 3.

When the temperature exceeds 1093 K, the contents of condensed  $\text{V}_2\text{O}_3(s2)$  and  $\text{V}_3\text{O}_5(s2)$  are lower compared to those in gas mixture 1. The concentration of  $\text{VO}(s2)$  is highest in gas mixture 3.

The amounts of  $\text{MnO}(s2)$  and  $\text{Mn}_2\text{SiO}_4(s2)$  are greater between 1093 and 1393 K in mixture 3 compared to mixture 1; however, in the 1393 – 1793 K range, their concentrations increase in mixture 1. In addition, an increase in hydrogen content in the gas phase leads to a higher concentration of  $\text{MnH}$ .

### CONCLUSIONS

The study of thermodynamic processes involved in the indirect reduction of titanomagnetite iron ore pellets using various gas atmospheres made it possible to identify patterns in the phase composition changes of the system depending on temperature and the composition of the reducing gas mixture.

Experimental results confirmed that in the temperature range of 500 – 1793 K, the equilibrium concentrations of silicon, aluminum, titanium, magnesium, and calcium remain virtually unchanged when different gas mixtures containing  $\text{CO}$ ,  $\text{N}_2$ ,  $\text{H}_2$ , and  $\text{CH}_4$  in varying proportions are used.

At the same time, significant changes in the concentrations of iron, vanadium, and manganese were observed depending on the composition of the gas mixture. For instance, in gas mixture 1 (20 %  $\text{CO}$  – 65 %  $\text{N}_2$  – 10 %  $\text{H}_2$  – 5 %  $\text{CH}_4$ ) a decrease in  $\text{Fe}_3\text{C}(s2)$  content and an increase in  $\text{Fe}(s1)$ ,  $\text{Fe}_3\text{O}_4(s2)$ ,  $\text{V}_2\text{O}_3(s2)$ ,  $\text{V}_3\text{O}_5(s2)$ ,  $\text{MnO}(s2)$ , and  $\text{Mn}_2\text{SiO}_4(s2)$  contents were observed in the 1393 – 1793 K temperature range.

In gas mixture 3 (50 %  $\text{CO}$  – 5 %  $\text{N}_2$  – 40 %  $\text{H}_2$  – 5 %  $\text{CH}_4$ ) a reduction in  $\text{Fe}_3\text{O}_4(s2)$  content and an increase in  $\text{FeO}(s2)$ ,  $\text{Fe}_3\text{C}(s2)$ ,  $\text{VO}(s2)$ ,  $\text{MnO}(s2)$ , and  $\text{Mn}_2\text{SiO}_4(s2)$  contents were noted in the 1093 – 1393 K temperature range.

The obtained results demonstrate the significant influence of the reducing gas mixture composition – particularly hydrogen content – on the phase equilibrium during

the indirect reduction of iron ore pellets. This has important implications for the optimization of technological processes in iron production.

## REFERENCES / СПИСОК ЛИТЕРАТУРЫ

- Digonskyi S.V., Ten V.V. Unknown Hydrogen: The Role of Hydrogen in the Polymorphism of Solids, Processes of Solid-Phase Reduction of Oxides and Sintering of Powders. St. Petersburg: Nauka; 2006:292. (In Russ.).  
Дигонский С.В., Тен В.В. Неизвестный водород: роль водорода в полиморфизме твердых веществ, процессах твердофазного восстановления оксидов и спекания порошков. Санкт-Петербург: Наука; 2006:292.
- Morozova O.N., Pavlenko A.A., Titov S.S. Methods of hydrogen production. *South Siberian Scientific Bulletin*. 2019;(4(28)):188–194. (In Russ.).  
<https://doi.org/10.25699/SSSB.2019.28.46373>  
Морозова О.Н., Павленко А.А., Титов С.С. Способы получения водорода. *Южно-Сибирский научный вестник*. 2019;(4(28)):188–194.  
<https://doi.org/10.25699/SSSB.2019.28.46373>
- Solodova N.L., Minigulov R.R., Emelyanycheva E.A. Hydrogen as a promising energy carrier. Modern methods of hydrogen production. *Bulletin of Kazan Technological University*. 2015;18(3):137–140. (In Russ.).  
<https://doi.org/10.24412/Fg4yW5JCGyE>  
Солодова Н.Л., Минигулов Р.Р., Емельянычева Е.А. Водород как перспективный энергоноситель. Современные методы получения водорода. *Вестник Казанского технологического университета*. 2015;18(3):137–140.  
<https://doi.org/10.24412/Fg4yW5JCGyE>
- Ershov Yu.L., Shakurov A.G., Parshin V.M., Kolesnikov A.G., Shishov A.Yu. Hydrogen era in Russian metallurgy. Report 1. *Steel in Translation*. 2021;51(11):839–845.  
<https://doi.org/10.3103/S0967091221110048>  
Ершов Ю.Л., Шакуров А.Г., Паршин В.М., Колесников А.Г., Шишов А.Ю. Водородная эра в отечественной металлургии. Сообщение 1. *Сталь*. 2021;(11):50–55.
- Ershov Yu.L., Shakurov A.G., Parshin V.M., Kolesnikov A.G., Shishov A.Yu. Hydrogen era in Russian metallurgy. Report 2. *Steel in Translation*. 2021;51(12):930–938.  
<https://doi.org/10.3103/S0967091221120044>  
Ершов Ю.Л., Шакуров А.Г., Паршин В.М., Колесников А.Г., Шишов А.Ю. Водородная эра в отечественной металлургии. Сообщение 2. *Сталь*. 2021;(12):48–56.
- Gao X., Zhang R., You Zh., Yu W., Dang J., Bai Ch. Use of hydrogen-rich gas in blast furnace ironmaking of V-bearing titanomagnetite: Mass and energy balance calculations. *Materials*. 2022;15(17):6078.  
<https://doi.org/10.3390/ma15176078>
- Okosun T., Nielson S., Zhou Ch. Blast furnace hydrogen injection: investigating impacts and feasibility with computational fluid dynamics. *JOM*. 2022;74:1521–1532.  
<https://doi.org/10.1007/s11837-022-05177-4>
- Yu X., Hu Z., Shen Y. Modeling of hydrogen shaft injection in ironmaking blast furnaces. *Fuel*. 2021;302:121092.  
<https://doi.org/10.1016/j.fuel.2021.121092>
- Suopajarvi H., Pongrácz E., Fabritius T. Bioreducer use in Finnish blast furnace ironmaking – Analysis of CO<sub>2</sub> emission reduction potential and mitigation cost. *Applied Energy*. 2014;124:82–93.  
<https://doi.org/10.1016/j.apenergy.2014.03.008>
- Liu Y., Shen Ya. Modelling and optimization of biomass injection in ironmaking blast furnaces. *Progress in Energy and Combustion Science*. 2021;87:100952.  
<https://doi.org/10.1016/j.pecs.2021.100952>
- Luo S., Zhou Ya., Yi Ch. Hydrogen-rich gas production from biomass catalytic gasification using hot blast furnace slag as heat carrier and catalyst in moving-bed reactor. *International Journal of Hydrogen Energy*. 2012;37(20):15081–15085.  
<https://doi.org/10.1016/j.ijhydene.2012.07.105>
- Xie H., Li R., Wang Zh., Yao X., Yu Q. Hydrogen production of bio-oil steam reforming combining heat recovery of blast furnace slag: Thermodynamic analysis. *International Journal of Hydrogen Energy*. 2019;44(47):25514–25523.  
<https://doi.org/10.1016/j.ijhydene.2019.08.014>
- Feliciano-Bruzual C. Charcoal injection in blast furnaces (Bio-PCI): CO<sub>2</sub> reduction potential and economic prospects. *Journal of Materials Research and Technology*. 2014;3(3):233–243. <https://doi.org/10.1016/j.jmrt.2014.06.001>
- Afanas'ev V.K., Gorlova S.N., Kuznetsova E.V., Sochnev A.V., Efanov G.I., Tolstoguzov V.N., Kuskov B.A. On the role of hydrogen in blast furnace process of iron production. *Obrabotka metallov: tekhnologiya, oborudovanie, instrumenty*. 2004;(4(25)):15–18. (In Russ.).  
Афанасьев В.К., Горлова С.Н., Кузнецова Е.В., Соцнев А.В., Ефанов Г.И., Толстогузов В.Н., Кусков Б.А. О роли водорода в доменном процессе получения чугуна. *Обработка металлов: технология, оборудование, инструменты*. 2004;(4(25)):15–18.
- Rogozhnikov S.P., Rogozhnikov I.S. Determination of degree of hydrogen usage in blast furnace. *Ferrous Metallurgy. Bulletin of Scientific, Technical and Economic Information*. 2020;75(10):1129–1134. (In Russ.).  
<https://doi.org/10.32339/0135-5910-2019-10-1129-1134>  
Рогожников С.П., Рогожников И.С. Определение степени использования водорода в доменной печи. *Черная металлургия. Бюллетень научно-технической и экономической информации*. 2020;75(10):1129–1134.  
<https://doi.org/10.32339/0135-5910-2019-10-1129-1134>
- Yalunin M.S., Vit'kina G.Yu., Dmitriev A.N., Zolotykh M.O., Alektorov R.V. Evaluation of the influence of reducing gas with an increased proportion of hydrogen on the efficiency of blast furnace smelting. In: *Heat Engineering and Informatics in Education, Science and Production (TIM'2022)*. Yekaterinburg; 2022:185–190. (In Russ.).  
Ялунин М.С., Витькина Г.Ю., Дмитриев А.Н., Золотых М.О., Алекторов Р.В. Оценка влияния газа-восстановителя с повышенной долей водорода на эффективность доменной плавки. В кн.: *Теплотехника и информатика в образовании, науке и производстве (ТИМ'2022)*. Екатеринбург; 2022:185–190.
- Shevelev L.N. Assessment of economic, energy and ecological efficiency of iron and steel production from ore-coal briquettes in electric-furnace melting facility with application of hydrogen fuel. *Ferrous Metallurgy. Bulletin of Scientific, Technical and Economic Information*. 2021;77(8):918–924. (In Russ.).  
<https://doi.org/10.32339/0135-5910-2021-8-918-924>  
Шевелев Л.Н. Оценка экономической, энергетической и экологической эффективности производства чугуна и

стали из рудоугольных брикетов в электросталеплавильном агрегате с использованием водородного топлива. *Черная металлургия. Бюллетень научно-технической и экономической информации.* 2021;77(8):918–924. <https://doi.org/10.32339/0135-5910-2021-8-918-924>

18. Vatolin N.A., Moiseev G.K., Trusov B.G. Thermodynamic Modeling in High-Temperature Inorganic Systems. Moscow: Metallurgy; 1994:352. (In Russ.).

Ватолин Н.А., Моисеев Г.К., Трусов Б.Г. Термодинамическое моделирование в высокотемпературных неорганических системах. Москва: Металлургия; 1994:352.

19. Rybenko I.A., Protopopov E.V. Thermodynamic modeling of iron recovery processes. *Izvestiya. Ferrous Metallurgy.* 2021;64(11):825–831. (In Russ.). <https://doi.org/10.17073/0368-0797-2021-11-825-831>

Рыбенко И.А., Протопопов Е.В. Термодинамическое моделирование процессов восстановления железа. *Известия вузов. Черная металлургия.* 2021;64(11):825–831. <https://doi.org/10.17073/0368-0797-2021-11-825-831>

20. Gamov P.A., Mal'kov N.V., Roshchin V.E. Thermodynamic modelling of the metals' reduction process from the Suroyam titanomagnetite concentrate. *Bulletin of the South Ural State University. Series: Metallurgy.* 2018;18(2):21–28. (In Russ.). <http://dx.doi.org/10.14529/met180203>

Гамов П.А., Мальков Н.В., Рошин В.Е. Термодинамическое моделирование процесса восстановления металлов из титаномагнетитовых концентратов Суроямского месторождения. *Вестник Южно-Уральского государственного университета. Серия: Металлургия.* 2018;18(2):21–28. <http://dx.doi.org/10.14529/met180203>

## Information about the Authors

## Сведения об авторах

**Andrei N. Dmitriev**, Dr. Sci. (Eng.), Prof., Chief Researcher of the Laboratory of Pyrometallurgy of Reduction Processes, Institute of Metallurgy, Ural Branch of the Russian Academy of Sciences

ORCID: 0000-0001-6446-0215

E-mail: andrey.dmitriev@mail.ru

**Yuliya E. Burova**, Junior Researcher of the Laboratory of Pyrometallurgy of Reduction Processes, Institute of Metallurgy, Ural Branch of the Russian Academy of Sciences

ORCID: 0009-0002-4591-700X

E-mail: menestrelfox@gmail.com

**Galina Yu. Vit'kina**, Cand. Sci. (Eng.), Leading Researcher, Head of the Laboratory of Pyrometallurgy of Reduction Processes, Institute of Metallurgy, Ural Branch of the Russian Academy of Sciences

ORCID: 0000-0002-1076-2709

E-mail: 20procents@mail.ru

**Nikolai M. Barbin**, Dr. Sci. (Eng.), Chief Researcher of the Laboratory of Pyrometallurgy of Reduction Processes, Institute of Metallurgy, Ural Branch of the Russian Academy of Sciences; Prof., Ural Institute of State Fire Service of EMERCOM of Russia

ORCID: 0000-0002-6709-4334

E-mail: nmbarbin@mail.ru

**Dmitrii I. Terent'yev**, Cand. Sci. (Chem.), Leading Researcher, Ural Institute of State Fire Service of EMERCOM of Russia

ORCID: 0000-0002-3991-4366

E-mail: sveripeu@mail.ru

**Андрей Николаевич Дмитриев**, д.т.н., главный научный сотрудник лаборатории пирометаллургии восстановительных процессов, Институт металлургии Уральского отделения РАН

ORCID: 0000-0001-6446-0215

E-mail: andrey.dmitriev@mail.ru

**Юлия Евгеньевна Бурова**, младший научный сотрудник лаборатории пирометаллургии восстановительных процессов, Институт металлургии Уральского отделения РАН

ORCID: 0009-0002-4591-700X

E-mail: menestrelfox@gmail.com

**Галина Юрьевна Витькина**, к.т.н., ведущий научный сотрудник, заведующий лабораторией пирометаллургии восстановительных процессов, Институт металлургии Уральского отделения РАН

ORCID: 0000-0002-1076-2709

E-mail: 20procents@mail.ru

**Николай Михайлович Барбин**, д.т.н., главный научный сотрудник лаборатории пирометаллургии восстановительных процессов, Институт металлургии Уральского отделения РАН; профессор, Уральский институт государственной противопожарной службы МЧС России

ORCID: 0000-0002-6709-4334

E-mail: nmbarbin@mail.ru

**Дмитрий Иванович Терентьев**, к.х.н., ведущий научный сотрудник, Уральский институт государственной противопожарной службы МЧС России

ORCID: 0000-0002-3991-4366

E-mail: sveripeu@mail.ru

## Contribution of the Authors

## Вклад авторов

**A. N. Dmitriev** – scientific guidance, formation of the basic concept, goals and objectives of the study.

**Yu. E. Burova** – data processing, visualization of research results, writing and editing the text.

**G. Yu. Vit'kina** – literary review, editing the text.

**N. M. Barbin** – software, reviewing and editing the text.

**D. I. Terent'yev** – editing the text.

**А. Н. Дмитриев** – научное руководство, формирование основной концепции, цели и задачи исследования.

**Ю. Е. Бурова** – обработка данных, визуализация результатов исследований, написание и редактирование текста статьи.

**Г. Ю. Витькина** – обзор публикации по теме статьи, редактирование текста статьи.

**Н. М. Барбин** – программное обеспечение, рецензирование и редактирование текста статьи.

**Д. И. Терентьев** – расчет, редактирование текста статьи.

Received 17.09.2024

Revised 06.11.2024

Accepted 28.02.2025

Поступила в редакцию 17.09.2024

После доработки 06.11.2024

Принята к публикации 28.02.2025



UDC 669.11:669.292.34

DOI 10.17073/0368-0797-2025-2-171-178



Original article

Оригинальная статья

## THERMODYNAMIC ANALYSIS OF CONDITIONS FOR IRON AND TITANIUM SEPARATION IN ILMENITE CONCENTRATE BY SELECTIVE REDUCTION OF ELEMENTS

K. I. Smirnov, P. A. Gamov, V. E. Roshchin , V. S. Samolin South Ural State University (76 Lenina Ave., Chelyabinsk 454080, Russian Federation) roshchinve@susu.ru

**Abstract.** The thermodynamic modeling method was used to determine the temperature of beginning of reduction of iron, vanadium, silicon, and titanium in ilmenite concentrate by carbon or hydrogen at different amounts of reducing agent in the system. The amount of excess carbon relative to the stoichiometry of the iron reduction reaction does not affect the temperature of reduction beginning, but determines their reduction degree and the amount of carbides formed. The amount of hydrogen in the system significantly affects the temperature of reduction beginning: with an increase in water amount, this temperature of each element decreases, but to a different extent. The wider temperature range of beginning of reduction by hydrogen and the quantitatively unequal effect of temperature create more opportunities for controlling the solid-phase selective reduction by hydrogen in comparison with carbon. In contrast to the carbothermic process, the solid-phase reduction of titanium by hydrogen is negligible at relatively low temperatures, at which titanium is reduced by carbon and forms carbides. The low solubility of hydrogen in solid iron excludes its influence on the behavior of elements at the stage of separation melting of solid-phase reduction products. This makes it possible to carry out reduction in hydrogen flow by changing the temperature and amount of hydrogen in the reducing gas mixture, and to control the processes of selective solid-phase reduction of elements. The use of hydrogen at the stage of solid-phase reduction makes it possible to selectively reduce iron with the storage of titanium oxides in the oxide phase in form of  $TiO_2$ , and after separation of the reduction products by melting, to obtain the products in demand (carbon-free iron and  $TiO_2$  concentrate).

**Keywords:** ilmenite, titanium dioxide, solid-phase selective reduction, carbon reduction, hydrogen reduction, production of carbon-free iron

**Acknowledgements:** The research was supported by the Russian Science Foundation (grant No. 23-29-10119, <https://rscf.ru/project/23-29-10119/>).

**For citation:** Smirnov K.I., Gamov P.A., Roshchin V.E., Samolin V.S. Thermodynamic analysis of conditions for iron and titanium separation in ilmenite concentrate by selective reduction of elements. *Izvestiya. Ferrous Metallurgy*. 2025;68(2):171–178. <https://doi.org/10.17073/0368-0797-2025-2-171-178>

## ТЕРМОДИНАМИЧЕСКИЙ АНАЛИЗ УСЛОВИЙ РАЗДЕЛЕНИЯ ЖЕЛЕЗА И ТИТАНА В ИЛЬМЕНитОВОМ КОНЦЕНТРАТЕ СЕЛЕКТИВНЫМ ВОССТАНОВЛЕНИЕМ ЭЛЕМЕНТОВ

К. И. Смирнов, П. А. Гамов, В. Е. Рощин , В. С. Самолин Южно-Уральский государственный университет (Россия, 454080, Челябинск, пр. Ленина, 76) roshchinve@susu.ru

**Аннотация.** Методом термодинамического моделирования определены значения температуры начала восстановления железа, ванадия, кремния и титана ильменитового концентрата углеродом или водородом при разном количестве восстановителя в системе. Количество избыточного углерода по отношению к стехиометрии реакции восстановления железа не влияет на температуру начала восстановления элементов, но определяет степень их восстановления и количество образующихся карбидов. Количество водорода в системе существенно влияет на температуру начала восстановления: с увеличением количества водорода температура начала восстановления каждого из элементов снижается, но в разной степени. Более широкий температурный интервал начала восстановления элементов водородом и количественно неодинаковое влияние температуры создают больше возможностей для управления твердофазным селективным восстановлением элементов водородом в сравнении с углеродом. В отличие от карботермического процесса твердофазное восстановление титана водородом ничтожно мало при относительно низких температурах, при которых титан восстанавливается углеродом и образует карбиды.

Малая растворимость водорода в твердом железе исключает его влияние на поведение элементов на стадии разделительной плавки продуктов твердофазного восстановления. Это позволяет проводить восстановление в потоке водорода путем изменения температуры и количества водорода в восстановительной газовой смеси, управлять процессами селективного твердофазного восстановления элементов. Использование водорода на стадии твердофазного восстановления позволяет селективно восстанавливать железо с сохранением оксидов титана в оксидной фазе в виде  $TiO_2$ , а после разделения продуктов восстановления плавлением получать востребованные продукты (безуглеродистое железо и концентрат оксида титана  $TiO_2$ ).

**Ключевые слова:** ильменит, оксид титана, твердофазное селективное восстановление, углеродное восстановление, восстановление водородом, получение безуглеродистого железа

**Благодарности:** Исследование выполнено при поддержке Российского научного фонда (грант № 23-29-10119, <https://rscf.ru/project/23-29-10119/>).

**Для цитирования:** Смирнов К.И., Гамов П.А., Рошин В.Е., Самолин В.С. Термодинамический анализ условий разделения железа и титана в ильменитовом концентрате селективным восстановлением элементов. *Известия вузов. Черная металлургия*. 2025;68(2):171–178. <https://doi.org/10.17073/0368-0797-2025-2-171-178>

## INTRODUCTION

Russia faces a shortage of raw materials for the production of pigment-grade titanium dioxide ( $TiO_2$ ) and metallic titanium. In 2019, the import of pigment-grade titanium dioxide amounted to 53.6 thousand tons, covering 67.5 % of domestic consumption [1]. Pigment-grade  $TiO_2$  is produced at the “Crimean Titan” plant (Armiansk) using the sulfuric acid process, while metallic titanium is manufactured using chloride technologies at the “VSMPO-AVISMA” facility (Berezniki) and the “Solikamsk Magnesium Plant” (Solikamsk).

Globally, the chloride process is the predominant method for producing pigment-grade titanium dioxide, as it has a lower environmental impact compared to the sulfuric acid process [2]. However, due to the lack of an efficient strategy for processing chlorination by-products, the chloride process typically relies not on ilmenite concentrate, but on natural rutile concentrates or high-titanium slags obtained through the pyrometallurgical Sorel process. The Sorel process, which involves electric arc smelting, is the primary pyrometallurgical method used to treat ilmenite concentrate. This process yields vanadium-rich pig iron and high-titanium slag. During smelting, 96 – 97 % of iron and 45 – 48 % of vanadium contained in the concentrate are transferred to the metallic phase. Titanium is partially reduced to lower oxides and, in some cases, to its metallic form, with up to 2 % of the titanium content entering the metal phase [3]. The Sorel process is highly energy-intensive due to the formation of a high-melting-point slag and is therefore employed primarily in regions with low-cost electricity [4].

A reduction in electricity consumption during the processing of ilmenite-based feedstock can be achieved by carrying out the reduction reactions in a separate unit designed for solid-phase metallization, using low-cost reductants and fuels. In this approach, the electric arc furnace is used solely for separating the metallization products. An assessment of using a metallized charge in electric arc smelting has shown that, at a metallization degree of approximately 70 %, the electricity consumption per

ton of high-titanium slag is reduced by about 35 %, and by a further 20 % when the contribution of sensible heat is considered [5].

Based on pilot tests for processing concentrates from the Chineiskoe deposit, a two-stage pyrometallurgical process was proposed for the recovery of iron, titanium, and vanadium [6]. This technology involves the preliminary reduction of iron with carbon in a rotary kiln, achieving a metallization degree of 90 – 93 %, followed by separation of hot metallized concentrate in an electric arc furnace to obtain vanadium pig iron and titanium slag. Although this process has been recommended for other medium- and high-titanium concentrates, it has not yet been implemented on an industrial scale.

Hydrogen can serve as an alternative reducing agent for iron during the processing of titanium-bearing iron ore materials. Both theoretical studies [7; 8] and experimental research [9 – 11] have demonstrated that hydrogen offers several advantages over carbon-based reductants, which is particularly important for the selective reduction of metals from complex ores.

Thermodynamic modeling is widely used to assess the conditions under which chemical reactions occur in metallurgical processes. In most cases, thermodynamic calculations are based on evaluating chemical reactions through changes in Gibbs free energy. This approach involves identifying the most probable reaction from among the possible ones by comparing  $\Delta G(T)$  values. However, in complex systems such as ores and concentrates, this type of calculation is labor-intensive and, in some cases, unfeasible due to the large number of components involved. Therefore, the use of computer-based software packages is considered the most efficient approach for modeling complex systems.

The thermodynamic modeling of element reduction from ilmenite concentrate has been explored in numerous studies [12 – 21]. Reference [12] examined the distribution of titanium, iron, and impurities between the metal and slag phases during carbon reduction, depending on the temperature range (1550 – 1750 °C) and slag basicity. In [13], the influence of  $CO-H_2$  gas mixture

composition was analyzed over a temperature range of 500–1200 °C. Study [14] investigated carbothermic reduction under vacuum conditions. According to [15], the lower titanium oxides formed during hydrogen reduction at temperatures above 827 °C can be used to reduce iron from ilmenite. Reference [16] examined the reduction process at 0.10132 MPa with varying amounts of ilmenite, carbon, and hydrogen. In [17], changes in Gibbs free energy were calculated for a number of reactions involved in the carbothermic reduction of elements in ilmenite across a broad temperature range (25–1650 °C). Study [18] also focused on carbothermic reduction from ilmenite concentrate under vacuum. In [19], the reduction process was studied using palm kernel biomass as a reductant at 1000–1200 °C. Reference [20] analyzed the influence of Na<sub>2</sub>CO<sub>3</sub> on reduction during electric smelting. Study [21] explored reactions occurring in Ar–H<sub>2</sub> gas mixtures with varying hydrogen content in 800–1000 °C temperature range. However, a comparative analysis of reduction conditions for elements in ilmenite concentrate using carbon versus hydrogen is lacking in the literature.

The objective of the present study is to compare, through thermodynamic modeling, the conditions of element reduction in ilmenite concentrate using carbon or hydrogen as the reducing agent.

## RESEARCH METHODOLOGY

Thermodynamic calculations were carried out using an ilmenite concentrate with the following composition (wt. %: O 42.6; Mg 0.4; Al 0.3; Si 0.7; Ti 24.0; V 0.3; Mn 0.4; Fe 31.3).

The equilibrium phase composition of the system components and the temperature sequence of their transformations during carbon or hydrogen reduction were determined using thermodynamic modeling with the Terra software package [22]. The calculations were based on the Terra thermodynamic database, supplemented by thermodynamic data for individual substances from reference sources [23–25]. The amount of reducing agent was set either at the stoichiometric level required for iron reduction or in excess. For carbon, the excess levels were 10, 20, 30, and 100 wt. %; for hydrogen, the amounts exceeded the stoichiometric requirement by factors of 10, 100, and 1000. The total pressure in the system was assumed to be constant at 0.10132 MPa. Equilibrium phase compositions were calculated over the temperature range of 750–1700 °C in 50 °C increments for carbon reduction and 500–1700 °C for hydrogen reduction. The calculated data on phase composition were tabulated and conventionally divided into three phases: metal (iron, titanium, vanadium, and silicon, including carbides and silicides), slag (oxides), and gas. The degree of metallization, as well as the composition of the metallic, slag,

and gas phases, were analyzed and presented in the form of graphical dependencies for clarity.

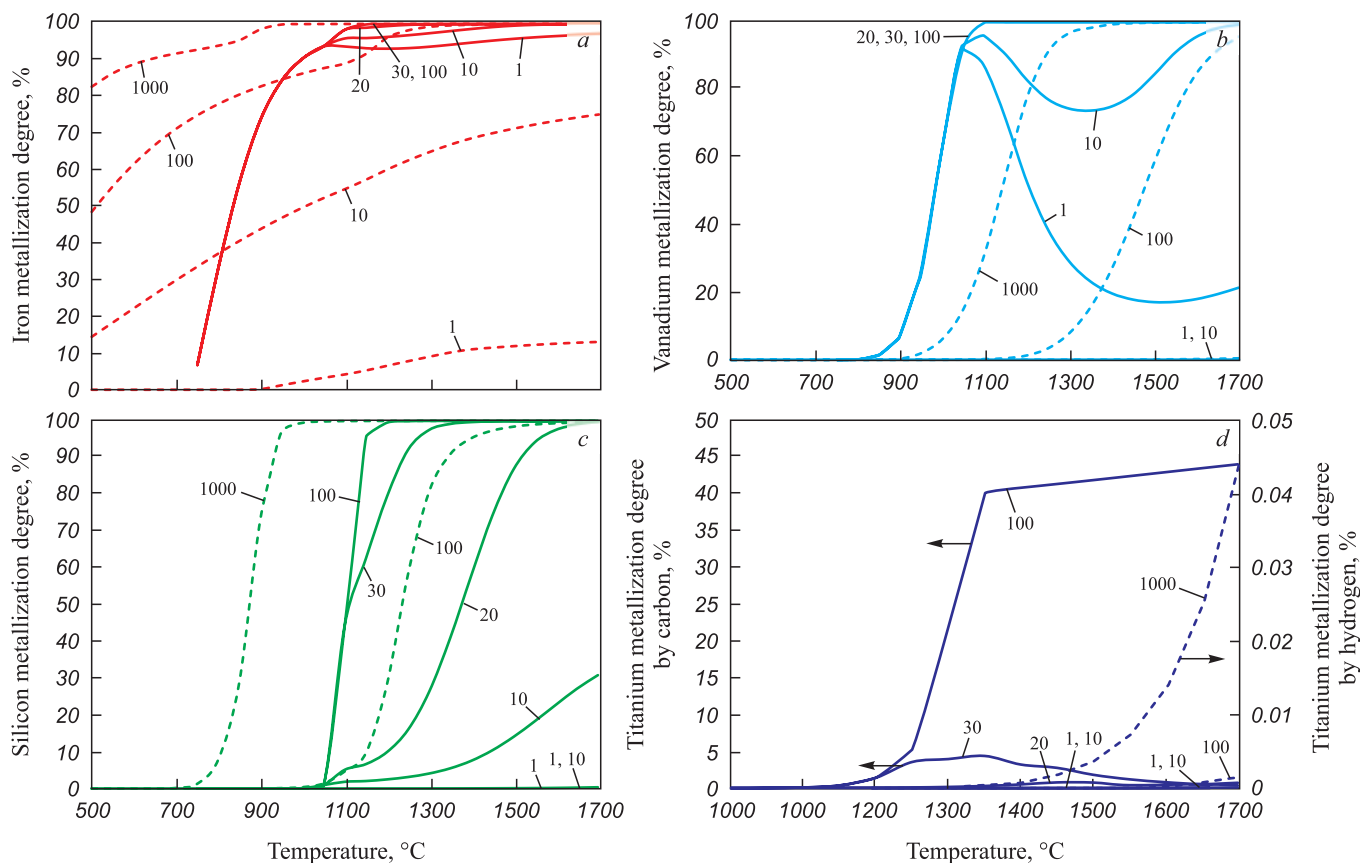
## MODELING RESULTS AND DISCUSSION

Based on the results of thermodynamic modeling, several elements in ilmenite concentrate – namely iron, titanium, vanadium, and silicon – were found to actively participate in the reduction process and contribute to the formation of the metallic phase (see Figure).

Among these, iron is the most readily reducible element. Its reduction by both carbon and hydrogen occurs across the entire range of temperatures and reductant quantities examined, with the only exception being hydrogen at its stoichiometric amount. Below 1050 °C, the degree of iron metallization with carbon increases steadily, regardless of the amount of reductant present. Above 1050 °C, metallization continues to rise, but the rate of increase varies depending on the level of carbon excess.

An increase in the amount of hydrogen in the system promotes a higher degree of iron metallization. The maximum degree of iron metallization by carbon reaches 99.39 % in the temperature range of 1250–1700 °C at a 100 wt. % excess of reductant relative to the stoichiometric amount. When reduced by hydrogen, the maximum degree of metallization reaches 99.36 % at 1700 °C with a 1000-fold excess of hydrogen. In both cases, complete reduction is not achieved due to the formation of the complex oxide FeAl<sub>2</sub>O<sub>4</sub>. In the carbon reduction system, iron in the metallic phase is primarily present in the form of iron carbide Fe<sub>3</sub>C, whereas in the hydrogen system it is found as a separate component. Reduced silicon binds part of the iron in the form of silicides FeSi and Fe<sub>3</sub>Si, forming in the carbon system at temperatures above 1050 °C, and in the hydrogen system at temperatures above 750 and 1200 °C.

Vanadium reduction by carbon is observed across the entire studied temperature range, whereas reduction by hydrogen occurs between 750 and 1700 °C. In the 800–1050 °C range, carbon reduction results in a progressive increase in the equilibrium degree of vanadium metallization, with vanadium carbide (VC) forming in the metallic phase. In calculations using stoichiometric or slightly excessive (10 wt. %) carbon, the degree of vanadium metallization decreases above 1050 °C, followed by an increase at temperatures above 1500 °C for stoichiometric carbon and above 1350 °C for 10 wt. % excess. This behaviour is attributed to the formation of not only vanadium carbides but also silicon carbides. With carbon excesses of 20, 30, and 100 wt. % over stoichiometry, the vanadium metallization degree increases with temperature, reaching 100 % at 1100 °C. In the case of hydrogen reduction, increasing the amount of hydrogen in the system leads to a decrease in the temperature at which vanadium begins to appear in the metallic phase. For stoichiometric



Effect of the amount of reducing agents on the degree of metallization of iron (a), vanadium (b), silicon (c) and titanium (d) (figures in the curves show excess reducing agent):  
 - - - - reduction with hydrogen; — — — — reduction with carbon

Влияние количества восстановителей на степень металлзации железа (a), ванадия (b), кремния (c) и титана (d) (цифры у кривых – избыток восстановителя):  
 - - - - восстановление водородом; — — — — восстановление углеродом

hydrogen and 10- and 100-fold excesses, these threshold temperatures are 1450, 1200, and 950 °C, respectively. The maximum equilibrium degree of vanadium metallization is observed at 1650 – 1700 °C and reaches 99.99 %.

Silicon reduction by carbon occurs over the temperature range of 1000 – 1700 °C. At 1000 and 1050 °C, the degree of silicon metallization is independent of the amount of carbon. Above 1050 °C, the metallization degree increases with both temperature and carbon content. The maximum degree of silicon metallization is observed at 1700 °C and amounts to 30.83, 99.52, 99.9, 99.95, and 100.00 % for stoichiometric carbon and 10, 20, 30, and 100 wt. % excesses, respectively.

Silicon reduction by hydrogen at a 1000-fold excess relative to the stoichiometric amount is observed within the temperature range of 650 – 1700 °C. As the hydrogen content in the system increases, the temperature at which silicon enters the metallic phase decreases – down to 1250 and 900 °C for 10-fold and 100-fold excesses, respectively. At stoichiometric hydrogen levels, no silicon reduction is observed. Within the range of 1350 – 1700 °C, a maximum silicon metallization degree of 100 % is reached

at a 1000-fold hydrogen excess. In both cases, silicon in the metallic phase is predominantly present as iron silicides FeSi and Fe<sub>3</sub>Si.

Titanium reduction by carbon occurs at temperatures of 1050 °C and above, while reduction by hydrogen is only observed at temperatures above 1550 °C and only in the case of a 1000-fold excess of hydrogen. When the carbon excess is below 10 wt. % of the stoichiometric amount, the titanium metallization degree remains negligible, reaching only 0.02 % at 1100 °C. With carbon excesses of 20, 30, and 100 wt. %, the maximum equilibrium degree of titanium metallization reaches 0.77, 4.37, and 44.02 % at 1450, 1350, and 1700 °C, respectively.

Solid-phase titanium reduction by hydrogen is not possible at stoichiometric levels or at hydrogen excesses below a factor of 100. The maximum degree of titanium metallization reaches only 0.05 % at 1700 °C, even at a 1000-fold excess of hydrogen over the stoichiometric amount. In the carbon system, titanium is present in the metallic phase in the form of titanium carbide (TiC), whereas in the hydrogen system it appears dissolved in the iron phase.

Selective reduction of iron from ilmenite is achievable with both carbon and hydrogen. For effective separation of the elements present in ilmenite concentrate, it is essential to achieve a high degree of solid-phase iron metallization while avoiding titanium metallization and ensuring that titanium is not reduced during the separation smelting of the solid-phase reduction products. Under the conditions required for high solid-phase iron metallization, other components of the ilmenite concentrate (vanadium, silicon, titanium) may also be partially reduced. However, titanium reduction is highly undesirable in this context. Vanadium, being one of the valuable components of ilmenite concentrate, can be recovered from both the metal and slag phases during further processing. However, the current technologies for vanadium recovery from the metal phase are associated with significant losses at all processing stages, which reduces the overall vanadium yield from the ore. Silicon, present in the concentrate as part of the gangue material, has no practical value when reduced to the metallic phase due to its low content.

The results of the calculations showed that iron reduction in ilmenite occurs at significantly lower temperatures when hydrogen is used as a reductant compared to carbon. Moreover, the degree of metallization is highly sensitive to the amount of hydrogen in the system. At the stoichiometric amount of hydrogen, the onset temperature of iron reduction is approximately 900 °C, while a 10-, 100-, or 1000-fold excess lowers this temperature to below 500 °C. In contrast, the onset temperature of iron reduction by carbon remains nearly constant at around 700 °C, regardless of the carbon excess.

Titanium is virtually not reduced by hydrogen, even when the hydrogen content exceeds the stoichiometric requirement for iron reduction by a factor of 1000. In contrast, in the presence of carbon, titanium forms a stable compound – titanium carbide (TiC) – which enables a relatively high degree of metallization. However, when carbon is limited, it is preferentially consumed in the reduction of other elements.

Vanadium exhibits similar behavior to titanium in the presence of carbon. However, due to its lower oxygen affinity, vanadium is reduced at comparatively lower temperatures – closer to those required for iron reduction. The extent of vanadium reduction by hydrogen depends strongly on the hydrogen content. At stoichiometric levels and even at a tenfold excess, vanadium is scarcely reduced. In contrast, at 100- and 1000-fold hydrogen excesses, the degree of metallization approaches 100 % at 1700 and 1400 °C, respectively. Notably, vanadium reduction by hydrogen occurs at higher temperatures than with carbon.

Unlike titanium and vanadium, silicon forms iron silicides. Its reduction is strongly influenced by the reductant's chemical activity. In the presence of excess carbon, silicon reduction begins at 1000 °C. By contrast, hydro-

gen reduction depends on the partial pressure of oxygen in the system. Under high hydrogen excess – 100 and 1000 times the stoichiometric amount required for iron reduction – silicon appears in the metallic phase at 950 and 750 °C, respectively.

It is worth noting that the temperature at which elements enter the metallic phase during carbon reduction does not depend on the amount of carbon in the system. Instead, the carbon content determines the extent to which the reduction reactions proceed. In contrast, the onset temperatures of element reduction by hydrogen  $T_{onset}$  are strongly influenced by the  $H_2O/H_2$  ratio in the system. For the system under study, the equilibrium values of the  $H_2O/H_2$  ratio are presented in the Table.

## CONCLUSIONS

The temperatures at which iron, vanadium, silicon, and titanium appear in the metallic phase during reduction of ilmenite concentrate by carbon are 700, 800, 1000, and 1150 °C, respectively, and are not affected by the amount of carbon present in the system. The excess carbon content relative to the stoichiometric requirement for the iron reduction reaction determines the extent of vanadium, silicon, and titanium reduction as the system temperature exceeds the onset temperature for the reduction of the corresponding element. By adjusting the carbon content and the process temperature, it is possible to control the development of reduction reac-

### Temperatures of the elements appearance in metallic phase and ratio of equilibrium amount of water vapor to hydrogen during reduction of elements from ilmenite by hydrogen

### Температуры появления элементов в металлической фазе и отношение равновесного количества паров воды к водороду при восстановлении элементов из ильменита водородом

Reducible element	Hydrogen excess	$T_{onset}$ , °C	$H_2O/H_2$ , wt. %
Fe	Stoichiometric	900	1.420
	10	<500	–
	100	<500	–
	1000	<500	–
Ti	1000	1550	0.013
	Stoichiometric	1450	2.790
V	10	1200	0.640
	100	950	0.079
	1000	750	0.008
	10	1250	0.660
Si	100	900	0.770
	1000	650	0.008

tions and achieve solid-phase selective reduction of iron or simultaneous reduction of iron, silicon, and vanadium while retaining titanium in the oxide phase.

The presence of carbon in excess of the stoichiometric amount for iron reduction leads to the formation of iron, vanadium, and silicon carbides. As the temperature increases during the pyrometallurgical separation stage, carbon contained in these carbides can partially reduce and bind titanium into carbides, thereby reducing the effectiveness of iron–titanium separation.

The onset temperatures for the reduction of iron, vanadium, silicon, and titanium from ilmenite concentrate by hydrogen span a broader range and are significantly influenced by the hydrogen content in the system. As the hydrogen concentration increases, the onset temperature for each element decreases, though to a different extent. This wider temperature window and the non-uniform temperature dependence of element reduction provide greater flexibility for controlling solid-phase selective reduction by hydrogen compared to carbon.

The negligible solubility of hydrogen in solid iron ensures that it does not affect the behavior of elements during the separation smelting of solid-phase reduction products. As a result, selective solid-phase reduction of elements can be carried out in a hydrogen stream, with process temperature serving as a control parameter for reduction selectivity. This approach eliminates the risk of titanium reduction and prevents the loss of titanium dioxide  $TiO_2$  during the separation of reduction products.

## REFERENCES / СПИСОК ЛИТЕРАТУРЫ

1. Leont'ev L.I., Volkov A.I. State and development of mineral resource base and metallurgical products to ensure Russia's import independence. In: *The Int. Sci. Conf. "Physico-Chemical Foundations of Metallurgical Processes" named after Academician A.M. Samarin. Vyksa. October 10-14, 2022.* Vyksa; 2022:18–36. (In Russ.).  
Леонтьев Л.И., Волков А.И. Состояние и развитие минерально-сырьевой базы и продукции металлургии для обеспечения импортнезависимости России. В кн.: *Международная научная конференция «Физикохимические основы металлургических процессов» имени академика А.М. Самарина. Выкса. 10–14 октября 2022 г.* Выкса; 2022:18–36.
2. Bogatyreva E.V. Production of Refractory Rare Metals: Metallurgy of Titanium and Its Compounds. Moscow: NUST MISIS; 2019:161. (In Russ.).  
Богатырева Е.В. Производство тугоплавких редких металлов: металлургия титана и его соединений. Москва: Изд. Дом НИТУ «МИСИС»; 2019:161.
3. Denisov S.I. Electrothermy of Titanium Slags. Moscow: Metallurgiya; 1979:165. (In Russ.).  
Денисов С.И. Электротермия титановых шлаков. Москва: Металлургия; 1979:165.
4. Alekseev L.F., Chentsov A.V., Shavrin S.V. Metallurgical evaluation of Ural ilmenite concentrates. In: *Complex Processing of Metallurgical Raw Materials*. Preprint. Yekaterinburg: UB RAS; 1994:27–35. (In Russ.).  
Алексеев Л.Ф., Ченцов А.В., Шаврин С.В. Металлургическая оценка уральских ильменитовых концентратов. В кн.: *Комплексная переработка металлургического сырья*. Препринт. Екатеринбург: УрО РАН; 1994:27–35.
5. Reznichenko V.A., Ustinov V.S., Karyazin I.A., Petrun'ko A.N. Electrometallurgy and Chemistry of Titanium. Moscow: Nauka; 1982:278. (In Russ.).  
Электрометаллургия и химия титана / В.А. Резниченко, В.С. Устинов, И.А. Карязин, А.Н. Петрунько. Москва: Наука; 1982:278.
6. Reznichenko V.A., Solov'ev V.I., Burmistrova T.M. Metallurgical evaluation of titanium-magnetite concentrate of the Chineyskoye deposit. *Kompleksnoe ispol'zovanie mineral'nogo syr'ya*. 1986;(2):60–63. (In Russ.).  
Резниченко В.А., Соловьев В.И., Бурмистрова Т.М. Металлургическая оценка титаномагнетитового концентрата Чинейского месторождения. *Комплексное использование минерального сырья*. 1986;(2):60–63.
7. Roshchin V.E., Gamov P.A., Roshchin A.V., Salikhov S.P. Prospects for the development of hydrogen technologies in the domestic metallurgy. *Ferrous Metallurgy. Bulletin of Scientific, Technical and Economic Information*. 2023;79(2):144–153. (In Russ.).  
<https://doi.org/10.32339/0135-5910-2023-2-144-153>  
Рошин В.Е., Гамов П.А., Рошин А.В., Салихов С.П. Перспективы освоения водородных технологий в отечественной металлургии. *Черная металлургия. Бюллетень научно-технической и экономической информации*. 2023;79(2):144–153.  
<https://doi.org/10.32339/0135-5910-2023-2-144-153>
8. Roshchin V.E., Smirnov K.I., Gamov P.A., Roshchin A.V. Fundamental features of hydrogen reduction of metals and feasibility of using hydrogen at the present stage. In: *Innovations and Complex Processing of Mineral Raw Materials – Actual Components of the Diversification of the Economy. Materials of the Int. Sci. and Pract. Conf.* Almaty; 2023: 153–155. (In Russ.).  
Рошин В.Е., Смирнов К.И., Гамов П.А., Рошин А.В. Фундаментальные особенности водородного восстановления металлов и целесообразность использования водорода на современном этапе. В кн.: *Инновации и комплексная переработка минерального сырья – актуальные составляющие диверсификации экономики. Материалы Международной научно-практической конференции*. Алматы; 2023:153–155.
9. Gamov P.A., Smirnov K.I., Roshchin V.E., Vyatkin G.P. Hydrogen technologies for decarbonization of ferrous metallurgy: Scientific background and technical capabilities. *Ferrous Metallurgy. Bulletin of Scientific, Technical and Economic Information*. 2024;80(7):47–53. (In Russ.).  
<https://doi.org/10.32339/0135-5910-2024-7-47-53>  
Гамов П.А., Смирнов К.И., Рошин В.Е., Вяткин Г.П. Оценка возможности селективного извлечения металлов из многокомпонентных оксидных материалов с применением водорода. *Черная металлургия. Бюллетень научно-технической и экономической информации*. 2024;80(7):47–53.  
<https://doi.org/10.32339/0135-5910-2024-7-47-53>

10. Kosdauletov N.Y., Roshchin A.V., Roshchin V.E. Production of high manganese slag by reducing iron and phosphorus from ferromanganese ores with hydrogen. *Chernye metally*. 2024;(2):4–9. (In Russ.).  
<https://doi.org/10.17580/chm.2024.02.01>  
Косдаuletov Н.И., Рошин А.В., Рошин В.Е. Получение высокомарганцевого шлага путем восстановления железа и фосфора из железомарганцевых руд водородом. *Черные металлы*. 2024;(2):4–9.  
<https://doi.org/10.17580/chm.2024.02.01>
11. Smirnov K.I., Gamov P.A., Samolin V.S., Roshchin V.E. Selective reduction of iron from ilmenite concentrate. *Chernye metally*. 2024;(7):19–23. (In Russ.).  
<https://doi.org/10.17580/chm.2024.07.03>  
Смирнов К.И., Гамов П.А., Самолин В.С., Рошин В.Е. Селективное восстановление железа из ильменитового концентрата. *Черные металлы*. 2024;(7):19–23.  
<https://doi.org/10.17580/chm.2024.07.03>
12. Moosavi-Khoonsari E., Siahbouni A.A., Kwon S.Y., Jones R., Mostaghel S. Thermodynamic modeling of ilmenite smelting and impurity distribution. *JOM*. 2024;76: 6511–6533. <https://doi.org/10.1007/s11837-024-06844-4>
13. Xiao W., Lu X.-G., Zou X.-L., Li C.-H., Ding W.-Z. Multiple gaseous reduction of ilmenite: Thermodynamic and experimental study. *Rare Metals*. 2015;34:888–894.  
<https://doi.org/10.1007/s12598-014-0264-9>
14. Run H., Pengsheng L., Yuehui Y., Jinzhu Z. Vacuum carbothermic reduction of Panzhihua ilmenite concentrate: A thermodynamic study. *Mineral Processing and Extractive Metallurgy Review*. 2017;38(3):193–198.  
<https://doi.org/10.1080/08827508.2017.1281129>
15. Yu H., Li C., Wei K., Li Y., Ma W. Effect of titanium suboxides on the reaction mechanism of hydrogen-reduced ilmenite. *International Journal of Hydrogen Energy*. 2023;48(5): 1747–1757. <https://doi.org/10.1016/j.ijhydene.2022.10.071>
16. Yunos N.F.M., Idris M.A., Nasrun N.A., Kurniawan A., Nomura T., Rezan S.A. Structural characterizations and phase transition on the reducibility of ilmenite ore with different carbon reductants by carbothermal reduction under hydrogen atmosphere. *Journal of Sustainable Metallurgy*. 2023;9:1716–1731.  
<https://doi.org/10.1007/s40831-023-00760-8>
17. He C., Zheng C., Dai W., Fujita T., Zhao J., Ma S., Li X., Wei Y., Yang J., Wei Z. Purification and phase evolution mechanism of titanium oxycarbide ( $TiC_xO_y$ ) produced by the thermal reduction of ilmenite. *Minerals*. 2021;11(2):104.  
<https://doi.org/10.3390/min11020104>
18. Zhang G., Gou H., Wu K., Chou K. Carbothermic reduction of Panzhihua ilmenite in vacuum. *Vacuum*. 2017;143:199–208.  
<https://doi.org/10.1016/j.vacuum.2017.06.016>
19. Setiawan A., Rhamdhani M.A., Pownceby M.I., Webster N.A.S., Harjanto S. Kinetics and mechanisms of carbothermic reduction of weathered ilmenite using palm kernel shell biomass. *Journal of Sustainable Metallurgy*. 2021;7(4): 1819–1837. <https://doi.org/10.1007/s40831-021-00457-w>
20. Myrzakulov M.K., Jumankulova S.K., Barmenshinova M.B., Martyushev N.V., Skeebea V.Y., Kondratiev V.V., Karlina A.I. Thermodynamic and technological studies of the electric smelting of Satpaevsk ilmenite concentrates. *Metals*. 2024;14(11):1211. <https://doi.org/10.3390/met14111211>
21. Wang Y., Yuan Z., Matsuura H., Tsukihashi F. Reduction extraction kinetics of titania and iron from an ilmenite by  $H_2$ -Ar gas mixtures. *ISIJ international*. 2009;49(2):164–170.  
<https://doi.org/10.2355/isijinternational.49.164>
22. Belov G.V., Trusov B.G. Thermodynamic Modeling of Chemically Reacting Systems. Moscow: Bauman MSTU; 2013:96. (In Russ.).  
Белов Г.В., Трусов Б.Г. Термодинамическое моделирование химически реагирующих систем. Москва: изд. МГТУ имени Н.Э. Баумана; 2013:96.
23. Thermodynamic Properties of Individual Substances. Guide. In 2 vols. Gurvich L.V., Khachkuruzov G.A., Medvedev V.A., etc. eds. Moscow: AN SSSR; 1962. (In Russ.).  
Термодинамические свойства индивидуальных веществ. Справочник. В 2 т. / Л.В. Гурвич, Г.А. Хачкурузов, В.А. Медведев и др. Москва: АН СССР; 1962.
24. Thermodynamic Properties of Individual Substances. Gurvich L.V., Veits I.V., Medvedev V.A., etc. eds. Moscow: Nauka; 1978–1982:623. (In Russ.).  
Термодинамические свойства индивидуальных веществ. Справочное изд. В 4 т. / Л.В. Гурвич, И.В. Вейц, В.А. Медведев и др. Москва: Наука; 1978–1982.
25. JANAF Thermochemical Tables. NSRDS – NBS37. Washington: Gove Printing Office; 1971:1144.

## Information about the Authors

## Сведения об авторах

**Konstantin I. Smirnov**, Research Associate of the Research Laboratory “Hydrogen Technologies in Metallurgy”, South Ural State University  
ORCID: 0009-0001-3678-2636  
E-mail: smirnovk@susu.ru

**Pavel A. Gamov**, Cand. Sci. (Eng.), Assist. Prof., Head of the Research Laboratory “Hydrogen Technologies in Metallurgy”, South Ural State University  
ORCID: 0000-0002-1474-644X  
E-mail: gamovpa@susu.ru

**Vasilii E. Roshchin**, Dr. Sci. (Eng.), Prof., Chief Researcher of the Research Laboratory “Hydrogen Technologies in Metallurgy”, South Ural State University  
ORCID: 0000-0003-3648-8821  
E-mail: roshchinve@susu.ru

**Константин Игоревич Смирнов**, научный сотрудник научно-исследовательской лаборатории «Водородные технологии в металлургии», Южно-Уральский государственный университет  
ORCID: 0009-0001-3678-2636  
E-mail: smirnovk@susu.ru

**Павел Александрович Гамов**, к.т.н., доцент, заведующий научно-исследовательской лаборатории «Водородные технологии в металлургии», Южно-Уральский государственный университет  
ORCID: 0000-0002-1474-644X  
E-mail: gamovpa@susu.ru

**Василий Ефимович Рошин**, д.т.н., профессор, главный научный сотрудник научно-исследовательской лаборатории «Водородные технологии в металлургии», Южно-Уральский государственный университет  
ORCID: 0000-0003-3648-8821  
E-mail: roshchinve@susu.ru

**Vladislav S. Samolin**, Postgraduate of the Chair “Pyrometallurgical and Foundry Technologies”, South Ural State University

**ORCID:** 0009-0003-1107-5788

**E-mail:** samolinvs@susu.ru

**Владислав Сергеевич Самолин**, аспирант кафедры «Пирометаллургические и литейные технологии», Южно-Уральский государственный университет

**ORCID:** 0009-0003-1107-5788

**E-mail:** samolinvs@susu.ru

## Contribution of the Authors

## Вклад авторов

**K. I. Smirnov** – addition of the database with thermodynamic characteristics of substances, thermodynamic calculation.

**P. A. Gamov** – formulation of the thermodynamic calculation methodology, analysis of the results.

**V. E. Roshchin** – formulation of the research task, formation of conclusions.

**V. S. Samolin** – preparation of graphic material.

**К. И. Смирнов** – дополнение базы данных термодинамическими характеристиками веществ, проведение термодинамического расчета.

**П. А. Гамов** – постановка методики термодинамического расчета, анализ результатов.

**В. Е. Рошчин** – постановка задачи исследования, формирование выводов.

**В. С. Самолин** – подготовка графического материала.

Received 01.12.2024

Revised 25.12.2024

Accepted 20.02.2025

Поступила в редакцию 01.12.2024

После доработки 25.12.2024

Принята к публикации 20.02.2025



UDC 66.046.581.4:669.054.82

DOI 10.17073/0368-0797-2025-2-179-187



Original article

Оригинальная статья

## PECULIARITIES OF THE PHASE COMPOSITION FORMATION OF STEELMAKING SLAGS AND EVALUATION OF THE POSSIBILITY OF OBTAINING MINERAL BINDERS WITH LOW CO<sub>2</sub> GENERATION ON THEIR BASIS

O. Yu. Sheshukov<sup>1, 2</sup> , M. A. Mikheenkova<sup>1, 2</sup>, D. K. Egiazar'yan<sup>1, 2</sup>,  
A. M. Mikheenkova<sup>2</sup>, M. V. Kleonovskii<sup>2</sup>, O. V. Matyukhin<sup>2</sup>

<sup>1</sup> Institute of Metallurgy, Ural Branch of the Russian Academy of Science (101 Amundsena Str., Yekaterinburg 620016, Russian Federation)

<sup>2</sup> Ural Federal University named after the first President of Russia B.N. Yeltsin (19 Mira Str., Yekaterinburg 620002, Russian Federation)

 o.j.sheshukov@urfu.ru

**Abstract.** The article presents the results of analysis of steelmaking slags formation. It is shown that currently two methods of steel refining are used in the steelmaking industry – oxidative and reducing. The method of oxidative refining is implemented in electric arc furnaces (EAF), and is primarily aimed at extracting phosphorus from the steel being smelted. Reducing refining is implemented in the ladle-furnace unit (LF) and is aimed at removing sulfur from steel. The features of these processes affect the formation of the phase composition of steelmaking slags. Under conditions of oxidative refining, wustite FeO, magnetite Fe<sub>3</sub>O<sub>4</sub>, larnite β-2CaO·SiO<sub>2</sub> and merwinite 3CaO·MgO·2SiO<sub>2</sub> are formed in EAF slags, and under conditions of reducing refining in LF slags, mayenite 12CaO·7Al<sub>2</sub>O<sub>3</sub>, periclase MgO, low-temperature modification of dicalcium silicate – γ-2CaO·SiO<sub>2</sub>, CaS and FeO. Of the minerals in the composition of EAF slags and LF slags, mayenite 12CaO·7Al<sub>2</sub>O<sub>3</sub> and larnite β-2CaO·SiO<sub>2</sub> have hydraulic activity. Based on the theoretical analysis of the formation of sulfated hydraulically active phases, the possibility of imparting properties of mineral binders to steelmaking slags by grinding without their additional thermal preparation is shown.

**Keywords:** LF slag, EAF slag, phase composition, binder, grinding, mineral binders, thermal treatment of slags, formation of phases in slags

**Acknowledgements:** The work was supported by PJSC Pipe Metallurgical Company, contract No. N112.210.011/23.

**For citation:** Sheshukov O.Yu., Mikheenkova M.A., Egiazar'yan D.K., Mikheenkova A.M., Kleonovskii M.V., Matyukhin O.V. Peculiarities of the phase composition formation of steelmaking slags and evaluation of the possibility of obtaining mineral binders with low CO<sub>2</sub> generation on their basis. *Izvestiya. Ferrous Metallurgy*. 2025;68(2):179–187. <https://doi.org/10.17073/0368-0797-2025-2-179-187>

# ОСОБЕННОСТИ ФОРМИРОВАНИЯ ФАЗОВОГО СОСТАВА СТАЛЕПЛАВИЛЬНЫХ ШЛАКОВ И ОЦЕНКА ВОЗМОЖНОСТИ ПОЛУЧЕНИЯ НА ИХ ОСНОВЕ МИНЕРАЛЬНЫХ ВЯЖУЩИХ ВЕЩЕСТВ С НИЗКОЙ ГЕНЕРАЦИЕЙ $\text{CO}_2$

О. Ю. Шешуков<sup>1,2</sup> , М. А. Михеенков<sup>1,2</sup>, Д. К. Егизарьян<sup>1,2</sup>,  
А. М. Михеенков<sup>2</sup>, М. В. Клеоновский<sup>2</sup>, О. В. Матюхин<sup>2</sup>

<sup>1</sup> Институт металлургии Уральского отделения Российской академии наук (Россия, 620016, Екатеринбург, ул. Амундсена, 101)

<sup>2</sup> Уральский Федеральный университет имени первого Президента России Б. Н. Ельцина (Россия, 620002, Екатеринбург, ул. Мира, 19)

 o.j.sheshukov@urfu.ru

**Аннотация.** В статье приведены результаты анализа механизма образования сталеплавильных шлаков. Показано, что в настоящее время в сталеплавильной отрасли используются два способа рафинирования стали – окислительный и восстановительный. Способ окислительного рафинирования реализуется в конвертерах и дуговых сталеплавильных печах (ДСП) и в первую очередь направлен на извлечение из выплавляемой стали фосфора, а восстановительное рафинирование происходит в агрегате ковш–печь (АКП) и направлено на удаление из стали серы. Особенности этих процессов сказываются на формировании фазового состава сталеплавильных шлаков. В условиях окислительного рафинирования в шлаках ДСП формируются вюстит  $\text{FeO}$ , магнетит  $\text{Fe}_3\text{O}_4$ , ларнит  $\beta\text{-}2\text{CaO}\cdot\text{SiO}_2$  и мервинит  $3\text{CaO}\cdot\text{MgO}\cdot 2\text{SiO}_2$ , а в условиях восстановительного рафинирования в шлаках АКП формируются майенит  $12\text{CaO}\cdot 7\text{Al}_2\text{O}_3$ , периклаз  $\text{MgO}$ , низкотемпературная модификация двухкальциевого силиката – шеннонит  $\gamma\text{-}2\text{CaO}\cdot\text{SiO}_2$ ,  $\text{CaS}$  и  $\text{FeO}$ . Из минералов в составе шлаков ДСП и АКП гидравлической активностью обладают майенит  $12\text{CaO}\cdot 7\text{Al}_2\text{O}_3$  и ларнит  $\beta\text{-}2\text{CaO}\cdot\text{SiO}_2$ . На основе теоретического анализа способов формирования сульфатированных гидравлически активных фаз показана возможность придания сталеплавильным шлакам путем помола свойств минеральных вяжущих веществ без их дополнительной термической обработки.

**Ключевые слова:** шлак АКП, шлак ДСП, фазовый состав, вяжущее, помол, минеральные вяжущие вещества, термическая обработка шлаков, формирование фаз в шлаках

**Благодарности:** Работа выполнена при финансовой поддержке ПАО «Трубная металлургическая компания», договор № Н112.210.011/23.

**Для цитирования:** Шешуков О.Ю., Михеенков М.А., Егизарьян Д.К., Михеенков А.М., Клеоновский М.В., Матюхин О.В. Особенности формирования фазового состава сталеплавильных шлаков и оценка возможности получения на их основе минеральных вяжущих веществ с низкой генерацией  $\text{CO}_2$ . *Известия вузов. Черная металлургия*. 2025;68(2):179–187. <https://doi.org/10.17073/0368-0797-2025-2-179-187>

## INTRODUCTION

At the turn of the 21<sup>st</sup> century, the steelmaking industry underwent radical changes. Due to increasing quality requirements for steel products combined with the declining quality of raw materials, high-intensity steel melting in ultra-high-power electric arc furnaces and methods of secondary steel treatment have become widespread. This led to changes in the structure and quality characteristics of steelmaking slags. In the previous century, the most common methods of steel production were the converter and open-hearth processes. The slags formed under such conditions had a stable crystalline structure, and their storage and processing did not pose significant challenges. The processing of these slags into commercial products was mainly carried out using the simplest methods – magnetic separation, crushing, and particle size classification – to meet the requirements of GOST 3344–83 “Slag crushed stone and sand for road construction. Technical specifications” [1].

The conditions for the formation of the phase and chemical composition of slags in the steelmaking industry

have changed significantly in recent years. The open-hearth method has become obsolete and is no longer used. Under modern conditions, two methods of steel refining are used in the steelmaking industry – oxidative and reducing. Oxidative refining is implemented in converter units and electric arc furnaces (EAF) and is primarily aimed at extracting phosphorus from the steel being smelted, while reducing refining is implemented in the ladle-furnace unit (LF) and is aimed at removing sulfur from steel. The specific features of these processes influence the formation of the phase composition of steelmaking slags.

The aim of this study is to analyze the specific features of steelmaking slag formation under current steel production conditions and to develop an optimal method for obtaining mineral binders based on these slag.

## PECULIARITIES OF STEELMAKING SLAG FORMATION

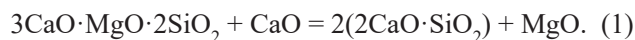
The processes of oxidative refining, carried out in converter and electric arc furnaces, differ only slightly, and the slags formed in these units are similar in terms of their phase and chemical composition. To ensure effec-

tive oxidative refining, a significant amount of burnt lime (CaO) is added to the furnace at the beginning of the melt. As a result of the interaction between CaO and the mill scale on the scrap metal, as well as with iron oxides formed during the oxygen blowing of molten steel, lime is assimilated and low-basic ( $\text{CaO}\cdot\text{Fe}_2\text{O}_3$ ) and high-basic ( $2\text{CaO}\cdot\text{Fe}_2\text{O}_3$ ) forms of calcium ferrite are formed in the slag. Simultaneously, during the oxygen blowing of molten steel, phosphorus pentoxide ( $\text{P}_2\text{O}_5$ ) enters the slag.  $\text{SiO}_2$ , an acidic oxide that enters the furnace along with contaminated scrap, displaces the amphoteric iron (III) oxide ( $\text{Fe}_2\text{O}_3$ ) from calcium ferrite, forming two silicate phases in the slag – dicalcium silicate ( $\beta\text{-}2\text{CaO}\cdot\text{SiO}_2$ ) and merwinite ( $3\text{CaO}\cdot\text{MgO}\cdot 2\text{SiO}_2$ ). At the same time, iron oxides enter the slag as independent phases. The dicalcium silicate formed in the slag exhibits a high-temperature polymorphic  $\beta$ -modification, known as larnite [2]. The formation of larnite in the slag is accompanied by partial isomorphous substitution of silicon-oxygen tetrahedra in the dicalcium silicate molecule by phosphorus pentoxide, which enters the slag during oxygen blowing. Due to the substitution of ions  $\text{SiO}_4^{4-}$  in the dicalcium silicate molecule by ions  $\text{PO}_4^{3-}$ , its ionic stabilization occurs, preventing the disintegration of dicalcium silicate during cooling. The other silicate phase, merwinite, is a magnesium-substituted analogue of dicalcium silicate. Magnesium oxide (MgO) forms due to the partial erosion of the periclase-based furnace lining by slag. As a result of all these processes, the final phase composition of the oxidative refining slag is formed [3], and consists of wustite (FeO) – 20.4 %, magnetite ( $\text{Fe}_3\text{O}_4$ ) – 24.1 %, larnite ( $\beta\text{-}2\text{CaO}\cdot\text{SiO}_2$ ) – 38.15 %, merwinite ( $3\text{CaO}\cdot\text{MgO}\cdot 2\text{SiO}_2$ ) – 15.9 %, and impurities – 1.45 %.

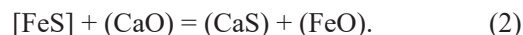
Steel from EAFs and converters is transferred to ladle units, where reducing refining is carried out in the ladle-furnace (LF) unit. When metal is tapped from the EAF or converter into the ladle, an effort is made to remove as much slag as possible. Nevertheless, a portion of the oxidative slag inevitably enters the ladle, forming the initial slag during the early stage of reducing refining. The phase composition of LF slag, as plotted on the  $\text{CaO}\text{-}\text{SiO}_2\text{-}\text{Al}_2\text{O}_3$  phase diagram and determined by the authors in studies on slag stabilization methods [2], is shown in Fig. 1.

Many of the identified phases contain magnesium oxide, since pure CaO was not used in phase formation; instead, a model slag with a chemical composition corresponding to typical LF slag containing approximately 10 % MgO was employed. Area *A* in Fig. 1 corresponds to the phase composition of EAF slag that entered the LF unit from the ladle iron, and only two phases remain

in area *A* – dicalcium silicate ( $\beta\text{-}2\text{CaO}\cdot\text{SiO}_2$ ) and merwinite ( $3\text{CaO}\cdot\text{MgO}\cdot 2\text{SiO}_2$ ). To enable desulfurization, burnt lime (CaO) is added to the LF unit, which reacts with merwinite and causes its decomposition according to the reaction



This phase composition corresponds to area *B* in Fig. 1. The interaction of free lime with sulfur in the metal leads to the following reaction



In area *B*, the slag viscosity is elevated, which hinders the desulfurization process. To reduce the viscosity, an alumina-based flux is added to the slag, and in area *C* (Fig. 1), the final phase composition of LF slag is formed [2], consisting of mayenite ( $12\text{CaO}\cdot 7\text{Al}_2\text{O}_3$ ) – 37.2 %, periclase (MgO) – 12.5 %, dicalcium silicate ( $\alpha\text{-}2\text{CaO}\cdot\text{SiO}_2$ ) – 41.4 %, approximately 1 % CaS, and the remainder FeO. During the cooling of LF slag, polymorphic transformations occur in the dicalcium silicate phase [2]. Five polymorphic modifications of dicalcium silicate are known, three of which are high-temperature forms ( $\alpha$ ,  $\alpha'_s$  and  $\alpha'_l$ ), and their successive transformations during cooling do not cause critical changes in LF slag. Since reducing conditions are maintained in the LF, iron oxides from the EAF slag are rapidly reduced to metallic a critical transformation is the polymorphic transition of larnite to shennonite<sup>1</sup>. Larnite ( $\beta\text{-}2\text{CaO}\cdot\text{SiO}_2$ )

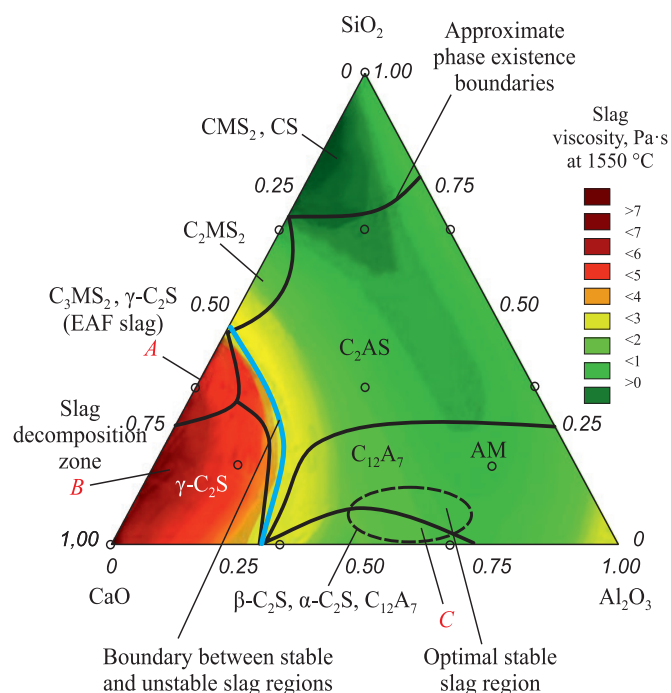


Fig. 1. Phase composition of LF slag [2]

Рис. 1. Фазовый состав шлака АКП [2]

<sup>1</sup> In Russian scientific literature, the term “shennonite” (ШЕННОНИТ) is commonly used to refer to the  $\gamma$ -polymorph of dicalcium silicate ( $\gamma\text{-}2\text{CaO}\cdot\text{SiO}_2$ ).

is a metastable modification of dicalcium silicate that, upon cooling below 525 °C, slowly transforms into shennonite ( $\gamma\text{-}2\text{CaO}\cdot\text{SiO}_2$ ). Since the true density of larnite ( $\beta\text{-}2\text{CaO}\cdot\text{SiO}_2$ ) is 3.28 g/cm<sup>3</sup> and that of shennonite ( $\gamma\text{-}2\text{CaO}\cdot\text{SiO}_2$ ) is 2.97 g/cm<sup>3</sup>, this polymorphic transformation leads to a 12 % volume increase, causing the slag to disintegrate into a powder-like fraction. As a result of these processes, larnite ( $\beta\text{-}2\text{CaO}\cdot\text{SiO}_2$ ) is absent in cooled LF slag, and shennonite ( $\gamma\text{-}2\text{CaO}\cdot\text{SiO}_2$ ) is present instead.

## LITERATURE REVIEW

The changed conditions of slag formation in the steel-making industry and the resulting phase composition require a more advanced approach to slag processing, taking into account current knowledge and developments in the formation of mineral binding agents based on such slags.

Due to stricter CO<sub>2</sub> emission regulations and environmental challenges associated with the storage and recycling of steelmaking slags, global efforts are being made to partially or completely replace components in general construction concrete – such as ordinary Portland cement, coarse aggregates (crushed stone, gravel), and fine aggregates (quartz sand). In [4], the use of converter slag with particle sizes of 5 – 20 mm as a substitute for coarse aggregates, and 0 – 5 mm for fine aggregates in general-purpose concrete, was investigated. It was shown that replacing natural aggregates with converter slag increases the concrete grade strength, allowing cement consumption to be reduced by 31 %. Similar findings are reported in [5], where the partial (30 %) replacement of natural aggregates with EAF slag resulted in improved physical and mechanical properties of the concrete. The authors concluded that EAF slag can be used to produce environmentally friendly concrete. In [6], concrete mixtures with 30 % fly ash replacing cement and 50 % EAF slag replacing coarse aggregate were tested for their physical and mechanical properties. The results demonstrated that the strength characteristics of these concrete mixtures surpassed those of conventional concrete made entirely with cement and natural aggregates. In [7], researchers investigated the replacement of coarse natural aggregates with EAF slag, while retaining natural quartz sand as the fine aggregate. It was observed that concrete containing EAF slag exhibited a faster strength gain during the first seven days of curing compared to concrete made with natural aggregates. Although the rate of strength development subsequently declined, the final grade strength of the slag-containing concrete remained higher. In [8], it was shown that eco-concrete incorporating 5 % aluminum slag and 20 % EAF slag as substitutes for natural aggregates demonstrated strength and durability levels comparable to those

of conventional concrete. A common feature across these studies is the use of slag primarily as a partial or complete replacement for natural aggregates, without altering the underlying mechanism of strength development based on Portland cement. However, this approach does not permit the complete elimination of Portland cement from the concrete mix, even though its production is a major source of CO<sub>2</sub> emissions.

A promising strategy for fully replacing Portland cement in concrete and mortar formulations involves the use of alkali-activated slag binders. The theoretical foundation for such binders was established by V.D. Glukhovskii [9], who proposed introducing various alkaline additives into slags prior to grinding. Upon hydration, these binders form insoluble calcium and sodium aluminosilicate hydrates – zeolites – capable of achieving compressive strengths of up to 200 MPa. At present, most studies in this area focus on the alkali activation of blast furnace slag [10] and EAF slag in combination with other industrial wastes [11 – 13]. The primary drawback of these binders is the need for extremely fine slag grinding and the presence of free alkalis in fully cured concrete, which may migrate to the surface and cause severe efflorescence. This issue is addressed in geopolymer binders, where free alkalis generated during activation are chemically bound within a three-dimensional polymer network [14]. This is achieved through the addition of specially treated metakaolins. Once incorporated into the polymer structure, the alkalis are immobilized and no longer migrate to the surface, effectively preventing efflorescence formation.

Since EAF slag contains a significant amount of iron oxides, and its silicate component consists primarily of dicalcium silicate ( $\beta\text{-}2\text{CaO}\cdot\text{SiO}_2$ ) and merwinite ( $3\text{CaO}\cdot\text{MgO}\cdot 2\text{SiO}_2$ ) – which decomposes at elevated basicity into two molecules of dicalcium silicate and periclase – the authors explored the possibility of simultaneously producing pig iron and Portland cement. This was to be achieved by increasing the slag's basicity through the addition of highly basic LF slag and extra lime. Laboratory studies and pilot-scale industrial trials confirmed the feasibility of this approach [15; 16]. It was established that mixing molten EAF slag, LF slag, and solid lime in a ratio of 64:17:17 %, respectively, allows for the simultaneous formation of Portland cement clinker and pig iron in proportions of 82 and 18 %, respectively. The Portland cement produced from this clinker demonstrated the following physical and mechanical properties:

- initial setting time – 175 min;
- final setting time – 285 min;
- volume stability – 0.2 mm;
- compressive strength after 2 days – 11.7 MPa;
- compressive strength after 28 days – 47.8 MPa.

According to GOST 31108, this cement meets the requirements for strength class 42.5 N. The chemical composition of the resulting pig iron complied with GOST 805 for foundry-grade pig iron of grade PL 1 and was as follows (wt. %: 3.13 C; 2.26 Mn; 0.109 Si; 0.036 P; 0.021 S).

## POTENTIAL PATHWAYS FOR TECHNOLOGY

### IMPLEMENTATION

Despite the positive outcomes of the trials, implementing this technology would require a complete reconstruction of steelmaking facilities, including the establishment of a dedicated slag secondary treatment section and a full reorganization of the logistics involved in slag transportation and processing.

In light of these challenges, an alternative approach was explored – the sulfate activation of steelmaking slags to impart the properties of mineral binding agents. In the construction industry, certain types of specialty cements are widely used, particularly gypsum-alumina cements based on calcium sulfoaluminates [17] and calcium sulfosilicates [18]. Gypsum-alumina cements are commonly applied for road and infrastructure repairs and are also used in rapid-setting and waterproofing systems – for example, the Emaco<sup>2</sup> line of fast-setting concretes was developed on the basis of such cements. Calcium sulfoaluminate and sulfoaluminoferrite binders are also well established in the production of expansive oil-well cements [19].

At present, several anhydrous minerals containing gypsum are known to possess strong binding properties. These include:

– calcium sulfosilicate (sulfospurrite  $2(\text{CaO} \cdot \text{SiO}_2) \cdot \text{CaSO}_4$  [17;18];

– calcium sulfoaluminate (yeelimite)  $3(\text{CaO} \cdot \text{Al}_2\text{O}_3) \cdot \text{CaSO}_4$  [17];

– calcium sulfoferrites, including low-basic  $3(\text{CaO} \cdot \text{Fe}_2\text{O}_3) \cdot \text{CaSO}_4$  and high-basic  $\text{CaO} \cdot \text{Fe}_2\text{O}_3 \cdot \text{CaSO}_4$  [20];

– a group of calcium sulfoaluminoferrites with the general formula  $\text{CaO}_n \cdot (\text{Al}_2\text{O}_3)_m \cdot (\text{Fe}_2\text{O}_3)_k \cdot (\text{SO}_3)_b$  [21].

These minerals are typically obtained by firing raw material mixtures at 1100 – 1300 °C, followed by either separate or joint grinding with Portland cement [17]. For EAF and LF slags, which contain mayenite ( $\text{C}_{12}\text{A}_7$ ) as well as dicalcium silicates ( $\beta\text{-}2\text{CaO} \cdot \text{SiO}_2$  and  $\gamma\text{-}2\text{CaO} \cdot \text{SiO}_2$ ), sulfate activation can be achieved through joint grinding with natural gypsum ( $\text{CaSO}_4 \cdot 2\text{H}_2\text{O}$ ).

The authors initially applied sulfate activation to LF slags. To prevent the development of internal stresses

during hydration of the resulting binder, which was produced by joint grinding of LF slag and gypsum, it was proposed to introduce additives that would enable the formation of a mineral binding agent following the principle of gypsum – cement – pozzolanic systems [22]. In this patented formulation, LF slag and gypsum act as the primary binder (cement), while pozzolanic additives include acidic sludges, various slags, and calcium carbonates – including EAF slag in amounts ranging from 9.5 to 23.0 %. The developed composite water-resistant gypsum-based binder made it possible to achieve compressive strengths in the range of 5 to 10 MPa in construction products.

## METHODOLOGY FOR OPTIMISATION

Further investigation of this binding system showed that increasing the proportion of EAF slag leads to a significant improvement in concrete strength. Notably, EAF slag can be added to the binder in the form of fine screening material (fraction 0 – 5 mm). Therefore, optimization of the strength properties of such concrete was carried out using experimental design methods, namely the simplex lattice method, with the test results described by a third-degree polynomial. The varying factors selected for the optimization were the contents of EAF slag, LF slag, and gypsum dihydrate in the raw mix. The intervals of variation for each factor are given in Table 1.

The scope of optimization is shown in Fig. 2.

According to the experimental plan, raw mixtures were prepared and mixed with water at a water-to-solid ratio of 0.4:1. The concrete was poured into standard molds and cured under air-dry conditions for seven days. After this curing period, compressive strength was measured and used as the response function.

## RESULTS AND DISCUSSION

The experimental plan and the results of compressive strength testing after 7 days are presented in Table 2.

Fig. 3 shows the overall distribution of the response function for the compressive strength of the slag-based binder.

Table 1. Intervals of the factors variation

Таблица 1. Интервалы варьирования факторов

Factor	Variation intervals, wt. %	
	upper	lower
EAF slag content	25	75
LF slag content	25	75
Gypsum dihydrate content	0	50

<sup>2</sup> Emaco is a registered trademark. URL: <https://mpkm.org/masterem-aco/?yclid=11188805335159930879> (accessed: October 9, 2024).

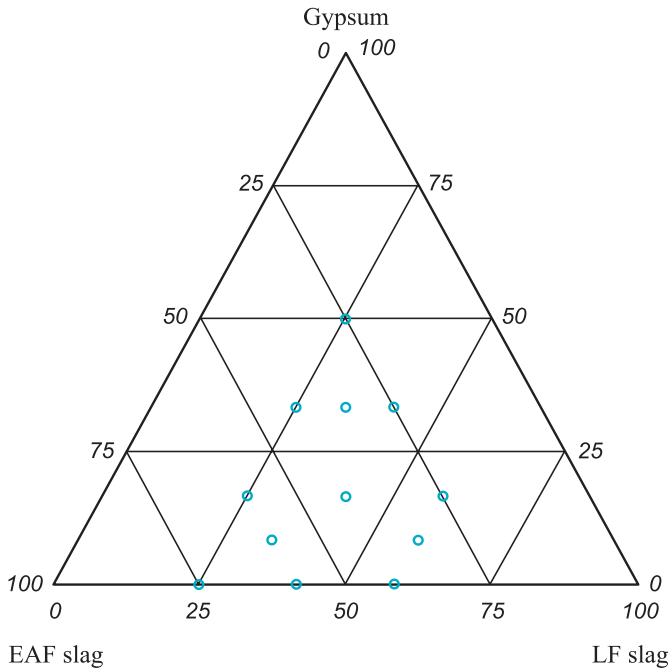


Fig. 2. Scope of optimisation

Рис. 2. Область проведения оптимизации

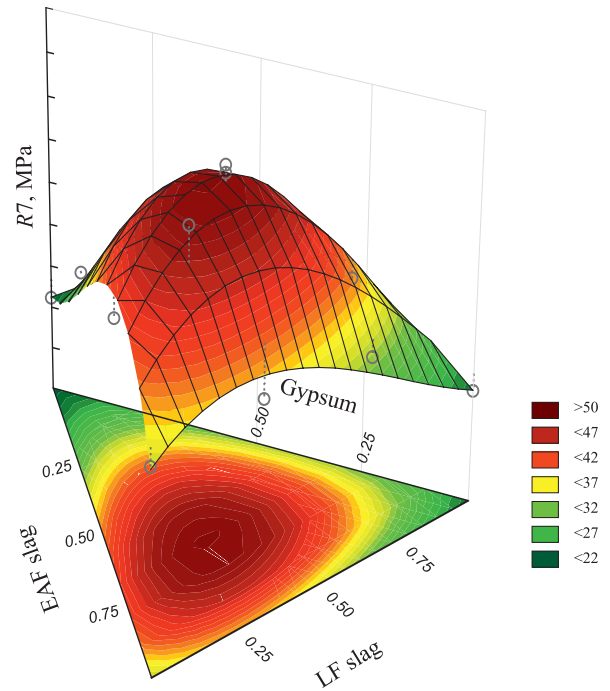


Fig. 3. General view of response function distribution for compressive strength of the binder

Рис. 3. Общий вид распределения функции отклика для предела прочности при сжатии вяжущего

Fig. 4 presents the isolines of equal compressive strength for the slag-based bind.

Point *A* in Fig. 4 corresponds to the maximum compressive strength of the binder – 50.4 MPa – achieved at an EAF slag content of 42.0 %, LF slag content of 42.0 %, and gypsum dihydrate content of 16.0 %.

The results of testing mineral binding agents based on steelmaking slags formed under modern steel production conditions confirm the feasibility of processing these slags using alternative approaches to those currently in use. Instead of limiting slag processing to con-

Table 2. Experimental plan and test results

Таблица 2. План проведения эксперимента и результаты испытаний

Content in the mix, wt. %			$R_{7c}$ , MPa
EAF slag	LF slag	gypsum	
41.67	58.33	0	33.5
25.00	58.33	16.67	33.4
33.33	33.33	33.33	34.2
33.33	58.33	8.33	37.2
58.33	41.67	0	35.2
41.67	25.00	33.33	34.5
75.00	25.00	0	34.2
41.67	41.67	16.67	50.8
25.00	41.67	33.33	31.2
25.00	75.00	0	23.2
41.67	41.67	16.67	49.9
25.00	25.00	50.00	21.1
58.33	33.33	8.33	52.1
58.33	25.00	16.67	39.8

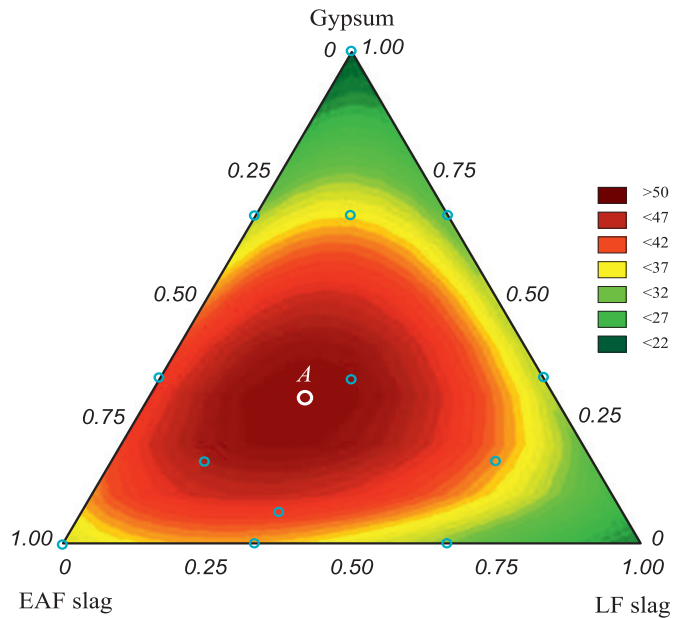


Fig. 4. Isolines of equal compressive strength when compressing the binder

Рис. 4. Изолинии равного предела прочности при сжатии вяжущего

ventional crushing and size classification, it is proposed to use steelmaking slags as raw materials for producing dry construction and concrete mixes. These products offer significantly higher market value compared to classified slag gravel and sand. Such mixes can be manufactured at existing dry mix production facilities, requiring only minimal modifications to the slag handling sections of metallurgical plants.

## CONCLUSIONS

Steelmaking slags generated during the steel smelting process contain hydraulically active phases that are capable of hardening upon contact with water. This study examined current methods for processing steelmaking slags and explored ways to impart the properties of mineral binding agents to them. A sulfate treatment method was proposed to activate the hydraulically active phases contained in the slags. As a result of sulfate activation, the resulting slag-based mineral binder exhibits high physical and mechanical properties, comparable to those of binders produced with Portland cement. It is recommended that this slag-based binder be used for the production of dry construction and concrete mixes suitable for both road building and general-purpose construction applications.

## REFERENCES / СПИСОК ЛИТЕРАТУРЫ

- Smirnov L.A., Sorokin Yu.V., Snyatinovskaya N.M., Danilov N.I., Eremin A.Yu. Processing of Man-Made Waste (based on the materials of programs for processing man-made formations of the Sverdlovsk region). Yekaterinburg: UIPC; 2012:607. (In Russ.).  
Смирнов Л.А., Сорокин Ю.В., Снятиновская Н.М., Данилов Н.И., Еремин А.Ю. Переработка техногенных отходов (по материалам программ по переработке техногенных образований Свердловской области). Екатеринбург: УИПЦ; 2012:607.
- Sheshukov O.Yu., Mikheenkova M.A., Nekrasov I.V., Egiazar'yan D.K., Metelkin A.A., Shevchenko O.I. Issues of Utilization of Steelmaking Refining Slags. Nizhny Tagil: NTI (branch) of UrFU; 2017:208. (In Russ.).  
Шешуков О.Ю., Михеенков М.А., Некрасов И.В., Егизарьян Д.К., Метелкин А.А., Шевченко О.И. Вопросы утилизации рафинировочных шлаков сталеплавильного производства. Нижний Тагил: НТИ (филиал) УрФУ; 2017:208.
- Leont'ev L.I., Sheshukov O.Yu., Mikheenkova M.A., Nekrasov I.V., Egiazar'yan D.K. Technological features of processing steelmaking slags into building materials and products. *Stroitel'nye materialy*. 2014;(10):70–74. (In Russ.).  
Леонтьев Л.И., Шешуков О.Ю., Михеенков М.А., Некрасов И.В., Егизарьян Д.К. Технологические особенности переработки сталеплавильных шлаков в строительные материалы и изделия. *Строительные материалы*. 2014;(10):70–74.
- Costa L.C.B., Nogueira M.A., Ferreira L.C., Elói F.P.F., Carvalho J.M.F., Peixoto R.A.F. Eco-efficient steel slag concretes: An alternative to achieve circular economy. *Revista IBRACON de Estruturas e Materiais*. 2022;(15):e15201. <https://doi.org/10.1590/S1983-41952022000200001>
- Diotti A., Cominoli L., Galvin A.P., Sorlini S., Plizzari G. Sustainable recycling of electric arc furnace steel slag as aggregate in concrete: Effects on the environmental and technical performance. *Sustainability*. 2021;13(2):521. <https://doi.org/10.3390/su13020521>
- Sekaran A., Palaniswamy M., Balaraju S. A study on suitability of EAF oxidizing slag in concrete: An eco-friendly and sustainable replacement for natural coarse aggregate. *The Scientific World Journal*. 2015;(1):1–8. <http://dx.doi.org/10.1155/2015/972567>
- Nguyen T.T.H., Phan D.H., Mai H.H., Nguyen D.L. Investigation on compressive characteristics of steel-slag concrete. *Materials*. 2020;13(8):1928. <http://dx.doi.org/10.3390/ma13081928>
- Javali S., Chandrashekar A.R., Naganna S.R., Manu D.S., Hiremath P., Preethi H.G., Kumar N.V. Eco-concrete for sustainability: utilizing aluminium dross and iron slag as partial replacement materials. *Clean Technology and Environmental Policy*. 2017;19:2291–2304. <http://dx.doi.org/10.1007/s10098-017-1419-9>
- Glukhovskii V.D., Pakhomov V.A. Slag-Alkali Cements and Concretes. Kiev: Budivelnik; 1978:184. (In Russ.).  
Глуховский В.Д., Пахомов В.А. Шлакощелочные цементы и бетоны. Киев: Будівельник; 1978:184.
- Artamonova A.V., Voronin K.M. Slag-alkaline binders based on blast-furnace granular slag of centrifugal impact grinding. *Tsement i ego primenenie*. 2011;(4):108–113. (In Russ.).  
Артамонова А.В., Воронин К.М. Шлакощелочные вяжущие на основе доменных гранулированных шлаков центробежно-ударного измельчения. *Цемент и его применение*. 2011;(4):108–113.
- Peys A., White C.E., Rahier H., Blanpain B., Pontikes Y. Alkali-activation of CaO-FeO<sub>x</sub>-SiO<sub>2</sub> slag: Formation mechanism from in situ X-ray total scattering. *Cement and Concrete Research*. 2019;122:179–188. <https://doi.org/10.1016/j.cemconres.2019.04.019>
- Peys A., White C.E., Rahier H., Blanpain B., Pontikes Y. Molecular structure of CaO-FeO<sub>x</sub>-SiO<sub>2</sub> glassy slags and resultant inorganic polymers. *Journal of the American Ceramic Society*. 2018;101(12):5846–5857. <https://doi.org/10.1111/jace.15880>
- Sedira N., Castro-Gomes J. Effects of EAF-Slag on alkali-activation of tungsten mining waste: mechanical properties. *MATEC Web of Conferences*. 2019;274:01003. <https://doi.org/10.1051/mateconf/201927401003>
- Dudnikov A.G., Dudnikova M.S., Redzhani A. Geopolymer concrete and its application. *Stroitel'nye materialy, oborudovanie, tekhnologii XXI veka*. 2018;(2):38–45. (In Russ.).  
Дудников А.Г., Дудникова М.С., Реджани А. Геополлимерный бетон и его применение. *Строительные материалы, оборудование, технологии XXI века*. 2018;(2):38–45.
- Mikheenkova M.A., Sheshukov O.Yu., Nekrasov I.V., Egiazar'yan D.K., Lobanov D.A. Production of mineral binder from steel-smelting slag. *Steel in Translation*. 2016;46:232–235. <https://doi.org/10.3103/S0967091216030098>

- Михеенков М.А., Шешуков О.Ю., Некрасов И.В., Егiazарьян Д.К., Лобанов Д.А. Придание сталеплавильным шлакам свойств минеральных вяжущих веществ. *Сталь*. 2016;(3):66–69.
16. Mikheenkoy M.A., Sheshukov O.Yu., Nekrasov I.V. A method for processing steelmaking waste to produce Portland cement clinker and cast iron. Patent RF no. 2629424. МРК7 С21В 3/04. *Bulleten' izobretenii*. 2017;(25). (In Russ.).  
Пат. 2629424 RU. Способ переработки отходов сталеплавильного производства с получением портландцементного клинкера и чугуна / Михеенков М.А., Шешуков О.Ю., Некрасов И.В.; заявлено 21.04.2016; опубликовано 29.08.2017. Бюллетень № 25.
17. Kuznetsova T.V. Aluminate and Sulfoaluminate Cements. Moscow: Stroiizdat; 1986:208 (In Russ.).  
Кузнецова Т.В. Алуминатные и сульфоалюминатные цементы. Москва: Стройиздат; 1986:208.
18. Atakuziev T.A. Sulfomineral Cements based on Phosphogypsum. Tashkent: FAN; 1979:152. (In Russ.).  
Атакузиев Т.А. Сульфоминеральные цементы на основе фосфогипса. Ташкент: ФАН; 1979:152.
19. Vyakhirev V.I., Frolov A.A., Krivoborodov Yu.R. Expanding Grouting Cements. Moscow: IRC RAO Gazprom; 1998:52. (In Russ.).  
Вяхирев В.И., Фролов А.А., Кривобородов Ю.Р. Расширяющиеся тампонажные цементы. Москва: ИРЦ РАО «Газпром»; 1998:52.
20. Kuznetsova T.V., Sychev M.M., Osokin A.P. Special Cements. St. Petersburg: Stroiizdat Spb; 1997:314. (In Russ.).  
Кузнецова Т.В., Сычев М.М., Осокин А.П. Специальные цементы. Санкт-Петербург: Стройиздат Спб; 1997:314.
21. Savchenko S.V. Sulfoaluminoferrite cements. *Tsement*. 1986;(3):11–12. (In Russ.).  
Самченко С.В. Сульфоалюмоферритные цементы. *Цемент*. 1986;(3):11–12.
22. Zuev M.V., Mamaev S.A., Mikheenkoy M.A., Stepanov A.I. Composite waterproof gypsum binder. Patent RF no. 2505504. IPC7 C04B 28/14. *Bulleten' izobretenii*. 2014;(3). (In Russ.).  
Пат. 2505504 RU. Композиционное водостойкое гипсовое вяжущее / Зуев М.В., Мамаев С.А., Михеенков М.А., Степанов А.И.; заявлено 13.7.2012; опубликовано 27.01.2014. Бюллетень № 3.

## Information about the Authors

## Сведения об авторах

**Oleg Yu. Sheshukov**, Chief Researcher of the Laboratory of Powder, Composite and Nano-Materials, Institute of Metallurgy, Ural Branch of the Russian Academy of Sciences; Dr. Sci. (Eng.), Prof., Director of the Institute of New Materials and Technologies, Ural Federal University named after the first President of Russia B.N. Yeltsin

ORCID: 0000-0002-2452-826X

E-mail: o.j.sheshukov@urfu.ru

**Mikhail A. Mikheenkoy**, Dr. Sci. (Eng.), Senior Researcher of the Laboratory "Pyrometallurgy of Ferrous Metals", Institute of Metallurgy, Ural Branch of the Russian Academy of Sciences; Prof., Ural Federal University named after the first President of Russia B.N. Yeltsin

ORCID: 0000-0002-7908-2955

E-mail: silast@mail.ru

**Denis K. Egiazar'yan**, Cand. Sci. (Eng.), Senior Researcher, Head of the Laboratory of Technogenic Formations Problems, Institute of Metallurgy, Ural Branch of the Russian Academy of Sciences; Assist. Prof. of the Chair of Metallurgy of Iron and Alloys, Ural Federal University named after the first President of Russia B.N. Yeltsin

ORCID: 0000-0002-9833-7191

E-mail: avari@mail.ru

**Aleksandr M. Mikheenkoy**, Postgraduate of the Chair "Metallurgy of Iron and Alloys", Ural Federal University named after the first President of Russia B.N. Yeltsin

E-mail: ma@osk66.ru

**Mikhail V. Kleonovskiy**, Engineer of the Chair "Metallurgy of Iron and Alloys", Ural Federal University named after the first President of Russia B.N. Yeltsin

ORCID: 0000-0002-8874-9061

E-mail: kleonovskiy@yandex.ru

**Oleg V. Matiukhin**, Cand. Sci. (Eng.), Assist. Prof. of the Chair "Thermal Physics and Informatics in Metallurgy", Ural Federal University named after the first President of Russia B.N. Yeltsin

E-mail: o.v.matiukhin@urfu.ru

**Олег Юрьевич Шешуков**, главный научный сотрудник лаборатории порошковых, композиционных и наноматериалов, Институт металлургии Уральского отделения РАН; д.т.н., профессор, директор Института новых материалов и технологий, Уральский федеральный университет имени первого Президента России Б.Н. Ельцина

ORCID: 0000-0002-2452-826X

E-mail: o.j.sheshukov@urfu.ru

**Михаил Аркадьевич Михеенков**, д.т.н., старший научный сотрудник лаборатории пирометаллургии черных металлов, Институт металлургии УрО РАН; профессор, Уральский федеральный университет имени первого Президента России Б.Н. Ельцина

ORCID: 0000-0002-7908-2955

E-mail: silast@mail.ru

**Денис Константинович Егiazарьян**, к.т.н., старший научный сотрудник, заведующий лабораторией проблем техногенных образований, Институт металлургии УрО РАН; доцент кафедры металлургии железа и сплавов, Уральский федеральный университет им. Первого Президента Б.Н. Ельцина

ORCID: 0000-0002-9833-7191

E-mail: avari@mail.ru

**Александр Михайлович Михеенков**, аспирант кафедры «Металлургия железа и сплавов», Уральский федеральный университет им. Первого Президента Б.Н. Ельцина

E-mail: ma@osk66.ru

**Михаил Витальевич Клеоновский**, инженер 1-й категории кафедры «Металлургия железа и сплавов», Уральский федеральный университет имени первого Президента России Б.Н. Ельцина

ORCID: 0000-0002-8874-9061

E-mail: kleonovskiy@yandex.ru

**Олег Владимирович Матиухин**, к.т.н., доцент кафедры теплофизики и информатики в металлургии, Уральский федеральный университет имени первого Президента России Б.Н. Ельцина

E-mail: o.v.matiukhin@urfu.ru

## Contribution of the Authors

## Вклад авторов

**O. Yu. Sheshukov** – basic studies of the phase composition of steel-making slags, development of a methodology for analyzing phase formation under conditions of oxidative and reductive refining, theoretical analysis of chemical and phase transformations in slags, development of methods for their optimization in order to improve hydraulic activity.

**M. A. Mikheenkova** – development of model slags for research, study of the phase composition of LF and EAF slags, analysis of their hydraulic activity; management of pilot industrial tests on the use of slags as binders.

**D. K. Egiazar'yan** – systematization of data on methods of processing steelmaking slags, development of methods for grinding slags and their use in the construction industry, including in the production of concrete using LF and EAF slags.

**A. M. Mikheenkova** – analysis of interaction of slags with additives, including exploring the possibilities of sulfate activation of steel slag for use in the cement industry; development of recipes and testing of slag-based binders.

**M. V. Kleonovskii** – study of the physical and mechanical properties of concretes based on steelmaking slags, conducting tests for the strength and durability of concretes with addition of slag, analysis of their environmental effectiveness in construction.

**O. V. Matyukhin** – theoretical review of literature on the use of slags in building materials, analysis of works on the alkaline activation of slags and their application in geopolymer binders.

**О. Ю. Шешуков** – исследование фазового состава сталеплавильных шлаков, разработка методики анализа фазообразования в условиях окислительного и восстановительного рафинирования, теоретический анализ химических и фазовых преобразований, разработка методов их оптимизации с целью улучшения гидравлической активности.

**М. А. Михеенкова** – разработка модельных шлаков для исследований, изучение фазового состава шлаков АКП и ДСП, анализ их гидравлической активности, руководство опытно-промышленными испытаниями по использованию шлаков в качестве вяжущих материалов.

**Д. К. Егиазарьян** – систематизация данных о способах переработки сталеплавильных шлаков, разработка методик помола шлаков и их использования в строительной промышленности, в том числе в производстве бетонов с использованием шлаков ДСП и АКП.

**А. М. Михеенкова** – анализ взаимодействия шлаков с добавками, в том числе исследование возможности сульфатной активации сталеплавильных шлаков для использования в цементной промышленности; разработка рецептур и тестирование вяжущих материалов на основе шлаков.

**М. В. Клеоновский** – изучение физических и механических свойств бетонов на основе сталеплавильных шлаков, проведение тестов на прочность и долговечность бетонов с добавлением шлаков, анализ их экологической эффективности в строительстве.

**О. В. Матюхин** – обзор литературы по использованию шлаков в строительных материалах, анализ работ по щелочной активации шлаков и их применению в геополимерных вяжущих.

Received 04.09.2024  
Revised 27.09.2024  
Accepted 23.10.2024

Поступила в редакцию 04.09.2024  
После доработки 27.09.2024  
Принята к публикации 23.10.2024



UDC 519.876.2

DOI 10.17073/0368-0797-2025-2-188-194



Original article

Оригинальная статья

## USING DIGITAL SIMULATION MODELS TO OPTIMIZE THE OPERATION OF COMPLEX PRODUCTION FACILITIES

A. V. Zimin<sup>1</sup>, M. E. Kornet<sup>2</sup> , I. V. Burkova<sup>3</sup>, V. V. Zimin<sup>1</sup><sup>1</sup> Siberian State Industrial University (42 Kirova Str., Novokuznetsk, Kemerovo Region – Kuzbass 654007, Russian Federation)<sup>2</sup> National University of Science and Technology “MISIS” (4 Leninskyii Ave., Moscow 119049, Russian Federation)<sup>3</sup> V.A. Trapeznikov Institute of Control Sciences, Russian Academy of Sciences (65 Profsoyuznaya Str., Moscow 117997, Russian Federation) [marya.kornet@gmail.com](mailto:marya.kornet@gmail.com)

**Abstract.** Using the example of formalized description of the converter production at JSC EVRAZ United West Siberian Metallurgical Plant consisting of two converter shops with two and three units, it is shown that the issues of planning production volumes and repairs of metallurgical units, building end-to-end schedules of units are complex and multifactorial tasks characterized by the discreteness and non-linearity of the functions describing them. The formalization of the tasks of optimizing production processes with specified constraints and criteria showed that features of the studied process of converter production make it almost impossible to build and use analytical solutions. The approach chosen by the authors to the solution (taking into account these circumstances) is based on the use of a digital discrete event simulation model. Such a model is a digital copy of the investigated process of converter production, reflects its structure, performance, technical condition and parameters: duration of converter campaign, duration of repair periods, etc. The model uses various control mechanisms to solve the problems of distributing the input flow of cast iron between converter shops, forming schedules for the operation of individual converters and their repairs, accumulates information as it functions for the purpose of optimizing and predicting the results of the operation process. It allows one to collect data on the operation of converter production and use predictive analytics tools to plan repairs, provides data that cannot be obtained directly on a physical object and which can be used to optimize system parameters, and generates datasets for visualizing individual results of the operation process.

**Keywords:** converter production, regulatory and current duration of campaign, schedule of operation and repairs of converters, design scheme of shop operation, discrete and nonlinear task, digital simulation model, computer modeling, numerical solution

**For citation:** Zimin A.V., Kornet M.E., Burkova I.V., Zimin V.V. Using digital simulation models to optimize the operation of complex production facilities. *Izvestiya. Ferrous Metallurgy*. 2025;68(2):188–194. <https://doi.org/10.17073/0368-0797-2025-2-188-194>

## ИСПОЛЬЗОВАНИЕ ЦИФРОВЫХ ИМИТАЦИОННЫХ МОДЕЛЕЙ ДЛЯ ОПТИМИЗАЦИИ РАБОТЫ СЛОЖНЫХ ПРОИЗВОДСТВЕННЫХ ОБЪЕКТОВ

А. В. Зимин<sup>1</sup>, М. Е. Корнет<sup>2</sup> , И. В. Буркова<sup>3</sup>, В. В. Зимин<sup>1</sup><sup>1</sup> Сибирский государственный индустриальный университет (Россия, 654007, Кемеровская область – Кузбасс, Новокузнецк, ул. Кирова, 42)<sup>2</sup> Национальный исследовательский технологический университет «МИСИС» (Россия, 119049, Москва, Ленинский пр., 4)<sup>3</sup> Институт проблем управления им. В.А. Трапезникова РАН (Россия, 117997, Москва, ул. Профсоюзная, 65) [marya.kornet@gmail.com](mailto:marya.kornet@gmail.com)

**Аннотация.** На примере формализованного описания работы конвертерного производства АО «ЕВРАЗ Объединенный Западно-Сибирский металлургический комбинат» в составе двух конвертерных цехов с двумя и тремя агрегатами показано, что вопросы планирования объемов производства и ремонтов металлургических агрегатов, построения сквозных графиков работы агрегатов являются сложными и многофакторными задачами, которые характеризуются дискретностью и нелинейностью описывающих их функционалов. Формализация задач оптимизации производственных процессов с заданными ограничениями и критериями показала, что особенности исследуемого процесса функционирования конвертерного производства делают практически невозможными построение и использование аналитических решений. Выбранный авторами подход к решению (с учетом указанных обстоятельств) базируется на использовании цифровой

дискретно-событийной имитационной модели. Такая имитационная модель представляет собой цифровую копию исследуемого процесса функционирования конвертерного производства, отражает его структуру, производительность, техническое состояние и такие параметры, как длительность кампании конвертеров, длительность ремонтных периодов и др. Модель использует различные механизмы управления для решения задач распределения входного потока чугуна между конвертерными цехами, формирования календарных графиков работы отдельных конвертеров и их ремонтов; накапливает информацию в ходе производственного процесса для целей оптимизации и прогнозирования результатов процесса функционирования; позволяет собирать данные о процессе функционирования конвертерного производства и использовать инструменты предиктивной аналитики для планирования ремонтов; предоставляет данные, которые невозможно получить непосредственно на физическом объекте и которые могут быть использованы для оптимизации параметров системы; формирует наборы данных для визуализации отдельных результатов процесса функционирования.

**Ключевые слова:** конвертерное производство, нормативная и текущая длительность кампании, график работы и ремонтов конвертеров, проектная схема работы цеха, дискретная и нелинейная задача, цифровая имитационная модель, компьютерное моделирование, численное решение

**Для цитирования:** Зимин А.В., Корнет М.Е., Буркова И.В., Зимин В.В. Использование цифровых имитационных моделей для оптимизации работы сложных производственных объектов. *Известия вузов. Черная металлургия.* 2025;68(2):188–194.  
<https://doi.org/10.17073/0368-0797-2025-2-188-194>

## INTRODUCTION

The tasks of planning repairs and calendar schedules for converter operation in the steelmaking production of a metallurgical plant have significant specific features, which are due to the discreteness, non-linearity, and strong interdependence of these tasks. It is advisable to approach such tasks as a comprehensive solution to a single general task, without decomposition, since under conditions of strong interrelations, decomposition does not allow for stable and effective solutions to individual subtasks due to the limitations imposed by the decomposition procedure [1; 2]. However, obtaining a comprehensive solution using analytical methods for the planning object under consideration is extremely difficult – if not entirely impossible. Therefore, the authors of the study decided to construct a discrete event digital simulation model of the functioning process of converter production at a metallurgical plant with two steelmaking shops, comprising two and three converters, respectively [3 – 5]. The presence of such a model makes it possible to find a comprehensive solution to the tasks under investigation.

## EVOLUTION OF SIMULATION MODEL CONCEPTS AND MODERN FUNCTIONAL REQUIREMENTS

The original concept of a simulation model was developed for industrial products, where a clear link existed between the simulation model and the product at every stage of its life cycle – from creation to disposal. As the approach evolved, it was extended to cover production processes as well [6 – 8]. According to the framework presented in [3], the evolution of simulation models progresses through four stages:

- 1 – physical objects (products) are created without any simulation model (i.e., no digital prototype);
- 2 – a simulation model (digital prototype) is used only at the design stage of the product;
- 3 – there is information exchange between the physical object and the digital model;

4 – physical object and digital model interact in real time, enabling continuous improvement of both the physical system and its digital counterpart.

This concept – involving real-time interaction between a physical object (or process) in the real world and its digital model in the virtual space, as well as the exchange of information between the two – reflects the idea of a digital twin [9 – 11].

Based on this classification, the goal of the present study is to develop a digital model of the functioning process of converter production at a metallurgical plant that corresponds to the third stage of this evolution. At the current stage, generally accepted functional requirements for such a digital model of converter production include the following:

- accurately representing the structure of production, the performance and technical condition of units, the duration of converter campaigns, the length of repair periods, and other key parameters;
- employing various control mechanisms to distribute the input flow of cast iron between converter shops and to generate calendar schedules for the operation and repair of individual converters;
- accumulating operational data over time for the purpose of optimizing and forecasting the performance of the production process;
- collecting data on the functioning of converter production and applying predictive analytics tools for repair planning;
- providing information that cannot be obtained directly from the physical object but is valuable for optimizing the performance parameters of converter production;
- generating datasets that support the visualization of individual aspects of the model's functioning process [12 – 14].

The virtual component of the digital twin consists of two main parts: the digital master and the digital shadow. The digital master contains the core information

required to construct the simulated process. The digital shadow represents the set of data that the functioning physical object (process) “casts” into the virtual space, along with models that allow for forecasting the properties of the process within certain limits [15 – 17].

### ELEMENTS OF FORMALIZED DESCRIPTION OF CONVERTER PRODUCTION FUNCTIONING PROCESS

**Basic concepts and notation.** Let us denote the steel-making production as  $O = \{O_I, O_{II}\}$ , which includes two shops. Here,  $O_I = \{o_1, o_2, o_3\}$  and  $O_{II} = \{o_4, o_5\}$ , meaning that the first shop includes three converters of the same type, and the second shop consists of two identical units. As the time interval for the planning tasks under investigation, we consider a sequence  $(T_1, T_2, \dots, T_j, \dots, T_p)$  of  $p$  months,  $T_j = (\Delta t_l | l = \overline{1, L_j})$  (where  $L_j$  denotes the number of days in the  $j$ -th month). Each converter is treated as a discrete unit operating in cyclical mode. When describing a converter, we introduce the tuple  $o_i = o(f_i, \rho_i, g_i, K_i, k_{ij}^b, r_i)$ , (where  $f_i$  – amount of steel produced by the unit per cycle (tons);  $\rho_i$  – consumption coefficient characterizing the need for cast iron  $g_i$  to produce one ton of steel ( $g_i = f_i \rho_i, \rho < 1$ );  $K_i$  – normative duration of the campaign of the converter (i.e. the number of heats the unit must perform on one lining from one cold repair to the next);  $k_{ij}^b$  – number of heats completed by the  $i$ -th converter at the beginning of the  $j$ -th planning period;  $r_i, v = \overline{1, 2, \dots}$  – durations (in days) of shutdowns (due to repair or waiting) for the  $i$ -th converter. Due to the uniformity of converters in each shop, the following equalities can be assumed:

$$f_i = f_I, i = \overline{1, 3}; \quad \rho_i = \rho_I, i = \overline{1, 3}; \quad (1)$$

$$g_i = g_I; \quad K_i = K_I, i = \overline{1, 3};$$

$$f_i = f_{II}, i = \overline{4, 5}; \quad \rho_i = \rho_{II}, i = \overline{4, 5}; \quad (2)$$

$$g_i = g_{II}; \quad K_i = K_{II}, i = \overline{4, 5}.$$

Let us denote by  $m_{ij}(\Delta t_l), m_{ij}(\Delta t_l), m_{Iij}(\Delta t_l)$  the number of heats produced by converter  $i$ , and by shops  $O_I$  and  $O_{II}$ , respectively, during the  $l$ -th day of the  $j$ -th period. Accordingly, we have

$$\sum_{i=1}^3 m_{ij}(\Delta t_l) = m_{Iij}(\Delta t_l); \quad (3)$$

$$\sum_{i=4}^5 m_{ij}(\Delta t_l) = m_{IIij}(\Delta t_l).$$

The calendar schedule of operation of the  $i$ -th converter in the  $j$ -th month is defined as the sequence

$$(m_{ij}(\Delta t_l) | l = \overline{1, L_j}). \quad (4)$$

If  $l$  is a day on which the converter undergoes repair or is placed in reserve, then  $m_{ij}(\Delta t_l) = 0$ .

We introduce the function  $k_{ij}(l)$ , which represents the number of heats performed by the  $i$ -th converter from the beginning of the campaign up to and including the  $l$ -th day of the  $j$ -th period. The values of this function are limited by the normative duration of the converter campaign

$$k_{ij}(l) \leq \begin{cases} K_I, & i = \overline{1, 3}, \\ K_{II}, & i = \overline{4, 5}. \end{cases} \quad (5)$$

Let us denote by  $k_{ij}^b$  the number of heats completed by the  $i$ -th converter at the beginning of the  $j$ -th planning period. Then, taking into account condition (4), the number of heats  $k_{ij}^e$ , produced by the  $i$ -th converter by the end of the  $j$ -th planning period can be represented as

$$k_{ij}^e = k_{ij}^b + \sum_{l=1}^{S_j} m_i(\Delta t_{s_l}), \quad (6)$$

where  $k_{ij}^e = k_{ij+1}^b$ .

**Structural constraints on the functioning of converters in the shops.** When a converter executes the calendar schedule of operation as defined in expression (4), the value of the function increases by  $m_{ij}(\Delta t_l)$  on each subsequent day, according to the rule:  $[k_{ij}(l) = k_{ij}(l-1) + m_{ij}(\Delta t_l)]$ , until it reaches the normative duration of the converter campaign. The function  $k_{ij}(l)$  has a “sawtooth” form, where the width of each “tooth” base depends on the calendar schedule of the converter’s operation and may span several planning periods. Once the maximum value is reached, the function retains this value until the end of the converter’s repair. Upon completion of the repair (or when the converter is placed in reserve), the function resets to zero. The fluctuations of the function  $k_{ij}(l)$  are regular in nature, but they do not follow a fixed period.

The design scheme of converter operation for Shop 1 is presented in Fig. 1. According to this scheme, simultaneous operation of all three converters is not allowed. Instead, the configuration assumes the continuous operation of two units, while the third is either undergoing repair or is held in reserve. This structure ensures that at any given time, exactly two converters are active, thereby maintaining a balanced operational load and enabling scheduled repairs without full production stoppage. Let us define the state  $s_{ij}(l)$  of the  $i$ -th converter of the first shop on the  $l$ -th day of the  $j$ -th planning period as follows:

$$s_{ij}(l) = \begin{cases} wr, & 0 \leq k_{ij}(l) \leq K; \\ rm, & k_{ij}(l) = K; \\ rz, & k_{ij}(l) = 0. \end{cases} \quad (7)$$

A description of the state transitions of the converters during the time interval from  $l(r_{11})$  to  $l(r_{31})$  (see Fig. 1) is presented in the corresponding Table.

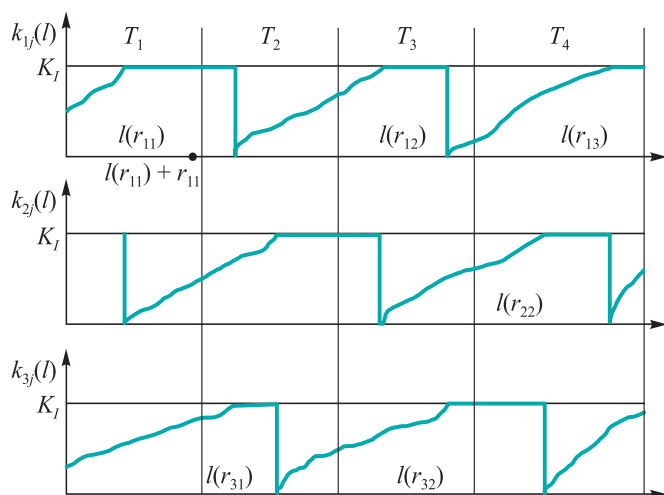


Fig. 1. Design operation scheme of converters of Shop 1

Рис. 1. Проектная схема работы конвертеров первого цеха

The design solutions and the repair management system for the second shop do not allow more than one cold repair to be carried out within a single planning period. Fig. 2 presents examples of permissible and unacceptable operational schemes for the converters in the second shop.

It should be noted that, in order to achieve maximum separation between the repairs of converters 4 and 5 – expressed in terms of the number of heats performed – the absolute difference between the values of the functions  $k_4(l)$  and  $k_5(l)$  must be as large as possible. The maximum value of this absolute difference equals  $K/2$  (Fig. 3). This maximum separation condition also applies to the first shop, since, according to the design scheme of converter operation, two out of the three units are in operation on each day.

**Quantitative constraints on converter operation.**

The simultaneous operation of units within the shops is subject to a set of technological constraints that define the allowable range for the number of heats per day in each shop, depending on whether one or two converters are operating at the same time:

$$\underline{m}_I^1 \leq m_{ij}(\Delta t_l) \leq \overline{m}_I^1, \quad i = \overline{1,3}, j = \overline{1,P}; \quad (8)$$

$$\underline{m}_{II}^1 \leq m_{ij}(\Delta t_l) \leq \overline{m}_{II}^1, \quad i = \overline{4,5}, j = \overline{1,P}; \quad (9)$$

**Operating procedure of converters of Shop 1**

**Порядок работы конвертеров цеха 1**

$i \backslash l$	$(l(r_{11}), l(r_{11}) + r_{11})$	$(l(r_{11}) + r_{11}, l(r_{31}))$
$s_{ij}(l)$	$rm$	$rz$
$s_{ij}(l)$	$wr$	$wr$
$s_{ij}(l)$	$wr$	$wr$

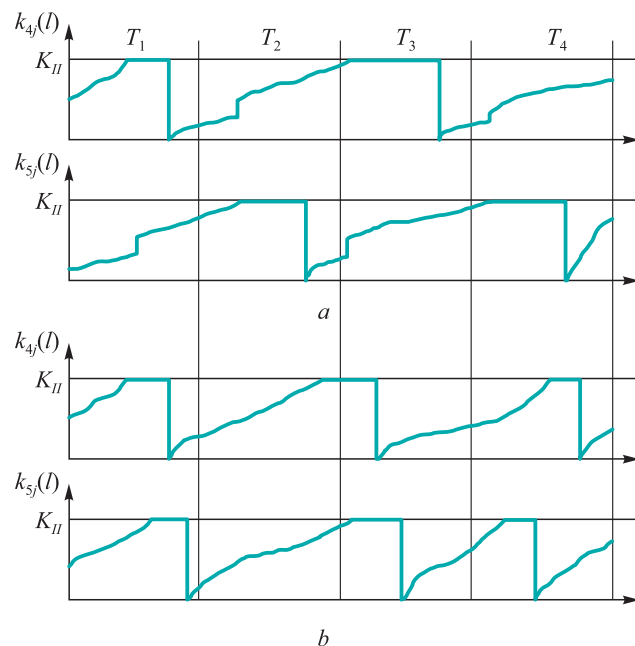


Fig. 2. Permissible (a) and unacceptable (b) operating schemes of converters 4 and 5 (in pos. a in the planning intervals  $T_1, T_3$  and  $T_4$ , two repairs are performed)

Рис. 2. Допустимая (a) и недопустимая (b) схемы работы конвертеров 4 и 5 (на поз. a в интервалах планирования  $T_1, T_3$  и  $T_4$  выполняются по два ремонта)

$$\underline{2m}_I^1 \leq [m_{ij}(\Delta t_l) + m_{i'j}(\Delta t_l)] \leq \overline{2m}_I^1; \quad (10)$$

$$i \neq i', \quad i, i' = \overline{1,3}, j = \overline{1,P};$$

$$\underline{2m}_{II}^1 \leq [m_{4j}(\Delta t_l) + m_{5j}(\Delta t_l)] \leq \overline{2m}_{II}^1, \quad j = \overline{1,P}, \quad (11)$$

where  $\underline{m}_I^1, \overline{m}_I^1, \underline{m}_{II}^1, \overline{m}_{II}^1, \underline{2m}_I^1, \overline{2m}_I^1, \underline{2m}_{II}^1, \overline{2m}_{II}^1$  represent the minimum and maximum number of heats produced

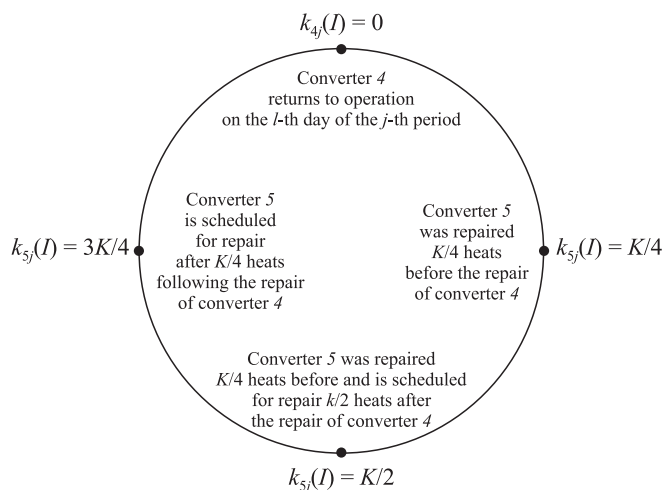


Fig. 3. Dependence of the absolute difference  $|k_4(l) - k_5(l)|$  on values of the functions  $k_4(l)$  and  $k_5(l)$

Рис. 3. Зависимость абсолютной разности  $|k_4(l) - k_5(l)|$  от значений функций  $k_4(l)$  и  $k_5(l)$

in the first and second shops, respectively, under two operating modes: with a single converter in operation, and with two converters in operation. Note that  $2m_l^1 < m_l^1$  and  $2m_{II}^1 < m_{II}^1$ , since otherwise, the shop would be unable to produce the number of heats within the ranges from  $m_l^1$  to  $2m_l^1$  and from  $m_{II}^1$  to  $2m_{II}^1$ , which does not correspond to actual operating conditions. Operation involving three converters simultaneously in the first shop is technologically infeasible.

Thus, the first shop, which according to the design solutions must operate continuously with two converters, can produce between  $2m_l^1$  and  $2m_{II}^1$  heats per day. Each unit may perform between  $m_l^1$  and  $m_{II}^1$  heats. The second shop, in the range from  $m_{II}^1$  to  $2m_{II}^1$  heats, can operate only with one converter (operating mode 1), in the range from  $2m_{II}^1$  to  $m_{II}^1$  it can operate with either one or two converters (operating mode 2), and in the range from  $m_{II}^1$  to  $2m_{II}^1$  it can operate only with two converters (operating mode 3) (Fig. 4).

**Determining the required daily cast iron production volumes in the blast furnace shop.** Cast iron, which serves as the main component of the converter charge, is produced by three blast furnaces (continuous-operation units). Each blast furnace is described by the following parameters: the average daily cast iron production volume  $g_q(\Delta t)$  at full capacity, which depends on the furnace volume; the production volume at reduced capacity  $g_q(\Delta t)/2$ , which may apply during periods of scheduled preventive maintenance, the overhaul schedule  $[r_q = \Delta t_l | l = (\overline{l_{qj}^b, l_{qj}^e})]$  typically carried out once every 4 – 5 years; the schedule  $r_{qj}^{ppr} = (\overline{l_{qj}^1, \dots, l_{qj}^v})$ , of planned preventive repairs during the  $j$ -th planning period, whose duration usually does not exceed 12 h (here  $q=1,3$  is the number of the blast furnace;  $l_{qj}^b, l_{qj}^e$  are the start and end dates of the overhaul, respectively;  $v$  is the number of planned preventive repairs in the  $j$ -th planning period).

Let  $g_{qj}(\Delta t_l)$  denote the planned cast iron production volume for the  $q$ -th blast furnace on the  $l$ -th day of the  $j$ -th planning period

$$g_{qj}(\Delta t_l) = \begin{cases} g_q(\Delta t), & l \notin (\overline{l_{qj}^b, l_{qj}^e}); \\ 0, & l \in (\overline{l_{qj}^b, l_{qj}^e}); \\ \frac{g_q(\Delta t)}{2}, & l \in (\overline{l_{qj}^1, \dots, l_{qj}^v}). \end{cases} \quad (12)$$

It is clear that the total cast iron production volume on  $l$ -th day is equal to

$$g_j(\Delta t_l) = \sum_{q=1}^3 g_{qj}(\Delta t_l), \quad l = \overline{1, L_j}. \quad (13)$$

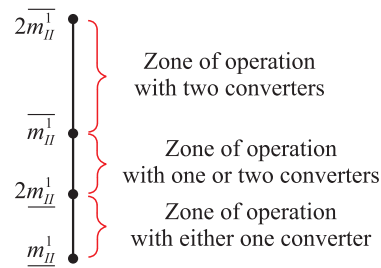


Fig. 4. Ranges of operating modes of converters of Shop 2

Рис. 4. Диапазоны режимов работы конвертеров второго цеха

The sequence  $(g_j(\Delta t_l) | l = \overline{1, L_j})$  describes the planned daily cast iron production of the blast furnace shop during the  $j$ -th planning period. Given the calendar schedule of converter operation defined by expression (4), the following equalities must hold

$$g_I \sum_{i=1}^3 m_{ij}(\Delta t_l) + g_{II} \sum_{i=4}^5 m_{ij}(\Delta t_l) = g_j(\Delta t_l), \quad l = \overline{1, L_j}. \quad (14)$$

### SPECIFIC FEATURES OF THE TASKS UNDER INVESTIGATION AND THE APPROACH TO THEIR SOLUTION

The main applied tasks that require solutions based on the above-described model representations of the object of study include:

1. Forming the schedules  $(m_{ij}(\Delta t_l) | l = \overline{1, L_j})$ ,  $(m_{Iij}(\Delta t_l) | l = \overline{1, L_j})$  of converter heats based on the cast iron production schedule  $(g_j(\Delta t_l) | l = \overline{1, L_j})$  for each  $j$ -th period, in order to determine monthly planned targets for the converter shops;

2. Forming the repair schedules for the converters

$$(l_{ij}^n, l_{ij}^e)_v \subset \bigcup_{j=1}^P T_j, \quad i = \overline{1, 5}, \quad v = \overline{1, 2, \dots}, \quad (15)$$

$$r_v = \begin{cases} l_{ij}^e - l_{ij}^n, & j = j'; \\ L_j - l_{ij}^n + l_{ij}^e, & j \neq j' \end{cases}$$

in the converter production shops, with the aim of planning the work of the maintenance services of the metallurgical plant;

3. Forming the operation  $[(m_{ij}(\Delta t_l) | l = \overline{1, L_j}) | i = \overline{1, 3}]$

and  $[(m_{ij}(\Delta t_l) | l = \overline{1, L_j}) | i = \overline{4, 5}]$  schedules of the converter shops, to ensure processing of incoming liquid cast iron from the blast furnace shop.

Thus, the main features of the investigated tasks include the discreteness and non-linearity of the functions, functionals, operators, parameters, and criteria that define these tasks. In particular, according to Fig. 3, one of the preferred criteria in calendar scheduling may be defined as follows

$$Q = \sum_{j=1}^P \left[ \left( |k_{ij}^e - k_{ij}^e| - 0,5K_I \right) + \left( |k_{4j}^e - k_{5j}^e| - 0,5K_{II} \right) \right] \rightarrow \min, \quad (16)$$

this criterion is aimed at ensuring the maximum separation of repairs of the two operating converters (expressed in terms of the number of heats performed). The corresponding functional  $Q$  belongs to the class of discrete and nonlinear functionals. The discreteness and non-linearity of the tasks hinder or make it impossible to build analytical models capable of identifying and ranking the set of admissible solutions.

Thus, the formalization of the studied tasks shows that the specific features of the process of functioning of converter production make it difficult – or practically impossible – to develop and apply analytical solutions. Considering these circumstances, the authors selected an approach based on the development and use of a digital discrete event simulation model, which:

- serves as a digital copy of the process of functioning of the converter production under study, reflects its structure, performance, technical condition, and parameters such as duration of converter campaigns, repair periods, and others;

- applies various control mechanisms to solve the tasks of distributing the input flow of cast iron between converter shops and forming calendar schedules for the operation and repair of individual converter;

- accumulates information over the course of its functioning for the purpose of optimization and forecasting of the process results;

- allows collecting data on the process of functioning of converter production and using predictive analytics tools to plan repairs;

- provides data that cannot be obtained directly on the physical object, but can be used to optimize the parameters of the system;

- generates datasets for the visualization of individual results of the functioning process [18 – 20].

## CONCLUSIONS

A significant interdependence, discreteness, and non-linearity of the tasks related to planning production volumes, repairs, and converter operation schedules have been demonstrated. The necessity of developing a digital discrete-event simulation model of the process of functioning of converter production at a metallurgical plant has been substantiated, in order to obtain numerical solutions to the tasks under study through computer modeling.

## REFERENCES / СПИСОК ЛИТЕРАТУРЫ

1. Lesdon L. Optimization of Large Systems. Moscow: Nauka; 1975:432. (In Russ.).  
Лэсдон Л. Оптимизация больших систем. Москва: Наука; 1975:432.
2. Hamann-Lohmer J., Lasch R. Production planning and scheduling in multi-factory production networks: A systematic literature review. *International Journal of Production Research*. 2021;59(7):2028–2054.  
<https://doi.org/10.1080/00207543.2020.1797207>
3. Prokhorov A., Lysachev M. The Digital Doppelganger. Analysis, Trends, and World Experience. Borovkov A.I. ed. Moscow: All'ansPrint; 2020:401. (In Russ.).  
Прохоров А., Лысачев М. Цифровой двойник. Анализ, тренды, мировой опыт / Научн. ред. проф. А.И. Боровков. Издание первое, исправленное и дополненное. Москва: ООО «АльянсПринт»; 2020:401.
4. Glaessgen E.H., Stargel D.S. The digital twin paradigm for future NASA and U.S. air force vehicles. In: *53<sup>rd</sup> AIAA/ASME/ASCE/AHS/ASC Structures, Structural Dynamics and Materials Conf. 20<sup>th</sup> AI. 23–26 April 2012, Honolulu, Hawaii*. <https://doi.org/10.2514/6.2012-1818>
5. The new age of manufacturing: Digital twin technology & IoT [Electronic resource]. URL: <http://www.innovation4.cn/library/r46394/>. (Accessed: 20.01.2025).
6. Modern manufacturing's triple play: Digital twins, analytics and the internet of things [Electronic resource]. URL: <https://www.nextspace.com/recommended-reading/modern-manufacturings-triple-play-digital-twins-analytics-and-iot>. (Accessed: 20.01.2025).
7. Digital doppelgangers in retail – who are they and why do you urgently need to get to know them? [Electronic resource]. Available at URL: [https://new-retail.ru/tehnologii/tsifrovye\\_dvoyniki\\_v\\_riteyle\\_kto\\_eto\\_takie\\_i\\_pochemu\\_s\\_nimi\\_srochno\\_nuzhno\\_znakomitsya5533/?ysclid=m8ajzyvqlj502045804](https://new-retail.ru/tehnologii/tsifrovye_dvoyniki_v_riteyle_kto_eto_takie_i_pochemu_s_nimi_srochno_nuzhno_znakomitsya5533/?ysclid=m8ajzyvqlj502045804). (Accessed: 20.01.2025). (In Russ.).
8. “15 key components of modern production” (Nano news net website) [Electronic resource]. Available at URL: <https://www.nanonewsnet.ru/articles/2017/15-klyuchevykh-komponentov-sovremennogo-proizvodstva>. (Accessed: 20.01.2025). (In Russ.).
9. Digital twins and digital shadows in high-tech industry. Available at URL: <https://4science.ru/articles/Cifrovie-dvoyniki-i-cifrovie-teni-v-visokotehnologichnoi-promishlennosti>. (Accessed: 20.01.2025). (In Russ.).
10. Key tools and formats for the development of the digital economy: “smart” digital twins and the NTI SPbPU Center [Electronic resource]. Available at URL: <https://nticenter.spbstu.ru/news/6722>. (Accessed: 20.01.2025). (In Russ.).
11. UK team to develop rapid virtual testing technique for manufactured components [Electronic resource]. URL: <https://www.theengineer.co.uk/content/news/uk-team-to-develop-rapid-virtual-testing-technique-for-manufactured-components/>. (Accessed: 20.01.2025).
12. Borovkov A.I., Ryabov Yu.A. Definition, development and application of digital twins: Approach of the NTI SPbPU Competence Center “New Production Technologies”. *Digital Substation*. 2019;(12):20–25. (In Russ.).  
Боровков А.И., Рябов Ю.А. Определение, разработка и применение цифровых двойников: подход Центра компе-

- тенций НТИ СПбПУ «Новые производственные технологии». *Цифровая подстанция*. 2019;(12):20–25.
13. Design with Confidence (Commentary). CIMdata [Electronic resource]. URL: <https://www.cimdata.com/de/resources/complimentary-reports-research/commentaries/item/3345-design-with-confidence-commentary/3345-design-with-confidence-commentary>. (Accessed: 20.01.2025).
  14. Rodič B. Industry 4.0 and the new simulation modelling paradigm. *Organizacija*. 2017;50(3):193–207. <https://doi.org/10.1515/orga-2017-0017>
  15. Mukherjee T., DebRoy T. A digital twin for rapid qualification of 3D printed metallic components. *Applied Materials Today*. 2019;14:59–65. <https://doi.org/10.1016/j.apmt.2018.11.003>
  16. Lind M. Digital thread. *Aras* [Electronic resource]. URL: <https://community.aras.com/b/english/posts/promise-of-the-digital-thread>. (Accessed: 28.05.2020)
  17. A new paradigm of digital design and modeling of globally competitive products of a new generation [Electronic resource]. Available at URL: <http://fea.ru/news/6721>. (Accessed: 20.01.2025). (In Russ.).
  18. Prokhorov I.M., Zimin A.V., Burkova I.V., Zimin V.V. Formulation and decomposition of the task of scheduling repairs and operation of steelmaking converters. *Management systems and information technologies*. 2024;(2(96)):38–40. (In Russ.).
- Прохоров И.М., Зимин А.В., Буркова И.В., Зимин В.В. Постановка и декомпозиция задачи календарного планирования ремонтов и работы конвертеров сталеплавильного производства. *Системы управления и информационные технологии*. 2024;(2(96)):38–40.
19. Kornet M.E., Zimin A.V., Burkova I.V., Zimin V.V. Planning BOF repair system in conditions of quasi-periodic operation of units. *Izvestiya. Ferrous Metallurgy*. 2024;67(6):738–743. <https://doi.org/10.17073/0368-0797-2024-6-738-743>
- Корнет М.Е., Зимин А.В., Буркова И.В., Зимин В.В. Планирование системы ремонтов конвертеров в условиях квазипериодического функционирования агрегатов. *Известия вузов. Черная металлургия*. 2024;67(6):738–743. <https://doi.org/10.17073/0368-0797-2024-6-738-743>
20. Prokhorov I.M., Zimin A.V., Burkova I.V., Zimin V.V. The procedure for solving the problem of scheduling repairs of converters in a steelmaking plant with two units. *Management systems and information technologies*. 2024;(2(96)):64–67. (In Russ.).
- Прохоров И.М., Зимин А.В., Буркова И.В., Зимин В.В. О процедуре решения задачи построения расписания ремонтов конвертеров сталеплавильного цеха с двумя агрегатами. *Системы управления и информационные технологии*. 2024;(2(96)):64–67.

## Information about the Authors

## Сведения об авторах

**Aleksei V. Zimin**, Dr. Sci. (Eng.), Assist. Prof., Head of the Chair of Automation and Information Systems, Siberian State Industrial University  
**ORCID:** 0000-0002-0485-9846  
**E-mail:** zimin.0169@yandex.ru

**Maria E. Kornet**, Senior Lecturer of the Chair of Engineering Cybernetics, National University of Science and Technology "MISIS"  
**ORCID:** 0000-0003-4100-5644  
**E-mail:** marya.kornet@gmail.com

**Irina V. Burkova**, Dr. Sci. (Eng.), Assist. Prof., Leading Researcher, V.A. Trapeznikov Institute of Control Sciences, Russian Academy of Sciences  
**ORCID:** 0000-0002-4671-0847  
**E-mail:** irbur27@mail.ru

**Valerii V. Zimin**, Dr. Sci. (Eng.), Prof. of the Chair of Automation and Information Systems, Siberian State Industrial University  
**ORCID:** 0000-0003-4152-3572  
**E-mail:** zimin1945@sibsiu.ru

**Алексей Валерьевич Зимин**, д.т.н., доцент, заведующий кафедрой автоматизации и информационных систем, Сибирский государственный индустриальный университет  
**ORCID:** 0000-0002-0485-9846  
**E-mail:** zimin.0169@yandex.ru

**Мария Евгеньевна Корнет**, старший преподаватель кафедры инженерной кибернетики, Национальный исследовательский технологический университет «МИСИС»  
**ORCID:** 0000-0003-4100-5644  
**E-mail:** marya.kornet@gmail.com

**Ирина Владимировна Буркова**, д.т.н., доцент, ведущий научный сотрудник, Институт проблем управления им. В.А. Трапезникова РАН  
**ORCID:** 0000-0002-4671-0847  
**E-mail:** irbur27@mail.ru

**Валерий Викторович Зимин**, д.т.н., профессор кафедры автоматизации и информационных систем, Сибирский государственный индустриальный университет  
**ORCID:** 0000-0003-4152-3572  
**E-mail:** zimin1945@sibsiu.ru

## Contribution of the Authors

## Вклад авторов

**A. V. Zimin** – formulation of the problem, formation of conclusions.  
**M. E. Kornet** – formulation of research tasks, development and implementation of the algorithm, analysis of results.  
**I. V. Burkova** – formulation of research tasks, data analysis.  
**V. V. Zimin** – technological description of the task, justification of the research direction, analysis of results.

**А. В. Зимин** – постановка проблемы, формирование выводов.  
**М. Е. Корнет** – постановка задачи исследования, разработка и реализация алгоритма, анализ полученных результатов.  
**И. В. Буркова** – постановка задач исследования, анализ данных.  
**В. В. Зимин** – технологическое описание поставленной задачи, обоснование направления исследований, анализ полученных результатов.

Received 20.12.2024  
 Revised 20.01.2025  
 Accepted 27.01.2025

Поступила в редакцию 20.12.2024  
 После доработки 20.01.2025  
 Принята к публикации 27.01.2025

Над номером работали:

*Л.И. Леонтьев, главный редактор*

*Е.В. Протопопов, заместитель главного редактора*

*Е.А. Ивани, ответственный секретарь*

*Л.П. Башенко, заместитель ответственного секретаря*

*Е.Ю. Потапова, заместитель главного редактора по развитию*

*О.А. Долицкая, научный редактор*

*В.В. Расенец, верстка, иллюстрации*

*Г.Ю. Острогорская, менеджер по работе с клиентами*

---

Подписано в печать 20.04.2025. Формат 60×90 <sup>1</sup>/<sub>8</sub>. Бум. офсетная № 1.  
Печать цифровая. Усл. печ. л. 11,0. Заказ 21934. Цена свободная.

---

Отпечатано в типографии Издательского Дома МИСИС.  
119049, Москва, Ленинский пр-кт, д. 4, стр. 1.  
Тел./факс: +7 (499) 236-76-17



Kuznetsk armor: The first frontiers of victory

Experience in producing rails from bainitic steels 30KhG2S2AFM and 30KhG2SAFN

Actual progress of production waste disposal problems

Initiation of melting at tilt grain boundaries in austenite depending on the misorientation angle

On the influence of rare-earth oxide additives on kinetics of borated layer formation and boron diffusion along grain boundaries during steel boriding

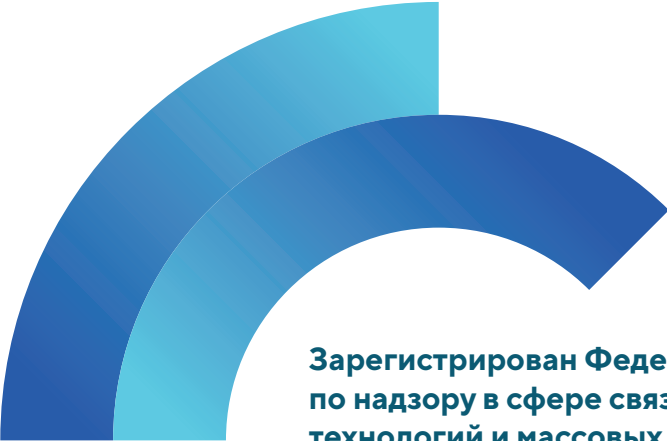
Thermodynamic second-order interaction coefficients of nitrogen with nickel and chromium in liquid steel

Thermodynamic modelling of reduction of iron ore materials by hydrogen-containing gases

Thermodynamic analysis of conditions for iron and titanium separation in ilmenite concentrate by selective reduction of elements

Peculiarities of the phase composition formation of steelmaking slags and evaluation of the possibility of obtaining mineral binders with low CO<sub>2</sub> generation on their basis

Using digital simulation models to optimize the operation of complex production facilities



**Зарегистрирован Федеральной службой  
по надзору в сфере связи, информационных  
технологий и массовых коммуникаций.  
Свидетельство о регистрации  
ПИ № ФС77-35456.**

**Подписной индекс 70383.**

